Development of Solar-Optical Models for Energy Performance Analysis of Draperies in Complex Fenestration Systems

by

Ned Yao-Te Huang

A thesis
presented to the University of Waterloo
in fulfillment of the
thesis requirement for the degree of
Doctor of Philosophy
in
Mechanical and Mechatronics Engineering

Waterloo, Ontario, Canada, 2018

© Ned Yao-Te Huang 2018

Examining Committee Membership

The following served on the Examining Committee for this thesis. The decision of the Examining Committee is by majority vote.

External Examiner	Thanos Tzempelikos Associate Professor
Supervisor(s)	Michael Collins Associate Professor
	John Wright Professor
Internal Member	Sean Peterson Associate Professor
	Zhongchao Tan Professor
Internal-external Member	Geoffrey Lewis Assistant Professor

Author's Declaration

I hereby declare that I am the sole author of this thesis. This is a true copy of the thesis, including any required final revisions, as accepted by my examiners.

I understand that my thesis may be made electronically available to the public.

Abstract

Window coverings have been used for many years to provide protection from undesired environmental conditions and to regulate indoor conditions. Models for complex fenestration systems (CFS), a term coined in the early 90's in light of optical and thermal complexity of shading elements, are essential in pursuing multiple objectives of modern building design. This research focuses on energy performance of one type of window shading, draperies.

Coupled with a rectangular pleated drape model, the conventional three-property Keyes Universal Chart (KUC) predicts shading effect of pleated drapes. This thesis offers a much improved KUC, the b&C model, which was developed using fabric solar-optical properties obtained by a highly accurate spectrophotometer. The improved KUC has largely eliminated the bias and reduced the uncertainty present in the original KUC. The b&C model, also a three-property KUC, uses manipulative functional relationships. A fourth property, fabric thickness, was explored to better correlate the three-property relationships, resulting in the customized KUC for increased accuracy.

Previous pleated drape models comprised only rectangular pleats (i.e., RPD). A triangular pleated drape (TPD) model was built for comparison with RPD. In parallel, an experiment was designed to measure and study the effects of fullness, pleating profile, and angle of incidence for selected fabrics. A comprehensive set of transmittance test results was attained using the Broad Area Illuminating Integrating Sphere (BAI-IS) system. Both RPD and TPD models were assessed with the experiment. Discussions on the effects of variables are offered.

The improved/customized KUC combined with a RPD/TPD model can be implemented in building energy simulation software or used as a stand-alone tool to determine the shading effect of a pleated drape on the solar heat gain.

Acknowledgements

Thank you, God, for your unprejudiced love.

Thank you, Prof. Collins, for your unparalleled patience and understanding. Your generosity and kindness forgive my flaws and motivate me to keep going at impossible times. I appreciate the most your gentle persistence that leads to the completion of this project. I could not ask for more under your supervision. I express my utmost appreciation to you for everything you provided.

Thank you, Prof. Wright, for all your advices and supports since my undergraduate study. You guided and believed in me. You inspire me to do the right things right and always strive for better writing. I am the most grateful for more than two decades of lecture, advice, encouragement, and support. And I appreciate the occasional burst into loud laughter that you and Prof. Collins have in our meetings. Thank you!

A special thank you goes to the thesis committee, Prof. Lewis, Prof. Tan, and Prof. Peterson, who have been very supportive and patient. Thanks to my external examiner, Prof. Tzempelikos from Purdue University, for your expertise in CFS and constructive comments in my KUC research.

Thank you, Prof. Stubley, for all TA and teaching observation opportunities. You showed me how learning and teaching can be both rewarding and enjoyable. I am especially moved by your effort to impart the virtue of honesty and teach students to think freely and as a real world engineer. My study is richer with these truly satisfying experiences.

I am also indebted to many people whom I have relied on for various assistances on campus. Thank you, Neil Griffett, for the LabVIEW/electronics related assistance. Thank you, Andy Barber, for all the hardware/electronics setup. Thanks to William Penney, Martha Morales, and

Mike Willson for computer-related help. Thanks to Jason Benninger and Robert Wagner for making the first frame. Thank you, Phil Laycock and Andrew Urschel, for advising/teaching me how to use machining tools. Thanks to Nathan Kotey and Victor Halder who previously worked on the topics of CFS and gave their precious time for discussions. Thank you, Will, Carsen, Alex, Ramin, Chris, and Julian, for the delightful office atmosphere and friendship. Special thanks to staffs at the UW libraries, CTE, and writing center for making my UW experience here so much better. I thank the University of Waterloo community that provided fifteen years of world-class education and life experiences.

Also, I received external help from friends. A big thank you, Joe, for the Ocean Optics spectrometer that was used in calibration and examination of the monochromator. Thank you, Debra (Fabricland Kitchener), for cutting so many fabric samples. Thank you, Lisa, for the useful fabric cutting tools.

For family, I thank my grandparents and my parents for their love.

My dear wife, Mei-Yu, whom I often take for granted, deserves the deepest appreciation from the bottom of my heart. You sustain me in every way you can and make sacrifices for realization of this study. You and your internal strengths are the backbone of my life. I thank God for bringing you into my life.

I thank you, my son and my daughter, because you always embrace all of me. I am simply blessed with your energy and joy.

All financial supports that make this research project possible are very much appreciated.

Dedication

This thesis is dedicated to all sentient beings.

Table of Contents

List of Figures

List of Tables

Nomenclature

Abbreviations

AGSL	Advanced Glazing System Laboratory (University of Waterloo)
ANSI	American National Standards Institute
ASHAE	American Society of Heating and Air-Conditioning Engineers
ASHRAE	American Society of Heating, Refrigerating and Air-Conditioning Engineers
ASHVE	American Society of Heating and Ventilating Engineers
ASRE	American Society of Refrigerating Engineers
ASTM	American Society for Testing and Materials
BAI-IS	Broad Area Illuminating Integrating Sphere
BFS	back fictitious surface
CFS	complex fenestration system
CPU	central processing unit
DAQ	data acquisition
DSB	downward-slope back (surface)
DSF	downward-slope front (surface)
ESR	external sample reflectance
FFS	front fictitious surface
FWHM	full width at half maximum
HVAC	heating, ventilation and air-conditioning
ILM	individual layer model
ISR	internal sample reflectance
KUC	Keyes Universal Chart
M	measurement
MR	measurement - rectangular
MT	measurement - triangular
N	number of measurements

NECB	National Energy Code for Building
NIR	near infrared
PbS	lead sulphide
PLA	phase lock-in amplifier
P	pleated drape model
PR	pleated drape model - rectangular
PT	pleated drape model - triangular
QTH	Quartz Tungsten Halogen
R	rectangular
ROC_S	rate of change in slope
S/N	signal-to-noise ratio
STRL	Solar Thermal Research Laboratory (University of Waterloo)
T	transmittance (dimensionless), triangular
TC	technical committee (of ASHRAE)
USB	upward-slope back (surface)
USF	upward-sloped front (surface)
UV	ultraviolet
UVS	UV silicon (silicon photo-diode)
YI	y-intercept

Symbols

/	upward-sloped (plan view)
\	downward-sloped (plan view)
A_o	openness (dimensionless)
AVG	average of a set of numbers
b	b coefficient of the b&C model
C	C coefficient of the b&C model
D	dark color fabric
Diff	difference between model prediction and measurement

E_D	direct solar irradiance (W/m^2)
f	focal length of a lens or mirror (cm)
F	view factor (dimensionless)
Fr	folding ratio (dimensionless)
G	irradiance (W/m^2)
I	incident flux (W/m^2), open Weave
IAC	interior attenuation coefficient (dimensionless)
II	semi-open weave
III	closed weave
J	radiosity (W/m^2)
L	light color fabric
M	medium color fabric
N	inward-flowing fraction of absorbed radiation
P	radiant energy transmitted by the sample
P_o	radiant energy incident upon the sample
q	solar flux gained per unit area (W/m^2)
RMS	root-mean-square defined as $(AVG^2 + STD^2)^{1/2}$
S	absorbed solar flux (W/m^2), slope (KUC), pleat spacing
SC	shading coefficient (dimensionless)
SHGC	solar heat gain coefficient (dimensionless)
STD	standard deviation of a set of number
T	temperature (K)
U-value	thermal resistance, heat transfer coefficient, or U-factor (W / m^2K)
W	pleat width
W_D	nominal band width per 1 mm slit opening (nm/mm)
W_E	nominal band width to be used for measurement (nm)
WL	wavelength (nm)
X	actual slit width (mm)
Z	source term for beam or diffuse radiation (W/m^2)

Greek Letters

α	absorptance (dimensionless), pleat angle
γ	wall-solar azimuth angle (local incident angle)
θ	incident angle
ρ	reflectance (dimensionless)
τ	transmittance (dimensionless)
Ω	profile angle

Subscripts

1, 2, 3	1^{st}, 2^{nd} and 3^{rd} coefficient of polynomial for openness lines in KUC
a	related to air temperature
assumed unknown	related to solar optical property predicted using KUC (vs measured)
avg	average
b	related to back surface of a layer
bb	beam-beam solar optical property
bd	beam-diffuse solar optical property
beam	related to beam radiation
bt	beam-total solar optical property
dd	diffuse-diffuse solar optical property
drape	related to pleated drape
f	related to front surface of a layer
fabric	related to flat fabric
full	full spectral range of interest
H	horizontal
i	related to the i^{th} layer or the i^{th} gap, index used in counting
in	related to indoor side
layer	related to drape layer
limit	related to boundaries of KUC

Lower	related to the constant openness line below fabric's data point
m	related to mean radiant temperature, Air Mass
measured	related to solar optical property measured (vs assumed unknown)
n	n^{th} integer
out	related to outdoor side
p	related to projected length
shaded	related to shaded window unit
sol	related to incident solar radiation
solar	related to solar transmittance
t	total
unshaded	related to unshaded window unit
Upper	related to the constant openness line above fabric's data point
V	vertical
yarn	related to yarn

Superscripts

m	related to flat fabric material

CHAPTER 1
INTRODUCTION

1.1 A Brief History of Window Coverings[1,2]

Driven purely by the basic physiological needs, human beings used a variety of coverings for protection and shelter from adverse weather conditions. Explicably, ancient desert civilizations needed ways to protect themselves from the harsh sun. As an example, they put together strips of cloth to form window blinds to shield themselves. When desired and possible, they wetted those strips of cloth to keep out dirt/sand and to provide cool air. Long before the idea of fashion was formalized[3], humans hung animal hides as curtains and placed them over doorways and openings. In this case, these curtains were there to define space as well as to offer privacy.

---

[1] This section provides a brief history of window coverings. Terms that are used today to describe various window coverings include blinds, curtains, drapes, and screens. These terms are written here in a less restrictive means to describe what and how human used them before. As history progressed and technology advanced, meanings of these words also have more definitive meanings.

[2] This section is a compilation based on the articles listed below.
Alex Hooper-Hodson. 2014 December. A History of Curtains and Drapes (Part 1 to Part 6).
http://www.homestyle-online.co.uk/curtains/a-history-of-curtains-drapes-part-one-the-renaissance/
The Editors of Encyclopedia Britannica. 2006 October. Curtain – Interior Decoration.
https://www.britannica.com/topic/curtain-interior-decoration
Amy Azzarito. 2011 March. Past & Present: History of Curtains.
http://www.designsponge.com/2011/03/past-present-history-of-curtains.html
Adrienne Chinn. The History of Curtains and Drapery through the Ages.
http://www.adriennechinn.co.uk/article12.htm
Classic Window Coverings. The History of Window Blinds
http://www.classiccoveringsbend.com/history-of-window-blinds
Helioscreen. 2012 January. A Brief History of Window Blinds
https://www.helioscreen.com.au/history-window-blinds/
DirectBlind 2016 July. 10 Super Interesting Facts about Blinds and Curtains
https://www.directblinds.co.uk/blog/interesting-facts-about-blinds-and-curtains/

[3] According to The Barnhart Dictionary of Etymology (1988), it was probably about the 14th century that a sense of style, fashion, manner of dress was first recorded. The English word of fashion first appeared in the 17th century.

The first Roman blind was devised to keep out dust and debris. People suspended damp pieces of cloth over windows and doorways. The sogginess in the blinds gave more weight (sturdier), trapped dirt, and even provided cooling. Textiles were not the only kind of material used in making blinds. The earliest known window blinds were probably assembled using bamboo by the Chinese, and reeds by the Egyptians. Even today, window shades made of bamboo and reeds are commercially available and regularly advertised by household hardware retailers.

The use of curtains marched along with advancements in household textiles (first linen, flax, followed by wool and later cotton and silk). From the evidence of excavations at Olynthus, Pompeii, and Herculaneum, portieres[4] appear to have been used as room dividers in classical antiquity. Mosaics from the 2nd to 6th century show curtains suspended from rods spanning arches. In England, only beds were curtained along a tester or canopy before the 17th century. Beds were so important because they represented the owner's wealth and status. Curtains for windows were almost non-existent. Instead, utilitarian wooden shutters (or heavy cloth) were more common, most likely, for regulating light and airflow (e.g. keeping the cold out). So curtains over doors appeared first. The hangings would be both decorative and practical in reducing the cold draft from room to room within the building.

The use of venetian blinds did not originate in Venice as the name might suggest. It was actually the Persians who invented and used venetian blinds through the late middle ages. Merchants introduced the eastern art to the Italian city of Venice where these blinds attained the well-known name and became popular across Europe through the 18th century.

[4] A portiere is a curtain hung in a doorway either to replace the door or for decoration.

The rolling types of blind came into play during the 17th and 18th century as window shades grew in popularity and developed in function and style. Likely, the rolling design emerged initially for the purpose of privacy and for protecting the costly textile.

1.1.1 Functions of Window Shades – Before and Today

It is notable that the prominent functions of these various coverings remain unchanged throughout history. It is also quite interesting that the use of blinds and curtains along with their intended functions can be explained and have been influenced very much by the different levels of human needs (e.g., Maslow's hierarchy of needs)[5]. These ancient inventions were originated from the most basic needs for survival (e.g., physiological and safety needs). When the basic level needs have been satisfied, then humans address the higher order needs (e.g., esteem needs such as achievement, status, and reputation). The bed curtain before the 17th century is a good example of the higher order needs. Similarly, the hierarchy of needs explains the reason why the idea/word of fashion did not appear earlier in history.

Today, although bed curtains are rarely seen, the various levels of human needs are apparent in the original functions of window coverings and later in the aesthetic aspects of those coverings. There is a great variety of window shades available today. Regardless of type, each of them has to meet multiple design objectives and fulfil modern requirements.

[5] Maslow's hierarchy of needs is a theory in psychology proposed by Abraham Maslow in his 1943 paper "A Theory of Human Motivation" in Psychological Review.

1.2 Background

1.2.1 Sustainability – The New Standard

Sustainability is becoming the new standard due to a growing list of energy and environmental concerns. Energy conservation is the first step and a key strategy to achieve sustainability. Studies (e.g., IPCC 2014 and Berardi 2015) show that buildings account for at least 30% of total energy use in North America as well as globally. Modern buildings have better insulation, allowing little heat transfer. As well, significant efforts have been made to improve window U-value (or U-Factor[6]). As buildings have better and better insulation, the complexity of windows effect and the associated solar heat gain on building energy use also increases.

1.2.2 Effects of Windows on Building Energy Use

Windows are one of the most influential envelope components to affect annual building HVAC energy consumption. Studies have shown that approximately 25% of consumption for the building sector is attributed to windows through heating, cooling, ventilation and lighting of buildings. For instance, Table 1.1 shows the energy lost/gain through windows (both conduction and solar heat gain) and opaque building envelope components from heating and cooling (Energetics Incorporated 2014). A positive value indicates the building component escalates heating (or cooling) load while a negative value implies the building component eases heating (or cooling) load. This data shows that windows have a significant impact on energy consumption, and therefore energy savings, in buildings. Consequently, as an example, NECB[7] limits the maximum

[6] U-Factor, also called thermal transmittance, is the overall heat transfer coefficient with SI units of W/(m^{2}K), and it is a measure of how well heat is transmitted through an assembly. The smaller the U-Factor, the higher the insulation value.

[7] NECB stands for National Energy Code for Building.

window to wall ratio to 40% for locations such as Toronto and Vancouver, and to 20% for Yellowknife and Iqaluit (based on the prescriptive compliance option)[8].

Table 1.1: Annual energy consumption attributable to fenestration and building components in 2010 (Quads)[9] (Energetics Incorporated 2014)

Building Component	***Residential***		***Commercial***	
	Heating	***Cooling***	***Heating***	***Cooling***
Roofs	1.00	0.49	0.88	0.05
Walls	1.54	0.34	1.48	-0.03
Foundation	1.17	-0.22	0.79	-0.21
Infiltration	2.26	0.59	1.29	-0.15
Windows (Conduction)	2.06	0.03	1.60	-0.30
Windows (Solar Heat Gain)	-0.66	1.14	-0.97	1.38

Among the building components, windows may occupy relatively small areas. Yet windows are clearly a weak point in any energy efficiency strategy. Thermally, they provide much less resistance than other building components, which is a detriment in both heating and cooling climates. From the solar heat gain perspective, they have the potential to either offset heating load or drive up cooling demand. As shown in Table 1.1, solar heat gain through windows offsets the heating load (negative value) in both the residential and commercial sectors. However, as buildings become better insulated, and/or as one moves to a more cooling dominated climate, increased cooling demand becomes a serious concern.

[8] Energy efficiency requirements can be set in different ways depending on types of regulation. For the prescriptive compliance method, each individual building component must achieve compliance with their specific energy efficiency requirements.

[9] 1 quad = 10^{15} BTU = 293.07 TWh

1.2.3 Complex Fenestration Systems - CFS

Solar radiation is a natural and inevitable source of light and heat for buildings. Window areas that are subject to high solar heat gain may cause overheating in a well-insulated building. Solar heat gain is usually the largest variable heat gain that affects peak cooling loads of a building. This is especially true given the current architectural trend toward highly glazed facades, especially in commercial buildings. A window design that is able to transition between high and low solar heat gains would be a great asset.

Advanced window technologies, such as smart glass, are available for controlling solar heat gain. A more conventional, much more economical and commonly implemented approach is to regulate solar heat gain by adding shading attachments such as venetian blinds, roller blinds, and draperies.

Window attachments are very popular and come in a wide variety of materials, weaves, fabrics, and colors. Their key benefits include low cost, ease of user control, privacy, aesthetics, and comfort (e.g., regulate solar heat gain, reduce glare, and etc.). The functions of conventional window attachments can be both an advantage and, sometimes, a drawback. The high level of user control entails manual adjustment/positioning to, for example, provide the most energy saving. Also, when deployed for privacy, shading attachments usually block outdoor views that may be desirable for the sense of connection to the outdoors. With added cost, there are ways to avoid or at least mitigate the drawbacks. One option is to use multiple shading layers. Automation of shades (including motors, sensors, controls, and timers) is also available and can be implemented to attain and optimize multiple benefits of these devices.

In any case, shading devices make a window “switchable” in various ways. Figure 1.1 shows a double glazing unit with a between-pane venetian blind (also known as an integral blind) and a

roller blind attached to the indoor side of the unit. Such a system is usually called a Complex Fenestration System (CFS). In general, CFS refers to a window system that incorporates one or multiple shading elements. The influence of CFS on building energy consumption fuels their technological advancement, increases system complexity, and generates a renewed interest in quantifying the effect of window shades on building energy performance.

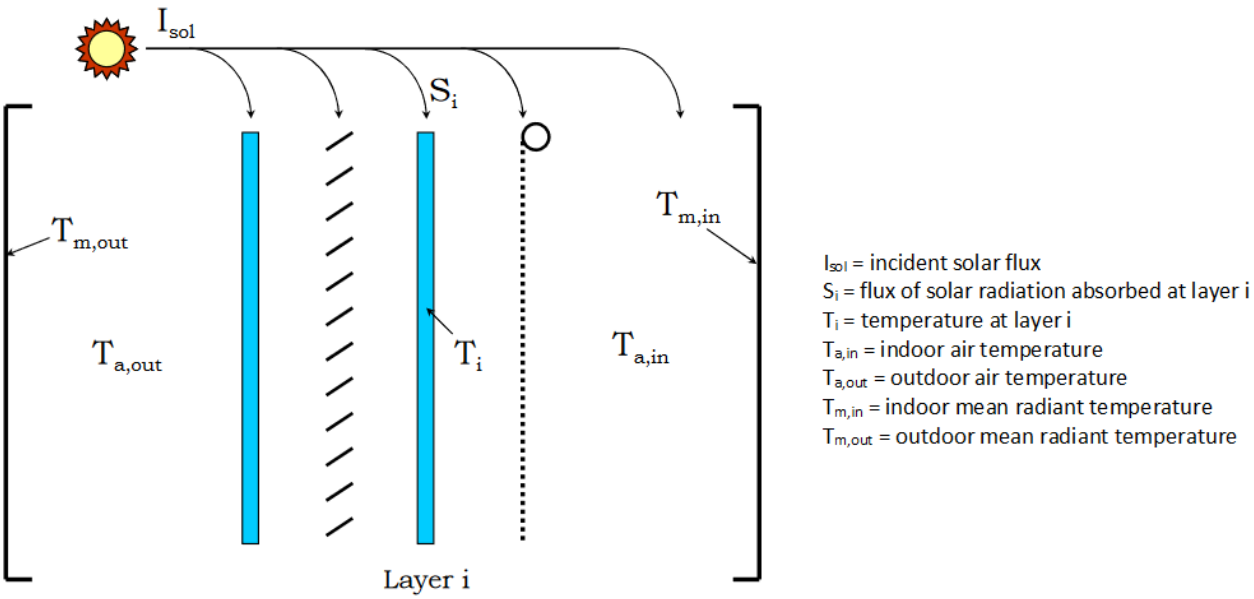

Figure 1.1: Example of a complex fenestration system (Wright et al. 2011)

1.2.4 Energy Flow through Fenestration Systems

CFS energy flow mechanisms include temperature driven heat transfer, solar heat gain, and infiltration. Due to an indoor-outdoor temperature difference, heat flows through a CFS by conduction, convection, and thermal radiation. The U-factor quantifies the combined mechanisms (conduction and longwave radiant exchange) of temperature driven heat transfer. Regardless of the indoor-outdoor temperature difference, solar radiation incident on a CFS either directly from

the sun or indirectly by reflection from the surroundings can be transmitted through the CFS. The amount of solar heat gain is measured in terms of the solar heat gain coefficient (SHGC).

Outdoor air entering the building through infiltration leads to increased heating or cooling loads. Windows and doors are responsible for a significant amount of infiltration in homes. So the effects of infiltration through fenestration systems are also a part of the overall energy analysis. For the center-glass (glazing area) analysis, however, infiltration does not need to be considered.

The center-glass analysis of energy transport through a fenestration system takes advantage of the fact that there is very little overlap between solar (shortwave) spectrum (< 2500 nm) and thermal (longwave) spectrum (> 2500 nm). Named solar-thermal separation, this fact allows the analysis to be carried out in two steps: (1) solar-optical and then (2) heat transfer analysis.

1.2.4.1 Heat Transfer Analysis

For thermal heat transfer analysis, an energy balance is imposed on each layer where net heat transfer must equal the absorbed solar radiation, which is determined from the first step, the solar-optical analysis. Thermal Individual Layer Models (ILMs) (e.g., Kotey et al. 2008, Wright et al. 2008, and Yahoda et al. 2004) are available for modelling each heat transfer mechanism.

1.2.4.2 Solar Optical Analysis

When solar radiation is incident on a fenestration system, the system can reflect, absorb, or directly transmit the radiation through the system. The absorbed portion flows either inward or outward by means of heat transfer. Figure 1.2 illustrates the energy flow of solar radiation incident on a simple one-layer fenestration system.

The flux of absorbed solar radiation can be calculated based on the solar optical properties, namely reflectance (ρ), absorptance (α), and transmittance (τ), for each layer in the system. The ratio of

solar heat gain (including transmitted portion plus the inward-flowing fraction of the absorbed portion) to incident solar radiation is defined as the solar heat gain coefficient (SHGC), or

$$q_b = E_D(\tau + N\alpha) \quad \textbf{(1.1)}$$

$$SHGC = \tau + N\alpha \quad \textbf{(1.2)}$$

where q_b is the total solar gain per unit area (W/m^2), E_D is the direct solar irradiance (W/m^2), τ is the solar transmittance, N is the inward-flowing fraction of the absorbed radiation, and α is the portion of E_D that is absorbed.

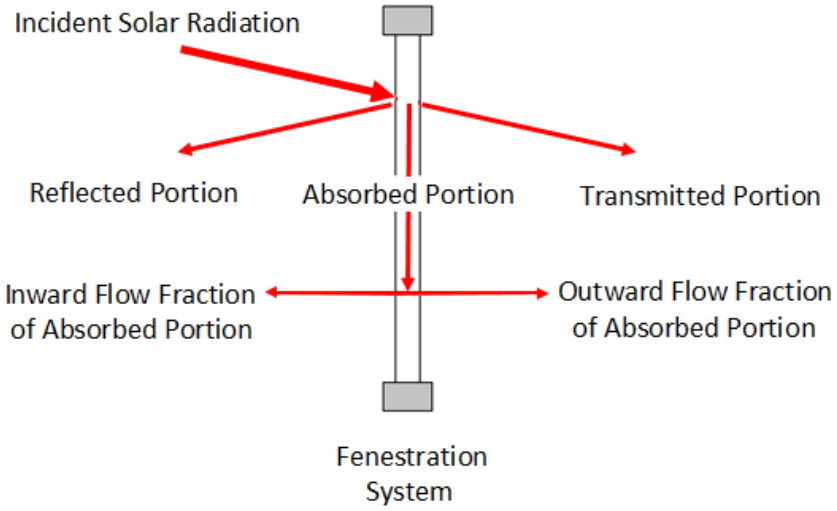

Figure 1.2: Illustration of solar heat gain flow through a fenestration system

Normal incidence beam-beam solar optical and longwave properties of glazing layers are well documented (e.g., LBNL 2008, Pettit 1979, Roos 1997, Pfrommer et al. 1995, and Furler 1991). Additionally, Wright et al. (2009) offers a practical approach to estimate the off-normal solar optical properties of glazing. Kotey et al. (2009a, 2009b, 2009c, 2009d, and 2009e) have developed solar optical Individual Layer Models (ILMs) for shading elements including slat type shades, drapes, roller blinds and insect screens.

1.3 Context of the Research

When energy conservation was not a main concern (e.g., before energy crisis in the 1970s), the indoor environmental qualities of a building could be easily achieved. The energy performance of fenestration systems was also not a top priority. As well, the indoor space conditioning of a building would be a much simpler problem if window areas could be just replaced by walls (such as a dungeon). Yet windows create aesthetically pleasing spaces in any building design. The key is to find an acceptable and optimized balance among several competing aspects of building design (e.g., comfort, daylighting, energy conservation, indoor environmental quality, privacy, security, and outdoor view).

Advanced window technologies and CFSs have become essential in pursuing multiple objectives of modern building design, including high building energy-efficiency and lower peak energy demand. As energy efficiency requirements become increasingly demanding, and indoor environmental quality requirements remain a high priority, the ability to accurately predict window performance becomes more important than ever before.

The increased application and development of CFS have also raised the need of authoritative guidance on accurate and efficient performance prediction methods and tools. Such methods could be useful for standardizing product ratings. As well, these tools may help building designers to pre-select window products and quantify their performance in buildings. However, CFS model development and implementation are still at a relatively early stage. Only recently has CFS thermal performance modelling been integrated into building energy simulation software (e.g., Wright et al. 2011, and Lomanowski and Wright 2009, 2012).

Wright (2008) developed a highly general multi-layer framework to predict center-glass energy performance indices (i.e., U-value and SHGC) of glazing systems with shading devices. The multi-layer framework incorporates Individual Layer Models (ILMs) with each layer assumed to have spatially homogenous behaviour (i.e., effective optical properties). These ILMs determine how one layer interacts with another (i.e., amount and different components of solar gain and heat transfer). Researchers have developed both thermal and solar-optical ILMs for shading devices such as venetian blinds, insect screens, roller shades and draperies. With the new multi-layer framework and available ILMs, Kotey et al. (2009) have shown that this approach is able to provide accurate solar optical and thermal characterization of shading devices.

This research project adds to this modelling effort, particularly in the area of solar optics. Specifically, efforts have been dedicated to aid the understanding and quantification of the effect of pleated drapes on building energy performance, particularly on SHGC. Some characteristics of drapes that can have an impact on both visual and energy performance include drape fabric materials, weaves, colors, and geometry as characterized by fullness or folding ratio. The next section provides a literature review on CFS studies with an emphasis on topics related to fabrics and pleated drapes.

1.4 Literature Review

1.4.1 Solar Shade Specifications Provided by Manufacturers

Today's window attachments usually come with a list of specifications that are used by designers for pre-selection and by business for product promotion. Solar shade providers generally brand their products into multiple lines by design/application and openness factor (OF) while various colors are generally available for each product line. Brochures or similar documents often promote product lines by highlighting the intended applications. As well, regardless of the designs and

intended applications, these marketing documents always include information on thermal and visual performance.

Some product guides may also include information on extended thermal analysis (e.g., SHGC) and visual impact (e.g., glare reduction, outdoor view visibility, and privacy). A comprehensive technical product guide for choosing a window covering fabric considers not only thermal and visual performance but also topics related to acoustic control, aesthetic aspects, building and window orientations, daylighting, environmental footprint of the product, occupant comfort, fabric material and physical properties, security (e.g., fire retardant), UV protection, etc.

Window attachment providers normally classify solar-optical properties into two groups: thermal and optical. Usually, they associate thermal performance with solar properties (i.e., Ts, Rs, and As) and visual performance with optical properties (i.e., Tv and OF). Respectively, Ts, Rs, and As are solar transmittance, reflectance, and absorptance while Tv and OF are visible transmittance and openness factor. This naming convention is not common in the research field, but it is widely used in the window shading industry.

Tv, visible transmittance, is determined with respect to the photopic response of the human eye. Tv is mostly linked to glare control. On the other hand, OF, openness factor, is typically considered with other fabric properties for determining the degree of visibility, glare control, and solar heat gain. OF and the three solar properties are discussed and defined below.

1.4.2 Nomenclature for Solar Optical Properties of Fabrics

To be consistent with previous CFS research studies, the nomenclature presented below are used throughout this thesis. Consider incident solar radiation on a fabric layer (Figure 1.3) with an incident angle of θ. The total (or beam-total) transmittance, τ_{bt}, includes an unscattered component,

τ_{bb}, and a scattered portion, τ_{bd}, as shown in Figure 1.3. The subscripts (bt, bb and bd) denote beam-total, beam-beam and beam-diffuse properties, respectively. In other words, these subscripts pertain to incident beam radiation where τ_{bb} and τ_{bd} account for beam-beam (unscattered) transmittance and beam-diffuse (scattered) transmittance, respectively. And the beam-total property is the sum of beam-beam and beam-diffuse components, or

$$\tau_{bt} = \tau_{bb} + \tau_{bd} \quad \textbf{(1.3)}$$

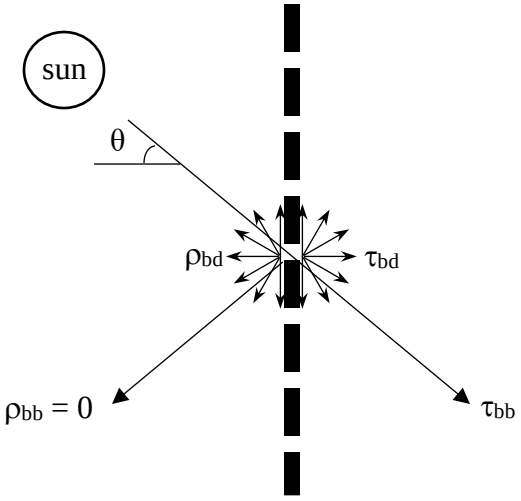

Figure 1.3: Solar optical properties of a fabric layer

In addition, openness (A_o) is a distinct term defined as the percent open area of a flat fabric. A_o is measured as τ_{bb} at normal incidence. So,

$$A_o = \tau_{bb}(\theta = 0) \quad \textbf{(1.4)}$$

Note that fabrics do not exhibit specular reflection, so $\rho_{bb} \approx 0$. The beam-total reflectance, ρ_{bt}, is therefore equal to the beam-diffuse reflectance.

$$\rho_{bt} = \rho_{bd} \quad \textbf{(1.5)}$$

For simplicity, ρ is consistently used to denote fabric reflectance in this thesis. So, unless stated otherwise, $\rho = \rho_{bt} = \rho_{bd}$ for fabric. Also, note that all solar optical properties provided by manufacturers are for normal incidence only (i.e. $\theta = 0$). And, these properties are beam-total properties. Therefore, $Ts = \tau_{bt}(\theta=0)$, $Rs = \rho_{bt}(\theta=0)$, and $OF = A_o = \tau_{bb}(\theta=0)$. Again, the naming convention presented in this section is general and will be used throughout the thesis.

1.4.3 Early CFS Researchers

As early as the 1930s, researchers at the American Society of Heating and Ventilating Engineers (ASHVE)[10] began to study the effect of heat gain/loss through windows (e.g., Miller 1932, Blackshaw et al. 1934, Houghten et al. 1934, Carr et al. 1939, and Houghten et al. 1941). This research group studied transmission of solar energy through glass, built two test houses, compared the energy requirements for a single-glazing test house to that for a double-glazing test house, and considered solar heat gain with and without shading.

Then, from the late 1940s to the late 1960s, ASHVE and then ASHRAE[11] undertook significant efforts to evaluate and quantify the impact of window shading. In the context of the now defunct Shading Coefficient (SC)[12], established CFS researchers such as Parmelee, Ozisik, Schutrum, Farber, Yellott, and Keyes laid the groundwork for much of the work that followed decades later.

---

[10] American Society of Heating and Ventilating Engineers (ASHVE) was founded in 1894 in New York City. In 1954, it changed its name to American Society of Heating and Air-Conditioning Engineers (ASHAE).

[11] American Society of Heating, Refrigerating and Air-Conditioning Engineers (ASHRAE) came from the 1959 merger of ASHAE and the American Society of Refrigerating Engineers (ASRE). ASHRAE, despite having "American" in its name, is an influential organization globally.

[12] SC is the ratio of solar gain through a window unit to the solar gain through 3mm clear float glass. It was introduced in 1963 ASHRAE Guide and Data Book. Standards have moved away from SC to SHGC.

In early work, studies on CFS performance depended largely on measurement in a solar calorimeter. As one of the earliest CFS researchers, Parmelee examined the effect of slat type sun shades on heat gain to the indoors using both mathematical analysis and experimental solar calorimetry (Parmelee et al. 1948, Parmelee et al. 1950, Parmelee et al. 1952, Parmelee et al. 1953).

Later, Ozisik and Schutrum performed similar measurements for roller shades (Ozisik and Schutrum 1959) and drapes (Ozisik and Schutrum 1960). They were the first to investigate the effect of pleating on the transmittance and reflectance of draperies. They limited both of their studies to single-glazed windows.

Furthermore, a team of researchers (Farber et al. 1963) performed a theoretical analysis of solar heat gain through double pane glazing units with both venetian blinds and draperies. They also provided a good summary of the previous studies mentioned above. The same research team carried out a parallel experimental study for comparison with their theoretical treatment (Pennington et al. 1964).

1.4.4 Antecedent of Keyes Universal Chart

Similar to Ozisik and Schutrum's work on drapes, Yellott experimentally determined the Shading Coefficient (SC) of draperies using the ASHRAE solar calorimeter (Yellott 1965). He measured the solar optical properties of fabrics as well as glass-drape combinations using a custom-made instrument. Based on these measurements, Yellott presented SC for various glass-drape combinations as a function of solar reflectance of the drape fabric. He also made frequent reference to Keyes work, which had not been published yet. Together Yellott and Keyes proposed that fabric properties be rated based on yarn reflectance, ρ_y, and fabric openness, A_o (the percent open area between fibers in a fabric). This approach was dubbed the yarn reflectance–openness (ρ_y–A_o)

system. A panel of seven untrained observers averaged over 80% correct in identifying 40 random fabrics using their system. Therefore, they concluded that visual estimation of fabric properties is accurate enough for this application.

In 1967, Moore and Pennington measured the solar optical properties of fabrics and glass-drapery combinations using various techniques. They recommended that fabric classifications be designated by fabric solar-optical properties, namely total transmittance (τ_{bt}) and total reflectance (ρ_{bt}), using their so-called ρ_{bt}–τ_{bt} system instead of the ρ_y–A_o system proposed by Yellott and Keyes. Moore and Pennington argued that A_o needed to be more accurately determined. Visual estimation may not be good enough depending on the fabric material, its thickness and other characteristics such as color. The energy passing through the interstices, plus that passing through the fabric material, is the transmitted energy. In addition, they pointed out that color may be misleading as to its reflective characteristic or ability to turn back the solar energy impinging on a fabric. For example, a dark glossy material may be more reflective than a light dull fabric. Note that yarn reflectance is hard, if not impossible, to measure. Discussions above on the two classification systems formed a good basis for the Keyes Universal Chart (KUC).

1.4.5 Keyes Universal Chart (KUC)

Although Keyes Universal Chart (KUC) was first published in the 1965 ASHRAE Guide and Data Book (ASHRAE 1965), and mentioned in the work of Yellott (1965), Keyes work itself was not published until 1967 (Keyes 1967). In his work, Keyes not only discussed the solar control ability of drapes but also their impact on other factors related to thermal comfort, sound (noise) control, and daylighting concerns.

Further, continuing from the arguments of Moore and Pennington, Keyes reasoned through the usefulness of the ρ_y–A_o system. He mentioned that if the fabric τ_{bt}–ρ_{bt} system were the only one employed, one would: a) have no fundamental understanding of what is physically happening between the yarn and radiant input, b) move into complete dependence on instruments, and c) give up the ability to predict other performance characteristics of the drape fabric. He asserted that the two systems complement each other; the fabric τ_{bt}–ρ_{bt} system for accurate prediction of shading effect, and the ρ_y–A_o system for approximation of shading effect without using instruments and for evaluation of other fabric characteristics. He reconciled the two systems and produced the KUC (Keyes 1967) shown in Figure 1.4.

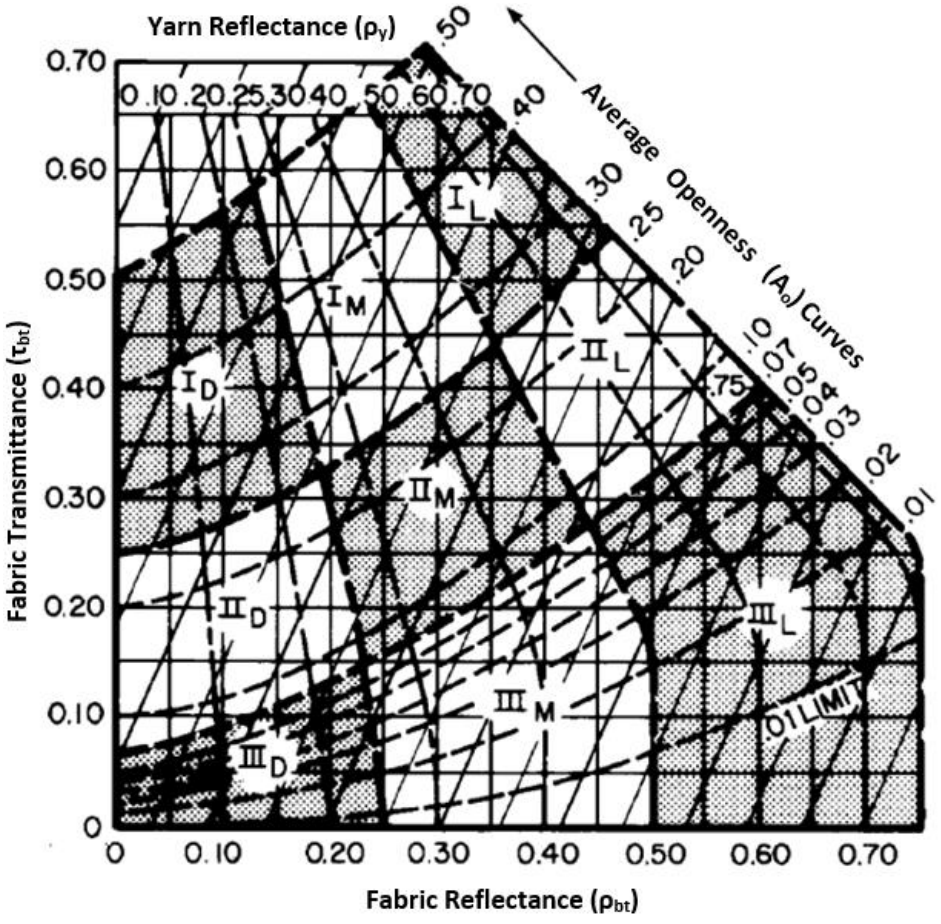

Figure 1.4: Keyes Universal Chart (Keyes 1967)

1.4.6 More Recent CFS Studies

It is well recognized how important CFS could be both for the control of energy consumption and peak load shaving. Fittingly, since the mid 1990s, ASHRAE Technical Committee 4.5: Fenestration (TC4.5) and others have paid significant attention to quantifying the benefits of shading devices placed on windows.

While not part of the TC4.5 efforts, one must include the work of Van Dyck and Konen (1982) who produced solar optical models of shades and CFS for implementation into their WIS software. They showed a theoretical model for analyzing a single glazing with an indoor shading device. Optical properties of shading devices including blinds, roller shades, and draperies were measured and used in their model for system optical properties.

Similarly, McCluney and Mills (1993) modelled solar optical properties of shade materials, and then applied the result to determine window system solar optical behaviors. Their goal was to use a simplified CFS model to compute a realistic estimate of the advantage of using shades to control solar heat gain. For windows without shades, the SHGC is insensitive for angles of incidence up to about 50 degrees. So one main simplification in their model is to assume that solar radiation is always at normal incidence. In addition, while McCluney and Mills acknowledged that almost all shades are diffuse reflectors, they also assumed a specularly reflecting shade. Therefore, with several other assumptions and as stated by McCluney and Mills (1993), their model has been limited to near normal incidence.

1.4.6.1 Matrix Layer Calculation

Innovation in window technologies necessitated added complexity in fenestration system analysis. Models and solar calorimetric methods became increasingly ineffective for determining solar optical and thermal characteristics of more complex fenestration systems. For this reason, Klems

developed a detailed method called the Matrix Layer Calculation (Klems 1994a, 1994b). The method has great potential to accurately quantify CFS both from solar heat gain and daylighting perspectives.

Using a scanning radiometer to compile a detailed solar optical map, this method relies on a full set of bi-directional solar optical properties for each layer in the system (Klems and Warner 1995). The complexity of this approach is a problem as it relies on difficult to obtain measurements (i.e., very time consuming and expensive) and is computationally intensive. This approach can provide a high level of detail regarding the directional nature of the solar radiation within or leaving the system, a desired capability for daylighting analysis. However, a lack of database or models of thermal and solar-optical properties for individual layers, and excessive CPU time needs, precludes the model's application in whole building energy simulations. Still the approach laid the groundwork for the efforts that followed.

1.4.6.2 Simplified Layer Method

A simplified and more practical approach is now available for determining the layer-by-layer absorption of solar radiation and transmission of solar radiation into the building (e.g., Klems 2001, Wright and Kotey 2006). Klems (2001) also introduced the Interior (solar) Acceptance Coefficient (IAC). Without changing the definition of IAC, IAC is now called Interior Attenuation Coefficient in the ASHRAE Handbook of Fundamentals. The IAC tables in newer ASHRAE versions replaced the shading coefficient tables in versions of the ASHRAE Handbook of Fundamentals prior to 2001. IAC is defined as ratio of the SHGC of a fenestration system with a shading device to the SHGC of the same fenestration system without the shading device, or

$$\mathrm{IAC} = \mathrm{SHGC}_{\mathrm{shaded}}/\mathrm{SHGC}_{\mathrm{unshaded}} \qquad \textbf{(1.6)}$$

1.4.6.3 CFS Models and Implementation into Building Simulation Software

Researchers at the Advanced Glazing System Laboratory (AGSL) and Solar Thermal Research Laboratory (STRL) of the University of Waterloo have made significant strides towards CFS modelling. They have not only produced accurate models of CFS performance but also implemented in code a methodology that allowed CFS models to be included in building simulation software where computational speed is important (Wright and Kotey 2006, Collins and Wright 2006, Wright et al. 2008, Barnaby et al. 2009, Wright et al. 2011, Lomanowski and Wright 2012, Foroushani et al. 2015).

1.4.6.4 Pleated Drape Model - Rectangular

In 2009, Kotey et al. performed research on determining solar optical properties of shading devices including venetian blind, roller blind, insect screen, and drape (Kotey et al. 2009a, 2009b, 2009c, 2009d, and 2009e). Kotey et al. (2009c) developed a pleated drape model based on a relatively simple geometry, rectangular pleats. For fenestration systems with drapes, most work was done in the 1960s, and the pleated drape model developed by Kotey et al. is the only theoretical model available since the one presented by Farber et al. in 1963. The IAC tables in the 2009 or newer version of ASHRAE Handbook of Fundamentals are results of the new model (Kotey et al. 2009a, 2009c, Wright et al. 2009, Barnaby et al. 2009).

1.5 Options for Determining SHGC

All work described above was undertaken for one purpose: estimating SHGC of a CFS. Based on the literature review, methods for determining SHGC are summarized below. Each option shows the process by which SHGC of a pleated drape is estimated from the properties of a flat fabric material. One may choose an option based on application, required accuracy, and/or available resources.

Option I: Build a full glass-drape test sample made of draped fabric and use direct measurement methods (e.g., using calorimeter) to determine SHGC.

Option II: Build a drape test sample made of draped fabric, measure ρ_{bt} and τ_{bt} (effective properties) of the pleated drape layer using direct measurement methods (e.g., using Broad Area Illuminating Integrating Sphere (BAI-IS) or integrated reading with pyrheliometer), and then perform the multi-layer analysis (Wright 2008) to determine SHGC.

Option III: Measure normal-incidence flat fabric properties including ρ_{bt}, τ_{bt}, and A_o using a spectrophotometer, apply drape ILM (i.e., off-normal fabric property models and the rectangular pleated drape model) to obtain drape layer effective properties, and then perform the multi-layer analysis to determine SHGC.

Option IV: When one or more flat fabric properties (i.e., ρ_{bt}, τ_{bt}, A_o) are not available:

a. Missing one fabric property: When two of the three properties are available, either use the KUC to determine the third property and follow Option III, or use the KUC to determine the categorized fabric properties and follow Option III.

b. Missing two fabric properties: When one of the three properties is available, use visual inspection and the KUC to determine fabric color (D: Dark, M: Medium, or L: Light) and openness (I: Open, II: Semi-open, or III: Closed). Then look up the IAC value in the ASHRAE Handbook, which is based on Option III above with estimated (or categorized) fabric properties, to determine SHGC.

c. Missing all three fabric properties: When none of the three properties is available, use visual inspection and the KUC to determine fabric color and openness. Then look up the

IAC value in the ASHRAE Handbook, which is based on Option III with estimated (or categorized) fabric properties, to determine SHGC.

Direct measurement methods (Option I and II) are considered more accurate, but costly and time consuming. Such methods are good for model development and validation purposes. In the case where no measurement device is available, one can use the visual inspection method (Option IV) with the KUC and the IAC tables in the ASHRAE handbook to estimate SHGC of pleated drape materials. The visual inspection method using the KUC and the IAC tables requires minimal cost and time with a reduced accuracy. Yet, when equipped with the KUC and IAC tables, visual inspection can be a very convenient tool for designers to estimate performance and consider design tradeoffs of a CFS during the early design phase.

Between direct measurement and visual inspection, a more balanced approach is to measure flat fabric properties using a spectrophotometer (Option III), which is a relatively quick and easy task compared to direct measurement methods. Then SHGC of pleated drape made from the measured fabric can be determined either by using the KUC with the IAC tables or by the multi-layer solar-thermal analysis with solar-optical models for pleated drapes.

The method of spectrophotometer measurements along with the solar optical models can be utilized as a stand-alone tool to determine the performance of a CFS, or it can be easily packaged in building simulation software. This method has been coded along with a drapery fabric library. In fact, fabric manufacturers will often know and supply ρ_{bt}, τ_{bt}, and A_o of their products, which can simply be used as input in the models.

1.6 Purpose and Objectives

The main purpose of this research is to provide simple but accurate tools that can be both used as a stand-alone tool and implemented in the multi-layer analysis as a solar-optical ILM to predict the CFS center-glass energy performance index, SHGC or IAC.

Specifically, this research focused on one type of window shading: draperies. For modelling draperies, the effect of pleating needs to be examined, using a pleated drape model. Also, KUC is a very convenient tool for designers as it correlates measured solar optical properties of fabric with eye-observed values to estimate the shading effect in terms of the historical SC or now the more widely recognized SHGC or IAC. In fact, KUC (Keyes 1967) along with the rectangular pleated drape model (Kotey et al. 2009c) are the basis for determining the IAC tables published in ASHRAE Handbook – Fundamentals since 2009. Therefore, the two key aspects for estimating the shading effect of draperies are (1) KUC and (2) a pleated drape model.

For KUC, Keyes established the original chart in 1967. Since then, it remained unchanged for half a century. Recognizing the value and flexibility of the KUC and its ρ_y–A_o system, however, a study (Collins et al. 2016) revealed the need to update the KUC.

For the pleated drape model, only the rectangular pleat geometry was considered in previous studies (Farber et al. 1963 and Kotey et al. 2009c). The rectangular pleating shape is only an approximation of the true pleating profile. In fact, there are so many pleating styles and techniques available that it is not feasible to survey all of them. Therefore, there is still much to learn about the effect of pleating geometry on SHGC. Furthermore, most experimental studies examined solar optical properties of either the glazing layers or the combination of the glazing layers and shading attachments. The author is not aware of any solar optical property measurement performed for the

pleated drape layer alone. Such sub-system layer measurements are crucial for model development and validation at the sub-system component level. The discussions above lead to the following three key objectives that are addressed in the next five chapters of the thesis:

(1) **An updated and improved KUC.** The first two sections in CHAPTER 2 examine the original KUC in detail and discuss the findings that lead to the search for an improved KUC. A database of fabric solar-optical properties was generated for updating the original KUC and presented in Section 2.3. Section 2.4 establishes a new methodology for KUC and presents the improved KUC (the b&C model). The model provides a functional relationship of fabric properties that can be manipulated by two model coefficients, b and C. The new methodology itself is an enhancement to the hand-drawn chart of the original KUC. The methodology allows variations and makes further analysis much more efficient. Building on the b&C model, CHAPTER 3 proposes a customized KUC approach, an extension to the b&C model that explores the possibility of using a fourth independent variable.

(2) **A triangular pleated drape model.** CHAPTER 4 offers a triangular pleated drape model for comparison with the rectangular model.

(3) **Pleated drape layer transmittance measurement.** CHAPTER 5 provides details of the experiment including test matrix, sample construction, limitations, the BAI-IS system setup and calibration, and measurement uncertainties. Then CHAPTER 6 presents and compares all results from the pleated drape models (both rectangular and triangular) and the measurements. Effects of incident angle, pleating (including pleating profile and folding ratio), and fabric properties are discussed.

CHAPTER 7 includes the conclusions and recommendations for further work.

CHAPTER 2
DEVELOPMENT OF THE IMPROVED KUC

2.1 Examination of the KUC[13]

2.1.1 Placement of Constant Openness Curves in the Original KUC

Keyes (1967) used a grid (coordinate) paper with the blank square surface missing to convey the concept of yarn reflectance (ρ_y) and fabric openness (A_o). He referred yarn to the grid and fabric open areas to the square openings. Having solar radiation impinging upon such a sheet, the openings allow direct transmission without any interference. The grid (yarn) that is present can absorb, reflect, and transmit the solar radiation. The reflectance of the fabric is, therefore, the reflectance of the yarn itself, ρ_y, multiplied by the decimal fraction of the surface that is present (i.e., $1 - A_o$).

$$\rho_{bt,fabric} = \rho_y \times (1 - A_o) \quad \textbf{(2.1)}$$

The transmittance of the fabric is 1) the transmittance of the sheet times the decimal fraction of the grid area, plus 2) the decimal fraction of the openings, allowing unrestricted transmission.

$$\tau_{bt,fabric} = \tau_{sheet} \times (1 - A_o) + A_o \quad \textbf{(2.2)}$$

Based on the use of ρ_y and A_o, Keyes needed three pieces of information to develop the KUC: $\rho_{bt,fabric}$, $\tau_{bt,fabric}$, and A_o. He was able to obtain this data for various fabric materials, colors and weaves from four sources (Keyes 1967): the Yellott Solar Energy Laboratory (Yellott), the

[13] Discussions presented in this section were largely published by the author (Collins et al. 2016).

University of Florida (Pennington), Pennsylvania State University (Pass), and from the Pittsburgh Plate Glass Company (Schutrum, Stewart, and Keyes).

As shown on the KUC (Figure 1.4), the x- and y-axis are $\rho_{bt,fabric}$ (or ρ) and $\tau_{bt,fabric}$ (or τ_{bt}) respectively. Keyes started by plotting ρ and τ_{bt}. To place the constant A_o curves, he plotted on the chart all data points within a range of the target A_o. Specifically, he categorized test data into ranges of A_o and then plotted a constant A_o curve for each range separately. For example, he plotted test data for all fabrics with A_o between 0.015 and 0.025. A curve fit to this data range was set to be the constant openness line of $A_o = 0.02$ as shown in Figure 2.1. As A_o and τ_{bt} should be nearly equal at $\rho = 0$ (i.e., dark thread with $\rho_y = 0$), the line was anchored at that point, at the left edge of the chart. In other words, Keyes drew the constant A_o lines starting at $\rho = 0$ with τ_{bt} being equal to the target A_o (i.e., Equation (1.4)) and passing through the group of plotted data points.

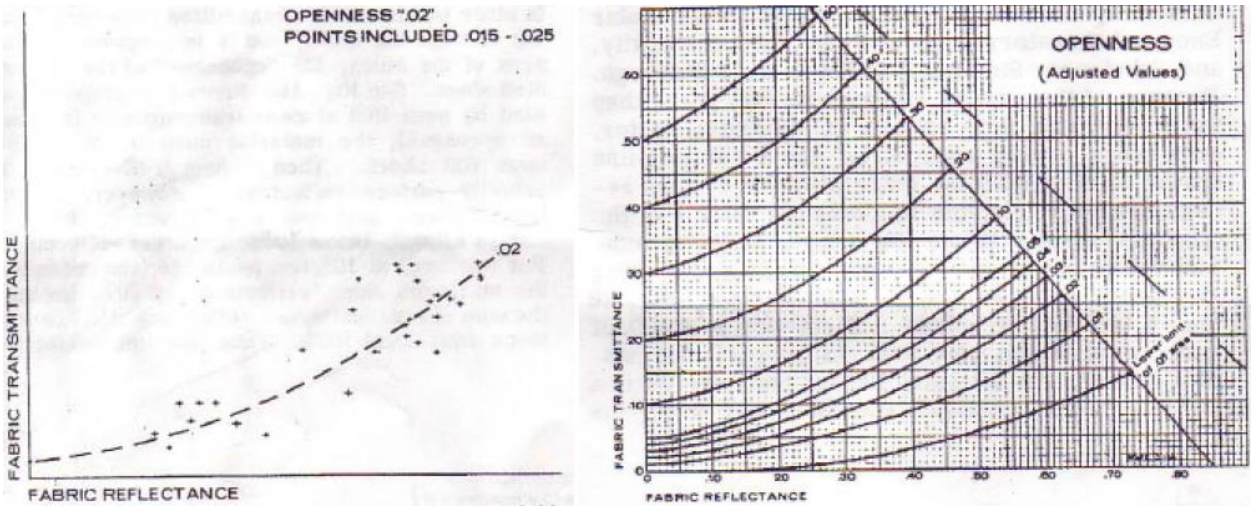

Figure 2.1: Development of openness lines on the KUC (Keyes 1967)

Note that, even with $A_o = 0$ (i.e., one cannot see through fabric), a certain amount of radiation can still penetrate the fabric by transmittance through fibers or by multiple reflections among fibers. So there are still scattered components, but no beam-beam transmission in this case. In other words,

$A_o = 0$ does not necessarily mean zero transmission. Figure 1.4 shows this effect as the area under the lowest ".01 LIMIT" line. Similarly, the same effect makes each line of constant A_o curve upward, indicating increased τ_{bt} (upward) as ρ_{bt} and ρ_y increase to the right.

Next, the diagonal line connecting ($\rho = 1$, $\tau_{bt} = 0$) and ($\rho = 0$, $\tau_{bt} = 1$) is the upper limit of the KUC. Data points beyond this limit require $\rho + \tau_{bt} > 1$, which is clearly not possible. So the plot takes on a triangular shape. Following this, yarn reflectance (ρ_y) was included, based on the approximation that ρ arises from a simple reflection in the area occupied by yarn (i.e., Equation (2.1)). The resulting ρ_y lines are shown in Figure 1.4. Although ρ_y is hard to measure, the openness concept offers a way to estimate ρ_y.

2.1.2 Fabric Classifications Outlined by Keyes

As a final step, Keyes added a general fabric classification to the KUC. The 1965 ASHRAE Guide and Data Book first introduced this classification system. Fabrics were classified by weave as Open (I), Semi-open (II), and Closed (III), and by color as Dark (D), Medium (M), and Light (L). Table 2.1 summarizes the classification system. Note that the nine categories shown in Table 2.1 correspond to the nine zones on the KUC (Figure 2.2).

Table 2.1: Classification of drapery fabrics by openness and yarn color of fabrics

	Dark (D)	**Medium (M)**	**Light (L)**
Open Weave (I) (> 25% open)	I_D	I_M	I_L
Semi-open Weave (II) (7 – 25 % open)	II_D	II_M	II_L
Closed Weave (III) (0 – 7 % open)	III_D	III_M	III_L

The KUC has remained virtually unchanged for 50 years. It has been published in the Fenestration Chapter of every ASHRAE Handbook of Fundamentals. The only significant change was the replacement of shading coefficient (SC) with interior attenuation coefficient (IAC) in the 2001 Handbook of Fundamentals (ASHRAE 2001).

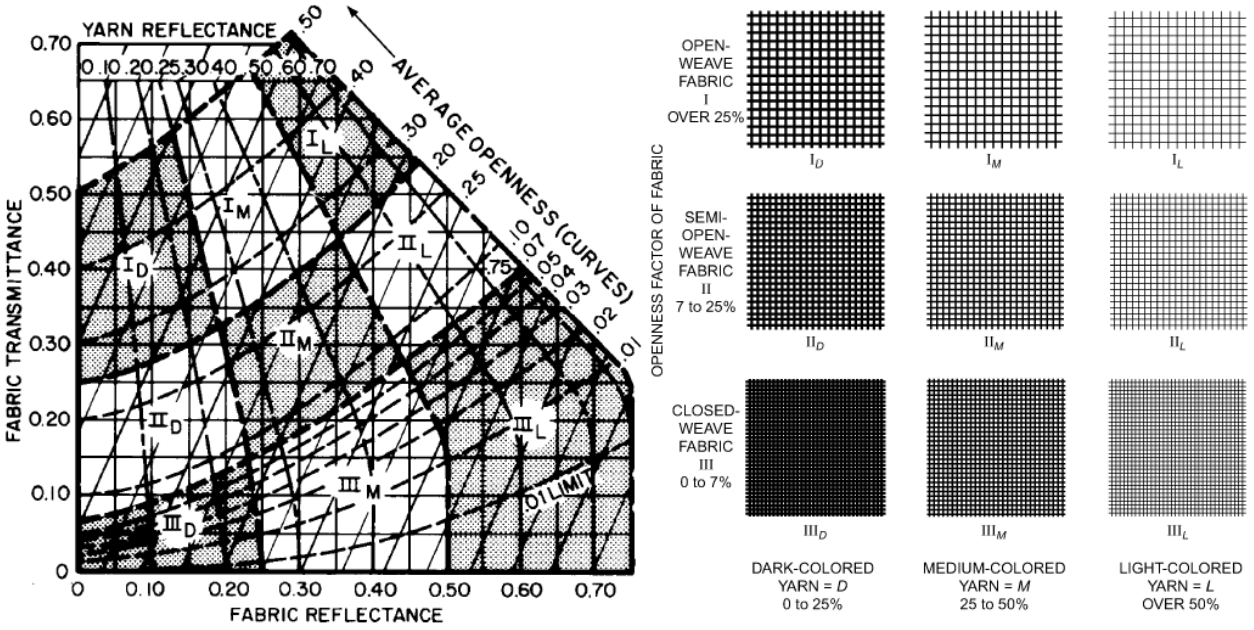

Note: Classes may be approximated by eye. With closed fabrics, no objects are visible through the material, but large light or dark area may show. Semi-open fabrics do not allow details to be seen, and large objects are clearly defined. Open fabrics allow details to be seen, and the general view is relatively clear with no confusion of vision. The yarn color or shade of light or dark may be observed to determine whether the fabric is light, medium, or dark.

Figure 2.2: Designation of drapery fabrics (Keyes 1967)

2.2 The Need to Update the KUC

2.2.1 Recently Measured Fabric Solar Optical Properties

ASHRAE Research Project 1311 recently developed new solar optical and thermal models, and a new solution methodology for modelling CFS in building simulation software (Wright et al. 2009). As part of that work, the link between the solar optical properties of shades and the solar optical properties of the materials from which shades are made was required. In several cases, those

models had already been developed. For example, Ozisik and Schutrum (1960) and Yellott (1965) had developed drapery models for determining the solar optical properties of a drapery layer based on the solar optical properties of fabric. The accuracy and limitations of these models needed to be established. And in the case of drapery, this required the measurement of solar optical properties of various fabrics.

Kotey et al. (2009a) examined nine fabrics in total, representing eight of the nine Keyes fabric categories, and a sheer fabric. He did not include a III_D (closed weave and dark) sample. All measured fabric properties came from a highly accurate UV/VIS/NIR spectrophotometer (Cary 5000). First, Kotey et al. obtained the data for specular (beam-beam) transmission (i.e., τ_{bb}), or openness (A_o), at normal incidence. Then, with the help of an integrating sphere attachment, the total reflectance, $\rho_{bt,}$ and total transmission, τ_{bt}, were measured. Complete details of the measurement method were documented (Kotey et al. 2009a). Table 2.2 reproduces the measurement results. Plotting the measured data on the KUC reveals some irregularities.

Table 2.2: Solar properties of various drapery fabrics (normal incidence)

Classification	A_o	Fabric ρ_{bt}	Fabric τ_{bt}
Sheer	0.45	0.19	0.80
I_L	0.26	0.42	0.56
II_L	0.01	0.56	0.43
III_L	0.01	0.68	0.30
I_M	0.33	0.23	0.64
II_M	0.02	0.32	0.28
III_M	0.01	0.38	0.20
I_D	0.23	0.15	0.32
II_D	0.05	0.21	0.23

2.2.2 Fabric Reflectance, Fabric Transmittance, and Openness

Recall that Keyes (1967) reconciled the ρ_y–A_o system with the ρ–τ_{bt} system. Equation (2.1) shows that ρ_y and A_o depend on each other. Therefore, one may reason that the reconciliation of the two systems is equivalent to an introduction of a third variable to the fabric τ_{bt}–ρ_{bt} system. In summary, KUC provides a relationship among three solar optical properties of fabrics: 1) ρ, 2) τ_{bt}, and 3) A_o.

2.2.3 Plotting Measured Solar Optical Properties on the KUC

While the validity of the older drapery models proved to be very good, the same could not be said for the KUC. Knowing any two fabric properties would enable one to read the third property using the KUC. As discussed in Section 2.2.1, these three fabric properties can also be measured, and they should ideally meet at a point on the KUC. However, given the complexity of fabric characteristics, it is improbable that the KUC is able to accurately relate the solar optical properties for all types of fabrics. Furthermore, Keyes approximated a constant A_o curve from multiple points representing a range of measured A_o values. So it was not expected that the three properties would meet exactly at a point. This was indeed the case for all fabrics measured by Kotey et al. (2009a).

2.2.4 Error and Bias of KUC

For a fabric, when its three properties do not converge to a point, the point disperses into three different points on the chart located by the three possible combinations (pairs) among the three properties: A_o–ρ_{bt}, A_o–τ_{bt}, and ρ_{bt}–τ_{bt}. They form a right triangle on the chart with the point paired by ρ_{bt} and τ_{bt} located at the right angle. So the triangle is bounded by τ_{bt} (horizontal leg), ρ_{bt} (vertical leg), and constant A_o (sloped) line. The constant A_o line can be approximated by the hypotenuse. Also, a triangle's hypotenuse can be facing either downward or upward. The smaller the triangle, the more accurate the KUC is for a specific sample. Using Kotey's fabric data (Table 2.2), Figure 2.3 shows 9 triangles, each triangle corresponding to a fabric sample.

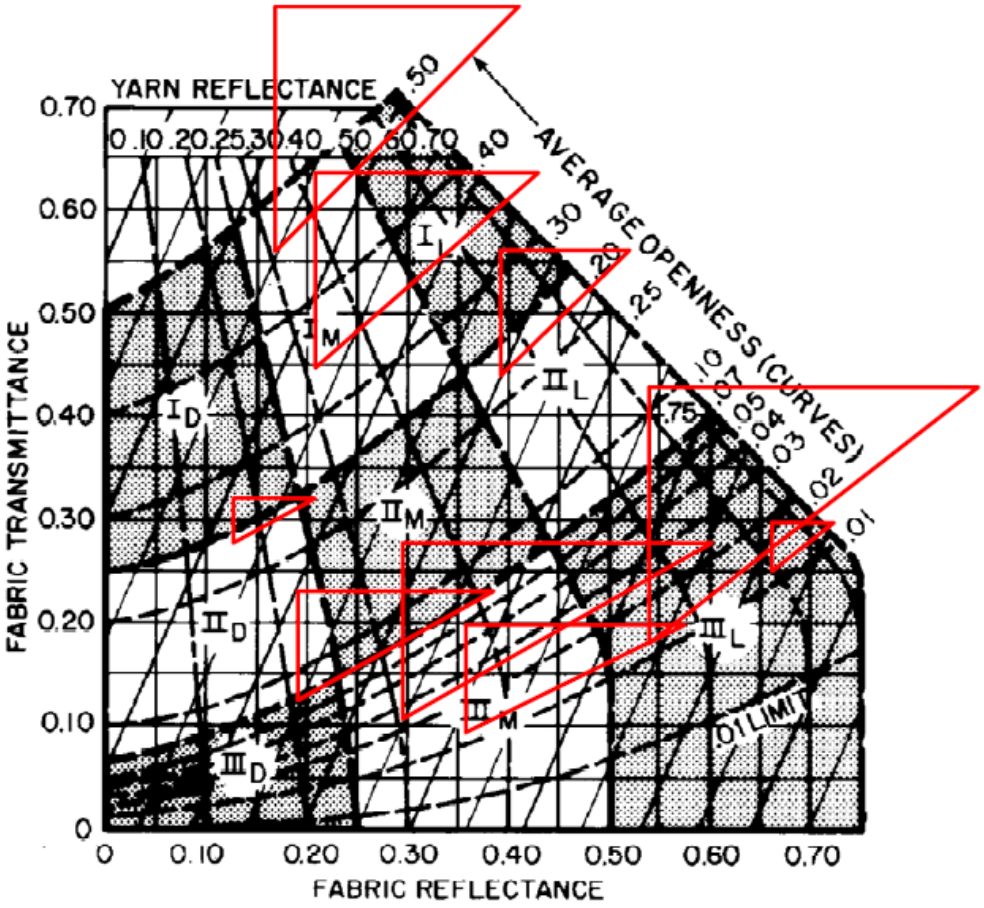

Figure 2.3: KUC (ASHRAE 2013) including data from Kotey et al. (2009a). This figure is taken from Collins et al. (2016)

As explained earlier, one should not expect that the three points would overlay one another in each case. However, they should be in close proximity: the triangles should be small. Furthermore, in the absence of bias, upward facing and downward facing triangles would both be present. This, however, was not the case. Figure 2.3 shows that not only are some of the triangles large, indicating chart inaccuracy, but also all of the triangles point in the same direction (hypotenuse facing downward). Also concerning is the fact that some points lie beyond the diagonal limit of the chart.

As shown in Figure 2.3, all triangles are facing downward. In such case, the $\rho_{bt} - \tau_{bt}$ data point is above the hypotenuse, suggesting that the KUC always overestimates A_o. Alternatively, depending

on which two of the three properties are measured and plotted, the KUC will always overestimate A_o, overestimate ρ_{bt}, or underestimate τ_{bt}.

2.2.5 Possible Sources of Error

It is unlikely that one can definitively show the origin of this error. Keyes (1967) obtained data from four sources, but at no point provided a detailed listing of the data or types of samples used. Concerning the methods by which each measurement was obtained; he referred to Pennington et al. (1964) for determining total reflectance and transmittance, and described a custom-built apparatus consisting of a slide projector, collimating tube, and photocell for measuring the openness (Figure 2.4). A photocell reading was taken both with and without the sample in place, and the ratio of these readings was reported as openness.

Reliance on the referenced data sources is also not helpful. In the paper by Ozisik and Schutrum (1960), they describes nine fabric samples, but no mention is made of the openness. They briefly describe the tests as being done outdoors using a pyrheliometer. In Pennington et al. (1964), only two samples are listed, also without openness data, and a brief reference is made to spectrophotometric measurement. To the authors knowledge, the work of Pass was never published, and it is unknown how many samples were tested, or how.

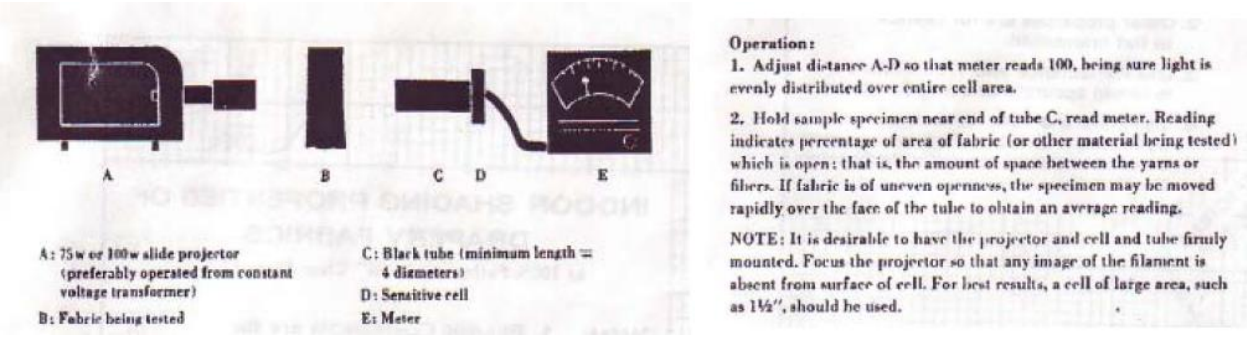

Figure 2.4: Keyes openness measurement apparatus (Keyes 1967).

Yellott's work (1965) is the best documented. Yellott describes all three properties for 17 fabrics, although fabric designations suggest he tested about 100 samples in total. He also describes his measurement procedure in detail. To measure total reflectance and transmittance, he uses the TRA-Scope (Figure 2.5). It consists of two frames rotating about the same axis, using the sun as a light source. One contains a fabric or glass sample, while the other contains a radiometer. To measure openness, an apparatus similar to the one described by Keyes was used, except the illumination source was the sun (Figure 2.5).

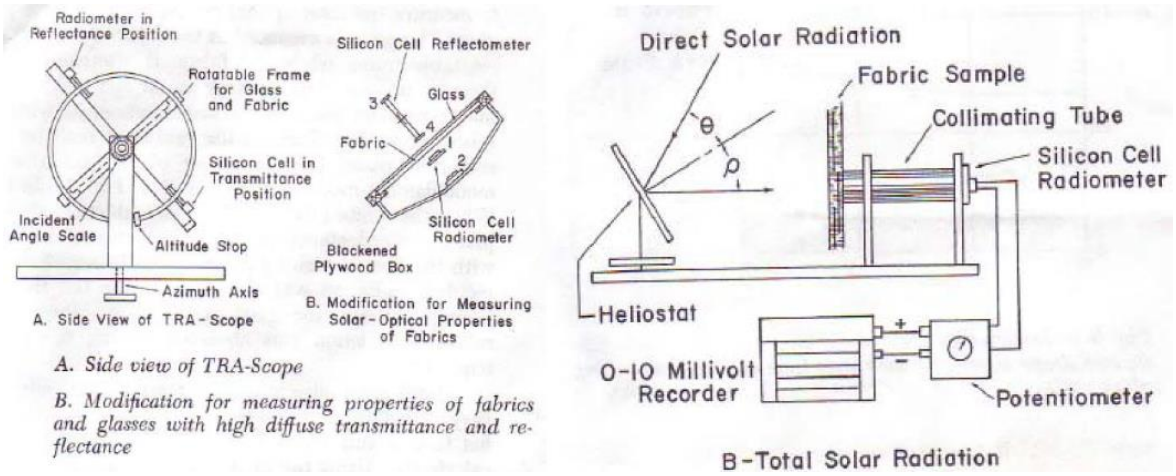

Figure 2.5: Yellott (1965) measurement setup: TRA-scope (Left) and A_o reading (Right)

Despite the lack of detail, the source of error most likely lies with the data used by Keyes, and not with the new measurements. Either Keyes' transmittance data was too low, his reflectance data too high, or his openness data was too high. The τ_{bt} and ρ_{bt} measurements shown in Table 2.2 were obtained using the same spectrophotometric process mentioned by Pennington et al. (1964) and endorsed by Keyes (1967). The modern shading studies described earlier endorse this approach.

In deference to the older studies, however, is the fact that the current spectrophotometric measurements come from far more accurate and reliable equipment. Still, one must presume that data used by Keyes are just as reliable. Regarding A_o, the τ_{bb} measurement obtained from the spectrophotometer is fundamentally no different from the one described by Keyes or Yellott and shown in Figure 2.4 and Figure 2.5. In the case of the spectrophotometric equipment, however, the equipment is far better designed and calibrated.

What is most likely the problem with the A_o measurements, however, is the acceptance angle associated with the collimating tube. Ideally, a measurement of beam-beam transmission would only include those light rays that pass directly through the fabric weave without changing direction. Unfortunately, if a single ray direction could be chosen, it would contain no energy, and the sensor would not pick up a reading. The measurement system must therefore be designed to accept all radiation within a cone that emanates from the sample. As the size of this cone increases, more scattered radiation is sensed, and the measured openness value becomes inflated. It is not known how large the acceptance angle was in the original experiments, but it is most definitely greater than the acceptance angle of the spectrophotometer used by Kotey et al. (2009a). No matter where the error lies, it is clear that the constant openness lines shown on the KUC are not placed accurately and should be updated.

2.3 SOLAR OPTICAL PROPERTY OF FLAT FABRICS

To further examine and resolve the error and bias of KUC discussed above in Sections 2.2.3 to 2.2.5, various fabrics have been selected and their solar optical properties measured. Without measured properties being available in the first place, the selection process first involved visual inspection with the intent to cover all regions of the KUC evenly. This was performed by the visual inspection method described by Keyes (1967). Visually selected fabrics were then measured and

their properties plotted on the KUC. Experience shows that Dark (D) category fabrics are relatively difficult to be correctly identified. As a result, relatively more fabrics are in the Medium (M) categories.

The measured properties are also required as input for the pleated drape models. This section offers details on the Cary 5000 spectrophotometer used for the fabric property measurements. A description of the integrating sphere inside the Cary 5000 and a brief survey on its theory are also included. Measurement techniques and data processing for transmittance and reflectance measurements are explained. Then, measurement results are presented. Most importantly, these measured fabric properties form the basis for developing the improved KUC.

2.3.1 Cary 5000 Spectrophotometer

The Cary 5000 UV-Vis-NIR spectrophotometer is a high performance device commercially designed and produced for photometric measurements in the 250-2500 nm range. The operation of the Cary 5000 is highly automated and controlled by the Cary WinUV software. Calibration and measurement procedures are relatively easy and quick. Because of its capabilities, it is an excellent apparatus for many purposes including this research project. Kotey gives a detailed description of the Cary 5000 spectrophotometer (Kotey 2009).

2.3.1.1 Measurement Using an Integrating Sphere

The Cary 5000 spectrophotometer is equipped with a 110 mm diameter integrating sphere. An integrating sphere consists of a hollow sphere with its inner surface coated with a layer of high reflectance material. An integrating sphere collects and integrates spatially and directionally all incoming radiation. Its inner surface is assumed to be Lambertian, reflecting light into all available solid angles with equal efficiency. An integrating sphere has at least one inlet port to admit light plus a port where detectors are located.

2.3.1.2 Integrating Sphere Theory

Sumpner (1892) described the theory of light-collecting hollow cavities. Ulbricht (1900) introduced the integrating sphere as a method for measuring the radiant flux of light sources and surface reflectance. Soon it became a standard instrument in photometry and radiometry. Integrating sphere theory has been extensively covered in the literature (e.g., Rosa and Taylor 1922, Jacquez and Kuppenheim 1955, Hisdal 1965a,b, Goebel 1967, and Tardy 1991) and derived from the general theory of radiation exchange between two differential elements of diffuse surfaces. Labsphere's technical guide (Labsphere 2013) gives a detailed discussion on integrating sphere theory and applications.

2.3.2 Measurement Method, Data Processing, and Results

The beam-diffuse transmittance, τ_{bd}, is measured with the sample in place and the reflection port open, allowing the transmitted beam component to escape while trapping the scattered radiation (Figure 2.6a). The beam-total (beam-beam plus beam-diffuse) transmittance, τ_{bt}, is measured with the reflection port covered (Figure 2.6b). The difference between the two readings is the beam-beam transmittance, τ_{bb}, which is equivalent to the openness factor, A_o. All measurements are for normal incidence, $\theta = 0$.

To measure the beam-diffuse reflectance, ρ_{bd}, the sample is mounted as shown in Figure 2.7a, allowing the incident beam to strike the sample at normal incidence and causing the beam-beam reflection component to exit through the transmission port. When the sample is mounted as shown in Figure 2.7b at a near normal incidence, both beam and diffuse components remain in the sphere and the detectors measure beam-total reflectance, ρ_{bt}. The beam-beam reflectance, ρ_{bb}, is simply the difference between the two reflectance readings. However, the shading layers considered do

not exhibit specular reflection, $\rho_{bb} \approx 0$, which was confirmed experimentally (Kotey 2009). The beam-total reflectance, ρ_{bt}, is therefore equal to the beam-diffuse reflectance, $\rho_{bt} = \rho_{bd}$.

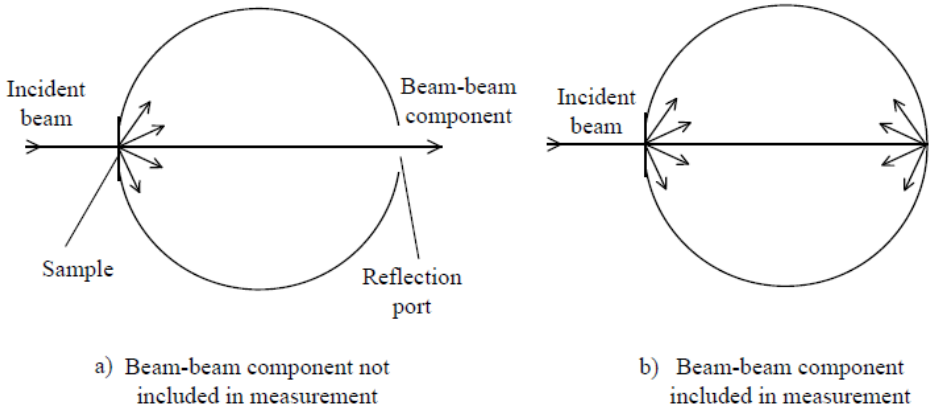

Figure 2.6: Beam-diffuse and beam-total transmittance measurements (Kotey 2009)

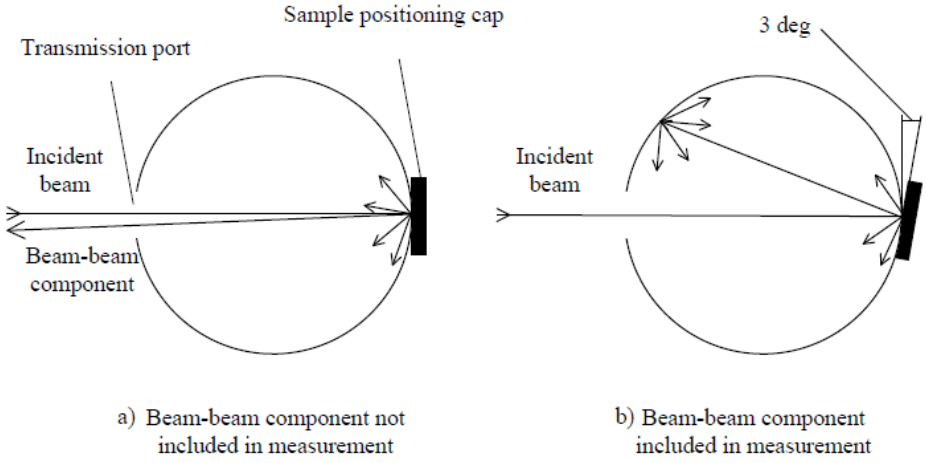

Figure 2.7: Beam-diffuse and beam-total reflectance measurements (Kotey 2009)

2.3.2.1 Weighted Average of Spectral Properties

Transmittance and reflectance measurements of the Cary 5000 utilize an artificial light source. Standard test methods have been developed for measuring solar optical properties with an artificial light source. The main advantage of using an artificial light source is its stability, enabling repeatable readings. Because an artificial light source has a different spectral irradiance profile

than natural sunlight, solar optical properties are obtained by calculating a weighted average of the corresponding spectral properties with a standard weighting function (e.g., solar spectral irradiance for Air Mass m = 1.5). Spectral measurement using a spectrophotometer with an integrating sphere provides the spectral solar-optical properties over the spectrum of interest.

Specifically, the solar spectrum is divided into 50 equal-energy wavelength intervals based on ASTM E891-87. Then, the solar optical properties can be determined following the 50-point selected ordinate method described in ASTM E903-96. For example, solar transmittance is calculated as:

$$\tau_{solar} = \frac{1}{n}\sum_{i=1}^{n} \tau(\lambda_i) \qquad \textbf{(2.3)}$$

where λ_i is the wavelength at the center of the i^{th} spectral interval and n = 50 (or the number of equal-energy wavelength intervals if a different range of solar spectrum is considered).

2.3.2.2 Measurement Results

For this study, spectral solar optical properties of 108 fabric samples have been measured. Including the nine fabrics measured by Kotey (2009a); there are 117 samples in total. These fabrics are numbered, and each of them has been given a name. Using the measured spectral property, weighted averages were calculated using the procedures described above in Section 2.3.2.1 for the solar wavelength range, 250 – 2500 nm. Appendix A: List of Fabric Samples and Their Properties lists the resulting solar optical properties for all 117 samples. Plotting fabric transmittance against fabric reflectance, Figure 2.8 shows the location of each measured fabric on the KUC without considering the openness data.

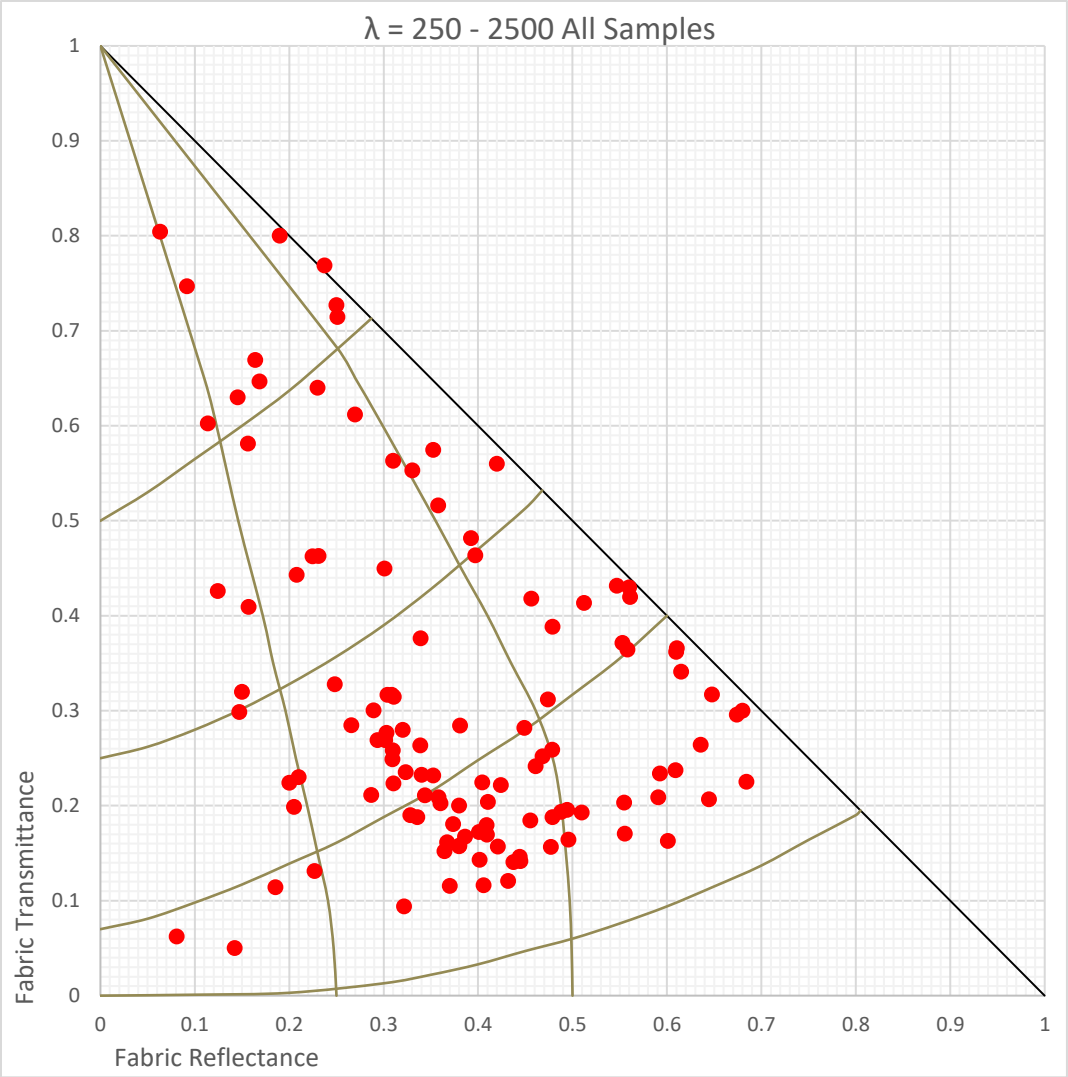

Figure 2.8: Fabric map showing τ_{bt} vs ρ on the KUC

2.3.3 Uncertainty Due to Non-uniformity in Flat Fabrics

When selecting a fabric, patterned fabrics with any kind of print have been deliberately avoided. Only plain fabrics were chosen to preclude the visible non-uniformity in the fabrics. Nonetheless, no fabric is perfectly uniform. This section lays out the effort given to quantify and correct the non-uniformity in the fabrics on the measured properties.

For those fabrics (22 out of 117 samples) that have been chosen to make pleated drape samples, their flat fabric properties were measured multiple times at different locations to identify any non-uniformity in the fabrics. The number of measurements depends on the degree of the non-uniformity. For each fabric, five random locations were measured. If all five measurements were within 0.01 of each other, no further measurement was made. Otherwise, up to 50 measurements were taken for measurement of the most non-uniform fabric.

Two highly non-uniform fabrics, #10 DecolineLining and #71 RoughRed, were chosen to demonstrate the effect of fabric non-uniformity. Fabrics #10 and #71 have been measured 50 times and 35 times, respectively. In addition, #22 SheerWhite01 and #26 BlusSoft01 have been measured 10 times each, also at various locations. For these four fabrics, all tests were performed for the visible spectral range 400 – 700 nm and results are presented in Figure 2.9.

Figure 2.9 shows four groups of spectral transmittance lines. As shown in the figure, a highly non-uniform fabric (e.g., #10 or #71) has a wide span in measurements whereas spectral transmittance lines of a uniform fabric (e.g., #22 or #26) fall within a narrow range. Distributions of measured τ_{bt} for the four fabrics are shown in Figure 2.10. The four graphs in Figure 2.10 have the same scale range (i.e., 0.125 or 12.5%). As expected, #10 and #71 span almost the whole range of 0.125 while #22 and #26 remain within 0.020.

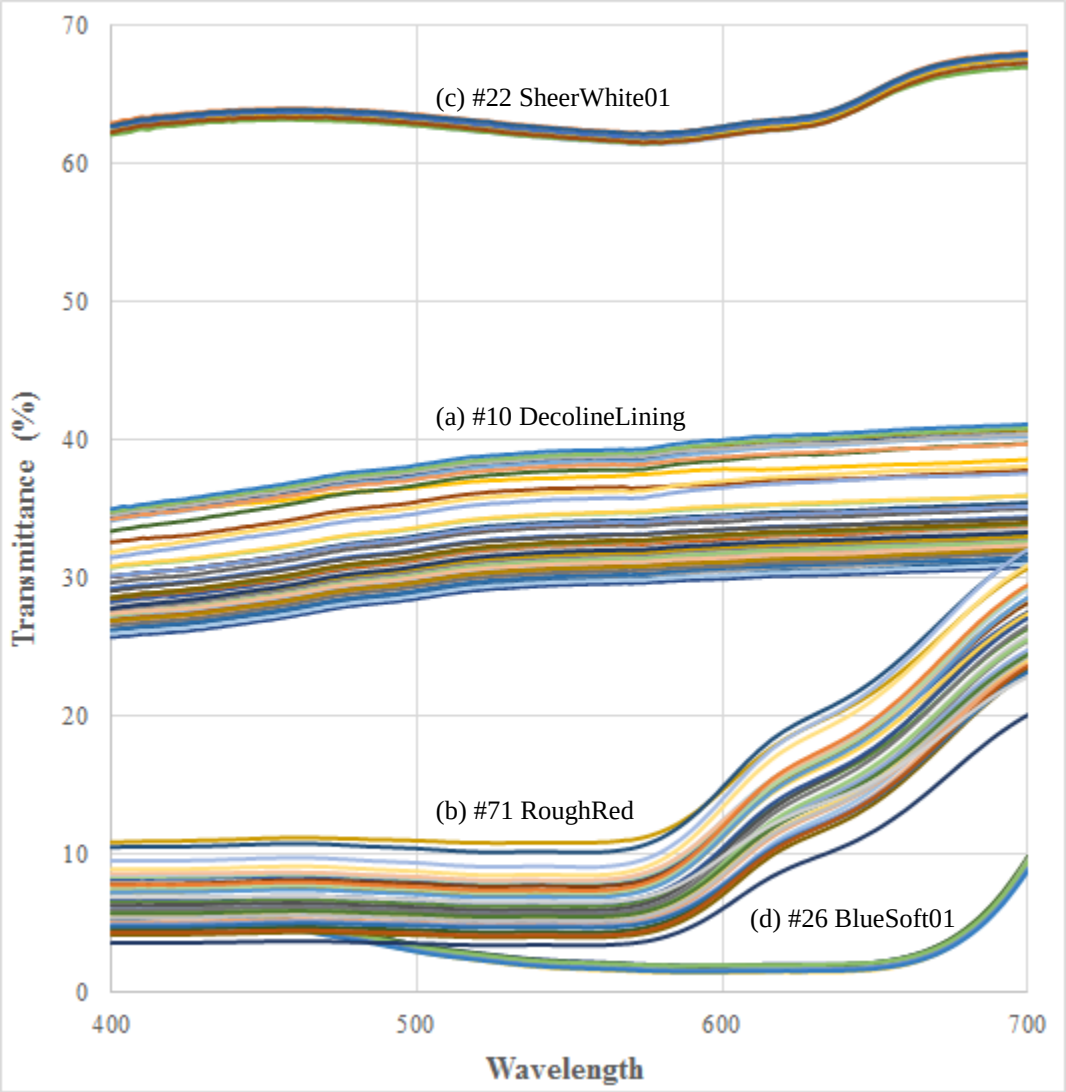

Figure 2.9: Spectral transmittance of Fabrics #10, #22, #26, and #71 for the wavelength range 400 – 700 nm

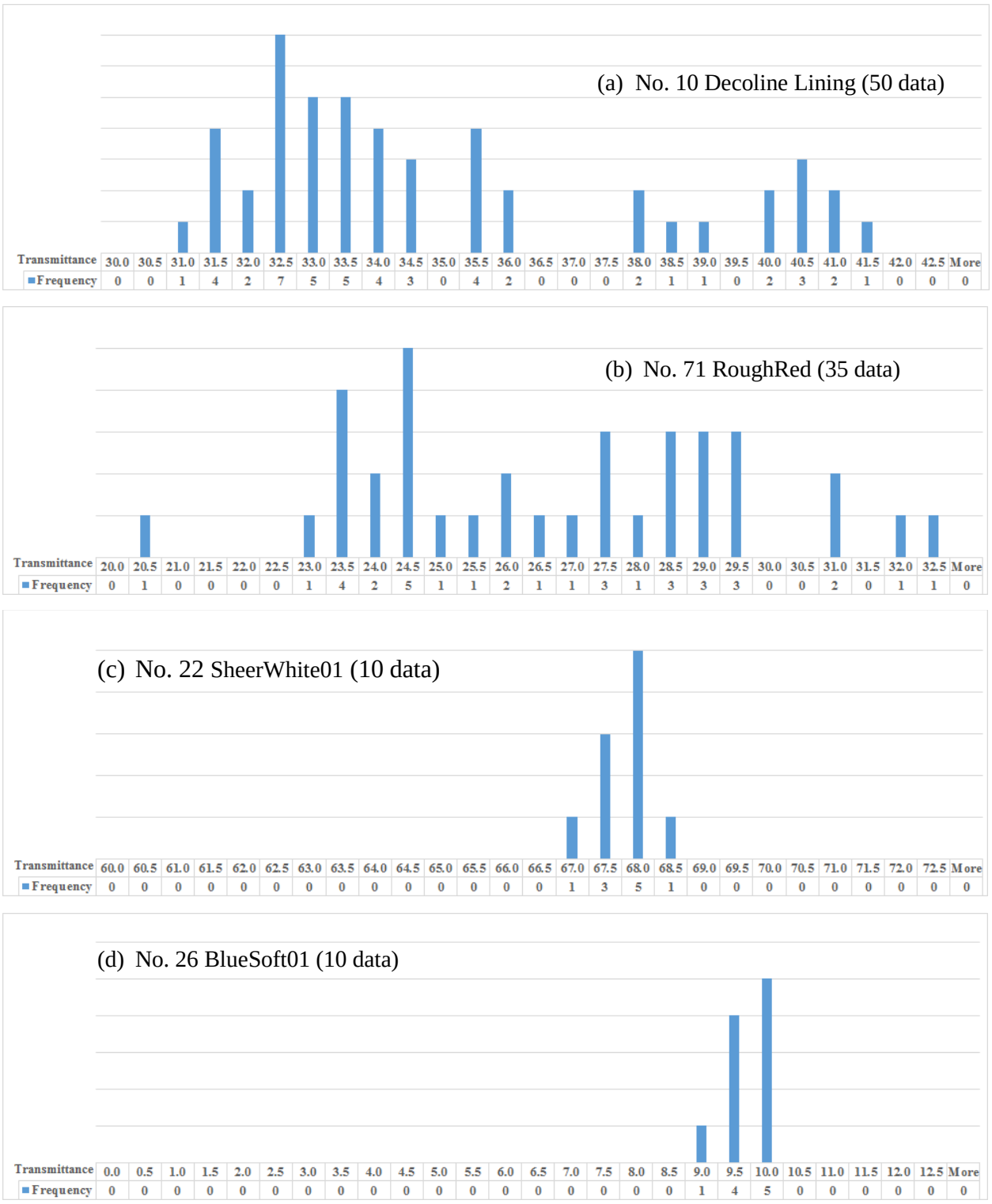

Note: Frequency is the number of measurements that fall within a specific range of transmittance. All four graphs have the same scale of 0.125 (to show the relative non-uniformity) at various spectral ranges: (a) 0.300 – 0.425, (b) 0.200 – 0.325, (c) 0.600 – 0.725, and (d) 0.000 – 0.125

Figure 2.10: Distribution of measured τ_{bt}

2.3.3.1 Non-Uniformity Correction Factors

Due to non-uniformity in a fabric, measured spectral τ_{bt} differs at various locations. However, as shown in Figure 2.9, the difference between any two measurements stays the same spectrally (i.e., the lines are almost parallel to each other). It has been confirmed that this "consistent" spectral difference is true across the entire spectral range of interest (i.e., 250 – 2500 nm). Therefore, it is reasonable to assume that the difference between two measurements at a specific wavelength can be applied to the whole range of interest.

Recall that the solar optical properties have been measured and evaluated for the full wavelength range 250 – 2500 nm. To correct fabric non-uniformity, multiple (5 to 50) measurements are taken and averaged at 700 nm. Then the average is compared to the single full-range measurement at 700 nm. The difference between the average (of multiple measurements at 700 nm) and the single full-range measurement at 700 nm is the correction factor.

As an example, the weighted average τ_{bt} of full range measurement is corrected as:

$$\tau_{bt,Corrected} = \tau_{bt,full} - (\tau_{bt,full@700} - \tau_{bt,avg@700}) \quad \textbf{(2.4)}$$

where the term inside the bracket is the correction factor.

All solar optical properties can be corrected following the procedures as described above. Table 2.3 lists the correction factors for the 22 fabrics that were used to build pleated drape samples.

Table 2.3: Correction factors for flat fabric properties

Fabric #	Correction Factors for		
	τ_{bt}	τ_{bd}	ρ_{bt}
01	0.0118	0.0026	-0.0057
08	0.0005	0.0001	-0.0043
10	0.0995	0.1056	-0.0410
13	0.0666	0.0100	-0.0038
20	0.0715	0.0170	-0.0037
22	0.0724	0.0575	0.0013
24	0.0117	0.0176	0.0025
26	0.0001	-0.0005	-0.0049
27	0.0190	0.0075	-0.0068
64	0.0141	0.0077	0.0004
66	0.0147	0.0112	0.0103
68	0.0000	0.0125	-0.0011
70	0.0298	0.0046	-0.0194
71	-0.0006	-0.0035	0.0291
72	0.0612	-0.0713	-0.0306
73	0.0066	-0.0044	-0.0013
75	0.0317	0.0121	-0.0064
77	0.0074	0.0137	0.0117
92	-0.0013	-0.0022	-0.0070
93	0.0085	0.0116	-0.0106
94	0.0538	0.0099	-0.0100
95	0.0171	0.0122	-0.0015

2.3.4 Section Summary

A total of 117 fabrics have been measured for their solar optical properties. Although patterned fabrics (visible non-uniformity) have been avoided, there is still invisible non-uniformity in the fabrics that can be significant. Fortunately, this uncertainty can be greatly reduced by applying a correction factor determined using the method described above. Keep in mind that the correction factors have been determined only for 22 fabrics that are used in the pleated drape layer measurements. This is largely because most fabric samples were small.

2.4 Development of an Improved KUC - The "b&C" Model

2.4.1 A Closer Look at the Constant A_o Lines and the Solar Optical Properties

Recall that Figure 1.3 shows the solar optical properties of a fabric layer. The beam-total property consists of a beam-beam component and a beam-diffuse component. In essence, a constant A_o line on the KUC predicts the split between the τ_{bb} and τ_{bd} that make up the total transmittance. So τ_{bb} is equivalent to the openness represented by the constant A_o line (Equation (1.4)), and τ_{bd} is the difference between τ_{bt} and A_o (Equation (1.3)), which is determined by the upward curvature of the A_o = constant line(s) on the KUC.

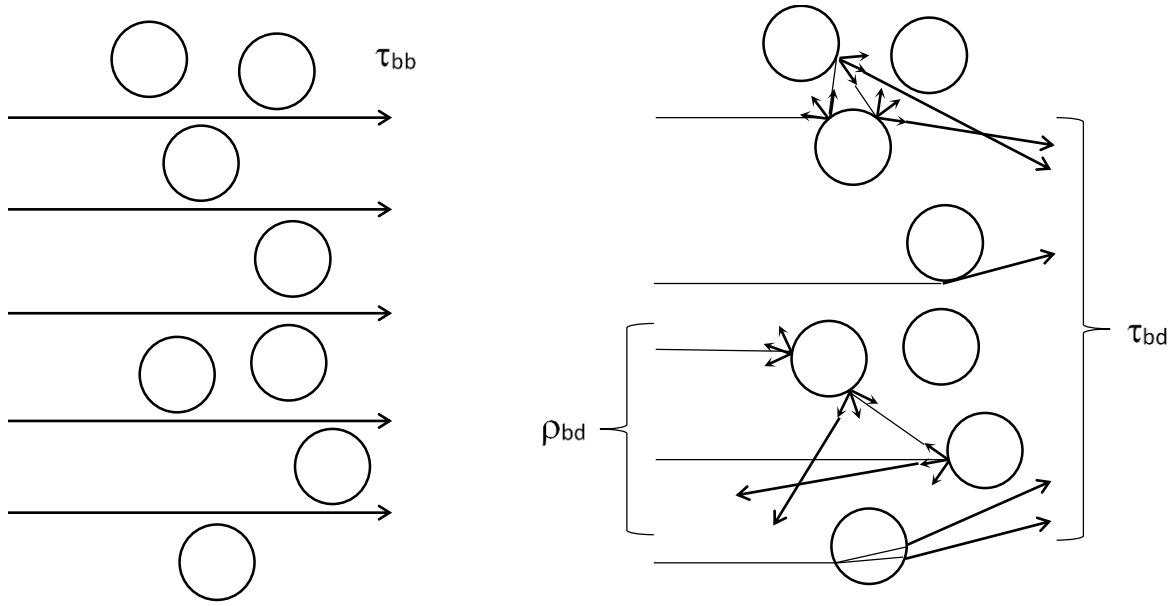

Figure 2.11: Illustration of (a) uninterrupted transmission through a fabric layer and (b) scattered components of reflectance and transmittance

Figure 2.11 demonstrates the possible radiation paths when radiation is incident on the fabric layer. Figure 2.11 (a) shows the uninterrupted transmission through interstices that makes up the τ_{bb} component. Figure 2.11 (b) shows various paths of radiation, which, when impinging on the yarn,

can be transmitted through fibers or reflected from fiber to fiber. As discussed earlier, fabrics, because of their irregular geometry, do not reflect specularly so ρ_{bt} consists of only scattered reflection as ρ_{bd} (Equation (1.5)). For the τ_{bd} component, Figure 2.11 (b) depicts how the beam passes through the fabric, scattered by the interactions of radiation and the fibers in a woven fabric. These interactions include optical phenomena such as diffraction, refraction, and multiple reflections as shown in the figure.

2.4.2 The "b&C" Model

A new model has been developed and proposed as an improved KUC using the measurement results presented in Section 2.3. This model is named the "b&C" approach. Equation (2.5) shows the proposed "b&C" model.

$$\tau_{bt} = (A_o + C\rho)(1+\rho)^{-1/b} \quad \textbf{(2.5)}$$

Coefficients "b" and "C" are two governing parameters that can be adjusted to alter the curvature of the constant A_o lines on the KUC, therefore predicting the split between the τ_{bb} and τ_{bd}.

There are three main characteristics of the constant A_o lines governed by Equation (2.5): the y-intercept (YI), initial slope (S), and rate of change in slope (ROC_S). These characteristics can be examined mathematically. Based on Equation (2.5), YI is equivalent to τ_{bt} at $\rho = 0$. Therefore, YI = A_o of a particular constant A_o line. S can be obtained by taking the derivative of τ_{bt} with respect to ρ (Equation (2.6)), and the curvature effect or ROC_S is the second derivative (Equation (2.7)).

$$S = \frac{\partial \tau_{bt}}{\partial \rho} = C(1+\rho)^{-1/b} + (-\frac{A_o}{b} - \frac{C}{b}\rho)(1+\rho)^{-1/b-1} \quad \textbf{(2.6)}$$

$$ROC_S = \frac{\partial S}{\partial \rho} = -\frac{2C}{b}(1+\rho)^{-1/b-1} + (\frac{A_o}{b^2} + \frac{A_o}{b} + \frac{C}{b^2} + \frac{C}{b})(1+\rho)^{-1/b-2} \quad \textbf{(2.7)}$$

As illustrated by Equations (2.6) and (2.7), the S and ROC_S of a constant A_o line depend on the two model parameters, b and C, as well as A_o and ρ. In other words, the influence of b and C differ through various ranges of A_o and ρ. This will be examined in detail in the following sections.

2.4.3 Model Requirements

The b&C model (Equation (2.5)) has been proposed because its form satisfies several known limits/conditions on the KUC. For instance, Equation (2.5) correlates the three solar optical properties of fabrics and provides constant A_o lines. Also, it satisfies the condition at the left edge of KUC where $\rho_{bt} = 0$ and $\tau_{bt} = A_o$. In addition, it provides the zero openness line that must begin at the bottom-left corner (where all three solar optical properties are zero) and curve upward as ρ_{bt} increases. These model requirements are discussed in detail as follows.

i. Relationship of the Solar Optical Properties

The main purpose of the KUC is to correlate the three solar optical properties: τ_{bt}, ρ_{bt}, and A_o. Equation (2.5) provides the required correlation since τ_{bt} is expressed as a function of ρ_{bt}, and A_o. Given coefficients b and C and with A_o held constant, Equation (2.5) results in a constant A_o line (i.e., in the form of τ_{bt} as a function of ρ_{bt}).

ii. Left Edge of the KUC ($\rho_{bt} = 0$)

At the left edge of the KUC (i.e., $\rho_{bt} = 0$), the model must satisfy the condition of $\tau_{bt} = A_o$, therefore, predicting the uninterrupted transmission component shown in Figure 2.11 (a). Equation (2.5) satisfies this requirement. As a special case, all three solar optical properties are equal to zero at the bottom left corner of the KUC. So, at $A_o = 0$ and $\rho_{bt} = 0$, $\tau_{bt} = A_o = 0$. (2.5 also satisfies this special case.

iii. The Zero Openness Line

When $A_o = 0$, the model must predict the scattered components of transmittance (τ_{bd}) as shown in Figure 2.11 (b). The zero openness line must start from the bottom left corner and then move upward as ρ_{bt} increases. This condition is met through the C coefficient in the model where C must be a positive number.

2.4.4 Effects of the b and C Coefficients on the Constant A_o Lines

The b&C approach starts from the fact that the purpose of KUC is to correlate the three fabric properties: ρ, τ_{bt}, and A_o. The simplest form of an equation for a constant A_o line that involves all three solar optical properties is:

$$\tau_{bt} = A_o(1 + \rho) \qquad \textbf{(2.8)}$$

Equation (2.8) is one particular form of the b&C model (i.e., C = 0 and b = -1). This equation produces straight constant A_o lines where A_o is the y-intercept (YI) as well as the slope (S) of its own line. Equation (2.8) satisfies model requirements (i) and (ii), but not (iii). To meet model requirement (iii) without affecting requirements (i) and (ii), the C coefficient is needed.

Introduction of the b coefficient does not invalidate any of the model requirements either. Instead the b coefficient comes with two effects for manipulating the constant A_o lines: 1) change in initial S and 2) the curvature effect (or change in ROC_S). In other words, varying the b coefficient will rotate all lines upward or downward around their YI (first effect) and force the line to curve upward or downward (second effect). Based on the value of b, intensities of these two effects vary.

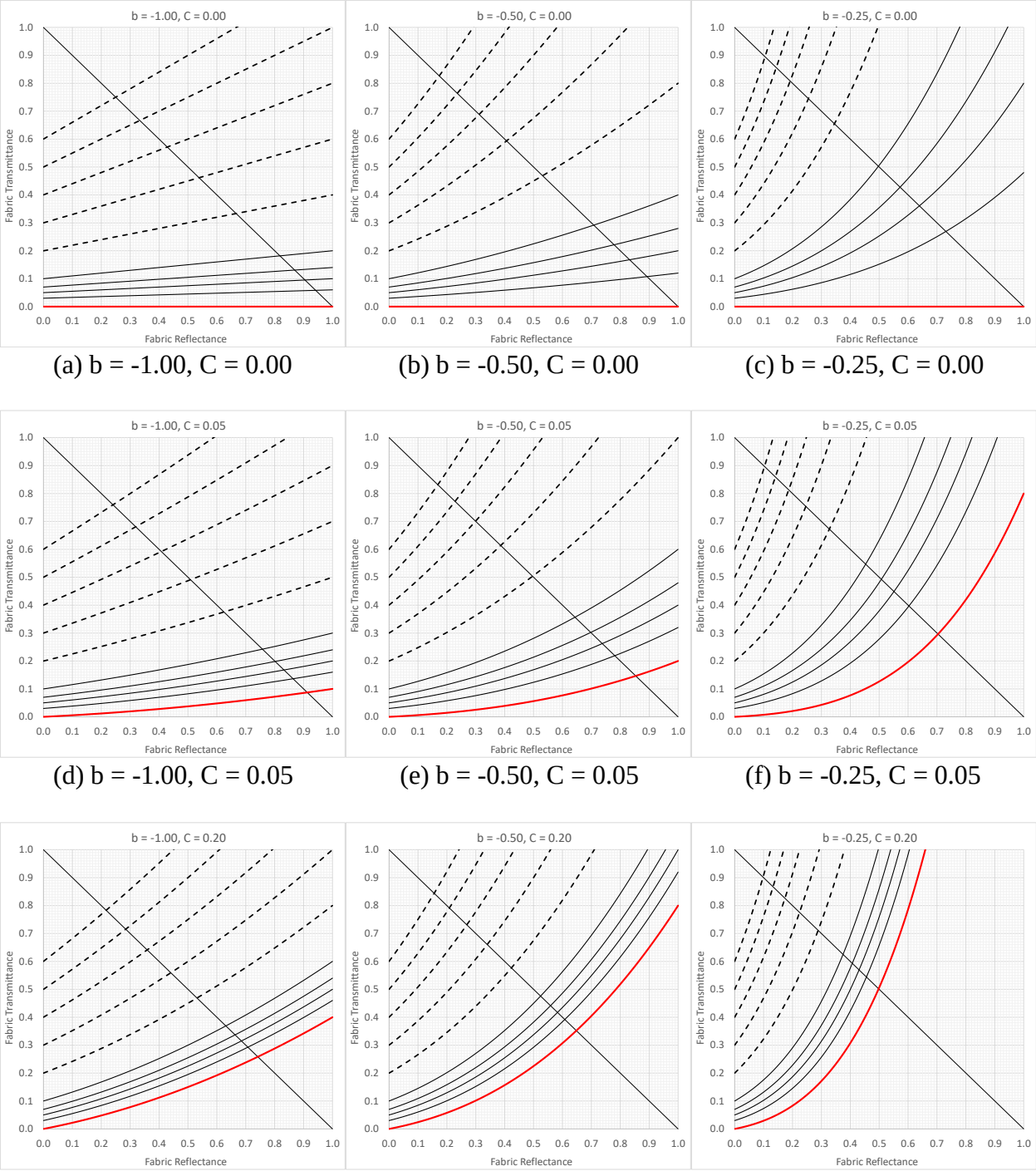

(a) b = -1.00, C = 0.00 (b) b = -0.50, C = 0.00 (c) b = -0.25, C = 0.00

(d) b = -1.00, C = 0.05 (e) b = -0.50, C = 0.05 (f) b = -0.25, C = 0.05

(g) b = -1.00, C = 0.20 (h) b = -0.50, C = 0.20 (i) b = -0.25, C = 0.20

Note: Red Line – Ao = 0. Solid Lines – Ao <= 0.10. Dashed Lines – Ao >= 0.20

Figure 2.12: Effect of b and C coefficients on openness lines

To put the effects of b and C into perspective, b is set to -1.00, -0.50, and -0.25 so that Equation (2.5) can be easily expanded and compared as shown in Table 2.4. Then set C = 0.00, 0.05, and 0.20. So there are in total 9 sets of b and C values. For each combination, the resulting constant A_o lines have been shown in Figure 2.12, which will be used to aid the following discussions.

Table 2.4: Equation (2.5) expanded with (a) b = -1.00, (b) b = -0.50, and (c) b = -0.25

$\tau_{bt} = (A_o + C\rho)(1+\rho)^{-1/b}$ Equation (2.5) is included here for reference.

b =	$\tau_{bt} =$	Equation
-1.00	$(C)\,\rho^2 + (1A_o + C)\rho + A_o$	**(a)**
-0.50	$C\rho^3 + (1A_o + 2C)\,\rho^2 + (2A_o + C)\rho + A_o$	**(b)**
-0.25	$C\rho^5 + (A_o + 4C)\rho^4 + (4A_o + 6C)\rho^3 + (6A_o + 4C)\,\rho^2 + (4A_o + C)\rho + A_o$	**(c)**

Strength of b Coefficient with ρ

If b = -1 (or -1/b = 1) and C is a non-zero positive number, the highest exponent applied to ρ is 2 (see Equation (a) in Table 2.4). As b increases toward zero, the highest exponent applied to ρ also increases and will be greater than 2 (see Equations (b) and (c) in Table 2.4). Therefore, the upward curvature of τ_{bt} increases with ρ. Recall that low constant A_o lines cover a wider range of ρ. Therefore, considering the ρ terms, the strength of b on the upward curvature is relatively strong for low A_o lines, but only at higher values of ρ.

Strength of b Coefficient with A_o

In addition to higher exponential terms with ρ terms, Equations (a), (b) and (c) in Table 2.4 also show that the upward curvature depends strongly on A_o. So, considering the A_o terms, b has a much stronger effect for high A_o lines than for low A_o lines, regardless of ρ.

Therefore, the b coefficient has a strong effect both at high A_o areas due to high initial S and at high ρ areas of the low A_o lines due to higher ROC_S. See a set of constant C in Figure 2.12 (e.g., Figure 2.12 (a), (b), and (c)) for illustration of these effects.

Strength of C Coefficient with ρ

Looking at the terms in the equations above, C's effect on τ_{bt} and, therefore, on the constant A_o lines is strongly linked to ρ. At high A_o, the limiting ρ is low, and therefore, the effect of C is weak. At low A_o, the effect of C is also weak in the low ρ region, but strong in the high ρ area (i.e., near the bottom right corner of the KUC). So C has a more localized effect on the constant A_o lines than b does. See a set of constant b in Figure 2.12 (e.g., (c), (f), and (i)) for illustration of the effect.

In fact, the C coefficient has been introduced for the $A_o = 0$ line where C has the strongest influence. Without the Cρ term (i.e., C = 0), the model would still work except for the $A_o = 0$ cases. If C is set to zero, the zero openness line becomes a horizontal line overlapping the x-axis (see red lines in Figure 2.12 (a), (b), and (c)). In other words, a model with C = 0 predicts that $\tau_{bd} = 0$ (i.e., no scattered component) when $A_o = 0$. So C must be greater than zero.

In summary, the C coefficient has a strong localized effect in the high-ρ (low-A_o) region. The b coefficient has a strong effect in the high A_o (low-ρ) region and a moderate effect in the high-ρ (low-A_o) region.

2.4.5 Determining b and C

The simplest form of a constant A_o line is a straight line starting at a point (0, A_o) on the left edge of the KUC and passing through the fabric's data point (ρ, τ_{bt}). Slope, or S, of a straight constant A_o line is defined as

$$S = (\tau_{bt} - A_o)/\rho = \tau_{bd}/\rho \qquad \textbf{(2.9)}$$

Based on the straight line assumption and the measured data presented in Section 2.3, straight constant A_o lines have been shown in Figure 2.13. These lines suggest that, on average, S increases with A_o, especially for the high A_o fabrics. This trend is also depicted in Figure 2.14.

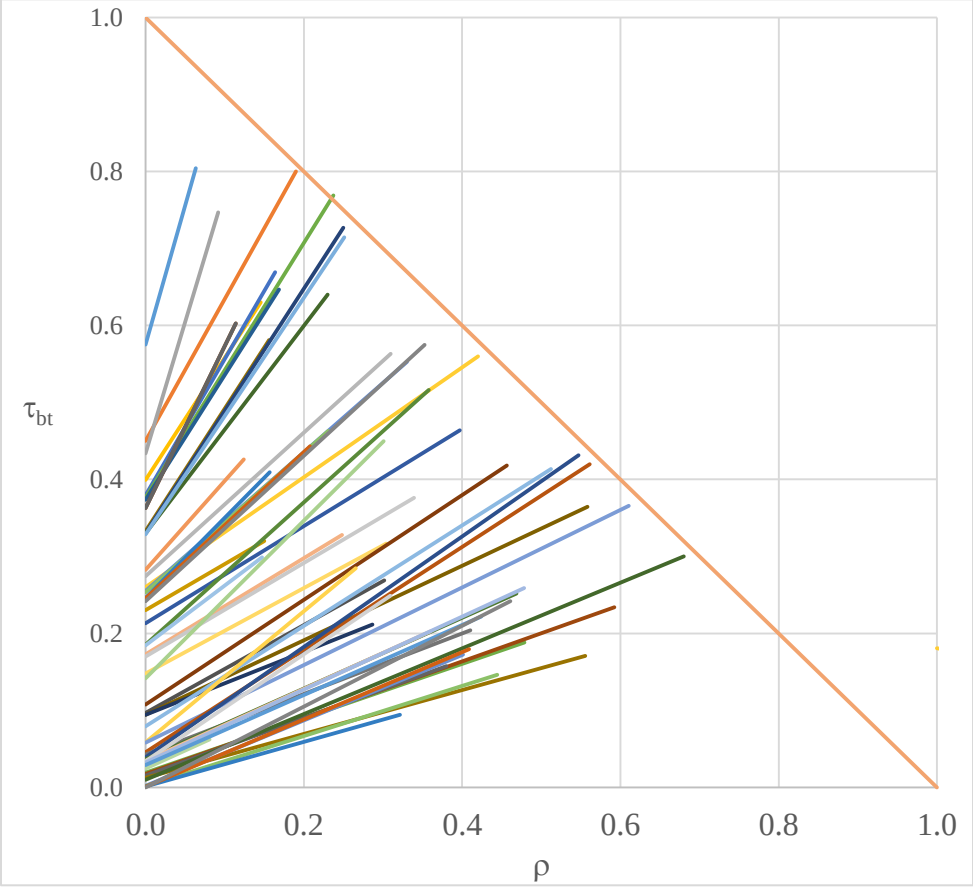

Figure 2.13: Straight constant Ao lines showing low slopes for low A_o fabrics and high slopes for high A_o fabrics

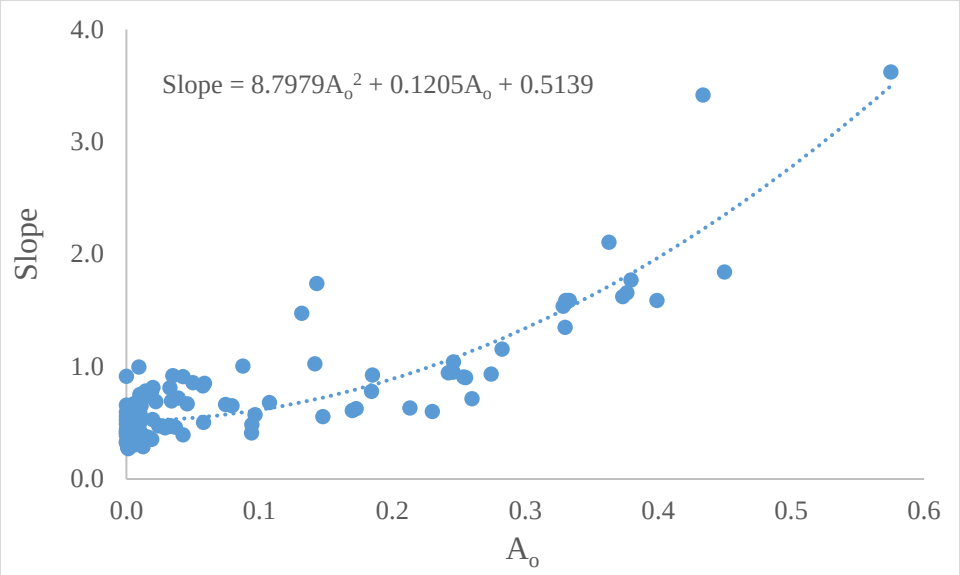

Figure 2.14: Slope based on (2.9 and measured fabric properties

The average S increases with A_o is an important trend as it suggests that the constant A_o lines should fan out (similar to as shown in Figure 2.13). Comparing Figure 2.13 to Figure 2.12 (a), it can be observed that Equation (2.8) (the most basic form of b&C model with b = -1 and C = 0) clearly under-predicts S (or over-predicts A_o).

Using the b&C model and measured fabric data, b can be calculated based on a given C. Figure 2.15 shows the calculated b versus A_o for all fabrics based on C = 0.0, C = 0.1 and C = 0.2. Recall that, although both b and C can influence the constant A_o lines, C's effect is local to the low-A_o and high-ρ area. This localized effect can be observed by monitoring the shift of the calculated b in Figure 2.15. As C increases, the calculated b decreases (i.e., downward shift) to various extents. For high A_o fabrics, the shift in b is insignificant (i.e., black o for C = 0.0, red Δ for C = 0.1, and blue □ for C = 0.2 shown in Figure 2.15 stay very closely together). Then, the shift in b increases as A_o decreases and as ρ increases.

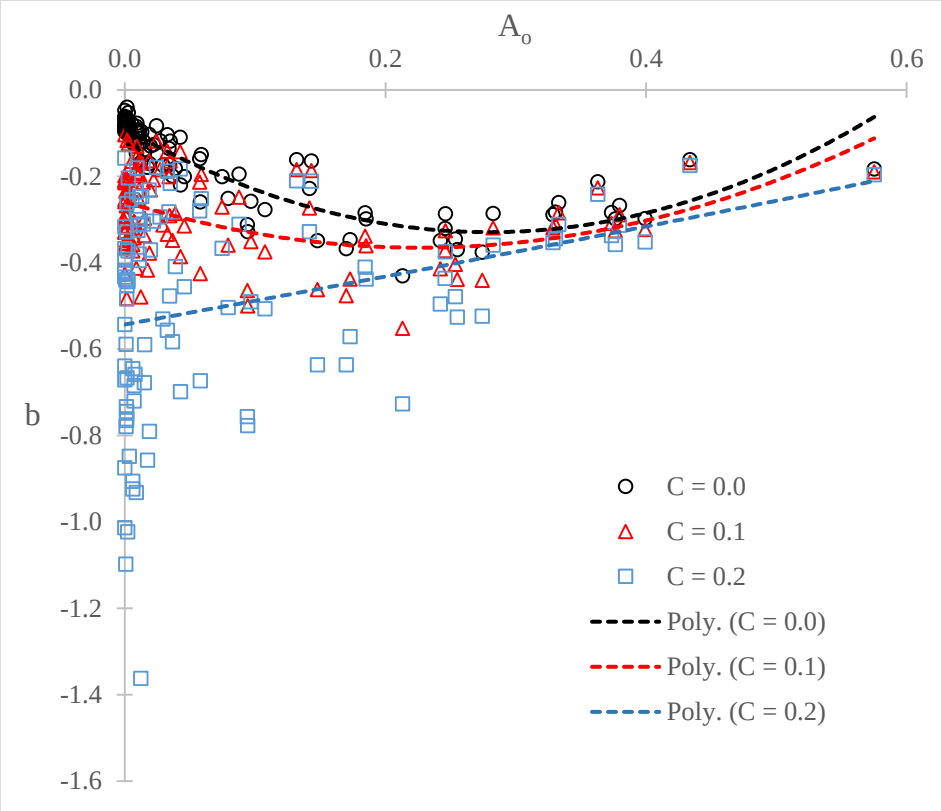

Figure 2.15: Calculated b based on C = 0.0, 0.1, and 0.2 versus A_o

Figure 2.14 shows that S should increase with A_o. Similarly, in order to have fan-out constant A_o lines, b also must increase (or at least stay constant) with A_o. As shown in Figure 2.15, b calculated with C = 0.0 and C = 0.1 show b decreasing for $A_o < 0.2$. Note that, when C is equal to 0.2, S in Figure 2.14 and b in Figure 2.15 both have a similar correlation with A_o. Both (averaged) S and b increase with A_o.

In fact, using the polynomial curve fitting for the calculated b, C must be > 0.18 (based on the current set of fabrics) so that calculated b would increase with A_o. On the other hand, C should be < 0.25 to maintain a reasonable downward shift in calculated b. For $0.18 < C < 0.25$, b can be assumed, and is proposed, to be a linear function of A_o (i.e., the curve fitting based on C = 0.2 shown in Figure 2.15 is virtually linear). Then, varying C (between 0.18 and 0.25) results in various

downward shift of b, and therefore, modifies the proposed linear function. The adjustment in the linear function does not significantly affect the overall result as it could be an improvement for a particular group of fabrics (e.g., high or low A_o) but a setback for another. So C should be chosen not only to optimize the overall result but also to retain the balance among all fabrics.

Based on the current set of fabric data and on the above discussion, C is proposed to be 0.22, and the resulting linear function is

$$b = 0.7951 \times A_o - 0.6421 \quad \textbf{(2.10)}$$

Based on the proposed b and C, the zero openness line is plotted and compared with fabrics with zero openness (Figure 2.16). By visual inspection, the $A_o = 0$ line passes through and follows the trend of $A_o = 0$ fabric data. Therefore, the proposed b&C model produces an excellent $A_o = 0$ line as well. Figure 2.17 displays the constant A_o lines (up to $A_o = 0.6$) based on the proposed values of b and C.

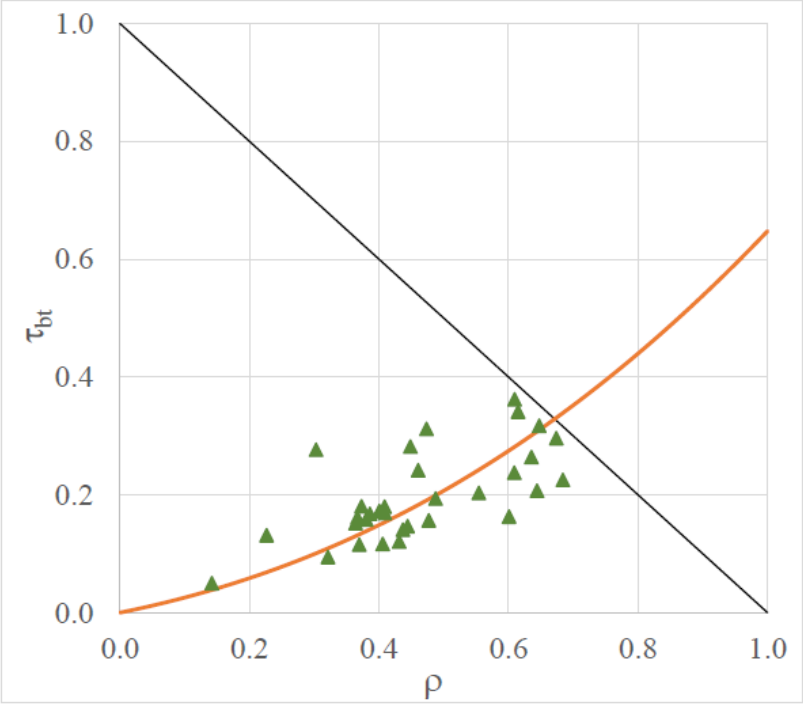

Figure 2.16: Fabrics with $A_o = 0$ and the $A_o = 0$ line.

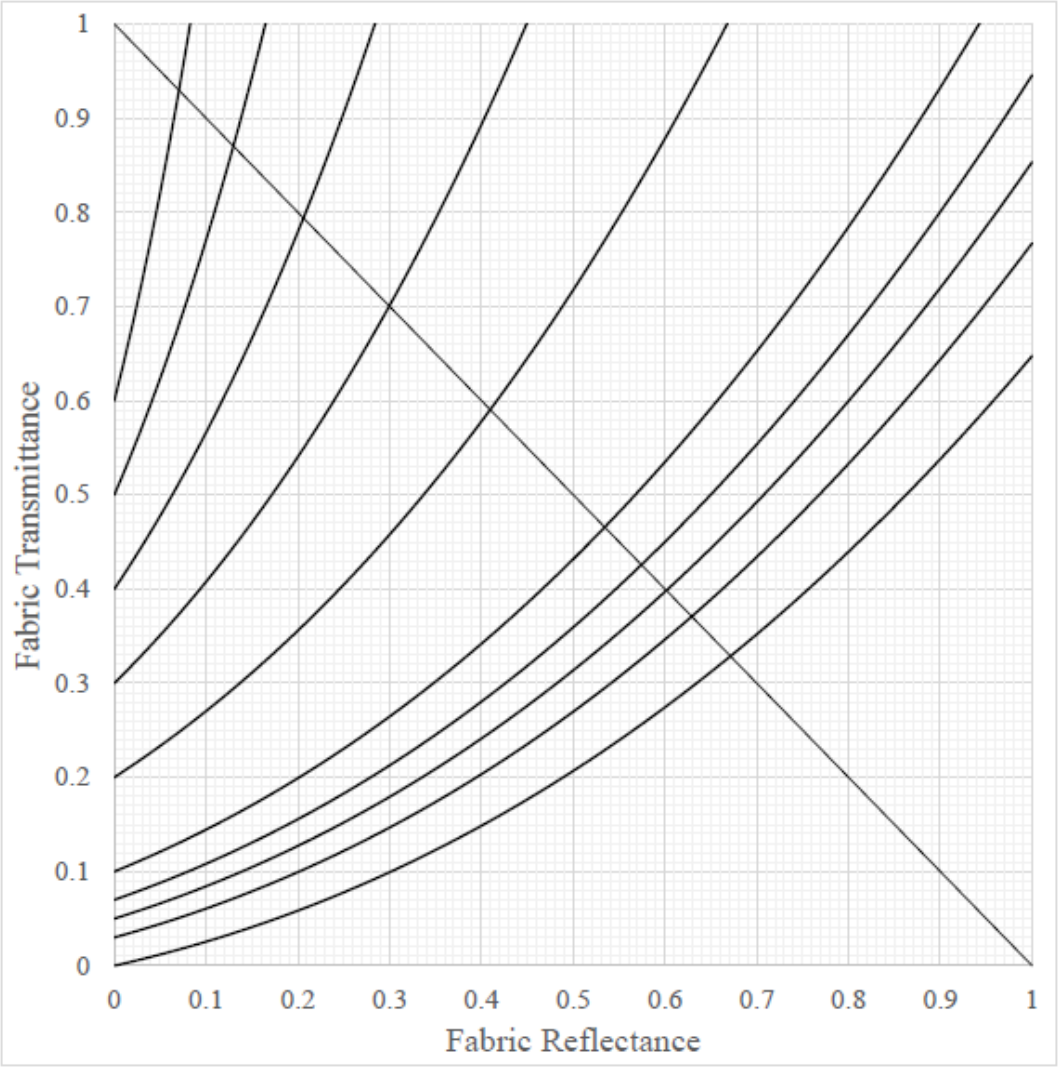

Figure 2.17: KUC based on the proposed b&C model

2.4.6 A Simplified KUC – The Slope Approach

Recall that Equation (2.9) defines slope (S) of a data point and Figure 2.14 plots S versus A_o. Having S as a function of A_o only (i.e., the dashed line shown in Figure 2.14), Equation (2.9) becomes an equation that relates the three solar optical properties. As shown in Figure 2.14,

$$S = 8.7979 \times {A_o}^2 + 0.1205 \times A_o + 0.5139 \qquad \textbf{(2.11)}$$

Keeping A_o constant, Equation (2.9) produces straight constant A_o lines with the y-intercept (YI) being equal to A_o and the slope (S) being calculated as a function of A_o (i.e., Equation (2.11)). In other words, Equations (2.9) and (2.11) provide a simplified KUC with straight lines (shown as solid lines in Figure 2.18). Note that the slope approach meets all the model requirements discussed in Section 2.4.3. If necessary, the slope of $A_o = 0$ line can be adjusted to, for example, evenly divide the zero openness fabric data by forcing the intercept (slope) to the required value.

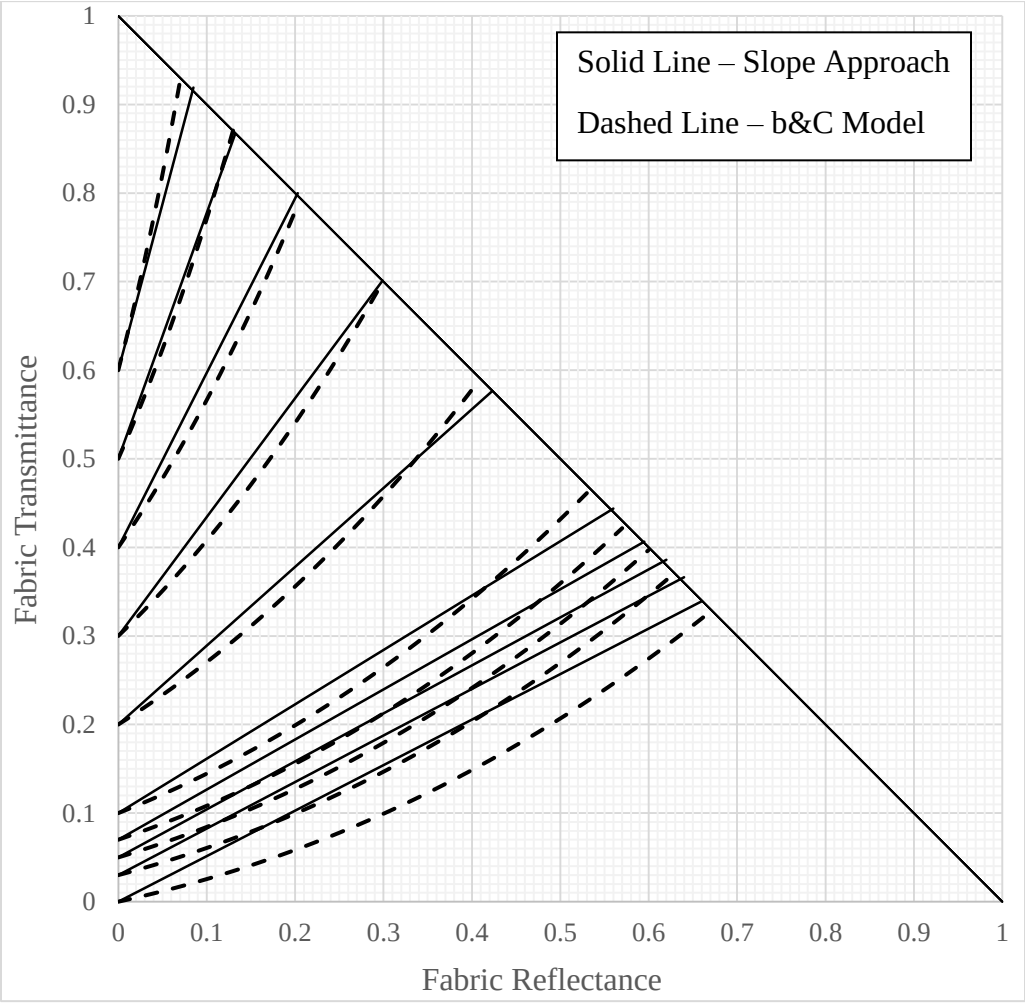

Figure 2.18: Comparison of KUC using the b&C model and simplified slope approach

2.4.7 Results

So far, plotting data points on the KUC has been done manually (e.g., Figure 2.3) and reading fabric properties from the KUC visually. In order to compare the b&C model to the original KUC, the original KUC has been reproduced in a methodical way so that plotting of data points can be automated. In other words, the original KUC has been reformulated mathematically. And given any two of the three solar optical properties (ρ_{bt}, τ_{bt}, and A_o), the third unknown property can be estimated with this new formulation. Appendix B: Mathematical Formulation of KUC layouts the procedures used to automate the plotting on the KUC. Results presented in this section were produced based on this formulation.

Figure 2.19 compares the results of the original KUC (shown on the left) to that of the refined KUC based on the b&C approach (right) for the open (top), semi-open (middle), and closed (bottom) fabrics. The original KUC, as discussed in Section 2.2.4, always over-predicts openness as each triangle hypotenuse faces the bottom-right. With the improved KUC, in general, the b&C model produces smaller triangles – some facing up and some facing down. The comparison shows that bias has been greatly reduced, and accuracy improved.

Table 2.5 shows the results of A_o predictions using the refined KUCs (slope approach and b&C model) and compares them to those predicted using the original KUC. The differences between measurements and predictions were averaged (AVG). Standard deviation (STD) was also presented to quantify the scattering of the data. Root-mean-square (RMS) is defined as $(AVG^2 + STD^2)^{0.5}$. Results are presented for all fabrics as a group as well as for various A_o ranges.

Overall, comparing the results of the original KUC to that of b&C model, the bias (AVG) has been greatly reduced from 0.082 to 0.014. STD has also been lowered from 0.061 to 0.041. Consequently, the improved KUC results in a much lower RMS (0.102 vs. 0.043).

To see how the improved KUC performs in various A_o ranges, the results are grouped by A_o into eight ranges of A_o as shown in Table 2.5. As expected, the original KUC over-predicts A_o in all ranges, and the over-prediction generally increases with A_o. For the b&C model, the AVGs are always within a few percent for all ranges (worst case for AVG is 0.034 for the $0.05 > A_o > 0.02$ group). Furthermore, there is a fairly consistent improvement in STD for all groups except for the $A_o > 0.4$ group. Note that, however, there are only three fabrics in the $A_o > 0.4$ group.

Comparison of the slope approach and the b&C model showed marginal difference. Considering the variety of fabrics, it is reasonable to conclude that these two methods perform equally well.

To summarize, the improved KUC largely eliminated the bias (AVG) of the original KUC as well as consistently gave lower uncertainty (STD). It would be very difficult, if not impossible, to eliminate this uncertainty due to the complexity and variety of fabrics. Therefore, the improvement in the overall results comes mainly from the reduction in bias (improved precision) and to a lesser extent from the improved STD (improved accuracy). The improvements are generally more significant at higher A_o ranges than at lower A_o ranges.

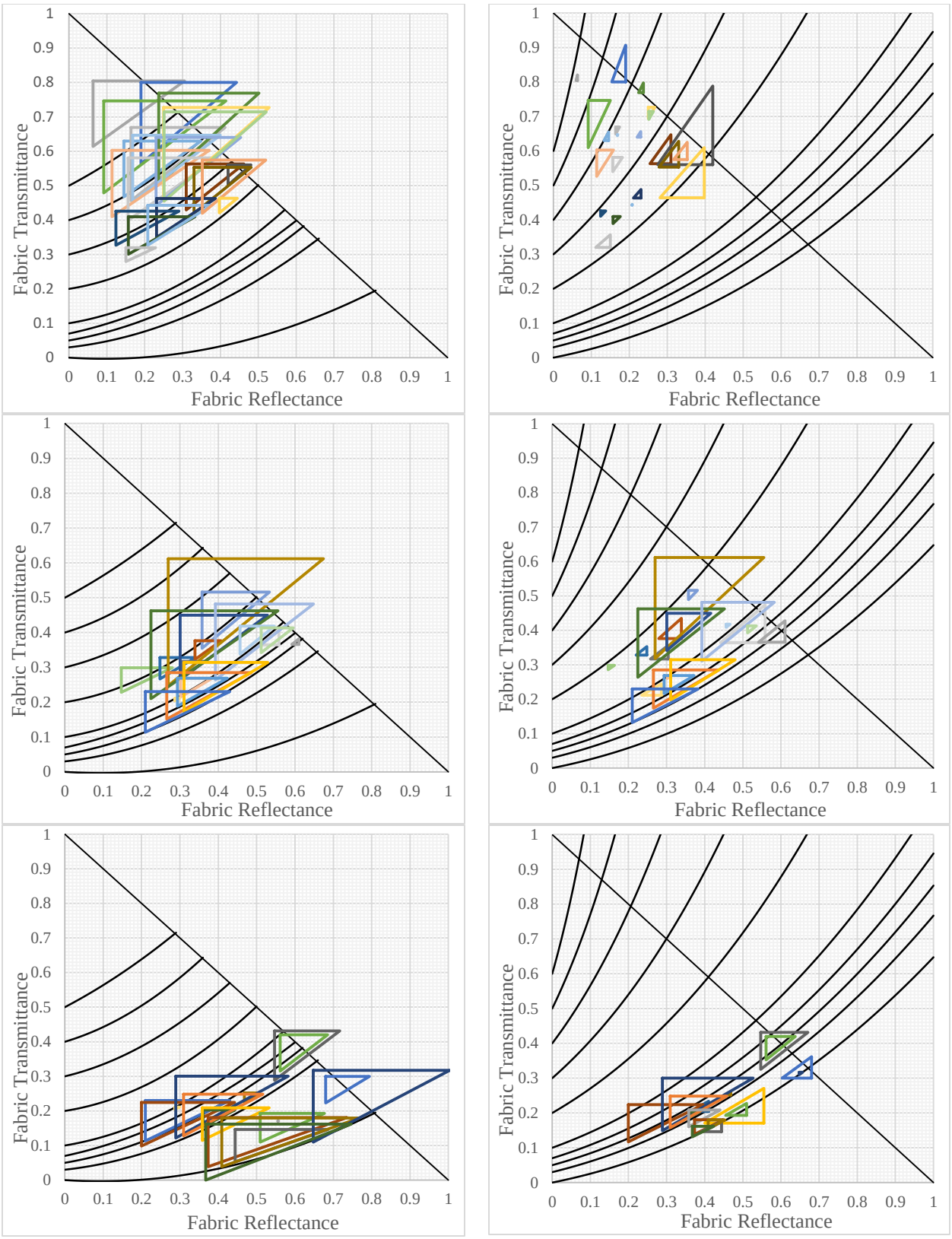

Figure 2.19: Comparison of KUC results – original (left) vs b&C model (right)

Table 2.5: Results of difference in A_o predictions using different methods

No. of Data	Ao Range		Slope	b&C	Keyes
		AVG	0.010	0.014	0.082
117 Fabrics	**All**	STD	0.036	0.041	0.061
		RMS	0.037	0.043	0.102
		AVG	0.009	0.009	0.222
3 Fabrics	**Ao > 0.4**	STD	0.051	0.052	0.033
		RMS	0.052	0.053	0.224
		AVG	-0.004	0.007	0.182
9 Fabrics	**0.4 > Ao > 0.3**	STD	0.016	0.017	0.029
		RMS	0.016	0.019	0.185
		AVG	-0.028	-0.023	0.093
10 Fabrics	**0.3 > Ao > 0.2**	STD	0.020	0.028	0.033
		RMS	0.035	0.036	0.099
		AVG	0.025	0.030	0.127
9 Fabrics	**0.2 > Ao > 0.1**	STD	0.060	0.061	0.092
		RMS	0.065	0.068	0.157
		AVG	0.018	0.023	0.074
10 Fabrics	**0.1 > Ao > 0.05**	STD	0.043	0.044	0.066
		RMS	0.047	0.050	0.099
		AVG	0.019	0.034	0.065
16 Fabrics	**0.05 > Ao > 0.02**	STD	0.040	0.033	0.046
		RMS	0.044	0.047	0.080
		AVG	0.017	0.020	0.059
31 Fabrics	**0.02 > Ao > 0.003**	STD	0.035	0.042	0.040
		RMS	0.038	0.047	0.071
		AVG	0.008	0.003	0.054
29 Fabrics	**0.003 > Ao**	STD	0.022	0.033	0.027
		RMS	0.023	0.033	0.061

2.5 Classification of Drapery Fabrics

One major advantage of KUC is the convenience of using eye-observed values for approximation of measured values and shading effect. One could estimate the fabric classification by comparison to a representative sample, and then look up IAC values for fabrics of that same classification. This convenient feature can be maintained by keeping the nine-region classification of drapery fabrics (see Table 2.1 and Figure 2.2) and the IAC tables in the ASHRAE handbook.

Since the openness lines that defined the nine regions have moved, the nine regions need to be redefined as well. However, in order to take advantage of the existing IAC tables, the nine regions and their representative fabrics should be maintained as much as possible for redefined regions. This section discusses and offers a revised nine-region classification (Figure 2.20 and Figure 2.21).

Recall that Keyes (1967) reconciled the ρ_y–A_o system with the ρ_{bt}–τ_{bt} system. The nine-region classification was based on the ρ_y–A_o system (Equation (2.1) described by Keyes). The nine regions on the KUC were defined by $\rho_y = 0.25$ and 0.50 and by $A_o = 0.07$, 0.25, and 0.50 as shown in Figure 2.2. For the revised chart (Figure 2.20 and Figure 2.21), the regions are defined by the constant A_o lines of the b&C model and by the ρ_y–A_o system (Equation (2.1)). Therefore, based on Equation (2.1), the constant ρ_y lines move accordingly with the constant A_o lines. As shown in Figure 2.20 and Figure 2.21, the A_o boundaries are horizontal axis, $A_o = 0.07$, $A_o = 0.20$, and $A_o = 0.40$ based on the improved KUC. Similarly, $\rho_y = 0.20$ and $\rho_y = 0.40$ are the constant ρ_y boundaries for Dark/Medium and Medium/Light categories respectively. These boundaries have been chosen to retain as much as possible the original regions and to have their representative fabrics remained in the same classifications (i.e., classifications of representative fabrics are not affected by the boundary changes).

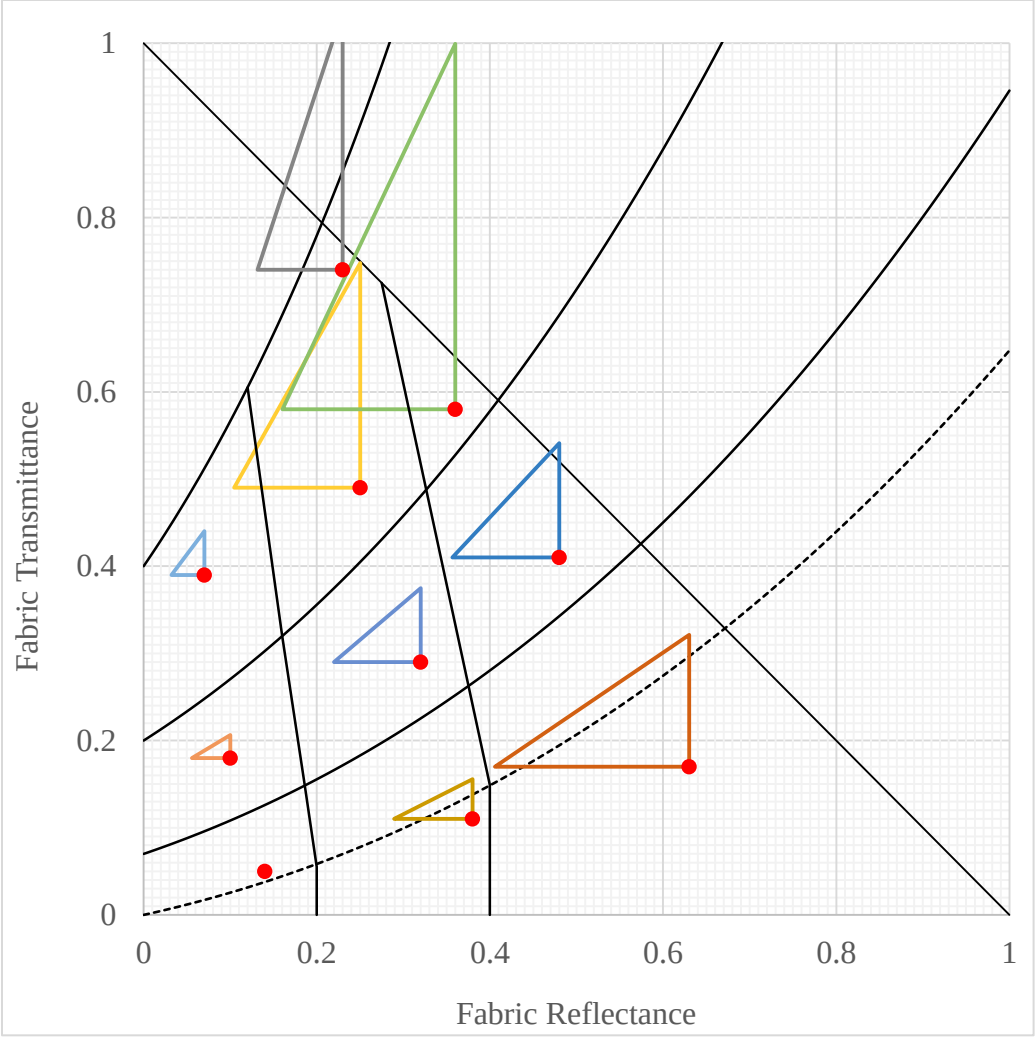

Figure 2.20: Representative fabrics of original KUC shown on the improved KUC

On the original KUC, a point near the center of each region is selected to represent typical (averaged) fabric properties. These representative points (where all three fabric properties meet) on the original KUC would disperse into three points each forming triangles on the improved KUC as shown in Figure 2.20. Notice that the triangles are now all facing the opposite direction. This is not an issue as any real fabric will be represented as a triangle on both the original and the improved KUC. Note that triangles are mostly contained in their classification region. Also, the point for the representative sheer fabric is now in the I_M (Open Fabric and Medium Color) category. This is

also not an issue because the reported IAC values in the ASHRAE handbook for the sheer and I_M categories are either the same or within 0.02 for all typical glazing and shade combinations. In fact, this observation reflects the increased accuracy that comes with the redefined regions.

By comparing the IAC values of the nine regions, one can also observe that IAC values are more sensitive to ρ_y than A_o. Again, the revised classification has been defined so that the existing IAC tables can still be used. It has been estimated that the IAC values will remain unchanged for the Dark (I_D, II_D, and III_D) categories and Closed-Weave (III_D, III_M, and III_L) categories and reduce slightly (less than 0.02) for the I_M, I_L, II_M, and II_L categories.

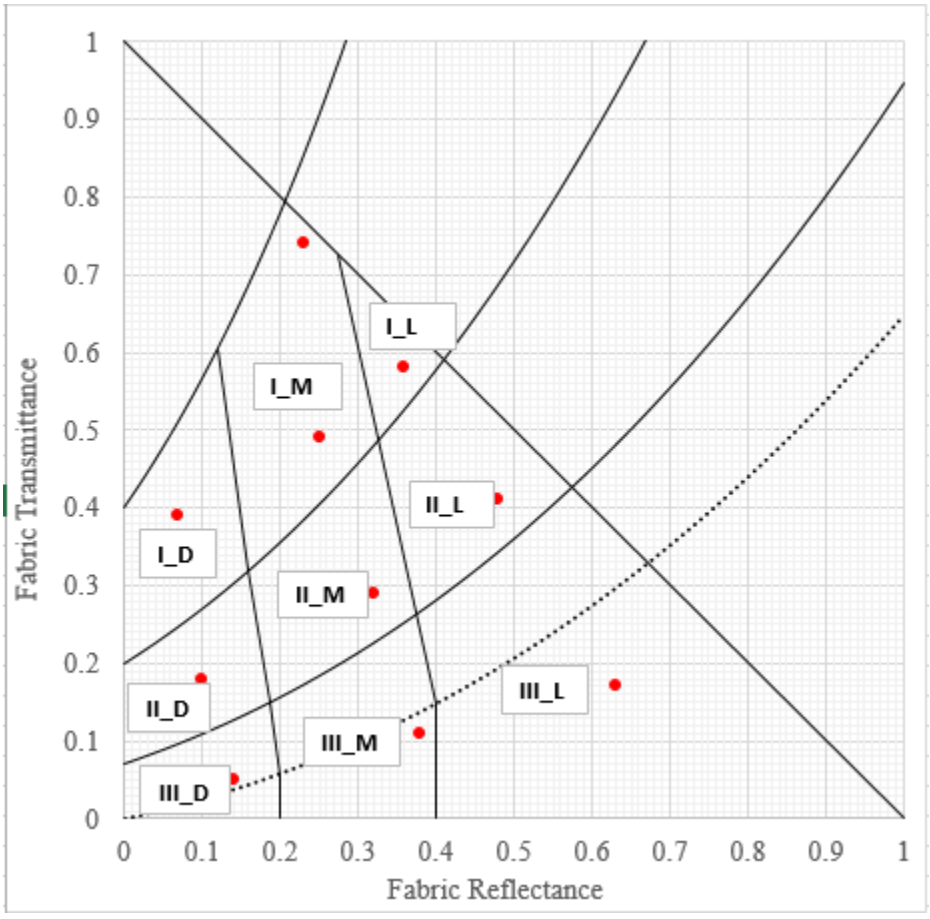

Figure 2.21: Proposed classification of drapery fabrics

2.6 Chapter Summary

This chapter provides two approaches to relate the three common fabric properties: ρ_{bt}, τ_{bt} and A_o. The slope approach is a quick and easy way to make a KUC when a database of fabric properties such as the one presented in Chapter 2.3 is available. Though more complicated than the slope approach, the b&C model is very versatile. The b and C coefficients allow users to adjust and design their own KUC for a specific set of fabrics. The slope approach gives straight openness lines while the b&C model results in curved openness lines. Regardless of the openness line profile, these two methods are comparable in relating the solar optical properties of flat fabrics based on the current set of fabric properties.

The improved KUC has largely eliminated the bias and reduced the uncertainty present in the original KUC. The improvement comes mainly from the high openness range with some improvement in the lower openness ranges.

Furthermore, the nine-region classification has been redefined based on the improved KUC. The boundaries of the nine regions are moved accordingly. However, these regions are redefined in a way that does not impact the use of the existing IAC tables.

CHAPTER 3
CUSTOMIZED KUC BASED ON FABRIC THICKNESS

It has been shown that the improved KUC (i.e., b&C model presented in CHAPTER 2) is a significant enhancement to the original KUC. Alongside the much improved predictions, as shown in Table 2.5, the b&C model provides a functional relationship between any two of the three conventional fabric solar-optical properties: τ_{bt}, ρ_{bt}, and A_o. Compared to reading a chart, this functional relationship offers efficient and consistent predictions, which make the following analysis and further development more feasible.

Recall that the b&C model gives constant A_o lines regulated by coefficients b and C. Also, recall that Figure 2.15 shows how the b coefficient varies with the C coefficient for all fabrics (Section 2.4.5). With the C coefficient fixed (e.g., C = 0.22), the b coefficient can be determined based on the best fit trend line (e.g., a linear function of A_o). While significant improvement has been achieved with this b&C model, further enhancement is possible by, for example, reducing the scatter of b along the best fit trend line.

This chapter presents an enhancement of the b&C model by exploring beyond the conventional three solar optical properties that are interrelated on the KUC. The investigation focuses on a physical property of fabrics, fabric thickness. The following sections discuss observations that lead to the introduction of fabric thickness as the fourth property. Analysis that demonstrate a few possible enhancements to the b&C model is offered as well.

3.1 An Observation – Results of the b&C Model for Fabric Subsets

Among the 117 selected fabrics, some of their names share the same label (e.g., Horizon, Open, ReflexGab, Singapore, 22111FV or etc.). Fabrics that share the same label are considered a subset and have the same physical properties. The only difference is in the color. Note that a subset of fabrics can be obtained from any retailer selling a type of fabric that is available in various colors. In total, there are twelve subsets among the selected fabrics. The properties were plotted on the improved KUC (i.e., the b&C model) to examine how the b&C model performs for each group. These plots are shown in part (a) of Figure 3.2 to Figure 3.13.

For two groups of fabrics, Sheer (Figure 3.4a) and ReflexGab (Figure 3.7a), the b&C model gives excellent results, very small triangles that do not face in one particular direction. Then, for each of the other groups, the b&C model results produce triangles all facing in the same direction. Therefore, observations made from Figure 3.2a to Figure 3.13a indicate that the b&C model may be tailored to a particular group of fabrics by shifting the constant A_o lines. When all triangles are facing downward, the constant A_o lines can be shifted upward. Similarly, when all triangles are facing upward, then downward shift of the constant A_o lines would reduce the bias. Therefore, further improvement is possible through customization of the model for fabrics of different color but made of the same material and weave. And the customized KUC would give results similar to those of Figure 3.4a and Figure 3.7a, smaller triangles, some facing upward and some facing downward.

3.2 Customized KUC using Direct Adjustment of b Coefficient

The key task in customizing a KUC for a fabric type is to determine the extent and direction of required shift for the constant A_o lines. Using the b&C model, the required shift for a fabric is equivalent to the difference between the calculated b coefficient (based on the measured solar-optical properties of the fabric) and the b coefficient determined using Equation (2.10). In other words, Equation (2.10) becomes

$$b_{avg} = 0.7951 \times A_o - 0.6421 + b_{diff,avg} \quad \textbf{(3.1)}$$

where $b_{diff,avg}$ is the required shift and the average vertical distance (for a subset) from the linear trend line (i.e., Equation (2.10)) shown in Figure 3.1. Applying this direct adjustment of the b coefficient the results are shown in Figure 3.2b to Figure 3.13b. Note how the constant A_o lines shift with the adjustment of b coefficient in each figure.

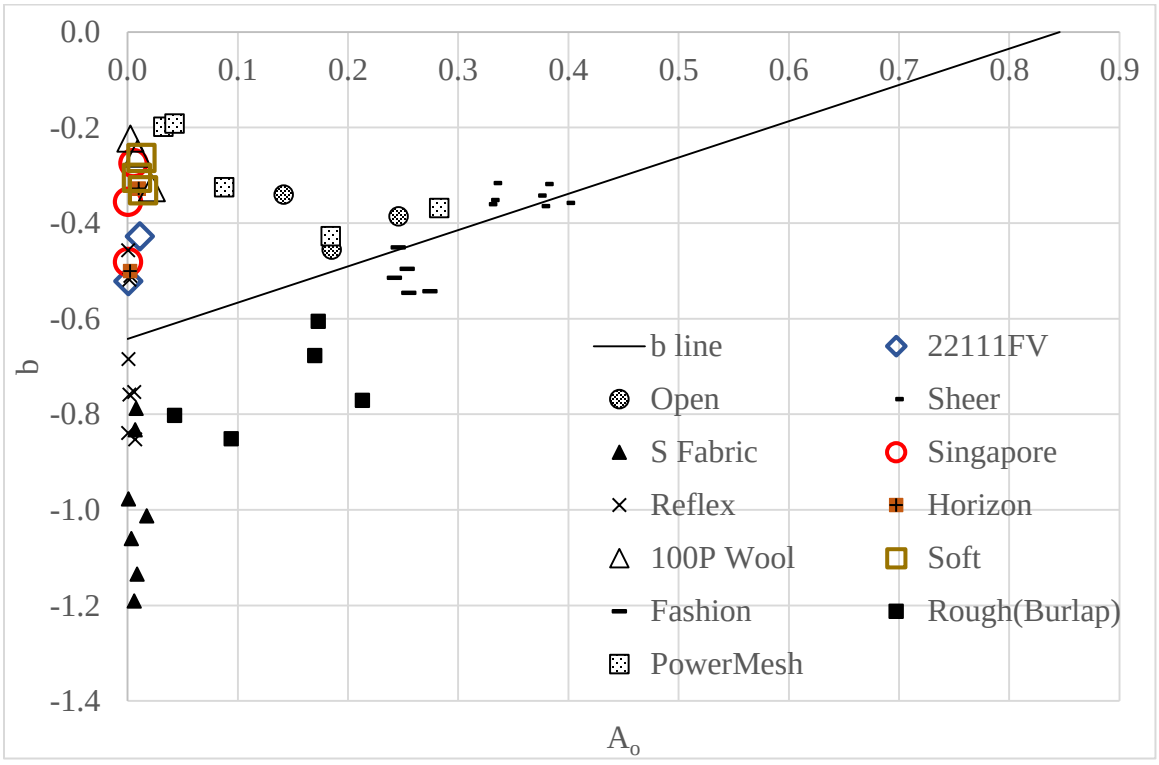

Figure 3.1: Location of calculated b coefficients for various fabric subsets

The direct adjustment method of customization is easy to do, but the adjustment is exclusive to fabrics used for determining the adjustment. Nonetheless, as shown in Figure 3.1, an adjustment (shift of constant A_o lines) in the right direction reduces the bias (for a particular subset) and is certainly better than no adjustment for most fabric groups. As shown in Figure 3.2b to Figure 3.13b, this method gives excellent results. Because of its simplicity and effectiveness, the direct adjustment is recommended for a group of fabrics that are made of the same material and weave.

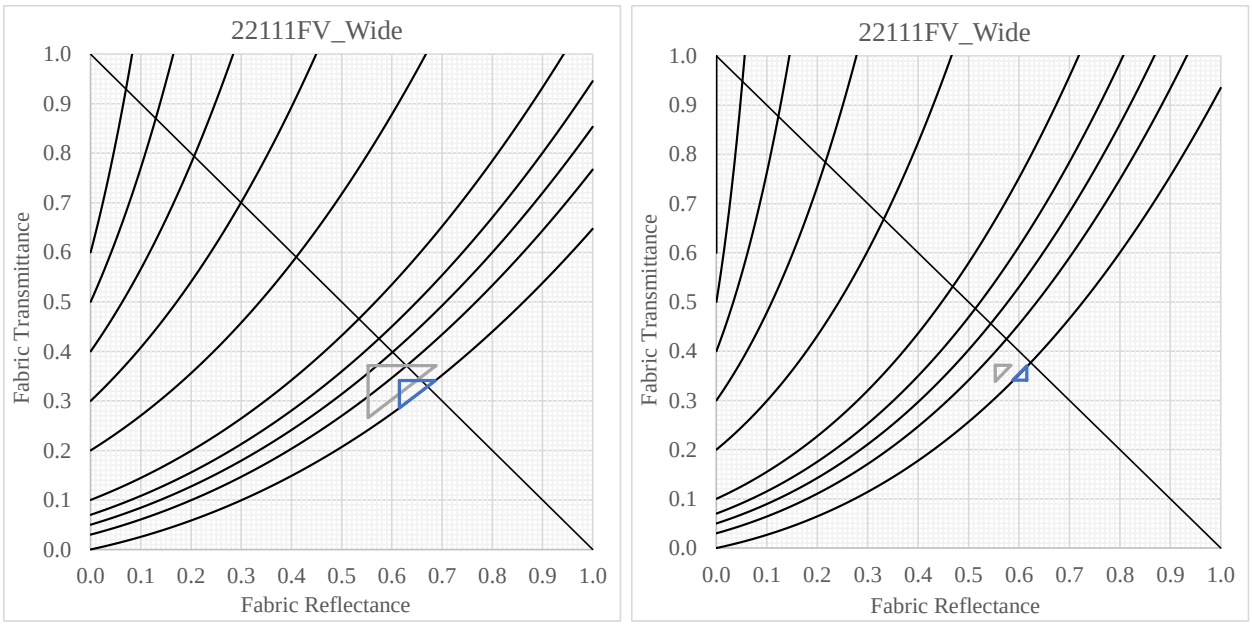

(a) b&C Model (b) w/ Direct Adjustment

Figure 3.2: Results for 22111FV_Wide fabrics (#2, 3) based on (a) the b&C model and (b) customized KUC by direct b coefficient adjustment

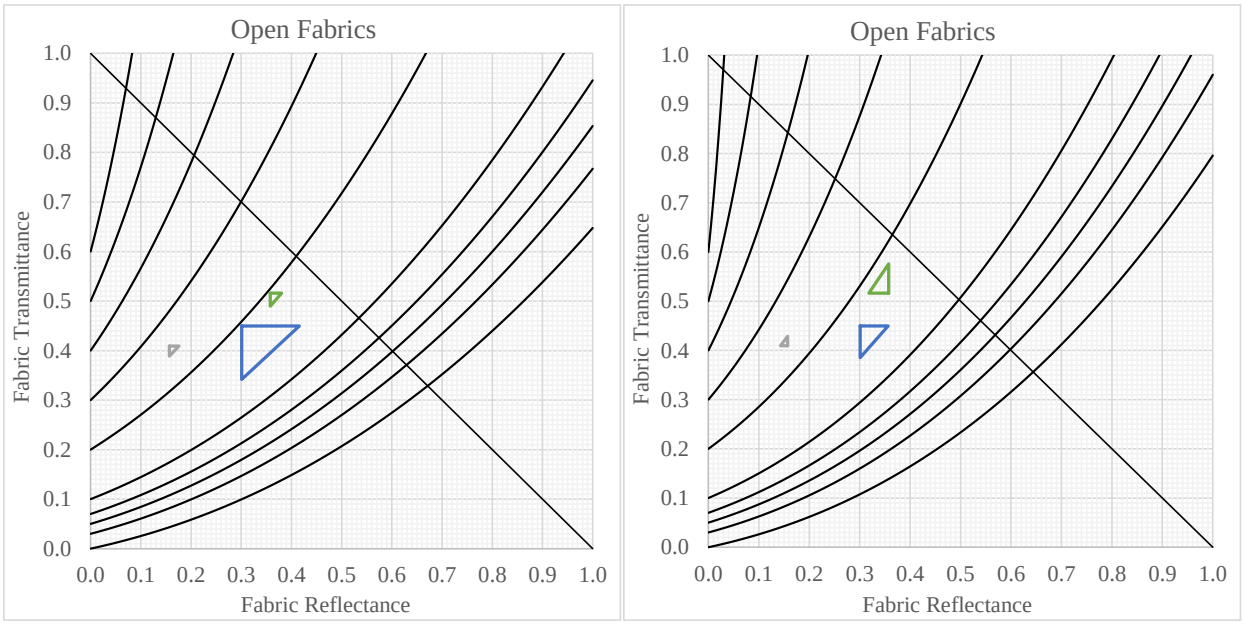

(a) (b)

Figure 3.3: Results for Open fabrics (#13, 68, 77) based on (a) the b&C model and (b) customized KUC by direct b coefficient adjustment

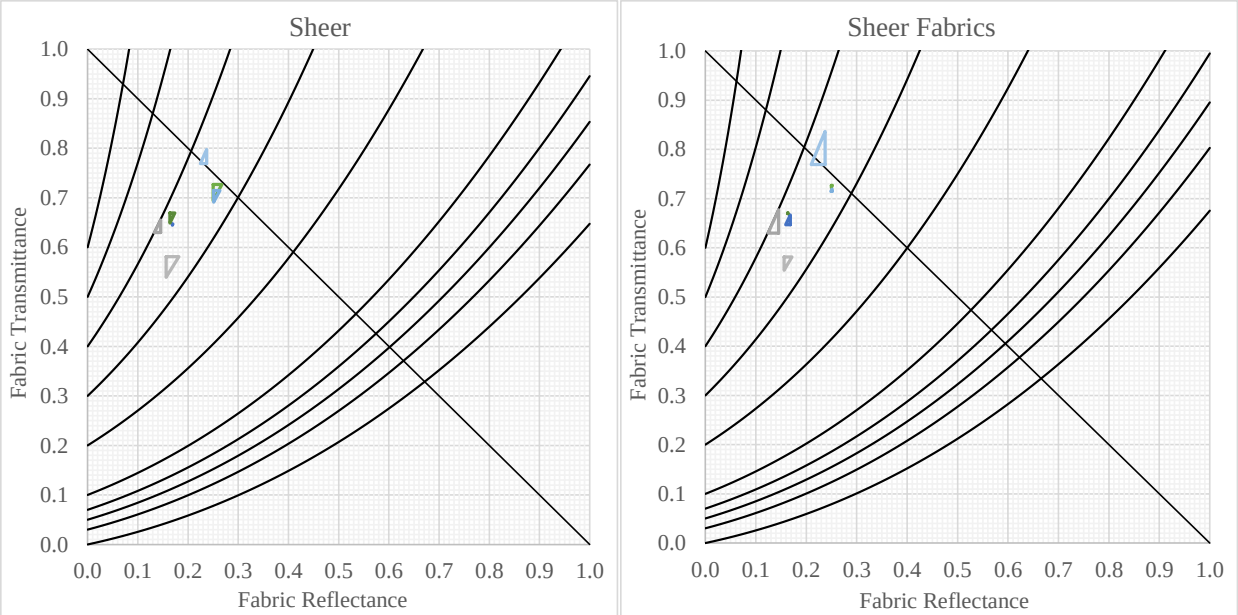

(a) (b)

Figure 3.4: Results for Sheer fabrics (#20, 21, 22, 59, 0-1, 0-4, 0-9) based on (a) the b&C model and (b) customized KUC by direct b coefficient adjustment

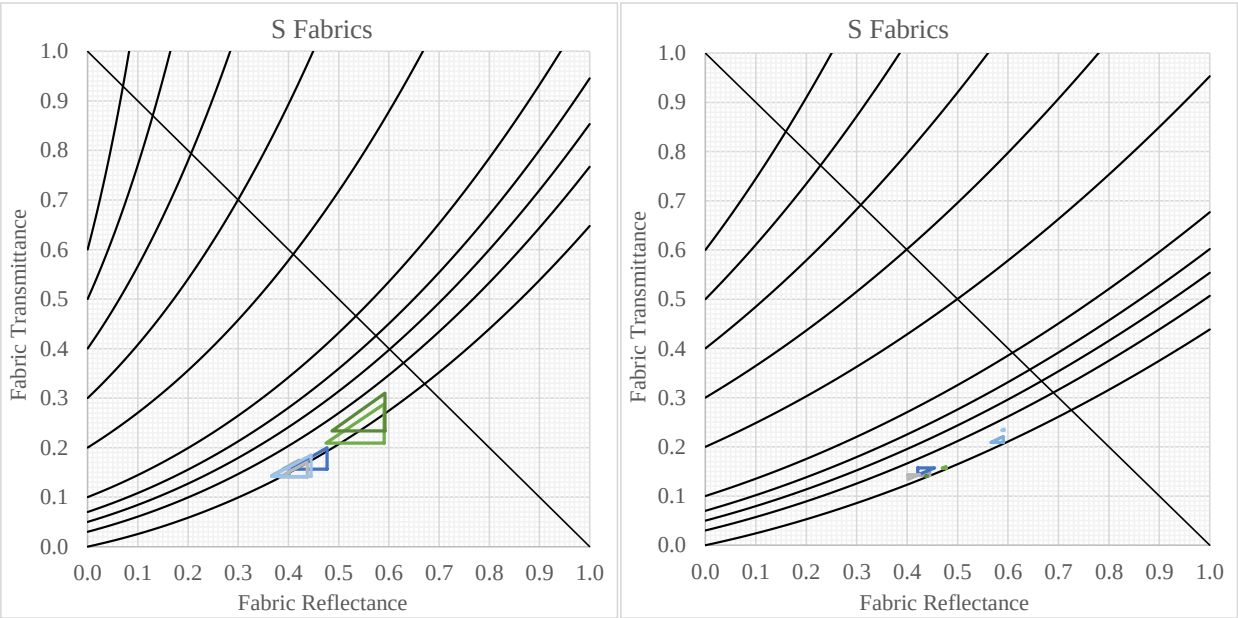

(a) (b)

Figure 3.5: Results for S fabrics (#34, 35, 36, 37, 38, 39, 80) based on (a) the b&C model and (b) customized KUC by direct b coefficient adjustment

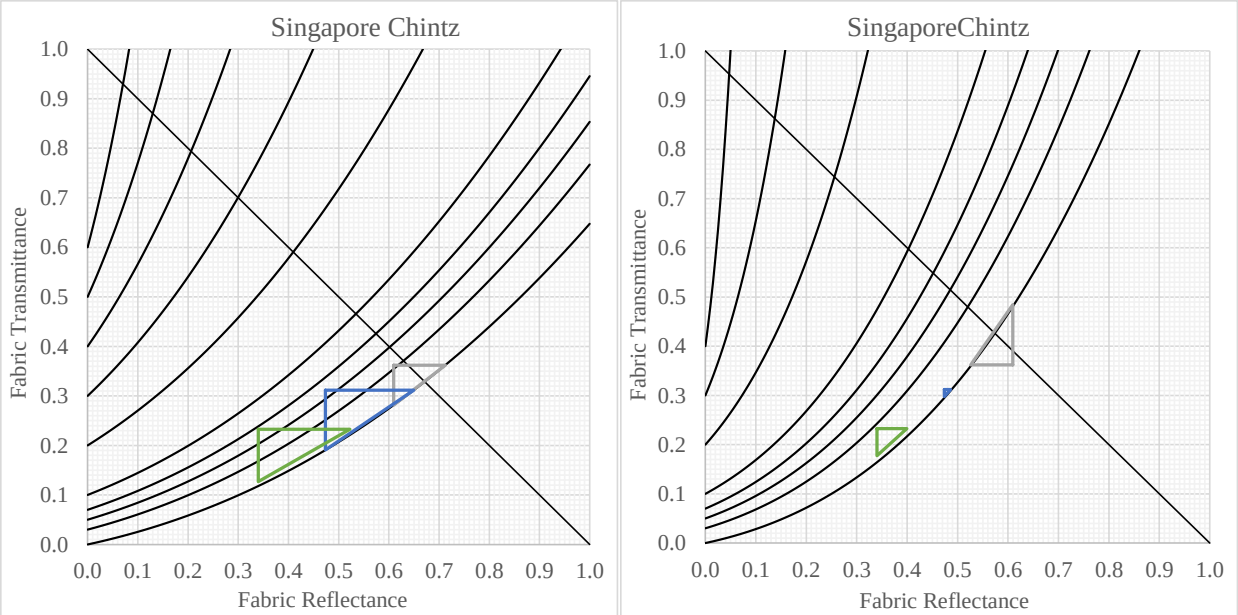

(a) (b)

Figure 3.6: Results for SingaporeChintz (#43, 44, 45) based on (a) the b&C model and (b) customized KUC by direct b coefficient adjustment

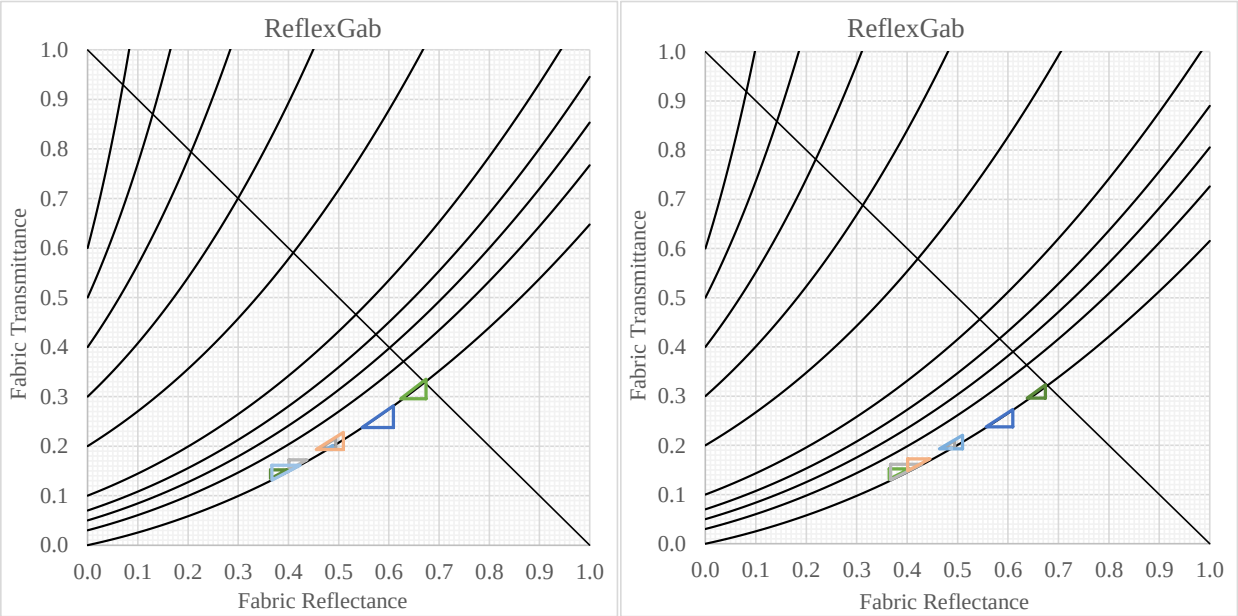

(a) (b)

Figure 3.7: Results for ReflexGab (#12, 24, 47, 48, 49, 85, 0-2, 0-8) based on (a) the b&C model and (b) customized KUC by direct b coefficient adjustment

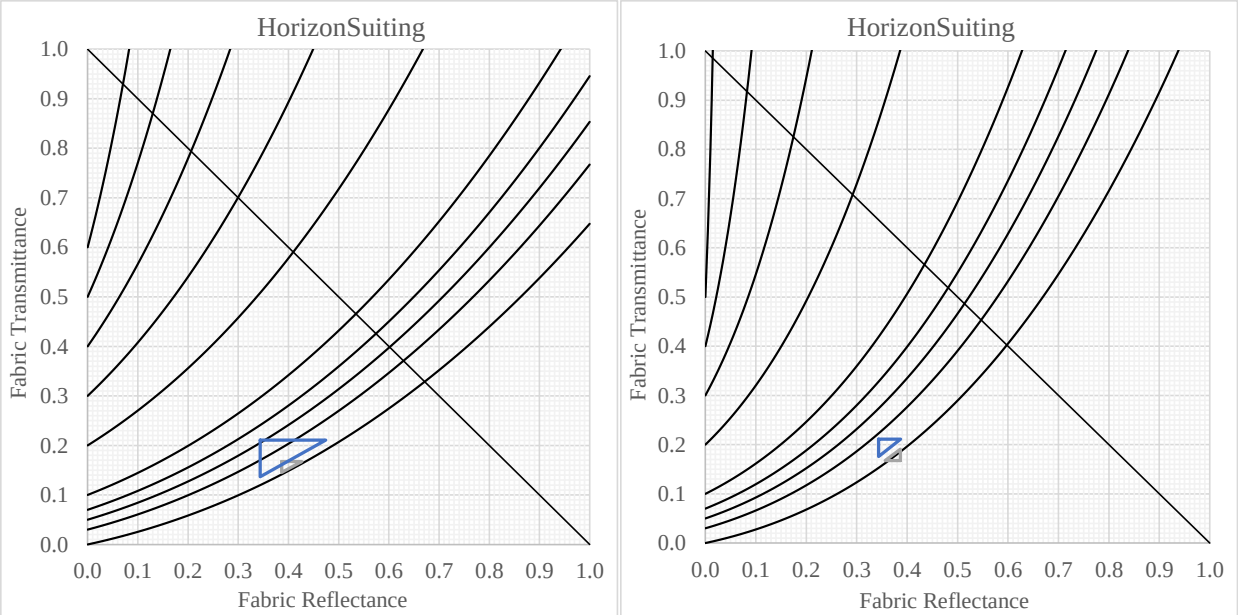

(a) (b)

Figure 3.8: Results for HorizonSuiting (#50, 51) based on (a) the b&C model and (b) customized KUC by direct b coefficient adjustment

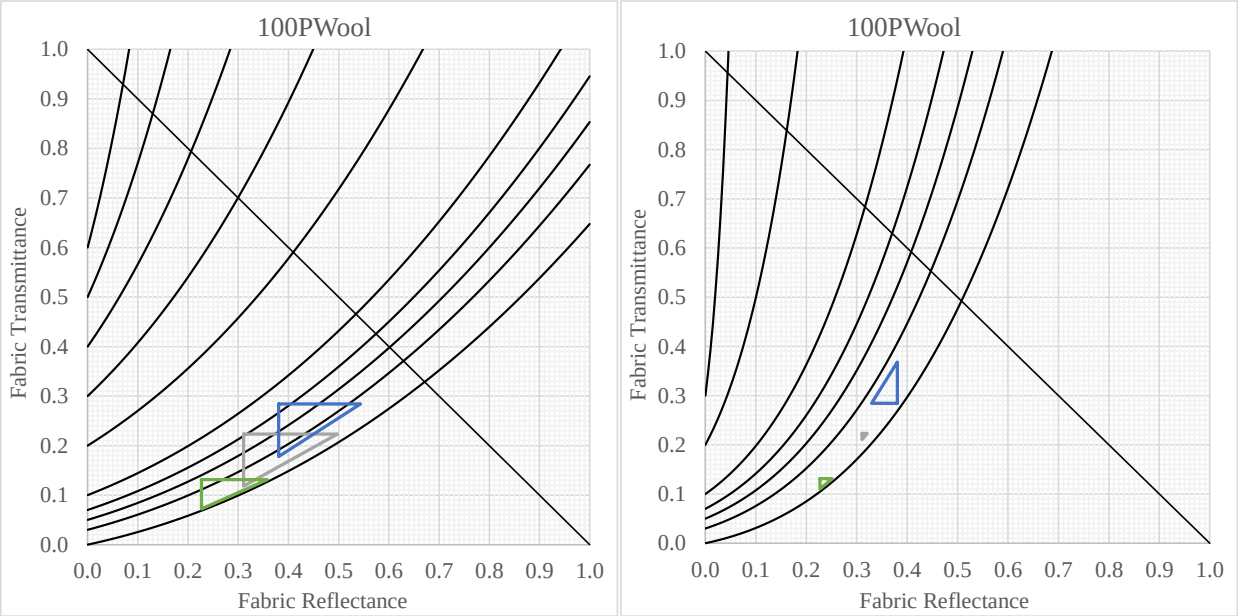

(a) (b)

Figure 3.9: Results for 100PWool (#54, 55, 56) based on (a) the b&C model and (b) customized KUC by direct b coefficient adjustment

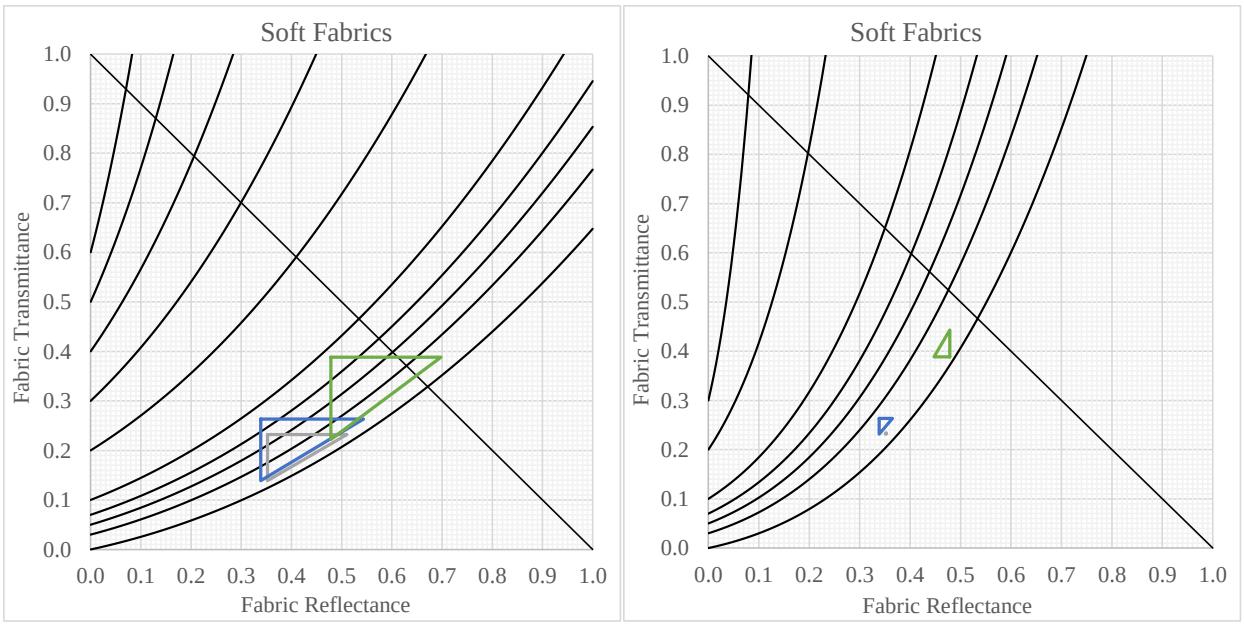

(a) (b)

Figure 3.10: Results for Soft fabrics (#57, 58, 60) based on (a) the b&C model and (b) customized KUC by direct b coefficient adjustment

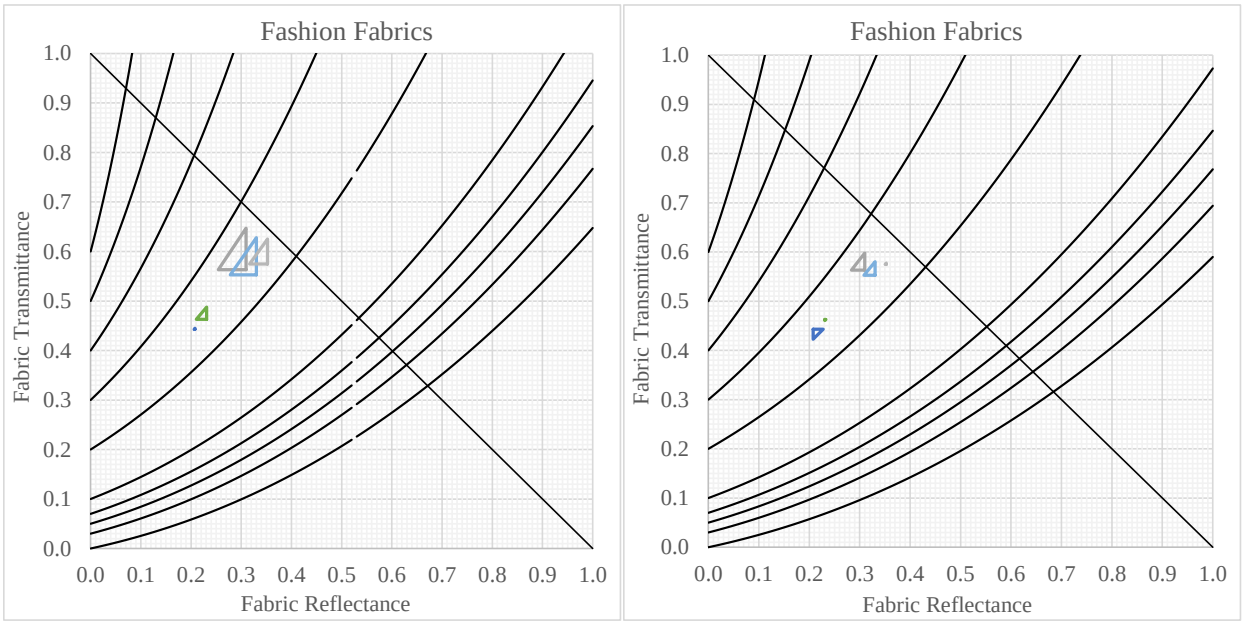

(a) (b)

Figure 3.11: Results for Fashion fabric (#64, 65, 66, 67, 88) based on (a) the b&C model and (b) customized KUC by direct b coefficient adjustment

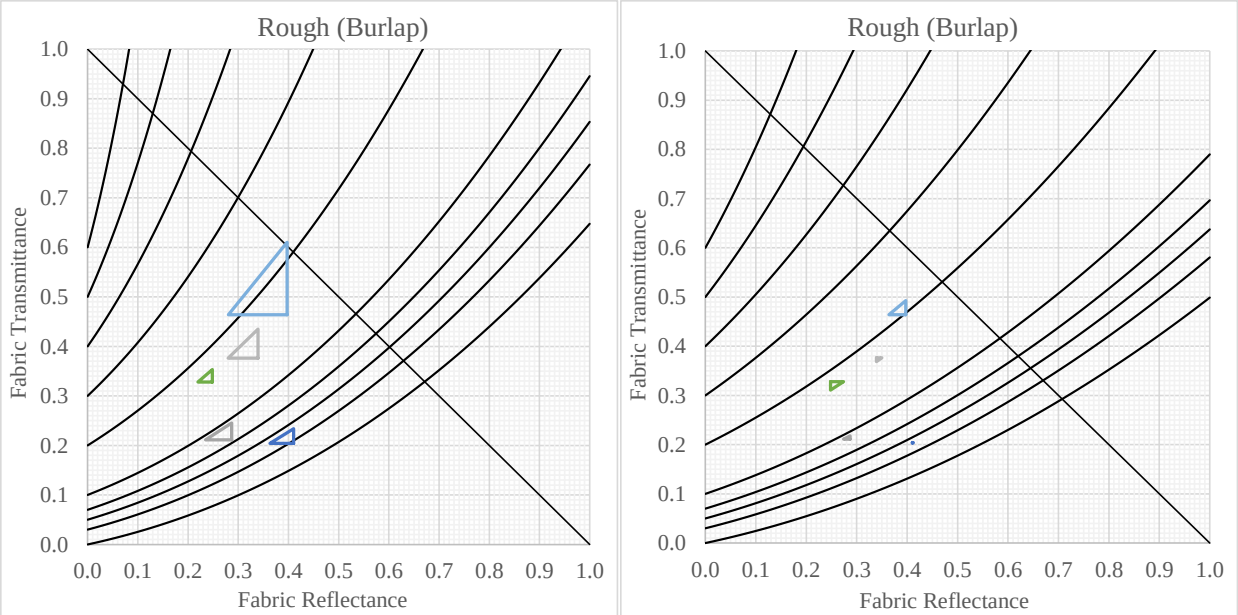

(a) (b)

Figure 3.12: Results for Rough/Burlap (#70, 71, 0-5, 0-6, 0-7) based on (a) the b&C model and (b) customized KUC by direct b coefficient adjustment

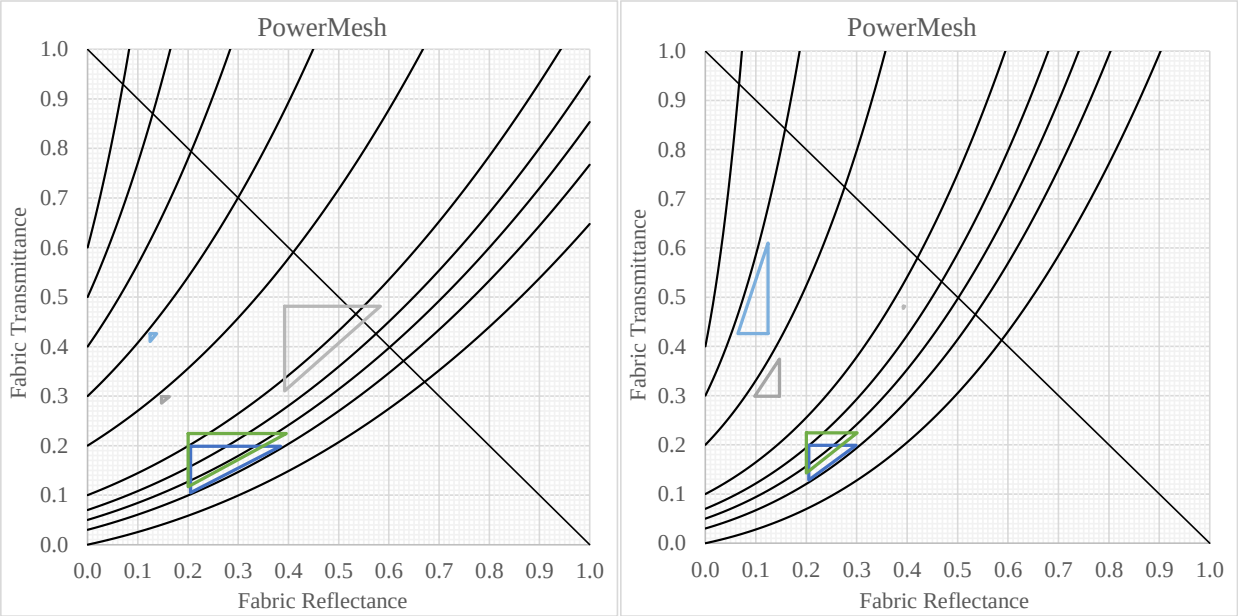

(a) (b)

Figure 3.13: Results for PowerMesh (#86, 92, 93, 94, 95) based on (a) the b&C model and (b) customized KUC by direct b coefficient adjustment

3.3 Generalized Customization Based on Fabric Thickness

While the direct adjustment approach (e.g., $b_{diff,avg}$ in Equation (3.1)) is easy and effective, it is also unique and can only be applied to a specific subset of fabrics. This section demonstrates a more general approach that can be more widely applied.

Figure 3.1 shows that calculated b coefficients of a fabric group tend to be concentrated in one region of the chart. In addition, fabrics higher on the chart are thinner while the lower ones are generally thicker. Based on Equation (2.10) and similar to the $b_{diff,avg}$ term in Equation (3.1), the shift from the model is b_{diff} for an individual fabric. It can be seen, and has been observed by visual inspection, that b_{diff} is generally linked to fabric thickness, t_f.

3.3.1 b_{diff} vs t_f

A digital vernier caliper was used for measuring fabric thickness. Once zeroed, fabric thickness, t_f, was measured by placing each sample between the jaws that are moved together with little pressure. These readings were recorded as the unpressed thickness in Appendix C: Measured Fabric Thickness and taken as a measure of t_f. The observation mentioned above (b_{diff} vs t_f) is depicted in Figure 3.14.

3.3.2 C vs t_f

A similar relationship between C and t_f was also sought. For instance, the b coefficient is calculated using Equation (2.10) and C coefficient determined as the unknown variable in the b&C model (instead of C = 0.22). Figure 3.15 shows the calculated C coefficients versus t_f.

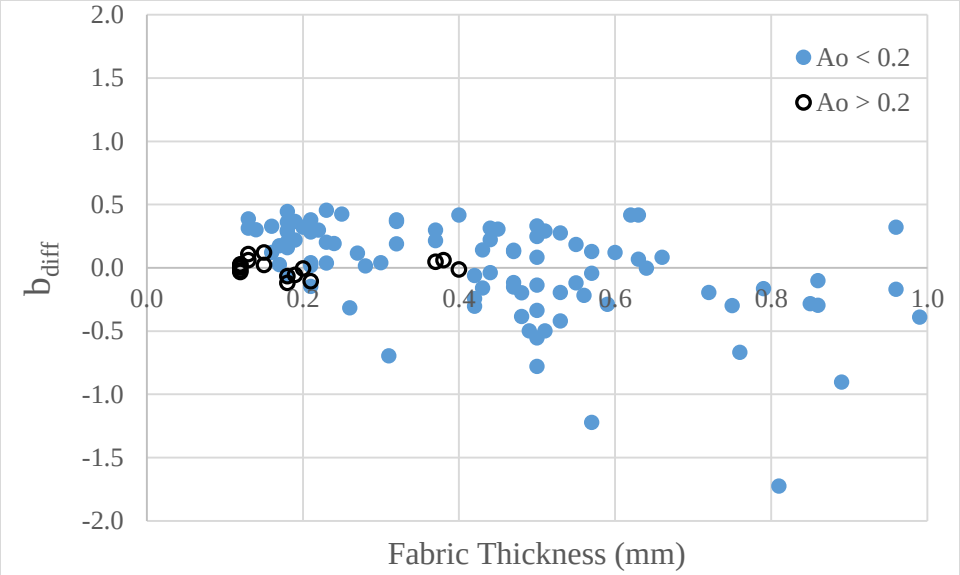

Figure 3.14: b_{diff} vs. measured fabric thickness

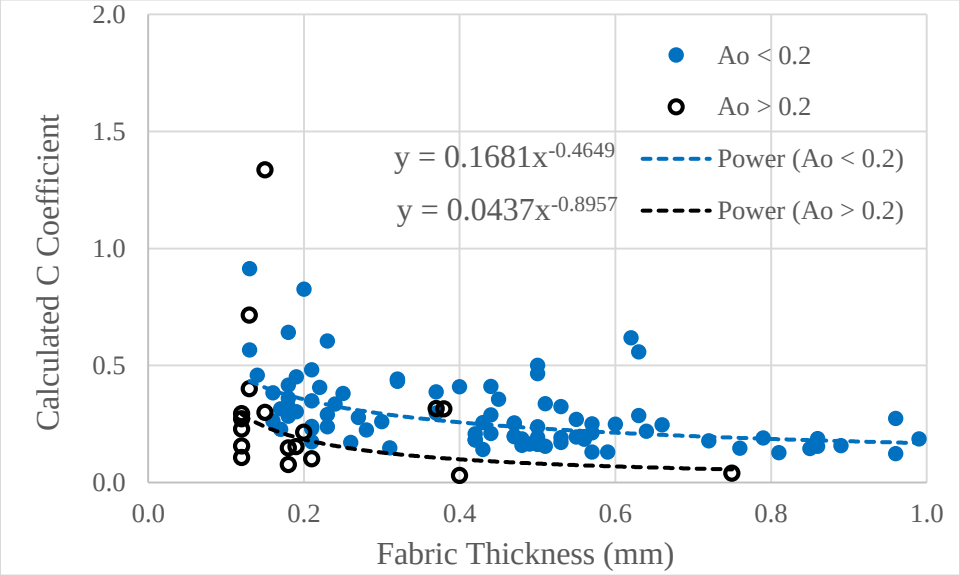

Figure 3.15: Calculated C coefficients vs. measured fabric thickness

3.3.3 Customized b&C Model

The more generalized approach is to have the b&C model customized based on the measured fabric thickness. Figure 3.14 and Figure 3.15 show that the customization can be done through the b coefficient (i.e., b_{diff} as a function of t_f) or the C coefficient (i.e., C as a function of t_f), respectively. Analysis shows that both customizations give similar and better results for A_o predictions than the b&C model. However, only customization through the C coefficient would also give better results than the b&C model for ρ and τ_{bt} predictions if they were the unknowns. This is also to say that, while both customizations work equally well in terms of A_o predictions, customization through the C coefficient produces triangles that are not only smaller but also closer to that of a right isosceles shape than customization through the b coefficient.

Furthermore, fabrics with different openness may be considered separately. Figure 3.15 shows that fabrics with $A_o > 0.2$ are mostly clustered below fabrics with $A_o < 0.2$. And there is no notable cluster for fabrics with $A_o < 0.2$. So there are two equations that govern the C coefficient, as shown in Figure 3.15 and in Equations (3.2) and (3.3).

$$C = 0.1681 \times t_f^{-0.4649} \text{ for } A_o < 0.2 \quad \textbf{(3.2)}$$

$$C = 0.0437 \times t_f^{-0.8957} \text{ for } A_o > 0.2 \quad \textbf{(3.3)}$$

The general guideline is to use the $A_o > 0.2$ equation (Equation (3.3)) for the C coefficient when one can see and read distinctly, for example, the text of a magazine behind the fabric. Lacking such a transparency, otherwise, Equation (3.2) should be used.

The two-equation customization scheme requires only an easy visual inspection (e.g., the transparency test) and a simple measurement of fabric thickness using a vernier caliper. It is an

enhancement to the improved KUC, the b&C model, which itself is a significant improvement to the original KUC.

3.3.4 Results of the Two-Equation Customization Scheme

The two-equation customization scheme is based on the b&C model (Equation (2.5)) where the b coefficient remains unchanged (Equation (2.10)), but the C coefficient (instead of being a constant) is based on Equations (3.2) and (3.3).

Figure 3.16 and Figure 3.17 compare the results of the improved KUC and the customized KUC. Enhancement offered by the customized KUC is not visually notable in the high A_o range, $A_o > 0.03$, shown in Figure 3.16. Results included in Table 3.1 reflect this observation as improvement, when compared to the improved KUC, is not consistent for the high A_o range. Yet, there is a consistent improvement for all other ranges, below $A_o < 0.3$, as shown in Table 3.1. As well, this consistent improvement can be observed in Figure 3.17. In general, the cluster of triangles shown in Figure 3.17 for $A_o < 0.3$ (from (a) to (b) in the figures) becomes "cleaner" as most triangles become smaller.

3.4 Chapter Summary

It has been shown that no one standard three-property KUC is able to suit all types of fabrics. This chapter sets a starting point in seeking additional fabric properties that may play a role in KUC. Although only with limited success, the two-equation customization scheme proves that fabric thickness is a possible fourth property. The potential of including other fabric properties should be explored.

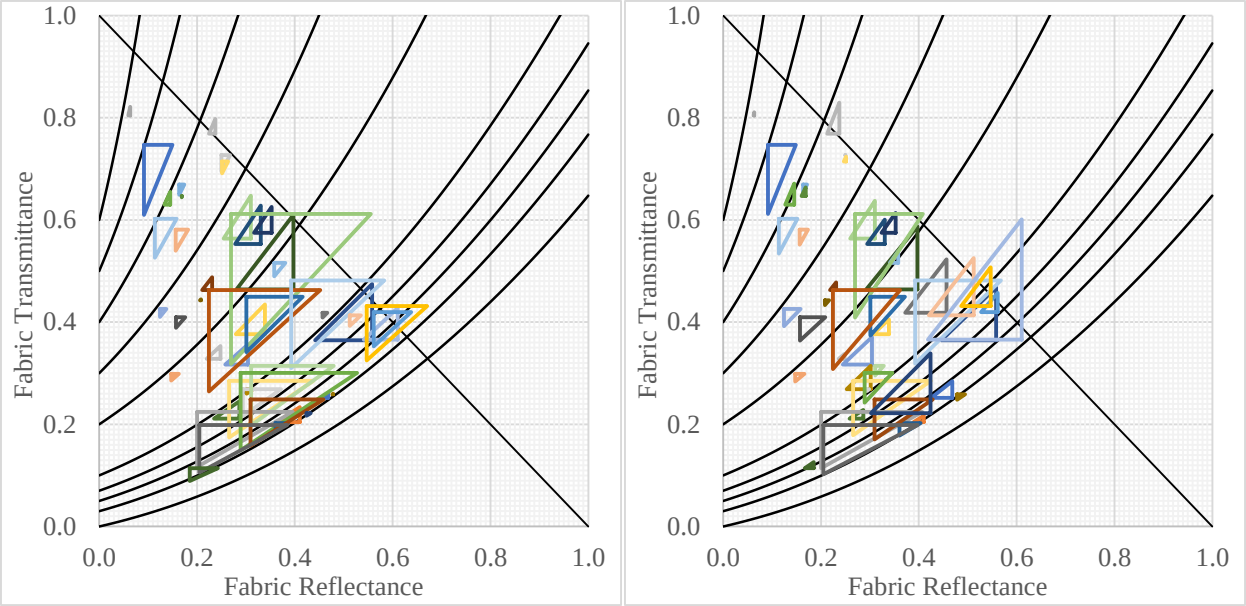

(a) Improved KUC – b&C Model

(b) Customized KUC – Two-equation Scheme

Figure 3.16: Comparison of the improved KUC (b&C model) and the customized KUC using the two-equation scheme for fabrics with $A_o > 0.03$

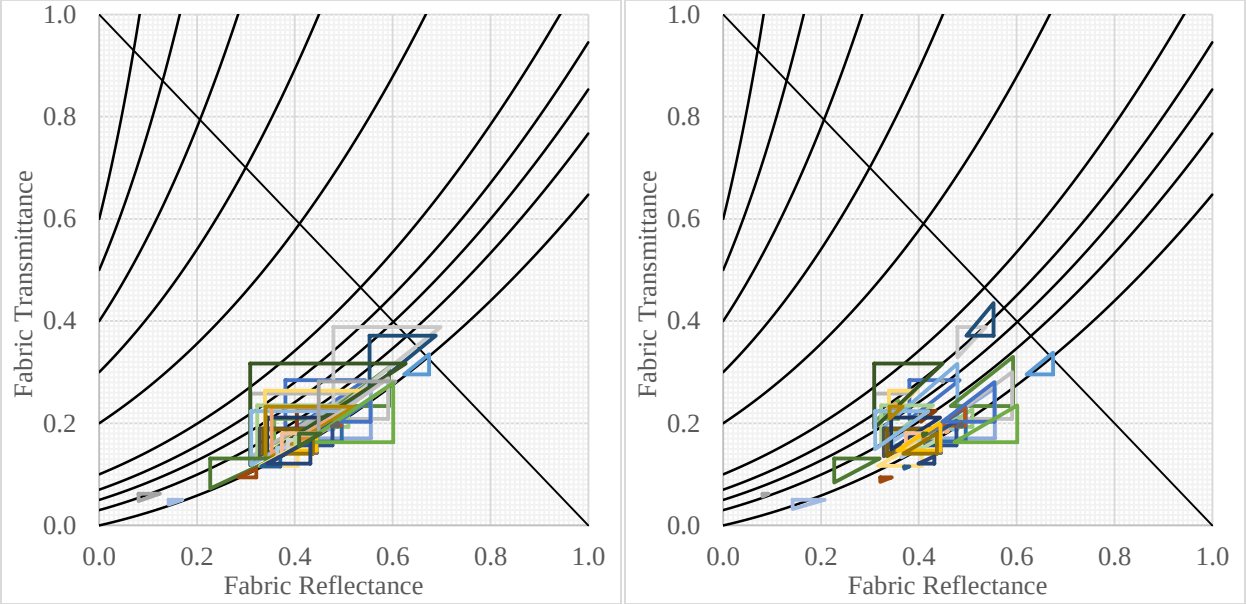

(a) Improved KUC – b&C Model

(b) Customized KUC – Two-equation Scheme

Figure 3.17: Comparison of the improved KUC (b&C model) and the customized KUC using the two-equation scheme) for fabrics with $A_o < 0.03$

Table 3.1: Results of the customized two-equation scheme compared to the original and the improved KUC using the b&C model

No. of Data	A_o Range		Original KUC	Improved KUC b&C Model	Customized KUC Two-Equation Scheme
117 Fabrics	**All**	AVG	0.082	0.014	0.007
		STD	0.061	0.041	0.029
		RMS	0.102	0.043	0.030
3 Fabrics	**Ao > 0.4**	AVG	0.222	0.009	0.015
		STD	0.033	0.052	0.045
		RMS	0.224	0.053	0.048
9 Fabrics	**0.4 > Ao > 0.3**	AVG	0.182	0.007	0.002
		STD	0.029	0.017	0.021
		RMS	0.185	0.019	0.021
10 Fabrics	**0.3 > Ao > 0.2**	AVG	0.093	-0.023	-0.007
		STD	0.033	0.028	0.020
		RMS	0.099	0.036	0.021
9 Fabrics	**0.2 > Ao > 0.1**	AVG	0.127	0.030	0.017
		STD	0.092	0.061	0.058
		RMS	0.157	0.068	0.061
10 Fabrics	**0.1 > Ao > 0.05**	AVG	0.074	0.023	-0.002
		STD	0.066	0.044	0.043
		RMS	0.099	0.050	0.044
16 Fabrics	**0.05 > Ao > 0.02**	AVG	0.065	0.034	0.011
		STD	0.046	0.033	0.029
		RMS	0.080	0.047	0.031
31 Fabrics	**0.02 > Ao > 0.003**	AVG	0.059	0.020	0.010
		STD	0.040	0.042	0.021
		RMS	0.071	0.047	0.023
29 Fabrics	**0.003 > Ao**	AVG	0.054	0.003	0.005
		STD	0.027	0.033	0.017
		RMS	0.061	0.033	0.018

CHAPTER 4
PLEATED DRAPE MODEL

If the solar optical properties of the flat materials used for draperies are known, the apparent solar optical properties of the pleated drape can be estimated (Farber et al. 1963, Kotey et al. 2009c). Currently the pleated drape ILM assumes rectangular pleating profile and takes the following inputs: pleating profile (geometry factors) and flat fabric solar optical properties (material factors). Then depending on the incidence angle, the model calculates the effective (individual) layer properties for determining SHGC. Furthermore, the effective properties of the pleated drape layer are required in the multi-layer analysis. Both Farber and Kotey approximated a drapery layer with a series of uniformly arranged rectangular pleats. For draperies, in addition, the current IAC tables in the ASHRAE handbook are results of solar thermal analysis using the pleated drape ILM developed by Kotey et al. (2009c). Therefore, the established IAC tables are also built based on the rectangular pleating profile. Farber et al. (1963) might have attempted to study other pleating geometries as they stated "Other configurations, such as sinusoidal, etc., are under study now." However, to the author's knowledge, the effect of other pleating profiles has not been examined and published until now.

Regardless the accuracy of the model, this model may not represent drapes with other pleating profiles (e.g., triangular, sinusoidal, and irregular). As well, the validity of the drapery layer model needs to be verified and improved if necessary.

Using the same methodology of Kotey et al. (2009c), a detailed model to determine the effective properties of pleated draperies is developed and presented in this chapter. While the ILM

developed by Kotey et al. (2009c) approximates a drape layer as a series of uniformly arranged rectangular pleats, the present ILM supposes that the pleats are of triangular shape. This is an important step to understand the effects of pleating profiles have on the solar heat gain. The following sections summarize the methodology and present the triangular drape layer ILM.

For any pleating profile (e.g., rectangular or triangular), draperies are generally described by % fullness (or folding ratio, Fr). Folding ratio describes the amount of fabric used to cover a specific window width. Specifically, Fr is the ratio of fabric width to window width (or pleated drape width), and % fullness is defined as

$$\% \text{ fullness} = (Fr - 1) \times 100\% \quad \textbf{(4.1)}$$

For example, a curtain that uses the least amount of material to cover the whole window width is a flat fabric. Such drape is said to have Fr = 1.0 and 0% fullness. Any fullness would be the extra fabric used across the width. Fullness not only provides a drape with a richer look but also provides more light and sound absorption. A drape that uses twice as much of a flat fabric to cover the same width would have 100% fullness and Fr = 2.0.

4.1 Triangular Pleated Drape Model

As the name suggests, the triangular pleated drape model consists of a series of triangular pleats. Figure 4.1 illustrates the configuration of the model, and Figure 4.2 shows a part of the cross-section. As shown in Figure 4.2, the geometry can be described by the pleat width (W) and pleat spacing (S). So, for triangular pleating profile, Fr = 2W/S.

4.1.1 Model Setup and Geometry

Consider beam radiation incident on a drape layer of triangular pleats (Figure 4.1). The plane of the drape layer is assumed parallel to window. The angle between the incident beam radiation and

the plane of drape layer is defined as incident angle, θ. For the purpose of comparison with the experimental study, vertical profile angle (or solar altitude) has been set to zero, $\Omega_V = 0$. Therefore, horizontal profile angle (or surface solar azimuth) is equal to the incident angle, $\Omega_H = \theta$.

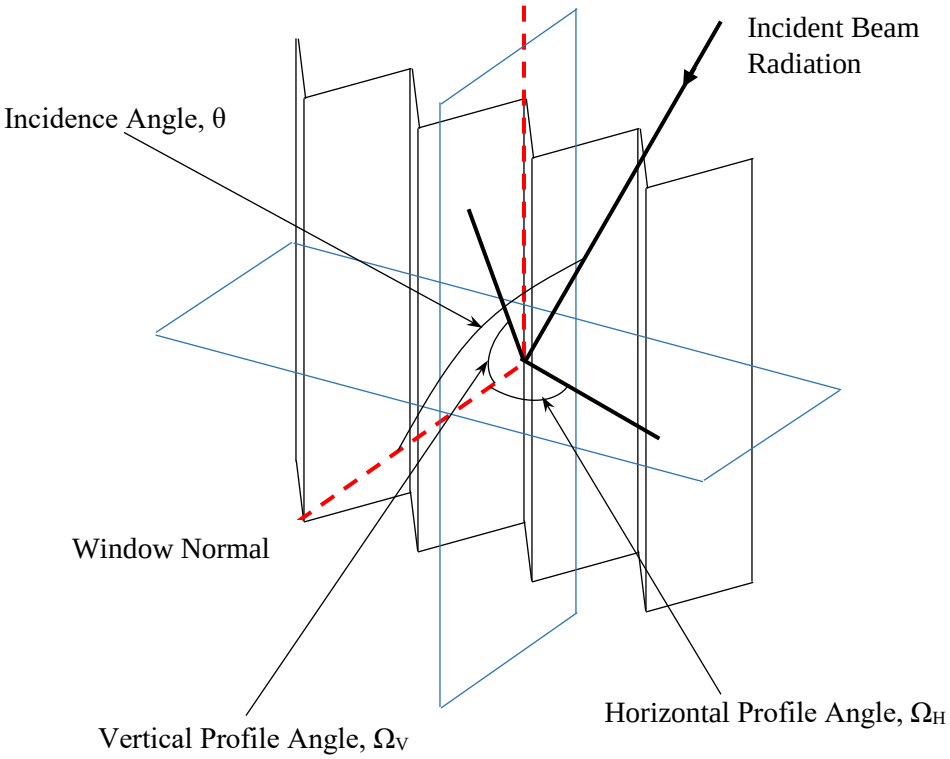

Figure 4.1: Configuration of drapery model showing solar angles

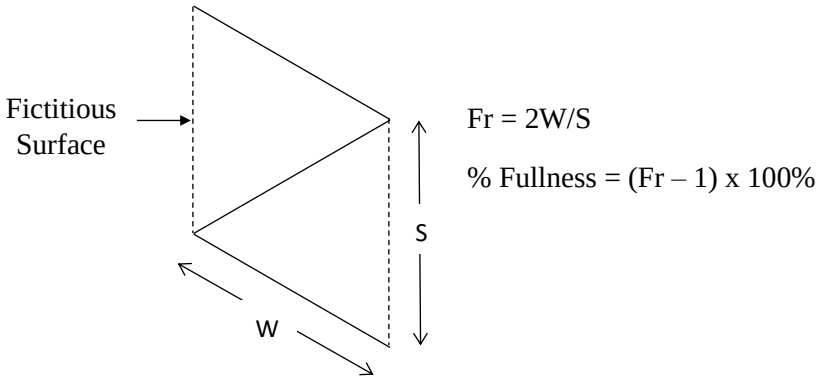

Figure 4.2: Cross-section of triangular pleats (plan view from top)

Note that the pleats are recurring so one pleat can represent the entire geometry. Figure 4.3 depicts a representative enclosure (plan view from top) that contains two pleats where sections ab and cd are the same surface in the model. Similarly, section ab is equivalent to section cd in the model.

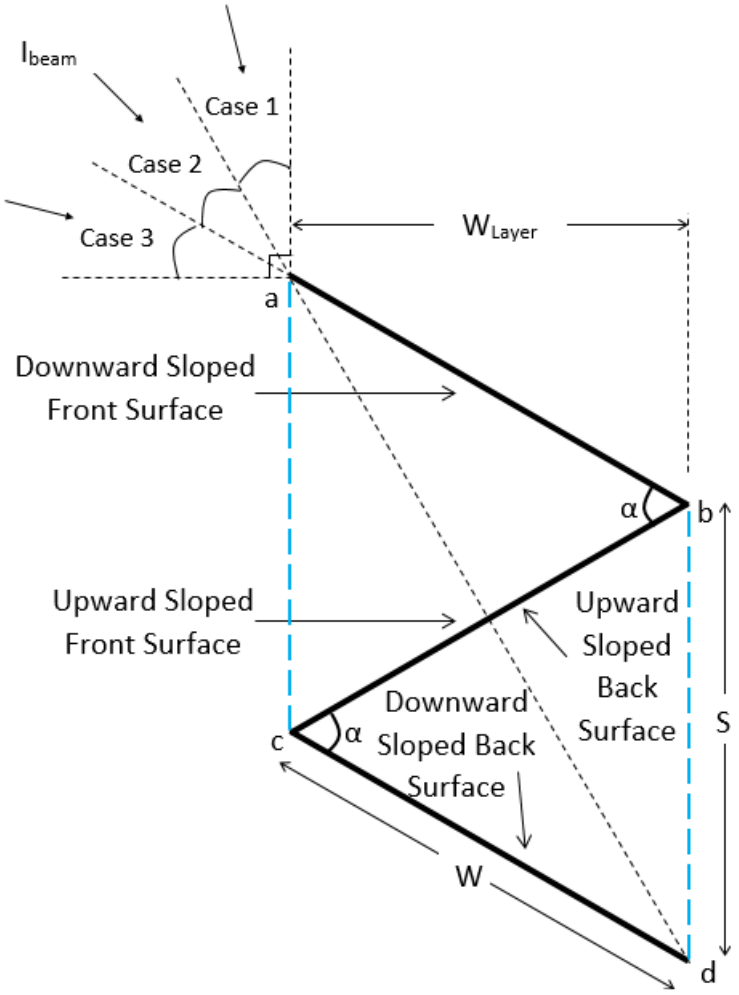

Figure 4.3: Triangular pleated drape model geometry setup

Beam radiation is coming from the front (left) side of the layer at an incidence angle, θ. This beam radiation goes through either direct transmission to the back (right) side of the layer or various interactions with the fabric. The effective beam-beam and beam-diffuse solar optical properties of

the pleated drape layer are determined by tracking all radiation components. Angle dependent solar properties of the fabric and the effect of beam and diffuse components, in both reflection and transmission, are included in the analysis.

There are front and back sides of the drape layer. As shown in Figure 4.3, the drape is folded back and forth and pleated at an angle, α. Every pleat takes the shape of an isosceles triangle with one side being overlapped with a preceding pleat. For the purpose of model analysis/setup, the side with a positive slope is defined as upward-sloped while the other side is downward-sloped (based on the plan view shown in Figure 4.3). Therefore, the drape layer alternates between upward-sloped and downward-sloped surfaces. And, as shown in Figure 4.3, the representative enclosure includes two fictitious surfaces, the front opening (ac) and the back opening (bd), and the following four surfaces: Upward-Sloped Front (USF), Downward-Sloped Front (DSF), Upward-Sloped Back (USB), and Downward-Sloped Back (DSB). Table 4.1 summarizes these surfaces.

Table 4.1: List of model enclosure surfaces

	Surface	**Description**	**Acronym**
Front Side	ac	Front Fictitious Surface	FFS
	ab	Downward-Sloped Front	DSF
	bc	Upward-Sloped Front	USF
Back Side	bd	Back Fictitious Surface	BFS
	bc	Upward-Sloped Back	USB
	cd	Downward-Sloped Back	DSB

The pleat angle, α, can be calculated from folding ratio (based on W and S) and vice versa. For example, Fr = 2.0 means that α = 60°. The incident angle and pleat angle, θ and α respectively, then define the local incidence (wall-solar azimuth) angle on pleat surfaces. Using the models developed by Kotey et. al. (2009a), the local incidence angle, γ, determines the off-normal solar optical properties of flat fabric. It can be shown that

$$\gamma_{USF} = \left|\frac{\pi}{2} - \theta - \frac{\alpha}{2}\right| \quad \textbf{(4.2)}$$

$$\gamma_{DSF} = \left|\frac{\pi}{2} + \theta - \frac{\alpha}{2}\right| \quad \textbf{(4.3)}$$

$$\gamma_{DSB} = \left|\frac{\pi}{2} - \theta + \frac{\alpha}{2}\right| \quad \textbf{(4.4)}$$

4.1.2 Solar Optical Properties of Flat Fabrics

The solar optical properties that are pertaining to beam or diffuse radiation incident on a surface include beam-beam, beam-diffuse, and diffuse-diffuse components of transmittance and reflectance. For radiation incident on the front surface of a fabric and following the same convention used by Kotey et al. (2009c), they are:

- $\tau^{m}_{f,bb}$ the front beam-beam transmittance
- $\tau^{m}_{f,bd}$ the front beam-diffuse transmittance
- $\tau^{m}_{f,bt}$ the front beam-total transmittance
- $\tau^{m}_{f,dd}$ the front diffuse-diffuse transmittance
- $\rho^{m}_{f,bb}$ the front beam-beam reflectance
- $\rho^{m}_{f,bd}$ the front beam-diffuse reflectance
- $\rho^{m}_{f,bt}$ the front beam-total reflectance
- $\rho^{m}_{f,dd}$ the front diffuse-diffuse reflectance

where the superscript m is used to designate a fabric material property as opposed to the corresponding effective solar optical property of the pleated drape. The beam-total component is the sum of the beam-beam and beam-diffuse components. Note that, as discussed in Section 2.3.2, $\rho_{f,bb}^{m}$ is assumed equal to zero. Henceforth, $\tau_{f,bt}^{m} = \tau_{f,bb}^{m} + \tau_{f,bd}^{m}$ and $\rho_{f,bt}^{m} = \rho_{f,bd}^{m}$. Similarly, for radiation incident on the back surface of a fabric, the corresponding properties are designated by replacing subscript f with subscript b.

4.1.3 Simplification and the Three Model Cases

Beam radiation incident on a drape layer is transmitted uninterrupted through fabric openings or, after multiple reflections, emerges in the forward direction as beam-diffuse transmission and in the backward direction as beam-diffuse reflection. Theoretically, at any angle of incidence, beam-beam transmissions through multiple fabric layers can take place before the beam radiation reach the other side of fabric as $\tau_{f,bb}$. Every transmission itself reduces the strength of beam radiation. Furthermore, multiple transmissions of beam radiation will entail incidence on alternating surfaces (i.e., between upward-sloped and downward-sloped surfaces), and one of the two (or both) incidence angles is likely to be high. Due to multiple transmissions and/or high incidence angles, fabric beam-beam transmittance is small, and therefore, the overall beam transmission is very small. Thus, as explained by Kotey (2009), it is reasonable to consider beam-beam transmission only when beam radiation is incident on the fabric for the first time. Subsequent transmission of incident beam radiation is deemed diffuse.

Based on the reasoning discussed above, the model breaks down into three cases depending on the angle of incidence, as depicted in Figure 4.3. For all three cases (Figure 4.4 (a) and (b), Figure 4.5 (a) and (b), and Figure 4.6 (a) and (b)), all or part of the Upward-Sloped Front (USF) surface (highlighted yellow by surface cf in the figures) is illuminated directly by incident beam radiation.

For Case 1, Figure 4.4 (a), the directly illuminated portion, cf, is less than half of the pleated drape width (or $0 < cf \pm W/2$). In this case, any transmitted beam radiation will hit a portion of the DSB surface (highlighted orange by surface cg in Figure 4.4 (a)). Then subsequent transmission of beam radiation through the DSB surface is considered diffuse. Case 1 condition continues to hold until the surface cg covers the entire DSB (i.e., until cg = cd).

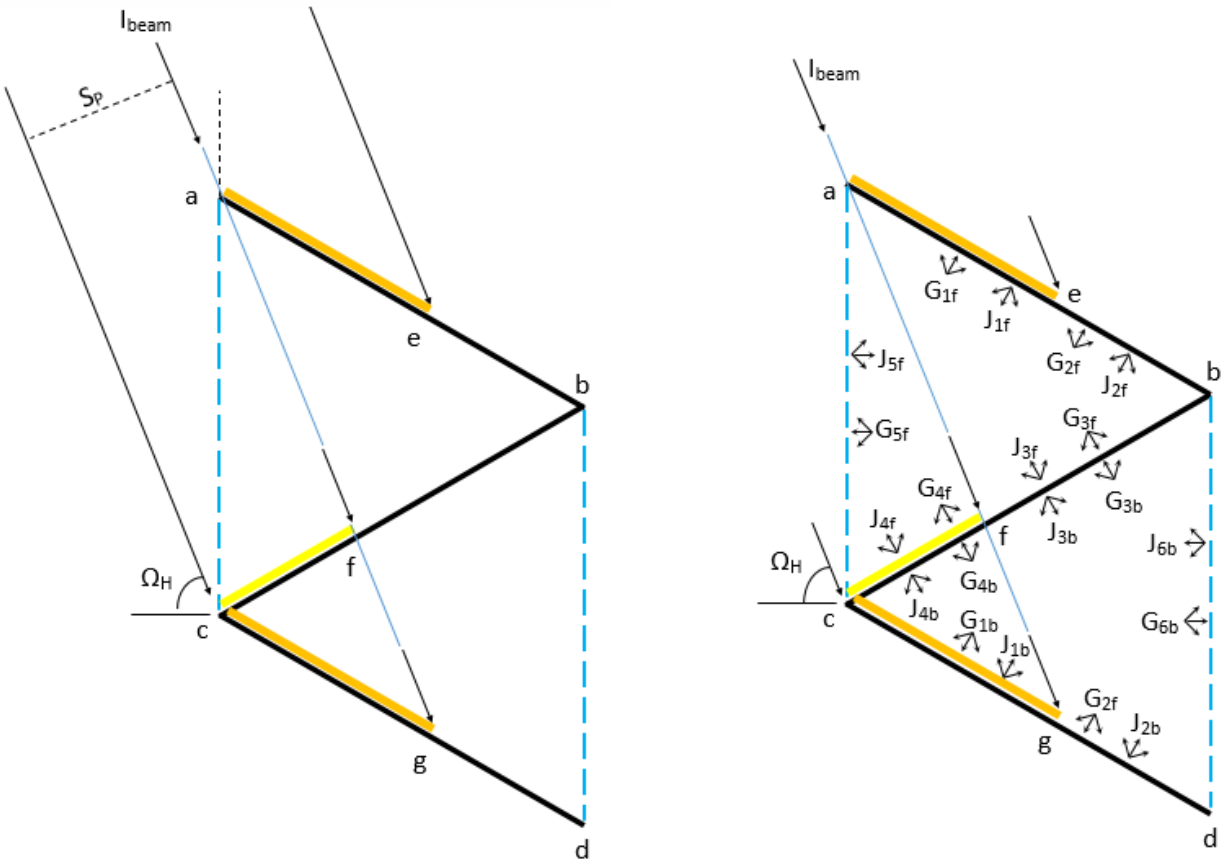

(a) (b)

Figure 4.4: Case 1 model for effective solar transmittance of pleated drape (a) beam-beam and (b) beam-diffuse

For Case 2, Figure 4.5 (a), the directly illuminated portion of cf is between W/2 and W (or W/2 < cf < W). In this case, a portion of the transmitted beam radiation hits the whole DSB surface (highlighted orange by surface cd in Figure 4.5 (a)), and subsequent transmission through DSB is diffuse. The rest hits the fictitious surface and reaches interior as $\tau_{f,bb}$ without further interference.

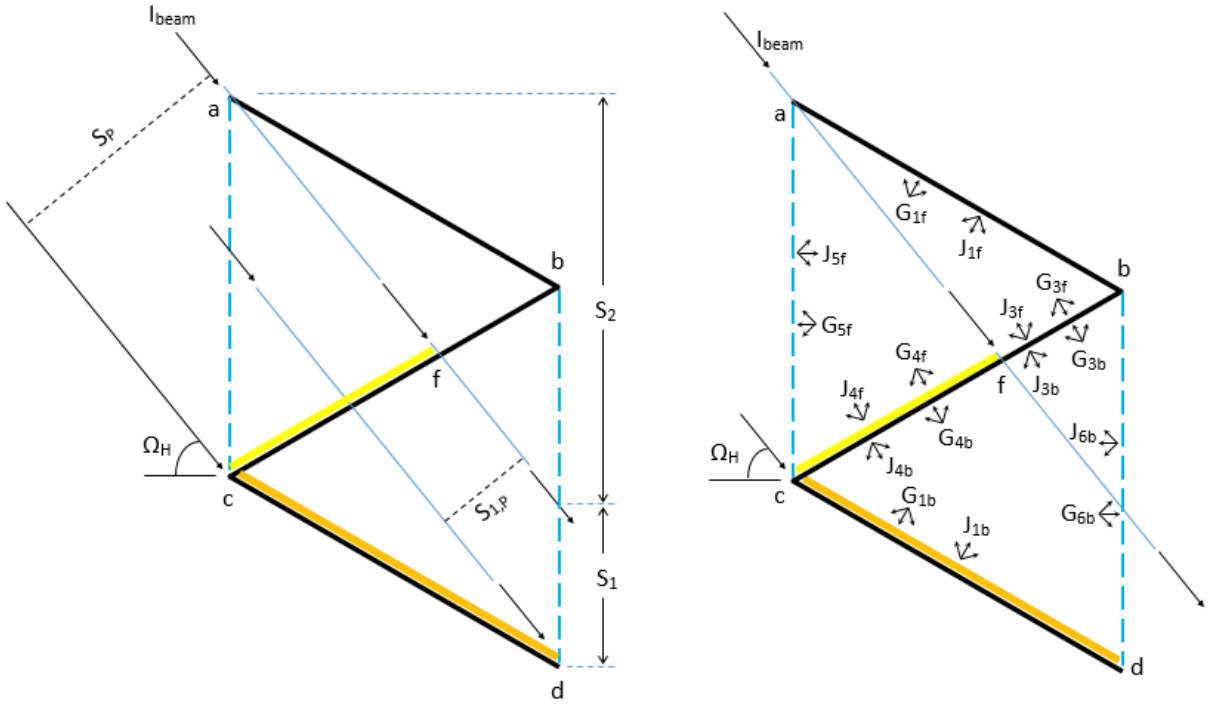

Figure 4.5: Case 2 model for effective solar transmittance of pleated drape (a) beam-beam and (b) beam-diffuse

For Case 3, Figure 4.6 (a), both of the front surfaces, USF (bc) and DSF (ab), are directly illuminated. In this case, all directly transmitted beam radiation hits fictitious surfaces and reaches interior as $\tau_{f,bb}$ after the first transmission without any interference.

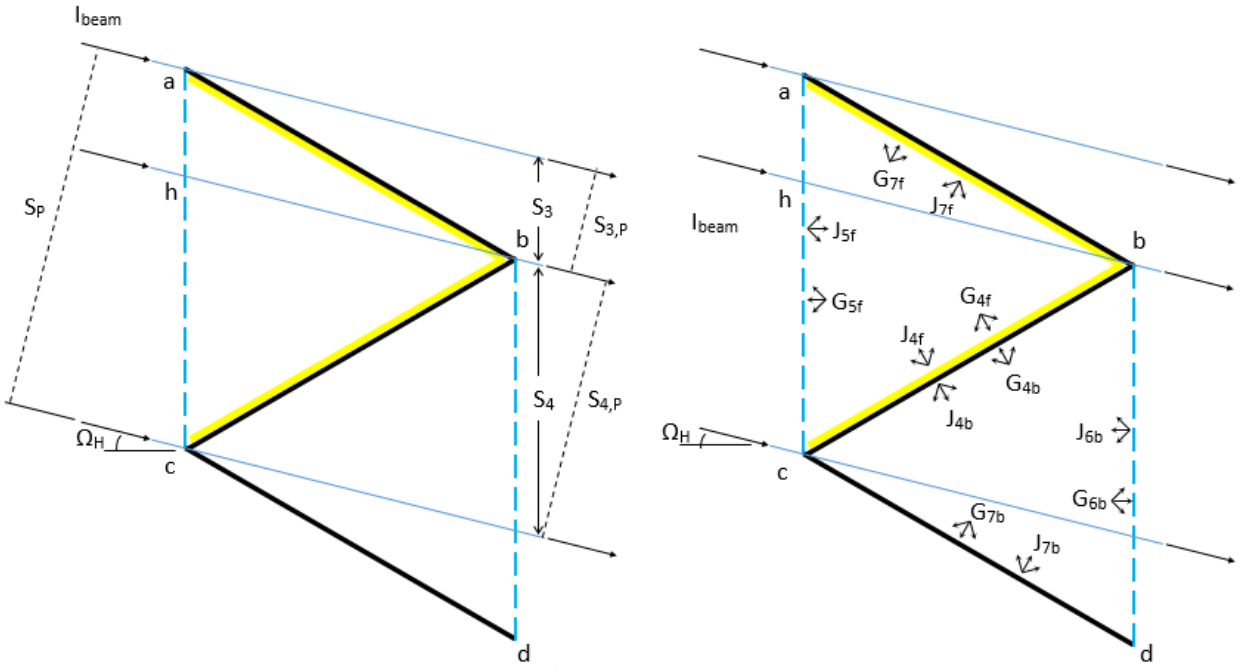

Figure 4.6: Case 3 model for effective solar transmittance of pleated drape (a) beam-beam and (b) beam-diffuse

4.1.4 Effective Beam-Beam Solar Optical Properties of Pleated Drapes

As discussed in Section 2.3.2, fabrics do not exhibit specular reflection. Therefore, the front beam-beam reflectance of the pleated drape, $\rho_{f,bb}$, is also zero.

The front beam-beam transmittance, $\tau_{f,bb}$, are determined based on the three model cases. $\tau_{f,bb}$ depends on the amount of direct transmission. For Case 1, all radiation that reaches interior must go through at least three fabric layers, and therefore, $\tau_{f,bb}$ is zero. As the incidence angle reduces toward Case 2, a portion of beam radiation goes through only one transmission before reaching the other side of the drape layer. When and after reaching Case 3, all transmitted beam radiation experiences only one transmission.

$\tau_{f,bb}$ can be calculated based on the fabric property and the portion of beam radiation experiencing only one transmission. For Case 2, $\tau_{f,bb}$ is the proportional to the ratio of $S_{1,P}$ to S_P as shown in Figure 4.5 (a). It is calculated by multiplying the ratio, ($S_{1,P}$ / S_P), to the off-normal (at the local incidence angle of γ_{USF}) beam-beam transmittance of the fabric, $\tau_{f,bb}^{m}(\gamma_{USF})$. For Case 3, $\tau_{f,bb}$ comes from transmissions of both USF and DSF surfaces. Beam-beam transmittance from DSF and USF encompass the distance, $S_{3,P}$ and $S_{4,P}$ respectively, as shown in Figure 4.6 (a). Table 4.2 summarizes the resulting effective $\tau_{f,bb}$ of the pleated drape model for all three cases.

Table 4.2: Effective beam-beam properties of pleated drape for all model cases

Case	$\tau_{f,bb}$	$\rho_{f,bb}$
1	$\tau_{f,bb} = 0$	$\rho_{f,bb} = 0$
2	$\tau_{f,bb} = \frac{S_{1,p} \cdot \tau^{m}_{f,bb}(\gamma_{USF})}{S_p}$	
3	$\tau_{f,bb} = \frac{S_{3,p} \cdot \tau^{m}_{f,bb}(\gamma_{DSF}) + S_{4,p} \cdot \tau^{m}_{f,bb}(\gamma_{USF})}{S_p}$	

4.1.5 Effective Beam-Diffuse Solar Optical Properties of Pleated Drapes

Incident beam radiation can filter through interstices of a fabric or interact with yarn. Beam radiation intercepted by yarn then transforms into transmitted or reflected diffuse radiations that can be traced as shown in Figure 4.4 (b), Figure 4.5 (b), and Figure 4.6 (b), each for the three model cases. For each case, a number of surfaces can be realized.

On the downward-sloped surface, any beam radiation would arrive either at the backside surface (DSB) in Cases 1 and 2 or at the front side surface (DSF) in Case 3. The section exposed to beam radiation at the backside is Surface 1 (section ae). Surface 2 is the section on the backside surface that is not being irradiated by any beam radiation. Surface 1 is present in Model Cases 1 and 2 while surface 2 is only present in Model Case 1. In Case 3, the incident beam radiation arrives at and covers the entire DSF surface. In this case, the entire DSF is represented by surface 7 as shown in Figure 4.6 (b).

Similarly, on the upward-sloped surface, there are Surface 3 (present in Model Cases 1 and 2) and Surface 4 (present in all three cases). The front and back openings are fictitious surfaces. They are,

respectively, surface 5 (section ac) and surface 6 (section bd); both are present in all three cases. Table 4.3 summarizes the applicable surfaces and their locations for each case.

Table 4.3: Applicable surfaces for each model case

Surface			Model Cases		
Number	**Section**	**Location**	**1**	**2**	**3**
1	ae	Downward-Sloped	✓	✓	
2	be	Downward-Sloped	✓		
3	bf	Upward-Sloped	✓	✓	
4	cf	Upward-Sloped	✓	✓	✓
5	ac	FFS	✓	✓	✓
6	bd	BFS	✓	✓	✓
7	ab	Downward-Sloped			✓

The analysis for determining the beam-diffuse solar optical properties involves radiant interactions among surfaces. Respectively, radiosity and irradiance are the radiant fluxes leaving and arriving at a surface per unit area. Note that a fabric has two sides. Therefore, for example, radiosity of a back surface i, J_{ib}, includes reflected irradiance, $\rho^{m}_{b,dd}G_{ib}$, on the same (back) side of the surface i (i = 1..7) and transmitted irradiance, $\tau^{m}_{f,dd}G_{if}$, on the other (front) side of that surface. In general, Equations (4.5) and (4.6) show the radiosity equations for a surface on the back and front of a fabric, respectively.

$$J_{ib} = \rho^{m}_{b,dd}G_{ib} + \tau^{m}_{f,dd}G_{if} + Z_{ib} \quad \textbf{(4.5)}$$

$$J_{if} = \rho^{m}_{f,dd}G_{if} + \tau^{m}_{b,dd}G_{ib} + Z_{if} \quad \textbf{(4.6)}$$

Surfaces that are illuminated by beam radiation generate a diffuse source term, Z_{ib} or Z_{if} (where i = 1, 4, and 7). Otherwise, the source term is zero. Furthermore, $J_{6b} = 0$ and $J_{5f} = 0$ for the two fictitious surfaces (ac and bd). For a given incident beam flux, I_{beam}, Table 4.4 lists the radiosity equations (Equations (4.7) to (4.18)) for all surfaces in this model.

Table 4.4: Summary of radiosity equations for all model surfaces

	Radiosity Equations	
Back Surfaces	$J_{1b} = \rho^{m}_{b,dd} G_{1b} + \tau^{m}_{f,dd} G_{1f} + \tau^{m}_{f,bb}(\theta_{USF}) \rho^{m}_{b,bt}(\theta_{DSB}) \frac{S}{ae} I_{beam}$	**(4.7)**
	$J_{2b} = \rho^{m}_{b,dd} G_{2b} + \tau^{m}_{f,dd} G_{2f}$	**(4.8)**
	$J_{3b} = \rho^{m}_{b,dd} G_{3b} + \tau^{m}_{f,dd} G_{3f}$	**(4.9)**
	$J_{4b} = \rho^{m}_{b,dd} G_{4b} + \tau^{m}_{f,dd} G_{4f} + \tau^{m}_{f,bd}(\theta_{USF}) \frac{S}{cf} I_{beam}$	**(4.10)**
	$J_{6b} = 0$	**(4.11)**
	$J_{7b} = \rho^{m}_{b,dd} G_{7b} + \tau^{m}_{f,dd} G_{7f} + \tau^{m}_{f,bd}(\theta_{DSF}) \frac{ah}{W} I_{beam}$	**(4.12)**
Front Surfaces	$J_{1f} = \rho^{m}_{f,dd} G_{1f} + \tau^{m}_{b,dd} G_{1b} + \tau^{m}_{f,bb}(\theta_{USF}) \tau^{m}_{b,bd}(\theta_{DSD}) \frac{S}{ae} I_{beam}$	**(4.13)**
	$J_{2f} = \rho^{m}_{f,dd} G_{2f} + \tau^{m}_{b,dd} G_{2b}$	**(4.14)**
	$J_{3f} = \rho^{m}_{f,dd} G_{3f} + \tau^{m}_{b,dd} G_{3b}$	**(4.15)**
	$J_{4f} = \rho^{m}_{f,dd} G_{4f} + \tau^{m}_{b,dd} G_{4b} + \rho^{m}_{f,bt}(\theta_{USF}) \frac{S}{cf} I_{beam}$	**(4.16)**
	$J_{5f} = 0$	**(4.17)**
	$J_{7f} = \rho^{m}_{f,dd} G_{7f} + \tau^{m}_{b,dd} G_{7b} + \rho^{m}_{f,bt}(\theta_{DSF}) \frac{ah}{W} I_{beam}$	**(4.18)**

The diffuse irradiance on each surface of model enclosure is coming from the radiosity of all surfaces in the model. Equations (4.19) and (4.20) show the diffuse irradiance equation for the back and front surfaces. Table 4.5 shows the full set of irradiance equations.

$$G_{ib} = \sum_{jb} F_{ibjb} J_{jb} \quad \textbf{(4.19)}$$

$$G_{if} = \sum_{jf} F_{ifjf} J_{jf} \quad \textbf{(4.20)}$$

Table 4.5: Summary of irradiance equations for all model surfaces

	Irradiance Equations	
Back Surfaces	$G_{1b} = F_{1b1b}J_{1b} + F_{1b2b}J_{2b} + F_{1b3b}J_{3b} + F_{1b4b}J_{4b} + F_{1b6b}J_{6b} + F_{1b7b}J_{7b}$	**(4.21)**
	$G_{2b} = F_{2b1b}J_{1b} + F_{2b2b}J_{2b} + F_{2b3b}J_{3b} + F_{2b4b}J_{4b} + F_{2b6b}J_{6b} + F_{2b7b}J_{7b}$	**(4.22)**
	$G_{3b} = F_{3b1b}J_{1b} + F_{3b2b}J_{2b} + F_{3b3b}J_{3b} + F_{3b4b}J_{4b} + F_{3b6b}J_{6b} + F_{3b7b}J_{7b}$	**(4.23)**
	$G_{4b} = F_{4b1b}J_{1b} + F_{4b2b}J_{2b} + F_{4b3b}J_{3b} + F_{4b4b}J_{4b} + F_{4b6b}J_{6b} + F_{4b7b}J_{7b}$	**(4.24)**
	$G_{6b} = F_{6b1b}J_{1b} + F_{6b2b}J_{2b} + F_{6b3b}J_{3b} + F_{6b4b}J_{4b} + F_{6b6b}J_{6b} + F_{6b7b}J_{7b}$	**(4.25)**
	$G_{7b} = F_{7b1b}J_{1b} + F_{7b2b}J_{2b} + F_{7b3b}J_{3b} + F_{7b4b}J_{4b} + F_{7b6b}J_{6b} + F_{7b7b}J_{7b}$	**(4.26)**
Front Surfaces	$G_{1f} = F_{1f1f}J_{1f} + F_{1f2f}J_{2f} + F_{1f3f}J_{3f} + F_{1f4f}J_{4f} + F_{1f5f}J_{5f} + F_{1f7f}J_{7f}$	**(4.27)**
	$G_{2f} = F_{2f1f}J_{1f} + F_{2f2f}J_{2f} + F_{2f3f}J_{3f} + F_{2f4f}J_{4f} + F_{2f5f}J_{5f} + F_{2f7f}J_{7f}$	**(4.28)**
	$G_{3f} = F_{3f1f}J_{1f} + F_{3f2f}J_{2f} + F_{3f3f}J_{3f} + F_{3f4f}J_{4f} + F_{3f5f}J_{5f} + F_{3f7f}J_{7f}$	**(4.29)**
	$G_{4f} = F_{4f1f}J_{1f} + F_{4f2f}J_{2f} + F_{4f3f}J_{3f} + F_{4f4f}J_{4f} + F_{4f5f}J_{5f} + F_{4f7f}J_{7f}$	**(4.30)**
	$G_{5f} = F_{5f1f}J_{1f} + F_{5f2f}J_{2f} + F_{5f3f}J_{3f} + F_{5f4f}J_{4f} + F_{5f5f}J_{5f} + F_{5f7f}J_{7f}$	**(4.31)**
	$G_{7f} = F_{7f1f}J_{1f} + F_{7f2f}J_{2f} + F_{7f3f}J_{3f} + F_{7f4f}J_{4f} + F_{7f5f}J_{5f} + F_{7f7f}J_{7f}$	**(4.32)**

The view factor, F_{ij}, which can be determined by Hottel's crossed string method, is the fraction of diffuse radiation leaving surface i that is seen by surface j. Subscripts i and j are applied to the given number of surfaces in each model case. Since a surface cannot see itself, $F_{ii} = 0$. Also, surfaces on the same plane cannot see each other. So, for example, $F_{1f2f} = 0$.

From the equations of J (Equations (4.7) to (4.18)) and G (Equations (4.21) to (4.32)) along with the diffuse source terms and the view factors calculated, a complete radiant analysis can be performed for beam-diffuse radiation. The J-G equation set is linear and can be solved by matrix reduction for a given I_{beam}. See Table 4.6 for the complete matrix, which applies to all three cases. The right-most column is the right-hand side (RHS) of the equations showing the diffuse source terms. By setting I_{beam} to unity and solving for the radiosities, the beam-diffuse transmittance and reflectance for the pleated layer are simply G_{6b} and G_{5f}, respectively.

$$\tau_{f,bd} = G_{6b} \quad \textbf{(4.33)}$$

$$\rho_{f,bd} = G_{5f} \quad \textbf{(4.34)}$$

Table 4.6 presents the J-G equation set in a matrix form.

The effective properties of the triangularly pleated drape layer, $\tau_{f,bt}$ and $\rho_{f,bt}$, are results (sum) of the effective beam-beam properties (Table 4.2) and effective beam-diffuse properties (Equations (4.33) and (4.34)).

4.2 Chapter Summary

A triangular pleated drape model was built and coded. The model code is included in Appendix D: Triangular Pleated Drape ILM. Results of the pleated drape models were compared to each other and to measurements. All results are presented in CHAPTER 6.

Table 4.6: Matrix of the J-G equation set

Left Hand Side												Right Hand Side
J_{1b}	J_{2b}	J_{3b}	J_{4b}	J_{6b}	J_{7b}	J_{1f}	J_{2f}	J_{3f}	J_{4f}	J_{5f}	J_{7f}	
-1	-	$\rho^{m}_{b,dd}F_{1b3b}$	$\rho^{m}_{b,dd}F_{1b4b}$	-	-	-	-	$\tau^{m}_{f,dd}F_{1f3f}$	$\tau^{m}_{f,dd}F_{1f4f}$	-	-	$-\tau^{m}_{f,bb}(\theta_{/})\rho^{m}_{b,bt}(\theta_{\backslash})\frac{S}{ae}I_{beam}$
-	-1	$\rho^{m}_{b,dd}F_{2b3b}$	$\rho^{m}_{b,dd}F_{2b4b}$	-	-	-	-	$\tau^{m}_{f,dd}F_{2f3f}$	$\tau^{m}_{f,dd}F_{2f4f}$	-	-	-
$\rho^{m}_{b,dd}F_{3b1b}$	$\rho^{m}_{b,dd}F_{3b2b}$	-1	-	-	-	$\tau^{m}_{f,dd}F_{3f1f}$	$\tau^{m}_{f,dd}F_{3f2f}$	-	-	-	-	-
$\rho^{m}_{b,dd}F_{4b1b}$	$\rho^{m}_{b,dd}F_{4b2b}$	-	-1	-	$\rho^{m}_{b,dd}F_{4b7b}$	$\tau^{m}_{f,dd}F_{4f1f}$	$\tau^{m}_{f,dd}F_{4f2f}$	-	-	-	$\tau^{m}_{f,dd}F_{4f7f}$	$-\tau^{m}_{f,bd}(\theta_{/})\frac{S}{cf}I_{beam}$
-	-	-	-	-1	-	-	-	-	-	-	-	-
-	-	-	$\rho^{m}_{b,dd}F_{7b4b}$	-	-1	-	-	-	$\tau^{m}_{f,dd}F_{7f4f}$	-	-	$-\tau^{m}_{f,bd}(\theta_{\backslash})\frac{ah}{W}I_{beam}$
-	-	$\tau^{m}_{b,dd}F_{1b3b}$	$\tau^{m}_{b,dd}F_{1b4b}$	-	-	-1	-	$\rho^{m}_{b,dd}F_{1f3f}$	$\rho^{m}_{b,dd}F_{1f4f}$	-	-	$-\tau^{m}_{f,bb}(\theta_{/})\tau^{m}_{b,bd}(\theta_{\backslash})\frac{S}{ae}I_{beam}$
-	-	$\tau^{m}_{b,dd}F_{2b3b}$	$\tau^{m}_{b,dd}F_{2b4b}$	-	-	-	-1	$\rho^{m}_{b,dd}F_{2f3f}$	$\rho^{m}_{b,dd}F_{2f4f}$	-	-	-
$\tau^{m}_{b,dd}F_{3b1b}$	$\tau^{m}_{b,dd}F_{3b2b}$	-	-	-	-	$\rho^{m}_{f,dd}F_{3f1f}$	$\rho^{m}_{f,dd}F_{3f2f}$	-1	-	-	-	-
$\tau^{m}_{b,dd}F_{4b1b}$	$\tau^{m}_{b,dd}F_{4b2b}$	-	-	-	$\tau^{m}_{b,dd}F_{4b7b}$	$\rho^{m}_{f,dd}F_{4f1f}$	$\rho^{m}_{f,dd}F_{4f2f}$	-	-1	-	$\rho^{m}_{f,dd}F_{4f7f}$	$-\rho^{m}_{f,bt}(\theta_{/})\frac{S}{cf}I_{beam}$
-	-	-	-	-	-	-	-	-	-	-1	-	-
-	-	-	$\tau^{m}_{b,dd}F_{7b4b}$	-	-	-	-	-	$\rho^{m}_{f,dd}F_{7f4f}$	-	-1	$-\rho^{m}_{f,bt}(\theta_{\backslash})\frac{ah}{W}I_{beam}$

CHAPTER 5
PLEATED DRAPE LAYER TRANSMITTANCE MEASUREMENTS

In order to further develop and validate solar optical model of pleated drape layers, an experiment has been designed to study draperies' solar transmittance. A standard test method for solar transmittance of materials using an integrating sphere has been develop by the American Society for Testing and Materials and outlined in ASTM E 903 (ASTM 1996). The flux measured by the photo-detector is proportional to the incident flux entering the integrating sphere. By placing a sample in front of the transmittance (inlet) port, the detector measures the radiant flux transmitted through the sample and entered into the integrating sphere. Then the ratio of the radiant energy transmitted by the sample (Sample Reading) to the energy incident upon the sample (Reference Reading) is equal to sample transmittance.

While the standard test method applies to flat and uniform materials, additional considerations are required for measuring spectral optical properties of thick, scattering, and spatially non-uniform samples such as the pleated drape samples. Milburn (1994) developed the optical-property measurement process for thick, scattering, and spatially non-uniform samples using a custom-designed broad-area illumination integrating sphere (BAI-IS) system. Halder et al. (2007) upgraded the BAI-IS system by replacing many of the measuring, control and data processing devices. This chapter provides detail discussions on the transmittance tests of pleated drape layers and the setup and calibration of the BAI-IS system.

5.1 Test Matrix

Transmittance measurements using the Broad Area Illumination Integrating Sphere (BAI-IS) system have been carried out for validating (both the triangular and rectangular) pleated drape models and for further model development. Measurements are performed to examine the shading effect of different pleat profiles and drape fullness. These tests cover off-normal incidence angles up to 60° (i.e., $\Omega_H = \theta$ = up to 60°).

The pleated drape layers are constructed with selected fabrics with various folding ratios (Fr) and pleating profiles (R – Rectangular and T – Triangular). Angle of incidence ranges from 0° to 60° with a 10° increment. Therefore, the experiment covers the following test matrix.

- Folding Ratios (Fr): 1.0 (flat fabric), 1.5, 2.0, 2.5
- Pleating Profiles: R – Rectangular and T – Triangular
- Fabrics: 20 selected fabrics
- Incidence Angles: 0°, 10°, 20°, ... , 60°

5.1.1 Folding Ratios

Most drapes have folding ratios (Fr) between 1.5 and 2.5. Drapes with Fr = 3.0 or above are not common. In addition, increasing Fr reduces the transmittance of the drape layer, especially at high angle of incidence. Therefore, tests with high Fr (3.0 or higher) may be difficult to do for some fabrics due to weak signal strength.

5.1.2 Pleating Profiles

There are many pleating styles available for draperies. It would be a daunting task to consider all possible pleating profiles. Although some drapes exhibit a rectangular or triangular profile, many have, for example, pinch pleats or other pleating styles. These pleating styles usually form a pleating profile that can be approximated by a rectangular or a triangular profile depending on the

pleating style. For example, Figure 5.1 (a) is best approximated by rectangular pleats where Figure 5.1 (b) and (c) should be approximated with triangular pleats. The triangular pleating style is used where a low stacking ratio is desired (i.e., requires less storage room when the drape is open to admit sunlight).

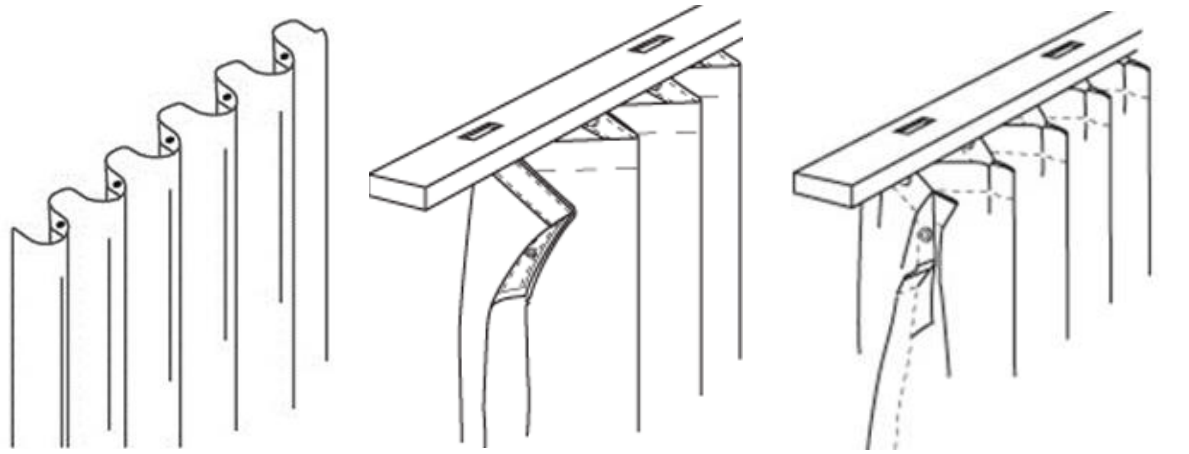

(a) (b) (c)

Figure 5.1: Examples of various pleating styles[14]

5.1.3 Fabric Selection

Fabrics were chosen so that the selection covers all nine categories of KUC (Figure 1.4 and Table 2.1). One fabric from each category was chosen. One additional fabric in each of the light-color (L) and open-weave (I) categories was chosen. This is because the effects of test variables are expected to be more noticeable for fabrics with high reflectance and high transmittance. Sheer is a popular drapery fabric whose properties fall outside (above) of the nine categories due to its high openness. For the sheer category, five fabrics of various openness and colors were selected.

[14] This image is taken online from www.drape.com

The Cary 5000 spectrophotometer is used to measured normal solar-optical properties of fabrics. Refer to Section 2.3.1 for details on measurement using the Cary 5000 and Section 2.3.2 for data processing of spectral data. The results are used for fabric selection and for input in the simulations.

5.1.4 Angles of Incidence

The turntable to which the integrating sphere and the sample mount structure are attached can rotate up to 60°. Therefore, the test matrix is limited to an incident angle of up to 60°. In general, increasing incident angle lowers transmittance with reduced signal strength.

5.2 Construction of Pleated Drape Samples

Two sample frames made of plexiglass have been built to support fabrics in a pattern of rectangular and triangular pleats. Figure 5.2 shows a picture of a sample frame. The frames are 60 cm by 38 cm (24" by 15"). The area is large enough for illumination at the largest angle of incidence, which is 60 degree. Design of the frame also allows pleats of various folding ratios.

As shown in Figure 5.2, tiny holes are drilled through the top and bottom of the frame. Distances between the drilled holes are based on the pleating profiles and folding ratios. Fishing lines pass through these holes and are pulled tightly with tension for supporting fabric in order to make the defined profiles and folding ratios as illustrated in Figure 5.3. The pleat spacing, S, is always 2 cm for rectangular pleats and 3 cm for triangular pleats.

Figure 5.2: A sample frame designed to allow various folding ratios of drapes

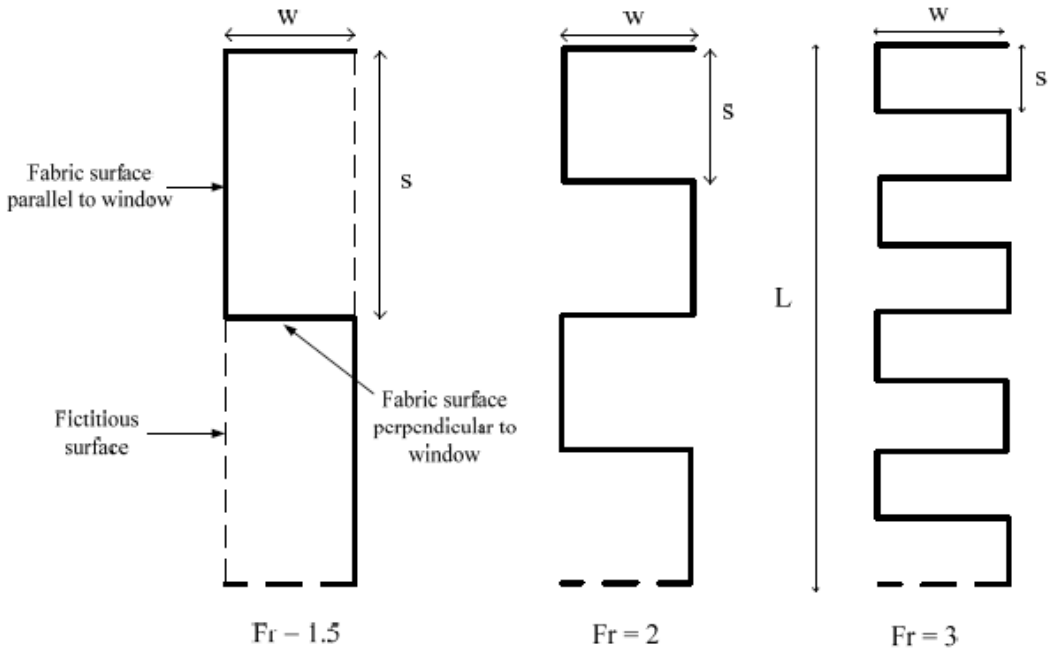

Figure 5.3: Illustration of folding ratio (drapery fullness) for square pleats (Kotey 2009)

5.3 Limitations (Signal Strength and Fabrics Physical Properties)

5.3.1 Signal Strength

Signal strength is an important factor for this experiment. It is difficult to obtain useful results in cases of weak signal strength. Transmittance (and therefore signal strength) depends strongly on aforementioned four variables of the test matrix. In general, signal strength decreases with

increasing angle of incidence although pleating profile can alter the effect of incident angle. Similarly, increasing Fr also reduces the signal strength. However, in a few cases, increasing Fr can increase the signal strength for some specific combinations of fabric properties and incident angle.

5.3.2 Physical Properties of Fabrics

Physical properties of fabrics are of great interest in fields such as textile research and processing (e.g., Azeem et. al. 2015 and Kenkare et. al. 2005). Fabrics have complex structures and various properties. The properties of woven fabric are decided upon its end use. Detailed discussions on properties of fabrics are not within the scope of this research. Instead, this sub-section introduces a few common physical properties for discussions of their effects on the pleated drape samples.

- Drape Coefficient: Drapability of a fabric is a combined effect of several factors such as stiffness, weight, thickness etc. Measurement for this parameter has continuously been developed, improved, and standardized since 1930. Now, drape coefficient is the most common among terms used to describe a fabric. Drape coefficient describes the ability of a fabric (circular specimen of known size) to deform when suspended under its own weight in specified conditions. The higher the drape coefficient, the less drapeable the fabric.

- Fabric Thickness: Fabric thickness is usually measured to gauge its effect on thermal, solar-optical, and mechanical properties of the fabric. For example, when choosing a fabric, one may want to consider how the thickness and construction of the fabric will play a roll in how warm it is, how easily it wrinkles, and whether it is sheer or opaque.

- Warp and Weft: Warp/weft refers to the threads that make up a woven fabric. Weft threads run from side to side whereas warp threads run along the length of the yardage. Yarn linear densities of warp and weft affect both solar-optical and physical properties of fabrics.

- Stretchability: Stretchability can be either unidirectional or bidirectional. In general, stretchability is greater weft-wise than warp-wise.

Ideally, the pleated drape sample would be of exactly rectangular or triangular shapes as approximated/assumed in the models (i.e., Figure 5.3 and Figure 4.2). However, this is not possible due to the physical properties of fabrics. For example, fabrics need to bend alternatively to make a pleated drape. As these fabrics fold around the supporting lines, fabrics with low drape coefficient would be able to form a sharper edge (better drapability) than fabrics with high drape coefficient. As a result, lower drape coefficient fabrics form the anticipated profiles better than higher drape coefficient fabrics do.

5.4 BAI-IS – Setup

While the Cary 5000 is easy to use and has excellent capabilities, it cannot measure the solar optical properties of thick and/or spatially non-uniform samples. The Cary 5000 has a small integrating sphere, and therefore a small inlet port. The small inlet port cannot capture all the scattering light. This is known as out-scattering loss. Also, the narrow beam of incident light source cannot irradiate a representative (broad) sample area.

Instead, the BAI-IS system is used to measure thick, scattering and spatially non-uniform samples. The BAI-IS system is a custom-built spectrophotometer specifically designed to overcome the limitations of the Cary 5000. First, it has a larger integrating sphere with an inlet port area that is large enough to cover a representative area of a non-uniform sample. Second, the broad beam illuminates a large sample area, allowing the in-scattering gain to offset the out-scattering loss.

To have confidence in the measurements made by the custom-built BAI-IS system, it is crucial that the experiment is properly setup and calibrated. The BAI-IS system consists of the following components and sub-systems:

a. **radiant source system** including lamp, reflective concentrator, kaleidoscope section, chopper disc, Fresnel lens,
b. **sample mount structure** including the rotating table and a stepper-motor-controlled traversing system that moves samples to block and unblock the sample (inlet) port of the integrating sphere,
c. **integrating sphere and monochromator** collecting and splitting the light into spectral components, and
d. **control and data processing system** including photo detectors, phase-lock amplifier, DAQ, a computer (LabVIEW).

Figure 5.4 shows the schematic of the BAI-IS. The setup and calibration of each component is described in the following sections.

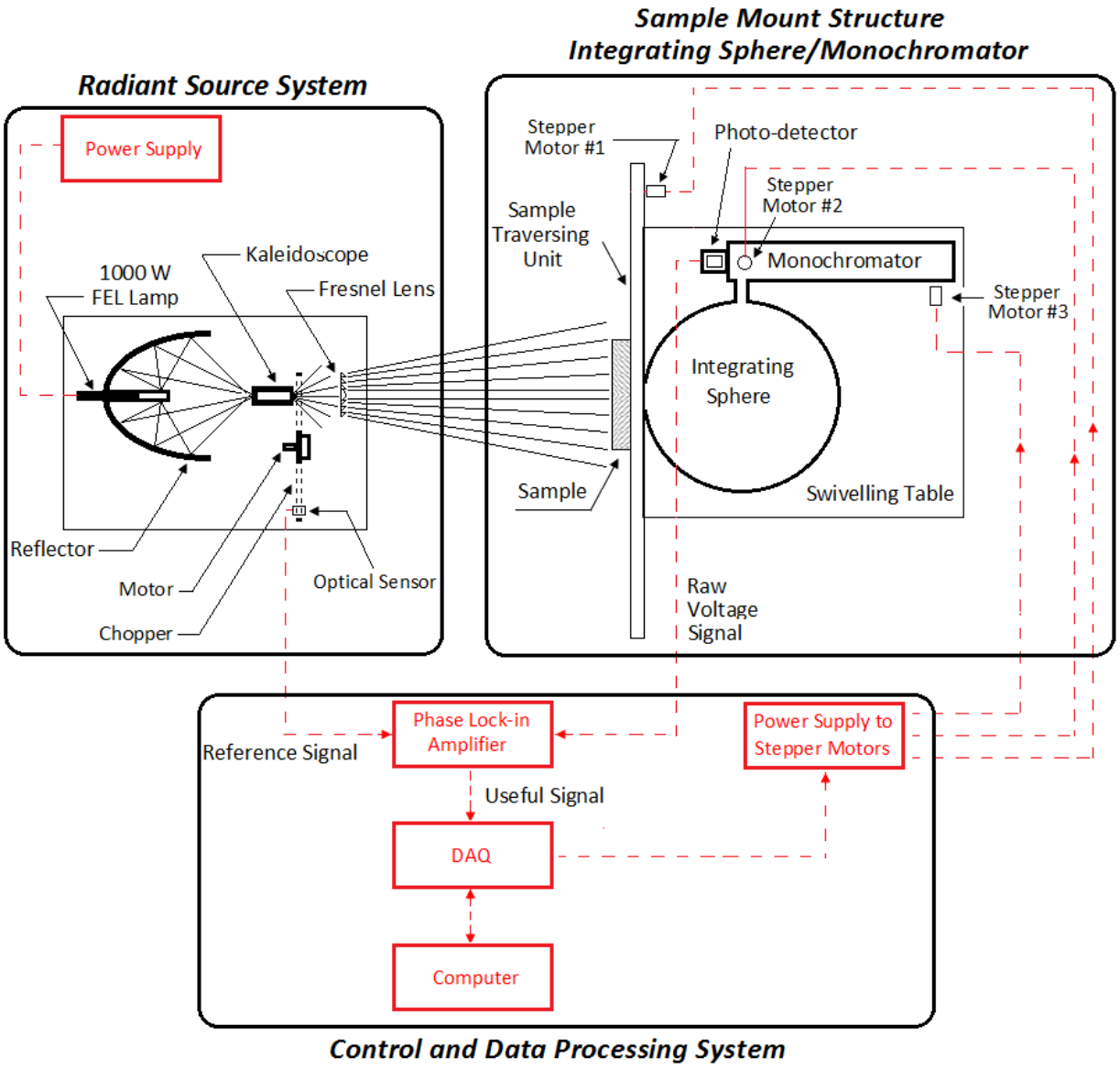

Figure 5.4: Schematic layout of the BAI-IS system

5.4.1 The Radiant Source System

The radiant source must provide quasi-collimated irradiation of nearly uniform intensity over a broad area at the inlet port of integrating sphere. Also, sufficiently strong intensity is required for detectors to attain a good signal-to-noise ratio. Therefore, the radiant source uses a 1000-Watt Quartz Tungsten Halogen (QTH) FEL[15] Lamp with color temperature of approximately 3200 K and with high output in the spectral region of interest (350 nm to 2500 nm). As shown in Figure 5.5, QTH lamps are good visible and near infrared sources because of their smooth spectral curve and stable output.

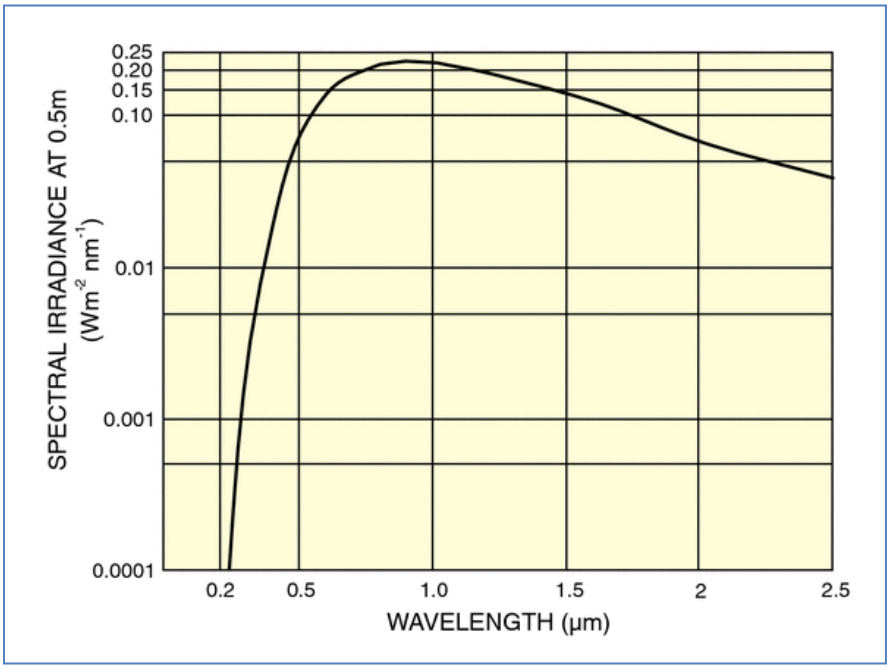

Figure 5.5: Typical spectral irradiance of 1000W FEL quartz tungsten halogen lamp[16]

[15] The FEL lamp is an ANSI standard 1000 watt quartz halogen lamp with a G9.5 medium 2-pin base.
[16] This figure is from Newport website.

5.4.1.1 Power Supply to QTH Lamps

An external power supply, ScienceTech Model 500-1K-QTH, designed for 120VDC 1000W QTH lamps is used to stabilize the output of QTH lamps. The 500-1K-QTH is a fixed DC stabilized switching power supply[17] that accepts 120/240VAC inputs and produces 120VDC output. Note that regardless of the input voltage, only the 120VDC 1000W QTH lamp can be used.

5.4.1.2 Ellipsoidal Reflective Concentrator

Radiation from the QTH lamp is directed by a rhodium coated ellipsoidal reflective concentrator[18]. The rhodium coating has an approximately 70% reflectivity and has superior resistance to tarnishing and scratching. As well, it has a very important characteristic for the present application: it normally does not form an oxide even when heated.

The QTH lamp should be located inside the concentrator so that its filament is at the focus of the ellipsoidal reflective surface. This maximizes the amount of light being redirected to the other focus point outside of the concentrator. Distance from center of ellipsoid to either focus, f, can be determined in terms of its major and minor radii, a and b:

$$f = \sqrt{a^2 - b^2} \qquad \textbf{(5.1)}$$

For the ellipsoidal concentrator, a = 19 cm (7.5”) and b = 12.3 cm (5.0”), giving f = 14.1 cm (5.6”).

5.4.1.3 Kaleidoscope and Fresnel Len

Irradiance uniformity is accomplished using a kaleidoscope section in combination with a Fresnel lens[19]. The kaleidoscope section is a square tube with smooth, specularly reflecting mirrored-walls. It acts as a light pipe that homogenizes non-uniform light source. The kaleidoscope output aperture

---

[17] Switching power supply is also called switched-mode power supply.
[18] Supplied by Melles Griot, Rochester, New York
[19] Supplied by Fresnel Technologies, Houston, Texas

is about 3 cm by 3 cm. To collect most of the light (i.e., to have good collection efficiency), a low f-number[20] lens should be used. The smaller the f-number the greater the radiant flux collected by the lens. Therefore, a Fresnel lens with a diameter of 20 cm is used. The lens is made of polycarbonate that has good high temperature resistance and a very low absorptance across the solar spectral range.

A diverging Fresnel lens is used to provide a magnification of about 15:1 to cover (45 by 45 cm) area of illumination at the sample plane. For reasonable directional uniformity across the sample area, the Fresnel lens is placed 3 m from the sample plane, and this dictates that the lens be about 20 cm from the kaleidoscope output aperture.

5.4.1.4 Optical Chopper Wheel

The chopper wheel is a 13-inch diameter disc made of a thin metal sheet with several openings. This optical chopper wheel rotates between the kaleidoscope and the Fresnel lens, allowing the radiant source to pass at a certain frequency. The chopping frequency is equal to the number of openings times the frequency of rotation. During the "open" position the detected signal comes from both the radiant source and background light. During the "close" position the radiant source is blocked, and only the background signal is collected. The chopping frequency provides a reference signal for the phase lock-in amplifier (PLA) to differentiate the background signal and generate the "wanted" signal that is from the radiant source only.

[20] For optical lens, f-number (also denoted as f/#) is defined as the ratio of its focal length to diameter of aperture.

5.4.2 Sample Mount

The sample mount is fixed onto a work table that can be rotated 60° counter-clockwise. This allows measurements with incident angles up to 60°. At 0° the sample plane is perpendicular to the incoming radiation.

As well, the sample mount can move horizontally across the sample plane with a traversing mechanism, positioning the sample either in front or away from the inlet port of the integrating sphere. Traversing of sample is controlled by a stepper motor drive mechanism.

5.4.3 Integrating Sphere and Monochromator

Light passing through a sample will be collected by the integrating sphere and split spectrally by the monochromator. The original system was developed by Doug Milburn for his PhD research in the early 1990s (Milburn 1994). Since then, both the hardware and the software of this system have been used, modified, upgraded, and rearranged around by various researchers for other projects. Because of its age and the way it has been built and used, the monochromator requires a thorough calibration, the biggest challenge of setting up the BAI-IS system.

5.4.4 Data Processing and Control Systems

After light goes through the monochromator and reaches the photo-detector, the detector sends a signal to the phase lock-in amplifier (PLA), which then sends the output signal to the DAQ/computer.

5.4.4.1 Detectors

The detector (model UVS/PBS-025/020-H from Electro-Optical System Inc.) is a combination of photo-detector/receiver that has both a photo-diode and a photo-conductor sandwiched together. Spectral responses of the Silicon photo-diode (UVS) and Lead Sulphide (PbS) photo-conductor are in the wavelength range of 200 – 1100 nm and 1000 – 3000 nm, respectively.

5.4.4.2 Phase Lock-in Amplifier (PLA)

The PLA receives both the input signal from the detector and the reference signal from the optical chopper sensor. The PLA is able to process signals buried in noise (i.e., mainly ambient light in this case). Following the check guide provided by Scitec Instruments Ltd., tests have been done to confirm that the PLA is working properly.

5.4.4.3 Control System

The BAI-IS utilizes LabVIEW software as an interface to control measurements and process results. Based on user input, LabVIEW drives three stepper motors: one turns the prism for wavelength selection, one adjusts the exit slit of the monochromator for spectral bandwidth selection, and one operates the sample traversing system.

5.5 Calibration of the Monochromator

The monochromator is Littrow-style quartz prism design taken from a Beckman DU spectrophotometer commercially produced in the 1950s. Milburn (1994) modified this monochromator and integrated it into the BAI-IS system. This monochromator has two control parameters: slit width and nominal wavelength. A slit width would give a specific nominal bandwidth (FWHM – full width at half maximum) within which the peak wavelength would be the nominal wavelength.

The spectral range of the monochromator specified in the literatures and in previous researches varies from 200 nm to 2200 nm. The spectral limits of the optical system inside the monochromator need to be verified. The control system has also been modified several times. The most recent documented work on the calibration of nominal wavelength is (Halder 2007). However, the positioning of the stepper motor vs. wavelength has again changed since then. As a result, the calibration curve reported by Halder (2007) cannot be used.

No information was previously reported on the calibration of spectral bandwidth. Milburn (1994), Jiang (2005), Halder (2007) all used the maximum slit width of 2 mm for maximum signal strength. Therefore, the spectral resolution of this device had never been tested. In summary, the following lists three key questions that need to be resolved for the calibration of monochromator.

a. What is the operational (spectral) range of this monochromator?
b. How does stepper motor position correspond to the nominal wavelength (i.e., calibration of nominal wavelength selection)?
c. How does the stepper motor position correspond to the slit/band width (i.e., calibration of spectral bandwidth)?

5.5.1 Beckman DU Quartz Spectrophotometer Documents

Although the BAI-IS system has been used for research for more than twenty years, no document was previously referenced on the Beckman DU quartz spectrophotometer. An effort has been made to find the relevant documents with the hope of finding useful information or answers for the questions listed above. As a result, some timeworn documents are located through the National Institute of Health (NIH) Office of History and Stetten Museum. These documents are listed in the end of the Reference section and important information has been summarized here.

Transmittance (T) is the ratio of the radiant energy transmitted by the sample (P) to the energy incident upon the sample (P_o). Both radiant energies must be obtained at the same wavelength, with the same spectral slit width. $T(\lambda) = P(\lambda) / P_o(\lambda)$

Spectral Slit Width is the range of waveband emerging from the exit slit, neglecting stray light and spherical aberrations.

Resolution is the ability of the instrument to distinguish between two closely spaced wavebands. The apparent transmittance will depend on the slit width and includes such influences as the transmittance profile curve within the wave band being transmitted and the variations of sensitivity of the sensors with respect to wavelength. It is usually possible to determine if these effects are significant by increasing or decreasing the slit width by a factor of two or more. For example, a change in apparent transmittance then indicates that these effects are pertinent.

Nominal Wavelength is selected by rotating the quartz prism inside the monochromator. In one of Beckman's documents, the wavelength scale is mentioned to have been calibrated from 200 to 2000 nm. However, in all other Beckman's documents, the optical system with integrated components is mentioned to provide a wavelength range from 220 to 1000 nm. Again, the wavelength range needs to be verified.

Half-Intensity Band Width (or **Nominal Band Width**) refers to the span of wavelengths leaving the monochromator, each of which contributes at least half as much energy as does the wavelength with the greatest energy. This is also referred as FWHM (Full Width at Half Maximum).

Figure 5.6 gives the band width versus wavelength relationship from which the required slit openings for a given spectral band width can be determined for any wavelength of interest. For measurements at a predetermined nominal band width, the necessary slit width must be calculated, taking into consideration that optical aberrations tend to increase that slit width by approximately 0.04 mm. If X is equal to actual slit width to be used at one wavelength, corresponding to the nominal band width, it may be calculated with the slit equation:

$$X = (W_E - 0.04*W_D)/W_D \quad \textbf{(5.2)}$$

where W_D is the nominal band width per 1 mm slit opening (Figure 5.6), and W_E is the nominal band width to be used for measurement.

The slit equation, along with Figure 5.6, is the most important piece of information obtained from the documents provided by the NIH Office of History and Stetten Museum.

The light emerging from any practical monochromator does not consist of a single wavelength but a group of wavelengths. When the light intensity is plotted as function of wavelength, a triangular curve would result similar to that in Figure 5.6 (see theoretical distribution of radiant energy with wavelength leaving exit slit in Figure 5.6 inset). The triangular distribution curve is an idealized result that would be obtained with a perfect optical system. In practice, unavoidable aberrations result in the effective widening of the slit image, and thus the triangle shown should be slightly wider and rounded at the bottom and top.

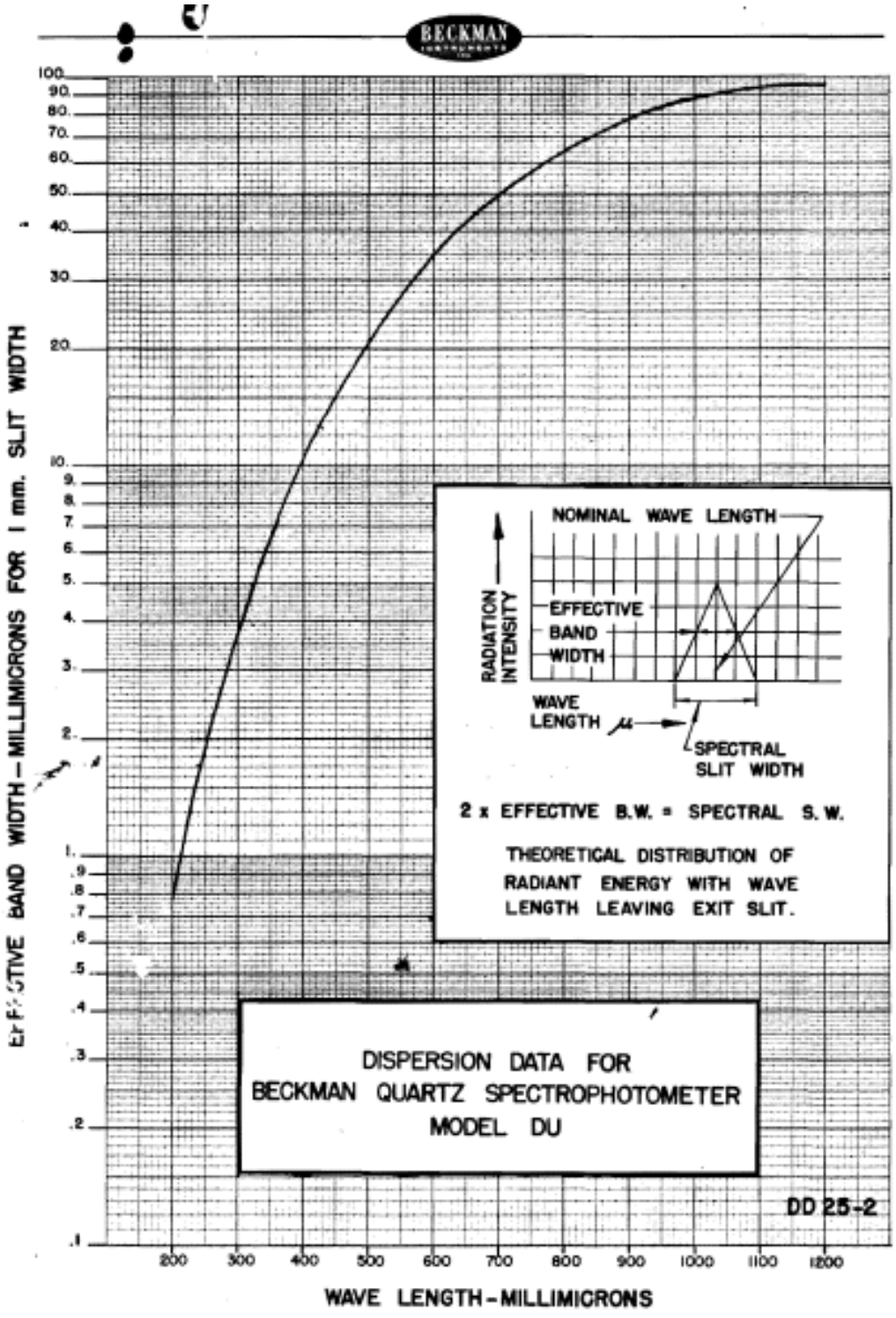

Figure 5.6: Bandwidth versus wavelength for 1 mm slit opening (Beckman Instruments)

5.5.2 Holmium Oxide Glass Measurements

A standard practice is to use holmium oxide glass to calibrate the monochromator because holmium oxide has many sharp, well documented, optical peaks in the visible range and some peaks in the NIR range. Figure 5.7 shows the spectral transmittance profile measured by the Cary 5000. The BAI-IS system is able to reproduce almost the same profile in the range of 380 nm to 1100 nm. For clarity, Figure 5.8 shows the comparison of the peak profiles in the visible range.

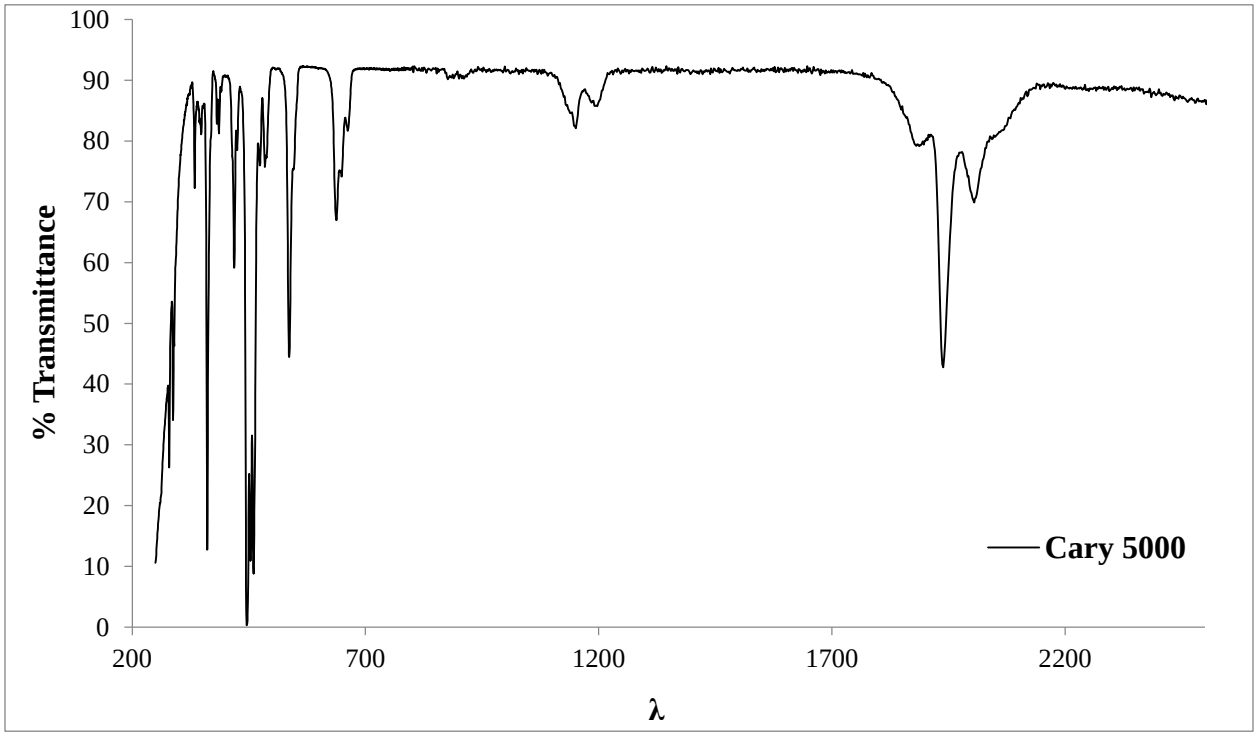

Figure 5.7: Spectral transmittance of holmium oxide glass measured by Cary 5000

Figure 5.8 shows that the BAI-IS is able to resolve the peaks in the visible range and has reasonable resolution in the NIR range. However, no sensible signal was obtained beyond 1100 nm. So peaks beyond 1100 nm were not resolved.

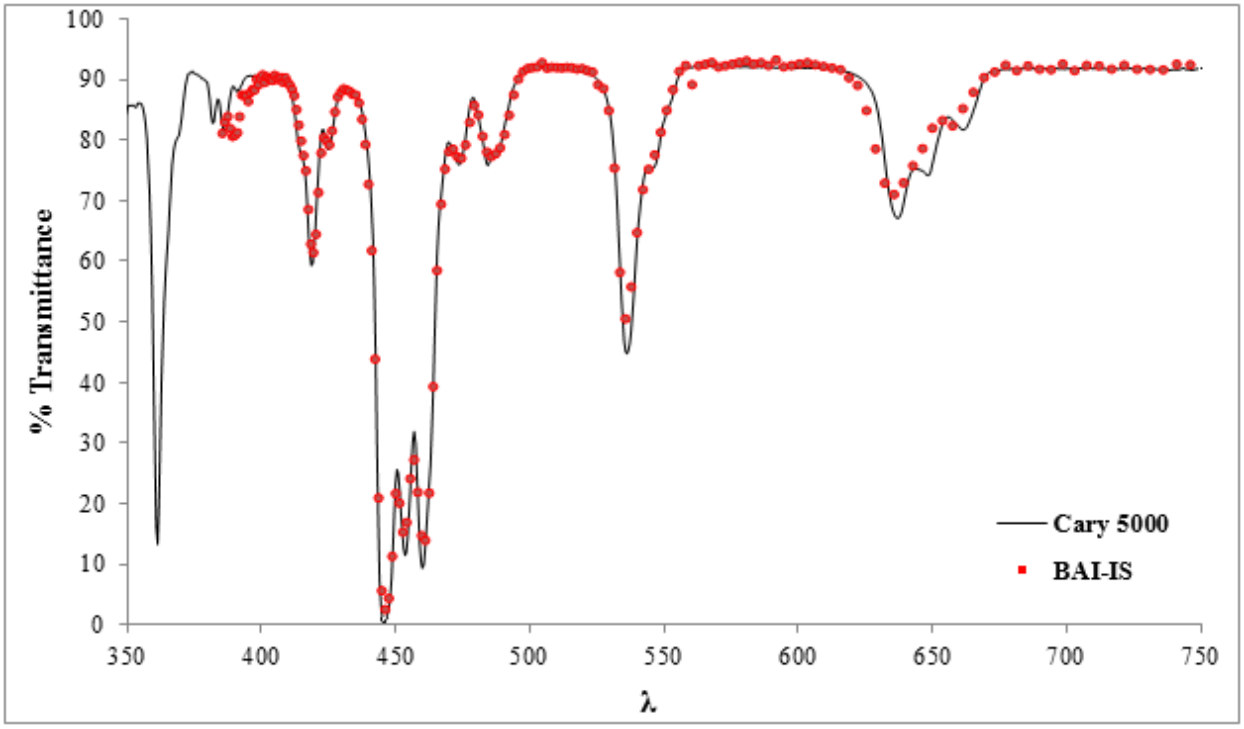

Figure 5.8: Comparison of spectral transmittance measurement of holmium oxide glass using Cary 5000 spectrophotometer (line) and BAI-IS (points) 386 – 750 nm

5.5.3 Ocean Optics Spectrometer Measurements

A spectrometer (Ocean Optics USB2000 Miniature Fiber Optic Spectrometer) was also used for spectral calibration of the monochromator. This spectrometer detects light intensity in the range of 200 to 1100 nm, which covers about 75% of the energy in the solar spectrum. This device is very useful as it gives an intensity profile in the detector range. When used with the BAI-IS system, the detector (i.e., the photo-detector shown in Figure 5.4) in the BAI-IS system was replaced by the Ocean Optics spectrometer system. Then, the measured intensity profile changes by varying the nominal wavelength and the slit width. A typical profile for a bandwidth is shown in Figure 5.9. As discussed in Section 5.5.1, this distribution profile would be a perfect triangle if the optical system of the monochromator were perfect.

The profile shown in Figure 5.9 provides very useful information for monochromator calibration. First, the wavelength at peak intensity is the nominal wavelength. Second, the nominal spectral bandwidth is approximately the bandwidth at the profile half height. Therefore, the relationship between the stepper motor positioning and the two control parameters of monochromator can be determined through measurements using various combinations of these two control parameters.

Using this approach, it has been confirmed that the monochromator is functional within the wavelength range of 380 to 1050 nm covered by the Ocean Optics USB2000 spectrometer.

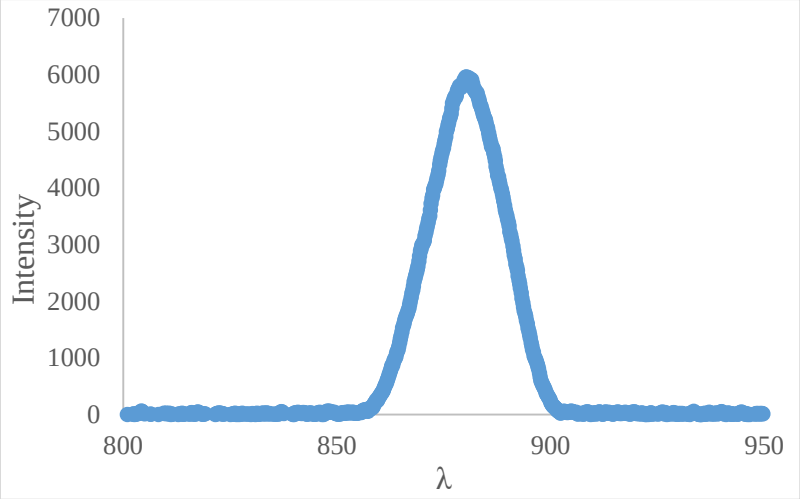

Figure 5.9: A typical light intensity profile within a bandwidth

5.5.4 Calibration of Nominal Wavelength

The nominal wavelength is controlled by a stepper motor that turns the prism. Light of different wavelengths is refracted differently and exits the prism at different angles. As the stepper motor turns, different wavelengths pass through the slit opening and exit the monochromator. With the Ocean Optics spectrometer system, a set of measurements has been done for various stepper motor/prism positioning. Figure 5.10 demonstrates intensity profiles measured at various wavelength with slit width = 0.1 mm.

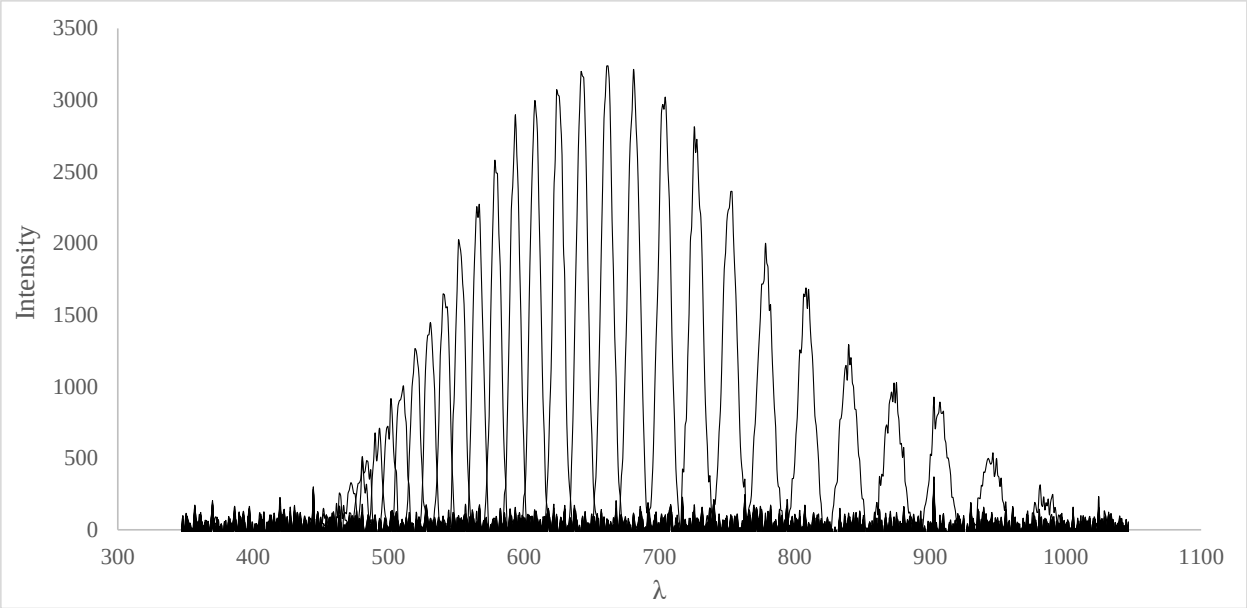

Figure 5.10: Intensity profiles measured for 0.1 mm slit width at different wavelength

5.5.4.1 Determining Nominal Wavelength

With the wavelength setting fixed (i.e., constant nominal wavelength), peak intensity should be at the chosen wavelength. However, measurements reveal that peak intensity consistently shifts toward higher wavelength as slit width increases. Figure 5.11 illustrates the shift of wavelength at peak intensity for a particular wavelength setting with various slit widths. Most likely, the shift of peak intensity toward higher wavelength is because the spectral irradiance of the QTH lamp peaks at close to 900 nm (Figure 5.5).

Therefore, the calibration of nominal wavelength is based on measurements with slit width of 0.1 mm, the narrowest slit recommended by the Beckman documentation. Figure 5.12 shows the new calibration curve. The reference point is at the limit switch. Curve fitting has been applied to the data and the resulting equation is shown in Figure 5.12. Any equation that relates the steps versus wavelength would work. In this case, the 6^{th} order polynomial gives the best estimate. Note that, if the limit switch location is moved, the curve will shift and need to be re-calibrated.

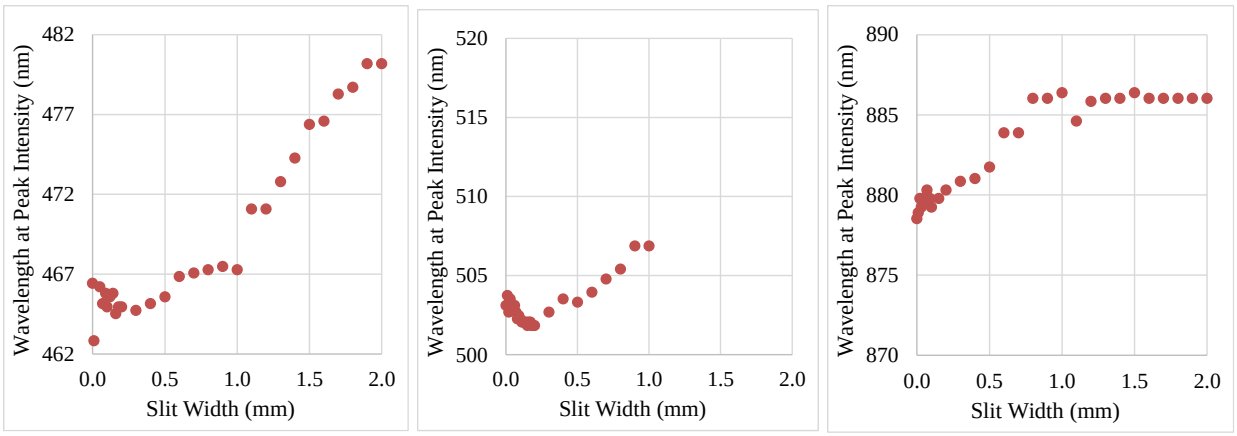

(a) Stepper Motor Steps = 57500 (b) Stepper Motor Steps = 55000 (c) Stepper Motor Steps = 45000

Figure 5.11: Wavelength at peak intensity shifts as slit width changes

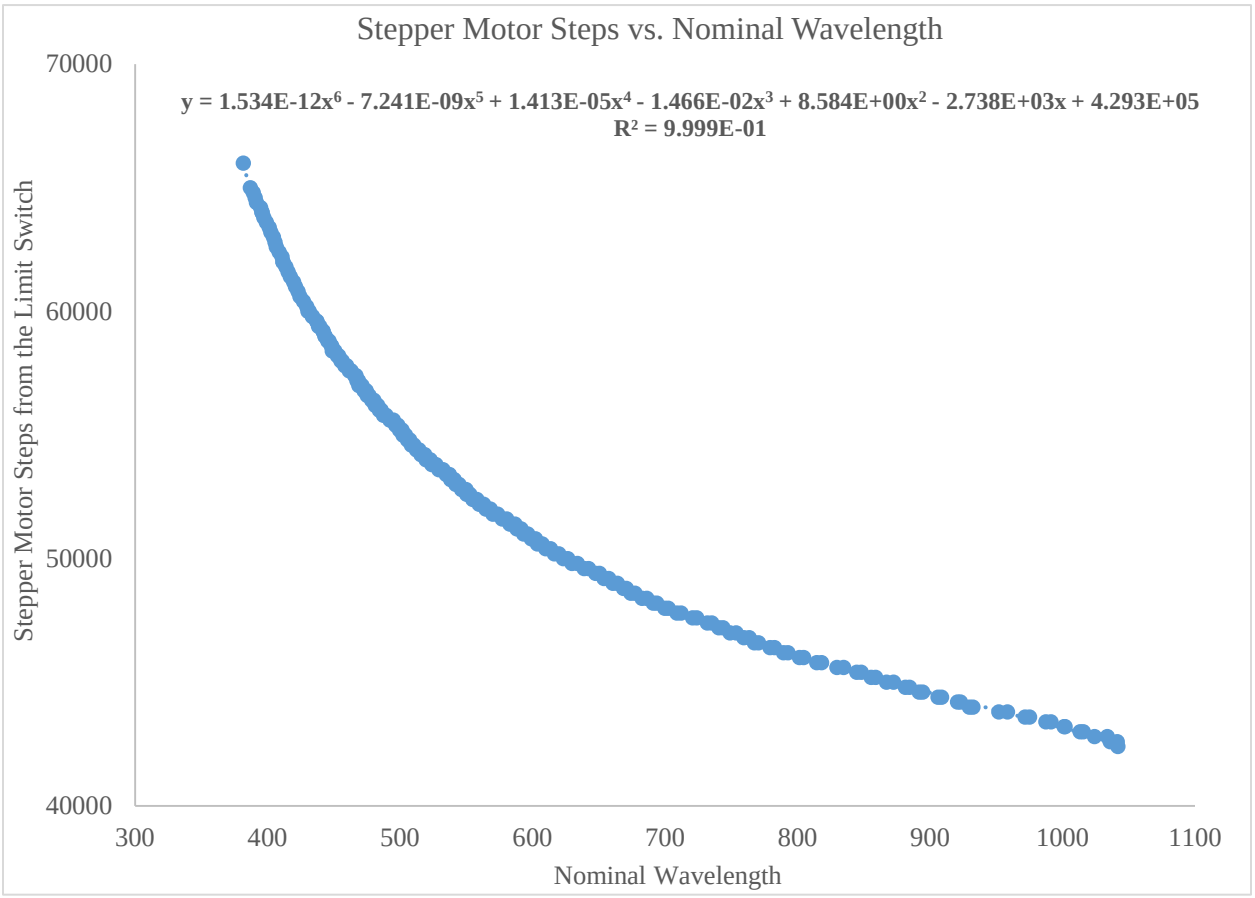

Figure 5.12: Calibration curve of stepper motor steps vs. nominal wavelength

5.5.5 Calibration of Nominal Spectral Bandwidth

The Ocean Optics spectrometer measurements can also be used to validate the relationship of slit width versus spectral bandwidth at a specific nominal wavelength described in the Beckman documentation (see Equation (5.2) and Figure 5.6). For example, the nominal wavelength in a measurement (e.g., Figure 5.9) is the wavelength corresponding to the peak intensity. Then, the bandwidth can be calculated for a given slit opening with Figure 5.6 and the slit equation (i.e., Equation (5.2)). The calculated bandwidth is compared and should be equal to the bandwidth at half height of the measured profile. Based on measured intensity profiles, it has been verified that Equation (5.2) and Figure 5.6 are valid. Note that slit width can be read visually from a graduated dial attached to the slit width adjustment shaft of the monochromator. Figure 5.13 shows a fitted curve for stepper motor position versus the slit width.

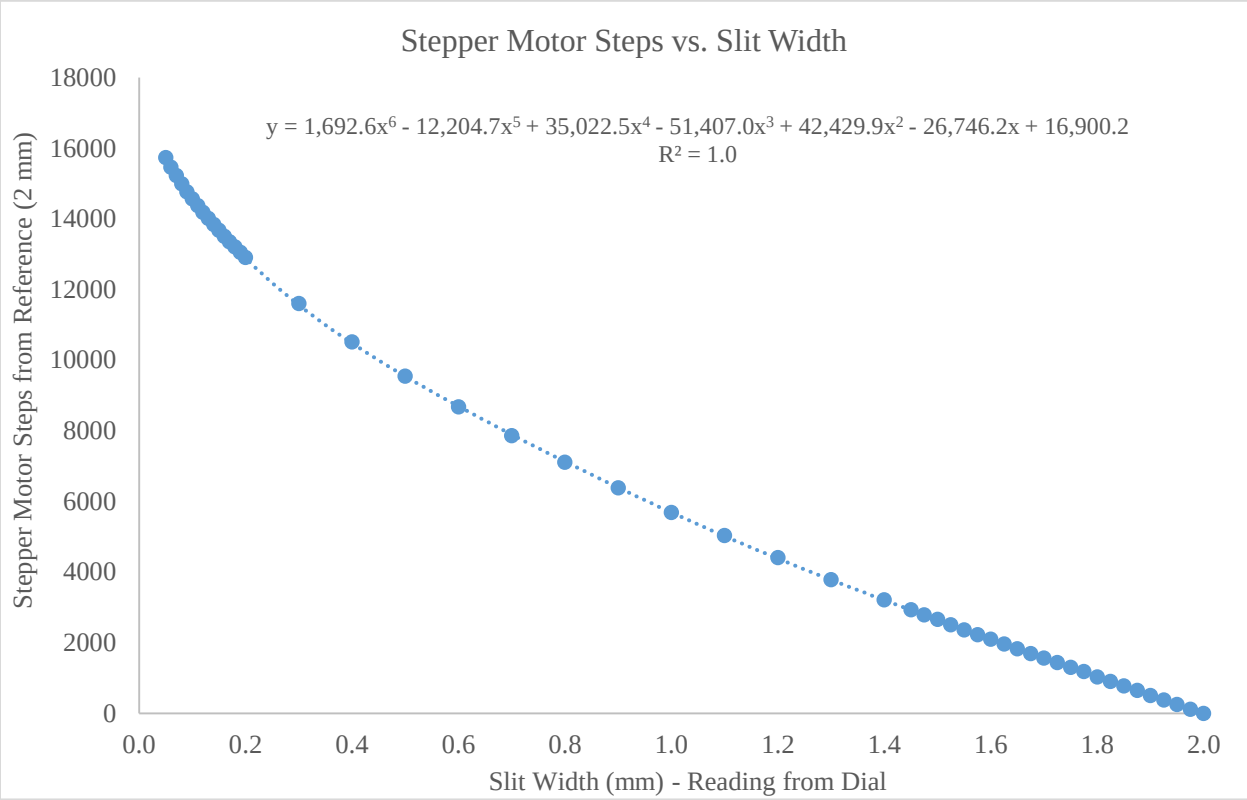

Figure 5.13: Number of stepper motor steps vs. slit width

5.6 Measurement Uncertainties

All measurements are subject to uncertainties. The uncertainty must be considered or estimated in order to interpret data correctly and draw meaningful conclusions. Determining the uncertainty of a measurement involves identifying the major process and variables and assessing their effect on the measurement. Per ASTM E903-96, random errors in solar optical property measurements are associated with signal detection and electronic processing. Errors are also introduced by the geometry of the integrating sphere system and the distribution of scattered or reflected light. Experience has shown that high level of accuracy is relatively difficult to achieve and depends strongly on operator skill, experience, and care, as well as on equipment design and maintenance. Based on ASTM E903-96 the following sections discuss random and systematic errors associated with measurements made using an integrating sphere.

5.6.1 Random Errors

The random uncertainty in the spectral properties measured with an integrating sphere is due almost entirely to the signal-to-noise (S/N) ratio of the detector–amplifier system. When the S/N ratio is high (e.g., usually in the visible range), the repeatability of measurements made on the same sample is usually better than ±0.5%. At the wavelengths near detector's spectral range limits where the S/N ratio is low, usually in the near infrared region, the uncertainty due to this source may exceed ±2.0%. These uncertainties can be reduced significantly by scanning for longer times at each wavelength. Carefully designed measurements can be repeatable to be within ±0.1%.

5.6.2 Systematic Errors

Simple integrating sphere theory (Goebel 1967) is based on four assumptions: (1) the sphere coating is uniform in reflectance over the entire inner surface of the sphere, (2) the sphere coating is a perfectly Lambertian reflector, (3) none of the reflected flux is lost out of the apertures of the

sphere, and (4) none of the reflected flux reaches the detector without being reflected at least twice by the sphere wall.

No integrating sphere design can completely realize these assumptions. However, they can be approached in a well-designed integrating sphere so that the resulting errors are small. Most commercially available integrating sphere reflectance attachments (e.g., Cary 5000) measure reflectance/transmittance factor, which is the ratio of the flux reflected/transmitted by a sample into a hemisphere to that reflected/transmitted by a completely reflecting/transmitting and perfectly diffusing surface under identical conditions of irradiation and collection. It does not measure the reflectance which is the ratio of the flux reflected into a complete hemisphere to the flux incident on the sample. The advantage of measuring reflectance/transmittance factor rather than reflectance/transmittance is that the ratio of the fluxes reflected by the sample and the comparison standard is automatically corrected for the major portion of the errors due to non-ideal characteristics of the sphere.

5.6.3 Uncertainties of Flat Fabric Property Measurements Using Cary 5000 Spectrophotometer

Uncertainty in integrating sphere measurements may be attributed to several errors as documented in ASTM E903-96. The Cary 5000 is a commercially designed spectrophotometer and uses 0% and 100% baseline calibration procedures (ANSI / ASHRAE 74-1988). Based on previous studies (Halder 2007, Kotey 2009), the equipment has an accuracy of ±0.1% or well below ±0.001 at 95% confidence level for raw measurements. A more significant uncertainty is attributed to the conversion of spectral data to solar properties. Since solar properties were obtained based on the ratio of sample/reference signals, uncertainties in both signals are correlated and tend to cancel, reducing the systematic error in measured properties (Chakroun et. al. 1993).

The most significant source of uncertainty for measuring flat fabric solar optical properties comes from the fabric non-uniformity (Section 2.3.3). The uncertainty due to fabric non-uniformity has been mitigated, if not eliminated, by determining and applying correction factors (Section 2.3.3.1).

5.6.4 Uncertainties of Pleated Drape Measurements Using the BAI-IS System

The BAI-IS system is custom-designed, and drape sample tests using the BAI-IS system is one of a kind measurement. This increases complexity of uncertainty analysis. The following are sources of uncertainty that have been considered for the BAI-IS components and measurement processes used in this research:

- Monochromator
    - wavelength selection
    - spectral bandwidth selection
- Experimental Setup
    - Internal Sample Reflectance error (ISR)
    - External Sample Reflectance error (ESR)
- Integrating Sphere Design
    - hot-spot error
- Data Processing
    - detectors, Phase Lock-in Amplifier (PLA), and DAQ
- Pleated drape sample
    - non-uniformity due to transmittance port seeing various pleat locations

5.6.4.1 Wavelength Selection Uncertainty

The nominal wavelength setting is controlled by changing the prism angle via linkages and a lead screw, which are driven by a stepper motor. Due to backlash effect in the mechanical linkages and stepper motor, the same stepper motor position does not mean the same prism angle. To reduce, if not completely eliminated, the backlash effect, a limit switch has been installed to ensure the same initial reference position for each measurement.

5.6.4.2 Uncertainty Due to Changing Spectral Bandwidth

Nominal spectral bandwidth can be adjusted with the slit width. For a fixed slit width, as discussed in Section 5.5, the bandwidth varies with the nominal wavelength. Based on Figure 5.6 and Section 5.5.1, Table 5.1 is generated and shows the slit widths required at various wavelength for a corresponding spectral bandwidth. The table shows that the BAI-IS system can have constant spectral bandwidths from 5 to 20 nm for the wavelength range of 400 to 1000 nm. However, keeping bandwidth constant requires a very narrow slit width at higher wavelength, leading to very low S/N ratio. Furthermore, adjusting the slit width multiple times during a test significantly increase the time required for measurements.

Table 5.1: Slit widths for corresponding nominal bandwidths at various wavelengths

WL (nm) = Norminal Wavelength								WE (nm) = Norminal bandwidth to be used for measureme								
WD (nm/mm) = Norminal bandwidth per 1 mm slit width								X (mm) = Actual slit width to be used at one wavelength								
WE(nm)	>>>	**1**	2	3	4	5	6	8	10	15	20	25	30	50	100	200
WL(nm)	*WD(nm/mm)*	X(mm)														
200	*0.78*	1.24														
215	*1*	0.96	1.96													
255	*2*	0.46	0.96	1.46	1.96											
285	*3*	0.29	0.63	0.96	1.29	1.63	1.96									
310	*4*	0.21	0.46	0.71	0.96	1.21	1.46	1.96								
325	*5*	0.16	0.36	0.56	0.76	0.96	1.16	1.56	1.96							
340	*6*	0.13	0.29	0.46	0.63	0.79	0.96	1.29	1.63							
355	*7*	0.10	0.25	0.39	0.53	0.67	0.82	1.10	1.39							
370	*8*	0.09	0.21	0.34	0.46	0.59	0.71	0.96	1.21	1.84						
380	*9*	0.07	0.18	0.29	0.40	0.52	0.63	0.85	1.07	1.63						
395	*10*	0.06	0.16	0.26	0.36	**0.46**	**0.56**	**0.76**	**0.96**	**1.46**	**1.96**					
495	*20*	0.01	0.06	0.11	0.16	**0.21**	**0.26**	**0.36**	**0.46**	**0.71**	**0.96**	1.21	1.46			
570	*30*		0.03	0.06	0.09	**0.13**	**0.16**	**0.23**	**0.29**	**0.46**	**0.63**	0.79	0.96	1.63		
635	*40*		0.01	0.04	0.06	**0.09**	**0.11**	**0.16**	**0.21**	**0.34**	**0.46**	0.59	0.71	1.21		
705	*50*			0.02	0.04	**0.06**	**0.08**	**0.12**	**0.16**	**0.26**	**0.36**	0.46	0.56	0.96	1.96	
770	*60*			0.01	0.03	**0.04**	**0.06**	**0.09**	**0.13**	**0.21**	**0.29**	0.38	0.46	0.79	1.63	
840	*70*			0.00	0.02	**0.03**	**0.05**	**0.07**	**0.10**	**0.17**	**0.25**	0.32	0.39	0.67	1.39	
915	*80*			0.00	0.01	**0.02**	**0.04**	**0.06**	**0.09**	**0.15**	**0.21**	0.27	0.34	0.59	1.21	
1030	*90*					**0.02**	**0.03**	**0.05**	**0.07**	**0.13**	**0.18**	0.24	0.29	0.52	1.07	
1200	*95*					0.01	0.02	0.04	0.07	0.12	0.17	0.22	0.28	0.49	1.01	2.07

Depending on the spectral properties of samples, non-constant bandwidth could affect the measurement results especially if the sample is spectrally selective. However, non-constant bandwidth does not have a significant effect here since fabrics are not spectrally selective.

For example, Figure 5.14 and Figure 5.15 show the spectral transmittance profiles measured, respectively for the holmium oxide glass (e.g., spectrally selective) and the red sheer fabric (e.g., a much smoother and typical profile for a fabric), using the BAI-IS system with various slit widths. The effect of slit width (and therefore bandwidth) on spectral transmittance is observable in the case of holmium oxide but not the red sheer fabric.

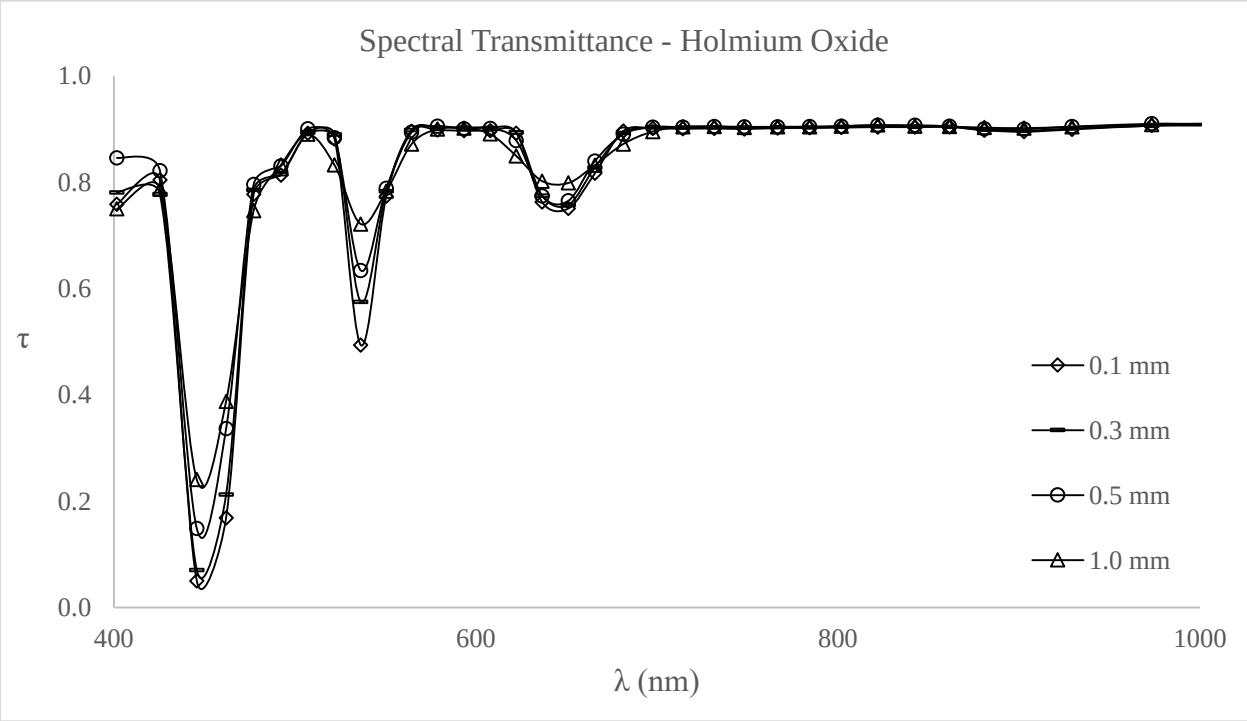

Figure 5.14: Spectral transmittance profiles of holmium oxide using BAI-IS with various slit widths

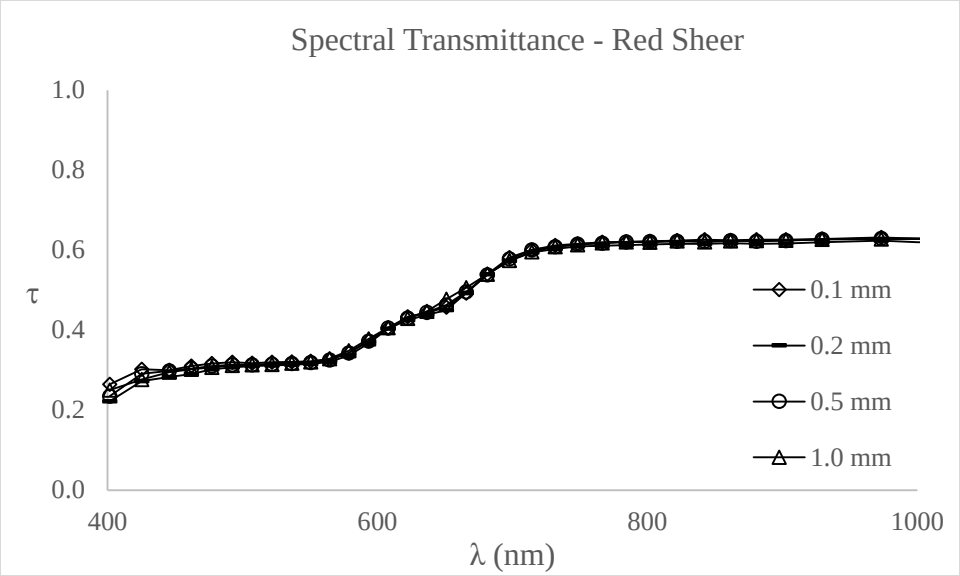

Figure 5.15: Spectral transmittance profiles of red sheer using BAI-IS with various slit widths

For the holmium oxide, the resulting weighted average (for each slit width) is 0.824 (0.1 mm), 0.829 (0.3 mm), 0.835 (0.5 mm), and 0.834 (1.0 mm). Similarly, for the red sheer fabric, the weighted averages are 0.481 (0.1 mm), 0.471 (0.2 mm), 0.478 (0.5 mm), and 0.478 (1.0 mm). These results show that the effect of slit/bandwidth on the weighted average is not significant even for the spectrally selective holmium oxide sample.

5.6.4.3 Internal and External Sample Reflectance Errors

BAI-IS transmittance measurements involve Internal Sample Reflectance (ISR) and External Sample Reflectance (ESR) errors that are caused by sample back reflectance (Milburn 1994). As shown in Figure 5.16 (a), some internally reflected ray leaving the sphere that would otherwise leave the sphere without sample blockage may now be reflected back into the sphere with the sample in place. As well, Figure 5.16 (b) shows that radiation transmitted through the sample (or from any surrounding structure) may be reflected by the sphere exterior and then by the back of the sample into the sphere.

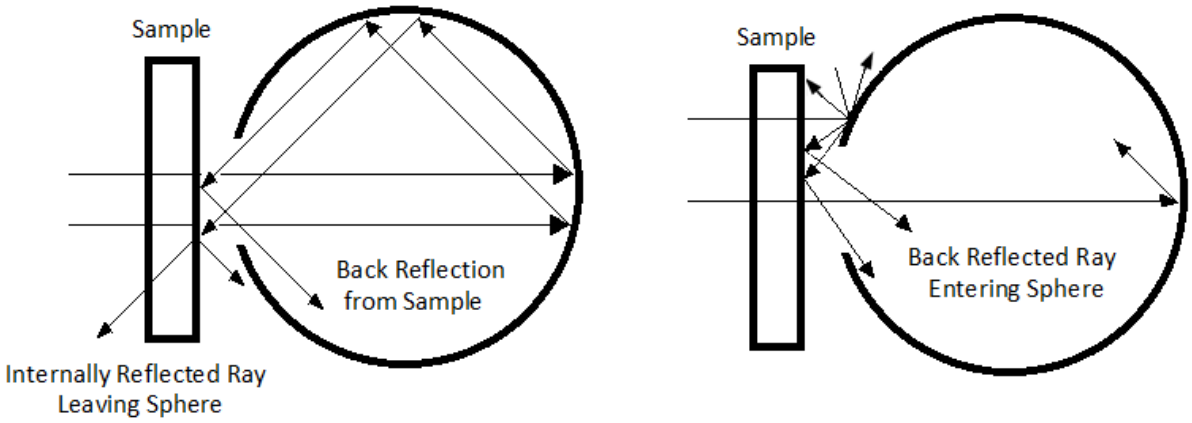

(a) ISR error caused by back reflectance (b) ESR error caused by back reflectance

Figure 5.16: Paths of radiation that cause ISR and ESR errors

The errors due to sample back reflectance may be significant. Milburn (1994) performed transmittance measurements of acrylic sample at 800 nm with various sample-to-sphere distance. The difference between two measurements could be more than 0.01 depending on how far the sample was away from the sample port. In order to minimize the difference, the sample is placed at least 12 cm away from the sample port.

5.6.4.4 Hot-Spot Error

A hot-spot is where the light source is first reflected inside the sphere as shown in Figure 5.17. The hot-spot error is caused by the overlap of the detector field-of-view (dashed lines in Figure 5.17) and the direct area of illumination. Generally the error is assumed small and ignored in measurements using integrating sphere. However, the hot spot moves with increasing incidence angle. A test shows that the hot spot effect is very large for incidence angles larger than 45° for the original baffle design. A new baffle (Figure 5.17 (b)) has been made and put in place to eliminate any direct view of hot spot.

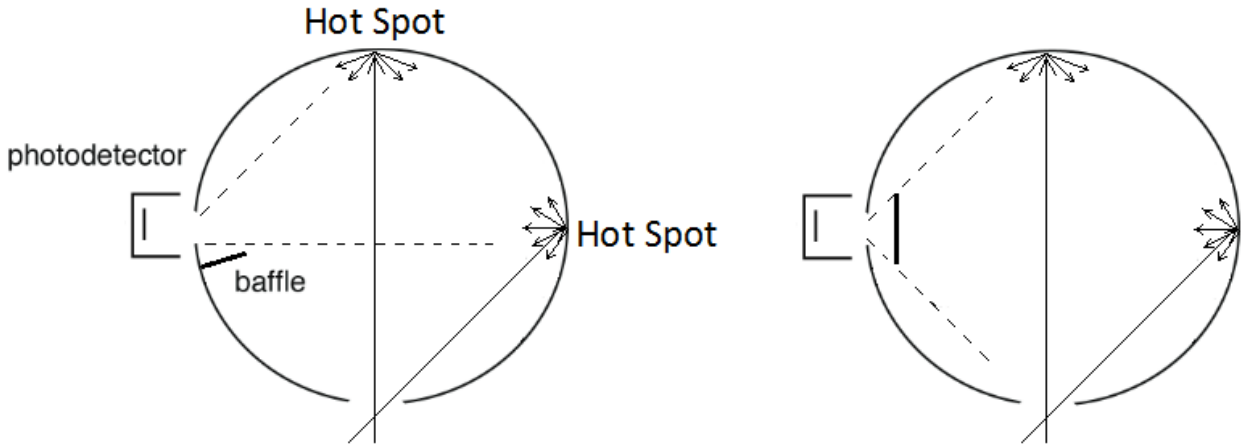

(a) Original baffle design (b) New baffle design

Figure 5.17: Comparison of the original and new designs of baffle to prevent hot-spot error

5.6.4.5 Data Processing System

Based on specifications given for the detector and electronic data processing systems, Halder (2007) performed an uncertainty analysis and reported a value of ±0.1% in solar transmittance for his sheer blind measurements. The ±0.1% was based on multiple-sample measurement. He recommended the number of measurements N ≈ 200 for $\lambda < 1000$ nm and N ≈ 400 for longer wavelengths.

Appendix E: Uncertainty Analysis includes an uncertainty analysis for the data processing system. The measurement uncertainty of a measurement can be high (i.e., > 10%) especially for low S/N cases. However, it can be greatly reduced by increasing sampling time and number. It has been estimated that the uncertainty can be reduced to within 1% with proper settings for the data processing system.

5.6.4.6 Pleated Drape Sample Non-Uniformity Uncertainty

Similar to the non-uniformity in the flat fabric sample (Section 2.3.3), pleated drape sample is an additional source of uncertainty. The projected view of a geometrically non-uniform sample on

the transmittance port of an integrating sphere may be different every time the sample is placed in front of the opening port. The degree of non-uniformity depends on the number of repeated pattern in the sample being "seen" by the opening. For example, in the case of a pleated drape sample, Figure 5.18 shows two possible projected views of the opening port on the sample. If the pleat size is relatively small, as shown in Figure 5.19, the port would see more pleats, and therefore a more uniform sample. In other words, the sample non-uniformity "disappears" when the opening port is relatively large.

Design constraints limit the port size to a maximum of 5% of the sphere surface area (Labsphere 2013). Having the port opening size fixed, the effect of sample uniformity depends the pleat size and folding ratio (Fr).

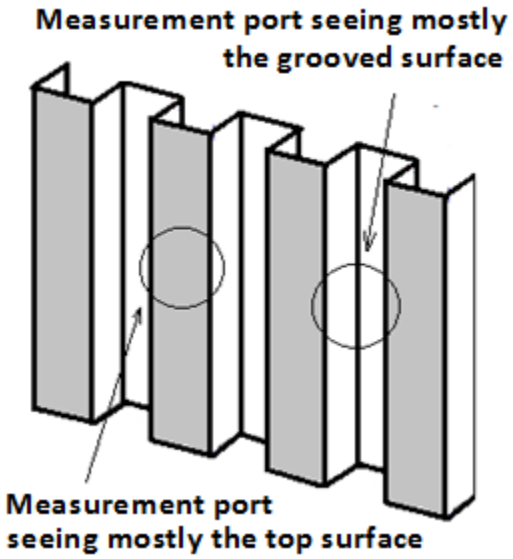

Figure 5.18: Transmittance port seeing mostly top (left) or grooved (right) surface of pleats

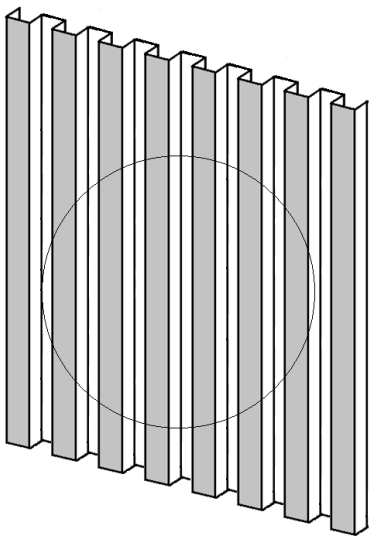

Figure 5.19: Transmittance port seeing several top and grooved surfaces

A set of tests has been performed to estimate the uncertainty in transmittance measurement of pleated drape samples using the BAI-IS system due to spatial non-uniformity of the samples. Fabrics used have openness ranging from the "Closed" to "Sheer" categories. The standard test method for solar transmittance of materials using an integrating sphere (ASTM E 903) is applied with one modification. Instead of one sample reading, six sample readings are taken, each at a slight shift in sample location. All tests use rectangular pleating profile with a pleat spacing (S) of 2 cm. The test matrix is shown in Table 5.2. Each test is performed at nominal wavelength of 401 nm, 536 nm, 651 nm, 784 nm, and 1025 nm to cover the spectral range of interest.

Table 5.2: Test matrix for pleated drape sample non-uniformity tests

Fabric ID	Fabric Name	Fr = 2	Fr = 3
0-3	Orange0001	$\theta = 0°, 30°$	
0-4	Rough_Medium0001	$\theta = 0°$	
0-7	Red0002 (Sheer)	$\theta = 0°, 30°$	$\theta = 0°, 30°$

Six sample readings of each test taken in the modified test procedures are recorded and averaged (AVG). Standard deviation (STD) for each set of six readings are calculated. Results are shown in Table 5.3. The uncertainty in the sample reading due to sample non-uniformity can be estimated by doubling STD or the ratio STD/AVG in terms of percentage (STD/AVG%).

As shown in Table 5.3, the STD/AVG ranges from 0.05% to 1.8%. Then 2 times STD would range from 0.1% to 3.6%. So the uncertainty due to sample non-uniformity could be significant and added to the overall uncertainty based on the results discussed above. However, except for one case, the uncertainty is always the highest at λ = 401 nm and generally decreases with increasing λ. Based on the typical spectral irradiance profile (for a 1000W FEL lamp) shown in Figure 5.5, the profile peaks at about 900 nm and decreases exponentially toward short wavelengths. This observation may imply that the uncertainty due to the non-uniformity is dominated by the uncertainty due to low S/N ratios (as discussed in Section 5.6.1).

Although the measurement uncertainty may be high for λ = 401 nm, it is generally insignificant at higher wavelengths. Therefore, the uncertainty due to the pleated drape non-uniformity can be ignored for the weighted average results.

5.7 Chapter Summary

Results of this experiment are presented in CHAPTER 6.

Table 5.3: AVG and STD of measured relative intensities at various wavelengths

Fabric ID	θ	FR	λ (nm)	AVG	STD	STD/AVG (%)
0-7	0°	2	401	3.077	0.018	0.571
			536	3.354	0.002	0.052
			651	4.792	0.006	0.134
			784	3.244	0.006	0.171
			1025	3.855	0.005	0.126
		3	401	1.198	0.011	0.893
			536	2.041	0.008	0.368
			651	3.510	0.010	0.295
			784	2.998	0.005	0.173
			1025	3.747	0.007	0.184
	30°	2	401	1.148	0.007	0.608
			536	1.661	0.007	0.451
			651	3.046	0.018	0.603
			784	2.729	0.010	0.373
			1025	3.455	0.018	0.515
		3	401	0.855	0.010	1.113
			536	1.027	0.019	1.813
			651	1.840	0.027	1.468
			784	1.945	0.012	0.629
			1025	2.329	0.008	0.354
0-4	0°	2	401	2.029	0.036	1.773
			536	1.246	0.005	0.362
			651	2.025	0.008	0.386
			784	1.645	0.005	0.314
			1025	2.288	0.007	0.316
0-3	0°	2	401	0.495	0.002	0.410
			536	0.511	0.002	0.337
			651	1.908	0.002	0.127
			784	1.727	0.002	0.113
			1025	1.523	0.002	0.122
	30°	2	401	1.513	0.018	1.179
			536	0.405	0.003	0.813
			651	1.412	0.007	0.500
			784	1.416	0.008	0.575
			1025	1.719	0.010	0.564

CHAPTER 6
RESULTS AND DISCUSSIONS

6.1 Presentation of Results

Based on the test matrix presented in Section 5.1, results of τ_{bt} have been generated using both of the pleated drape models presented in CHAPTER 4. The current chapter presents and compares the results of the pleated drape models with the BAI-IS measurements presented in CHAPTER 5. Recall that there are twenty fabrics selected for the test (Section 5.1.3). These fabrics are itemized and listed in column (1) of Table 6.1. The next four columns of Table 6.1 summarize all table and figures (of the twenty selected fabrics) used for presenting and comparing the predicted and measured results.

Column (2) of Table 6.1 lists, for each of the 20 fabrics, the tables (Table 6.2 to Table 6.21) that present both predicted (abbreviated to P) and measured (abbreviated to M) τ_{bt} based on the test matrix (Section 5.1): Fr (Flat, 1.5, 2.0, 2.5), θ (0°, 10°, 20° ... 60°), and pleating profiles (rectangular – abbreviated to R and triangular – abbreviated to T). Results are grouped by PR, PT, MR, and MT where the abbreviations indicate the result type (P or M) and the pleating profile (R or T). For instance, PR designates predicted results based on a rectangular profile. Similarly, MT refers to measured results with a triangular profile.

Column (3) of Table 6.1 lists the corresponding figures comprising four plots each and showing the matrix results for the four groups: (a) PR, (b) PT, (c) MR, and (d) MT. The effect of Fr and θ on τ_{bt} is best seen through observation of the column (3) figures.

Then results are rearranged in various plots for further examination. These plots are assembled into figures that are listed in columns (4) and (5) of Table 6.1. Each of the column (4) figures has seven plots that compare predicted and measured (P vs M) results of different pleating profiles and various Fr. The seven comparisons are for flat (Fr = 1.0), R 1.5, R 2.0, R 2.5, T 1.5, T 2.0, and T 2.5 where R and T stand for rectangular and triangular, respectively, and the numerals indicate the Fr values. Plots in the column (4) figures allow direct comparison between the results of pleated drape model predictions and BAI-IS measurements. Similarly, column (5) figures have six plots each, three for the pleated drape model and three for measurements. These plots compare results of the rectangular and triangular profiles (i.e., R vs T). There are only six plots in each of these figures since Fr = 1 is flat for both profiles. Plots in column (5) figures are best for examining the effect of pleating profiles.

Table 6.1: Summary of tables and figures

Fabrics	All Predicted and Measured τ_{bt} Listed and Plotted in 4 Groups (PR, PT, MR, MT)		P vs M	R vs T
(1)	(2)	(3)	(4)	(5)
#01 2600BX_Sheeting	Table 6.2	Figure 6.1	Figure 6.2	Figure 6.3
#08 DarkBrown01	Table 6.3	Figure 6.4	Figure 6.5	Figure 6.6
#10 DecolineLining	Table 6.4	Figure 6.7	Figure 6.8	Figure 6.9
#13 GreyOpen01	Table 6.5	Figure 6.10	Figure 6.11	Figure 6.12
#20 SheerBlack01	Table 6.6	Figure 6.13	Figure 6.14	Figure 6.15
#22 SheerWhite01	Table 6.7	Figure 6.16	Figure 6.17	Figure 6.18
#24 White05	Table 6.8	Figure 6.19	Figure 6.20	Figure 6.21
#26 BlueSoft01	Table 6.9	Figure 6.22	Figure 6.23	Figure 6.24
#27 Yellow05	Table 6.10	Figure 6.25	Figure 6.26	Figure 6.27
#64 FashionBlack01	Table 6.11	Figure 6.28	Figure 6.29	Figure 6.30
#66 FashionLight01	Table 6.12	Figure 6.31	Figure 6.32	Figure 6.33
#68 GreenOpen01	Table 6.13	Figure 6.34	Figure 6.35	Figure 6.36
#71 RoughRed	Table 6.14	Figure 6.37	Figure 6.38	Figure 6.39
#72 Thin01	Table 6.15	Figure 6.40	Figure 6.41	Figure 6.42
#73 Thin02	Table 6.16	Figure 6.43	Figure 6.44	Figure 6.45
#75 Thin04	Table 6.17	Figure 6.46	Figure 6.47	Figure 6.48
#77 WhiteOpen01	Table 6.18	Figure 6.49	Figure 6.50	Figure 6.51
#92 PMB01	Table 6.19	Figure 6.52	Figure 6.53	Figure 6.54
#94 PMBOpen	Table 6.20	Figure 6.55	Figure 6.56	Figure 6.57
#95 PMY	Table 6.21	Figure 6.58	Figure 6.59	Figure 6.60

6.2 Effects of Fr, θ, Pleating Profiles, and Fabric Properties on τ_{bt}

In order to aid the understanding of the results presented in tables and figures listed in Table 6.1, general discussions on the effects of test variables are offered. Such discussions also establish terms that are used to facilitate discussions for individual fabric and any further analysis. These effects are:

- Blockage Effect (Due to Increasing Fr)
- Enclosure Effect (Due to Increasing Fr)
- Global θ Effect (Due to Varying θ)
- Local θ Effect (Due to Varying θ and Pleating Profile)
- Combined Effect of Fr, θ, and Pleating Profile
- Effects of Fabric Solar Optical Properties
    - Insensitivity Effect
    - Effect of A_o on Blockage and Global θ Effects

6.2.1 Blockage Effect (Due to Increasing Fr)

Pleated drapes have a Fr greater than one. Drapes with higher Fr have more fabric material present in the path of radiation than those with lower Fr. Therefore, in general, increasing Fr reduces τ_{bt}. So one effect of increasing Fr is called the "blockage" effect.

Regardless the pleating profile or θ, the blockage effect is a general effect that τ_{bt} reduces as Fr increases. This trend can be observed in the results of most fabrics (i.e., column (2) tables and column (3) figures of Table 6.1). As an example, Table 6.5 and Figure 6.10 show the results for Fabric #13, and the trend of τ_{bt} reduces with increasing Fr is observed everywhere on Figure 6.10 with a few exceptions at low θ for rectangular pleating (i.e., PR and MR). With the few exceptions, the blockage effect is still present. However, it is offset by the enclosure effect.

6.2.2 Enclosure Effect (Due to Increasing Fr)

Another effect of increasing Fr is called the "enclosure" effect. Consider incident beam radiation on a flat fabric, the properties pertaining to the layer are τ_{bb}, τ_{bd}, and ρ_{bt}. Note that all reflected radiation is considered diffuse. Also, for any pleating profile, Fr dictates the width of that pleating profile. As Fr increases from 1 (flat), the drape starts to form pleats (an enclosure). Then a portion of the ρ_{bt} component encounters the pleated fabric. So another effect of Fr is that the pleated drape layer traps more reflected radiation as Fr increases (deeper pleats) or less as Fr decreases. One can relate high Fr to an integrating sphere with a small opening or vice versa where the opening is the fictitious surface considered in the pleated drape model (see Figure 4.2, Figure 4.3, and Table 4.1).

The enclosure effect may offset the blockage effect in that one (enclosure) effect increases τ_{bt} while the other (blockage) decreases it. Intuitively, τ_{bt} is expected to decrease with increasing Fr. This is true for most cases except for fabrics with high reflectance. The higher the reflectance, the stronger the radiation field in the enclosure (e.g., integrating sphere's highly reflecting surface). Furthermore, transmittance of a fabric allows the trapped radiation to be transmitted. So, in theory, the strongest enclosure effect is when $\rho = 0.5$ and $\tau = 0.5$. With a strong enough enclosure effect, it could dominate and override the blockage effect. In such cases, τ_{bt} at higher Fr layer can exceed τ_{bt} at lower Fr.

The best example for illustrating this effect is Fabric #10 (see Table 6.4 and associated figures). The enclosure effect shows up in both the predicted results and the measured results of Fabric #10.

6.2.3 Global θ Effect (Due to θ)

The term "global" indicates that the window normal is the reference for specifying the incident angle. Also, the term "global" is added to exclude the effect that pleating profiles have on local

incidence angles. In general, the effect of increasing (global) θ is similar to the blockage effect. The higher θ, the more the blockage (to the incoming radiation). And τ_{bt} approaches zero as θ increases.

For example, based on the results of rectangular pleating profile shown in Figure 6.10 (a) and (c), τ_{bt} reduces with increasing (global) θ. This trend is more evident for high Fr and at high θ. Then, for the triangular pleating profile, the change in pleating profile alters the "local" θ, which in turn affects the general trend at lower θ.

6.2.4 Local θ Effect (Due to θ and Pleating Profile)

The term "local" describes how pleating profiles change the local angle of incidence, which in turn affects the general trend of increasing global θ. So, as global θ increases from 0°, the local θ may increase or decrease.

For example, consider a right-angle triangular profile (i.e., triangular profile with Fr = 1.414). At normal incidence (i.e., global θ = 0°), solar radiation is striking everywhere on the fabric surface at an angle (local θ) of 45°. Then at an incidence angle of θ = 45°, local θ is 0° for all incident radiation, and the right-angle triangular profile acts the same as the square pleats with global θ = 0°. So, one can expect maximum effective layer transmittance at θ = 45° (instead of at the normal incidence, θ = 0) for the right angle triangle pleating profile.

As a result, while the maximum τ_{bt} for the rectangular pleating profile with a fixed Fr is always at θ = 0, the incident angle at which the maximum τ_{bt} is measured or predicted can range from 0° to about 40° for a triangular pleated layer. This is termed the local θ effect. As an example, see Figure 6.10 (b) and (d).

6.2.5 Combined Effects of θ, Fr, and Pleating Profile

All variables affect τ_{bt}, and their effects are not independent of each other. A special case of the local θ effect for rectangular pleated drapes is that, at normal incidence (i.e., θ = 0), the local θ is either 0° or 90° regardless of Fr. As a result, increasing Fr has a relatively weak effect on τ_{bt} in this case. This is because most solar radiation needs to penetrate only one layer of fabric to enter the room at normal incidence. As θ increases, local θ everywhere moves away from 0° and 90°, and the effect of increasing Fr becomes stronger as well due to the consequent multiple layer transmission. Take Figure 6.10 (a) and (c) as examples. The (vertical) range of τ_{bt} for various Fr is the smallest at θ = 0. The vertical span lengthens as θ increases. In other words, the blockage effect (i.e., due to increasing Fr) is stronger at high θ than at low θ.

For the triangular pleating profile, as shown in Figure 6.10 (b) and (d), the resulting τ_{bt} range for various Fr is the narrowest near θ = 20°. The increased τ_{bt} range at lower θ is due to the local θ effect, and the increased range at higher θ is due to the multiple layer transmission as discussed above for the rectangular pleating profile.

6.2.6 Effects of Fabric Properties

The extent of effects described above varies as these effects are further influenced by fabric properties. For instance, a low transmitting fabric would not experience a strong blockage effect or the θ effect (both global and local). Similarly, a fabric with low ρ would have a weak enclosure effect regardless of its transmittance. So the lower the solar optical properties of a fabric, the weaker the discussed effects.

6.2.6.1 Insensitivity Effect

The term insensitivity effect is used to describe cases where fabrics with low solar optical properties are insensitive to change in variables. Regardless of the changes in variables, the range

of measured or predicted τ_{bt} is always between 0 and τ_{bt} of a fabric (or, in a few cases, slightly higher due to the enclosure effect). So, any change would be small when the possible range is small (i.e., for low transmitting fabrics).

The best example for illustrating the insensitivity effect is Fabric #1 2600Bx Sheeting (τ_{bb} = 0.0146, τ_{bt} = 0.0258, ρ_{bt} = 0.0418). As shown in Figure 6.1, Figure 6.2, and Figure 6.3, the results are insensitive to any variables due to very low solar optical properties.

6.2.6.2 On Combined Effect of Variables

As discussed in Section 6.2.5, the blockage effect (i.e., due to increasing Fr) is more evident at high θ. The blockage effect is also important at low θ for the triangular pleating profile. Note that the extent of blockage effect also depends strongly on A_o. For example, compare Fabric #13 (Figure 6.10) to Fabric #20 (Figure 6.13) and Fabric #24 (Figure 6.19). Fabric #20 (A_o = 0.3451) experiences a stronger blockage effect than Fabric #13 (A_o = 0.1919). And the blockage effect is weaker for Fabric #24 (A_o = 0.0006). Therefore, the extent of blockage effect depends strongly on A_o. Note that the blockage effect mainly affects the τ_{bb} component. So, as A_o decreases and as the τ_{bd} component becomes dominant, the blockage effect diminishes.

Table 6.2: #01 2600BxSheeting – calculated and measured τ_{bt} for various θ and Fr

#01 2600BxSheeting (τ_{bb} = 0.0146, τ_{bt} = 0.0258, ρ_{bt} = 0.0418)														
	Pleated Drape Models (P)							BAI-IS Measurements (M)						
		Rectangular (R)			Triangular (T)				Rectangular (R)			Triangular (T)		
θ	Flat	1.5	2.0	2.5	1.5	2.0	2.5	Flat	1.5	2.0	2.5	1.5	2.0	2.5
0	0.026	0.024	0.023	0.022	0.011	0.006	0.004	0.038	0.029	0.019	0.020	0.017	0.011	0.012
10	0.025	0.021	0.019	0.016	0.011	0.007	0.005	0.038	0.027	0.019	0.017	0.017	0.011	0.012
20	0.023	0.018	0.014	0.010	0.014	0.010	0.009	0.034	0.027	0.019	0.012	0.020	0.014	0.012
30	0.020	0.015	0.010	0.006	0.017	0.016	0.011	0.028	0.025	0.017	0.007	0.024	0.016	0.011
40	0.016	0.011	0.007	0.004	0.021	0.015	0.010	0.020	0.022	0.013	0.003	0.026	0.015	0.009
50	0.011	0.009	0.006	0.003	0.020	0.012	0.005	0.012	0.020	0.009	0.002	0.025	0.013	0.005
60	0.007	0.008	0.004	0.001	0.015	0.005	0.003	0.005	0.017	0.006	0.001	0.020	0.006	0.002

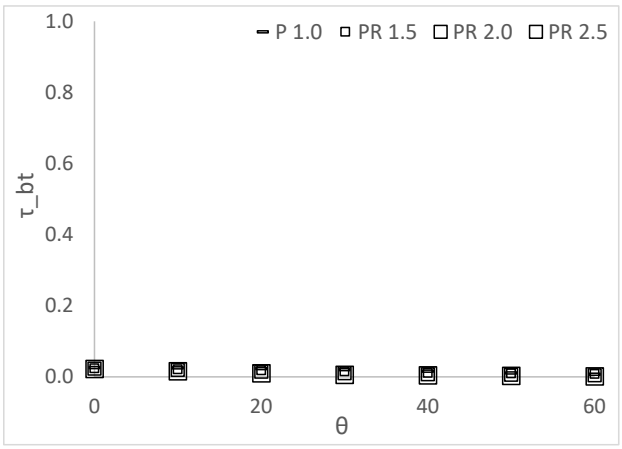

(a) Pleated Drape Model – Rectangular

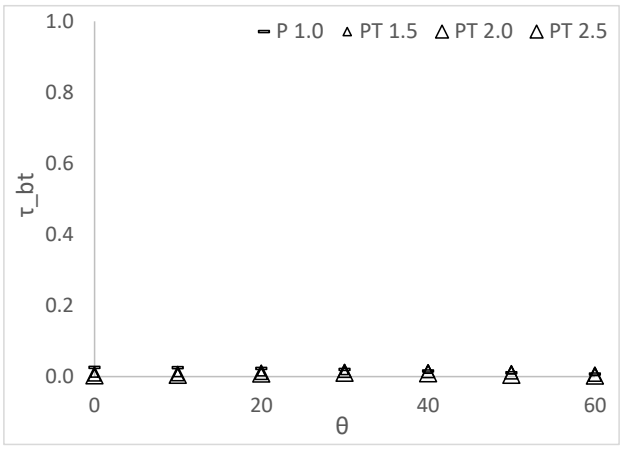

(b) Pleated Drape Model – Triangular

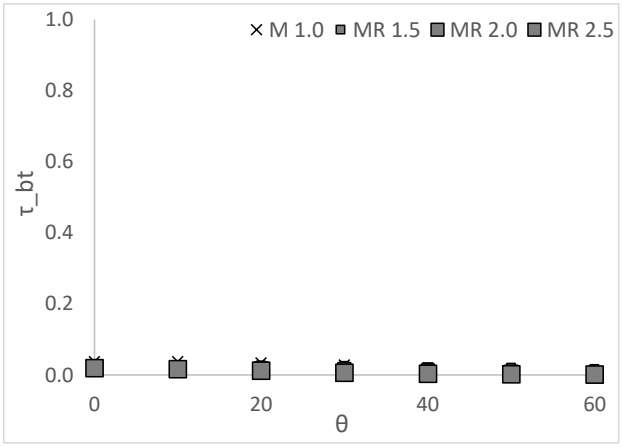

(c) BAI-IS Measurements – Rectangular

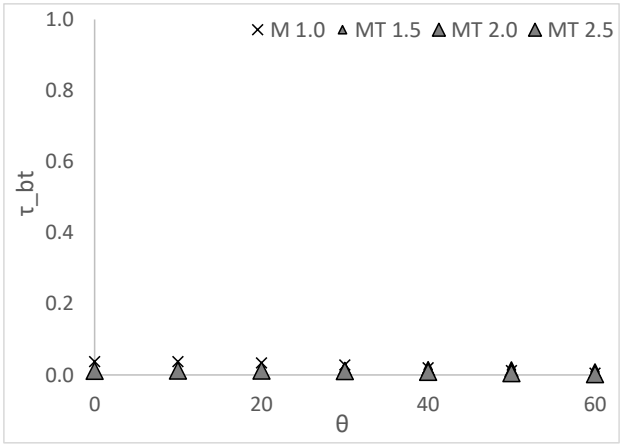

(d) BAI-IS Measurements – Triangular

Figure 6.1: #01 2600BxSheeting – calculated and measured τ_{bt} for various θ and Fr

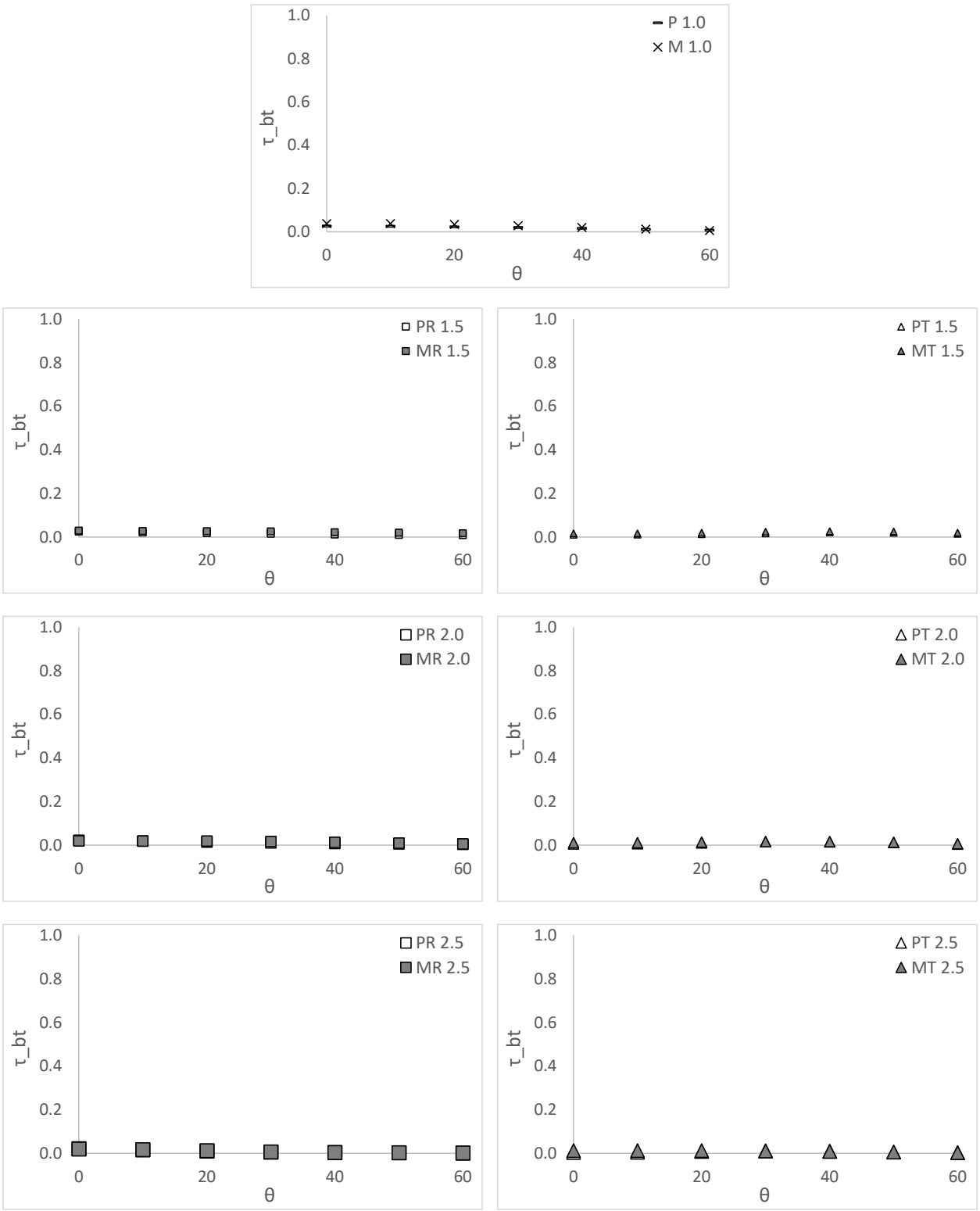

Figure 6.2: #01 2600BxSheeting – prediction vs measurement

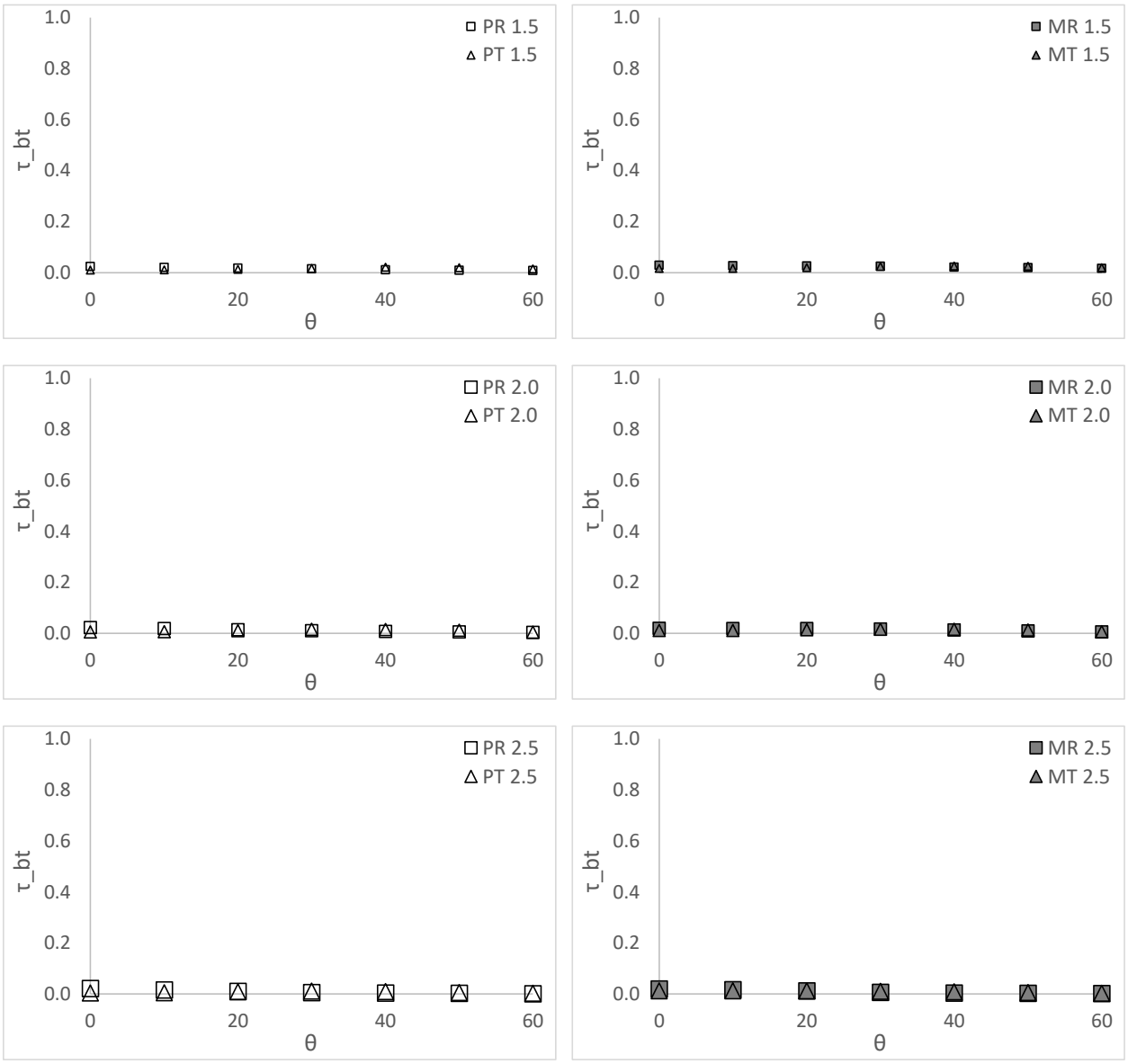

Figure 6.3: #01 2600BxSheeting – rectangular vs triangular profile

Table 6.3: #08 DarkBrown01 – calculated and measured τ_{bt} for various θ and Fr

#08 DarkBrown01 (τ_{bb} = 0.0000, τ_{bt} = 0.1156, ρ_{bt} = 0.2933)														
	Pleated Drape Models (P)							BAI-IS Measurements (M)						
		Rectangular (R)			Triangular (T)				Rectangular (R)			Triangular (T)		
θ	Flat	1.5	2.0	2.5	1.5	2.0	2.5	Flat	1.5	2.0	2.5	1.5	2.0	2.5
0	0.115	0.100	0.090	0.084	0.063	0.043	0.033	0.113	0.091	0.097	0.103	0.097	0.092	0.111
10	0.113	0.095	0.080	0.069	0.065	0.046	0.036	0.110	0.090	0.095	0.099	0.095	0.087	0.109
20	0.108	0.087	0.069	0.054	0.069	0.054	0.046	0.107	0.090	0.093	0.094	0.097	0.087	0.106
30	0.099	0.078	0.058	0.040	0.077	0.068	0.052	0.106	0.091	0.092	0.089	0.097	0.087	0.103
40	0.086	0.068	0.047	0.032	0.090	0.069	0.051	0.100	0.086	0.087	0.079	0.097	0.083	0.094
50	0.072	0.058	0.040	0.029	0.091	0.067	0.050	0.092	0.083	0.083	0.071	0.093	0.078	0.083
60	0.055	0.051	0.036	0.025	0.085	0.063	0.045	0.083	0.082	0.071	0.061	0.087	0.069	0.074

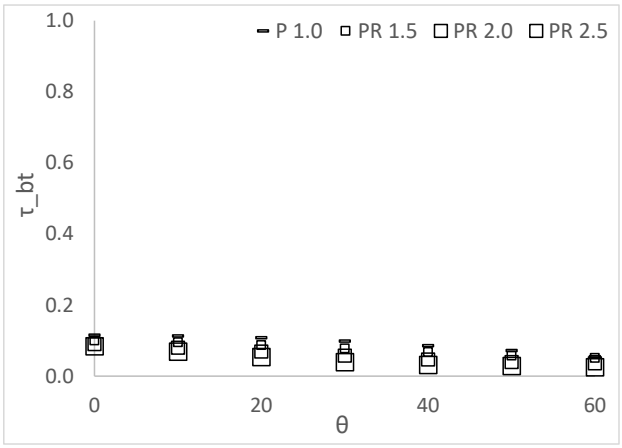

(a) Pleated Drape Model – Rectangular

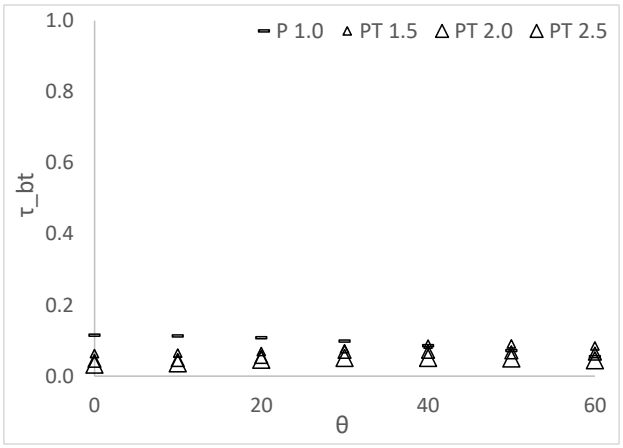

(b) Pleated Drape Model – Triangular

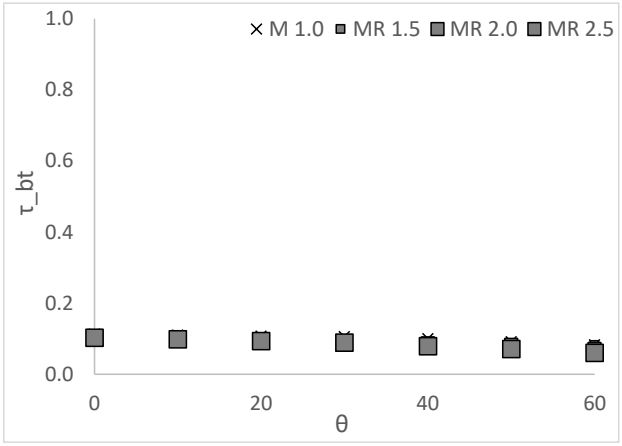

(c) BAI-IS Measurements – Rectangular

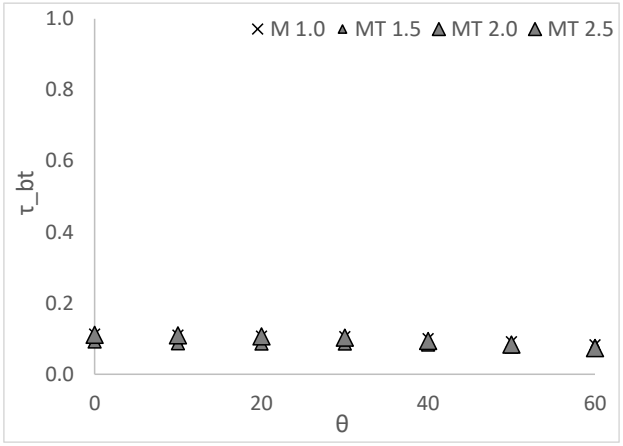

(d) BAI-IS Measurements – Triangular

Figure 6.4: #08 DarkBrown01 – calculated and measured τ_{bt} for various θ and Fr

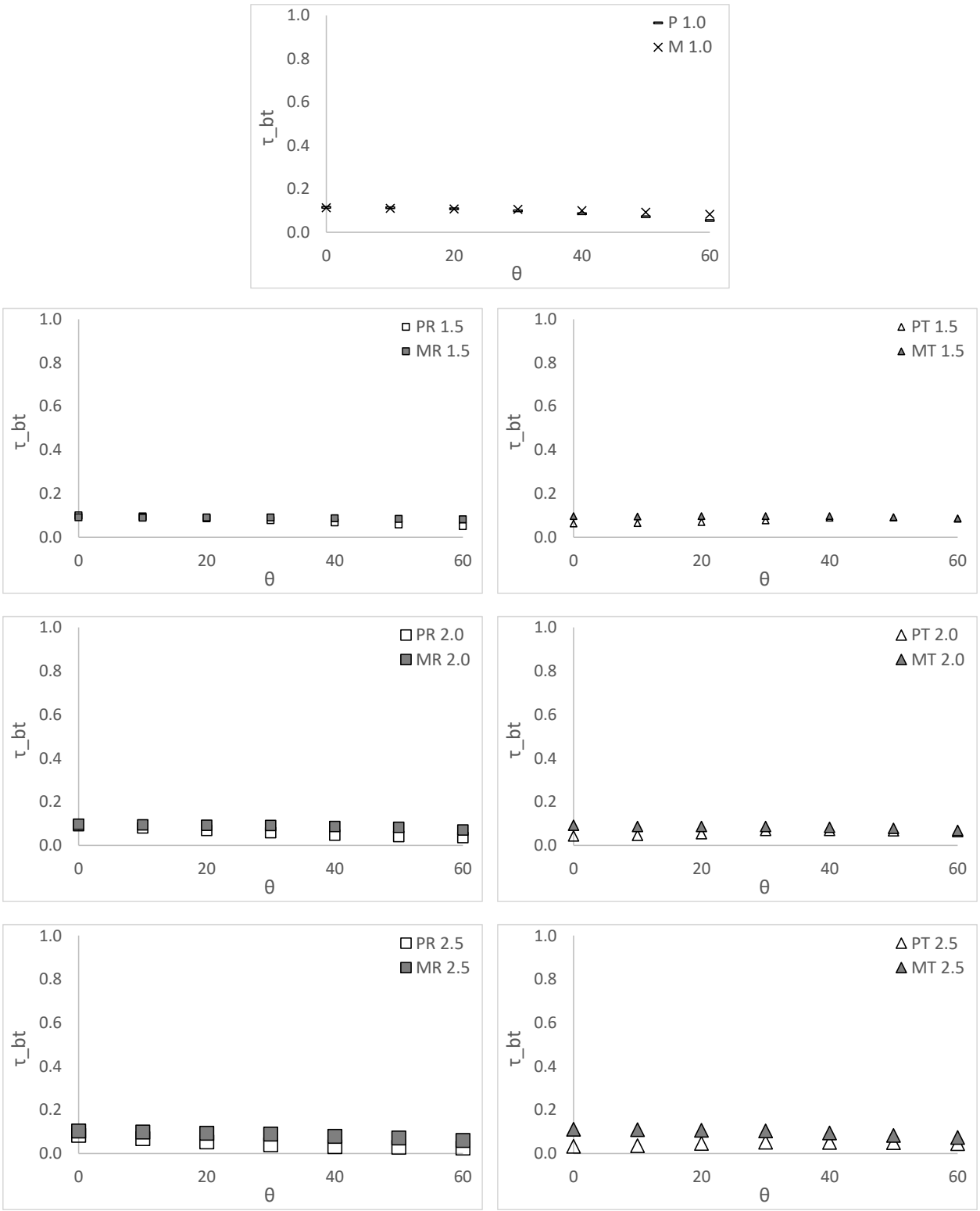

Figure 6.5: #08 DarkBrown01 – prediction vs measurement

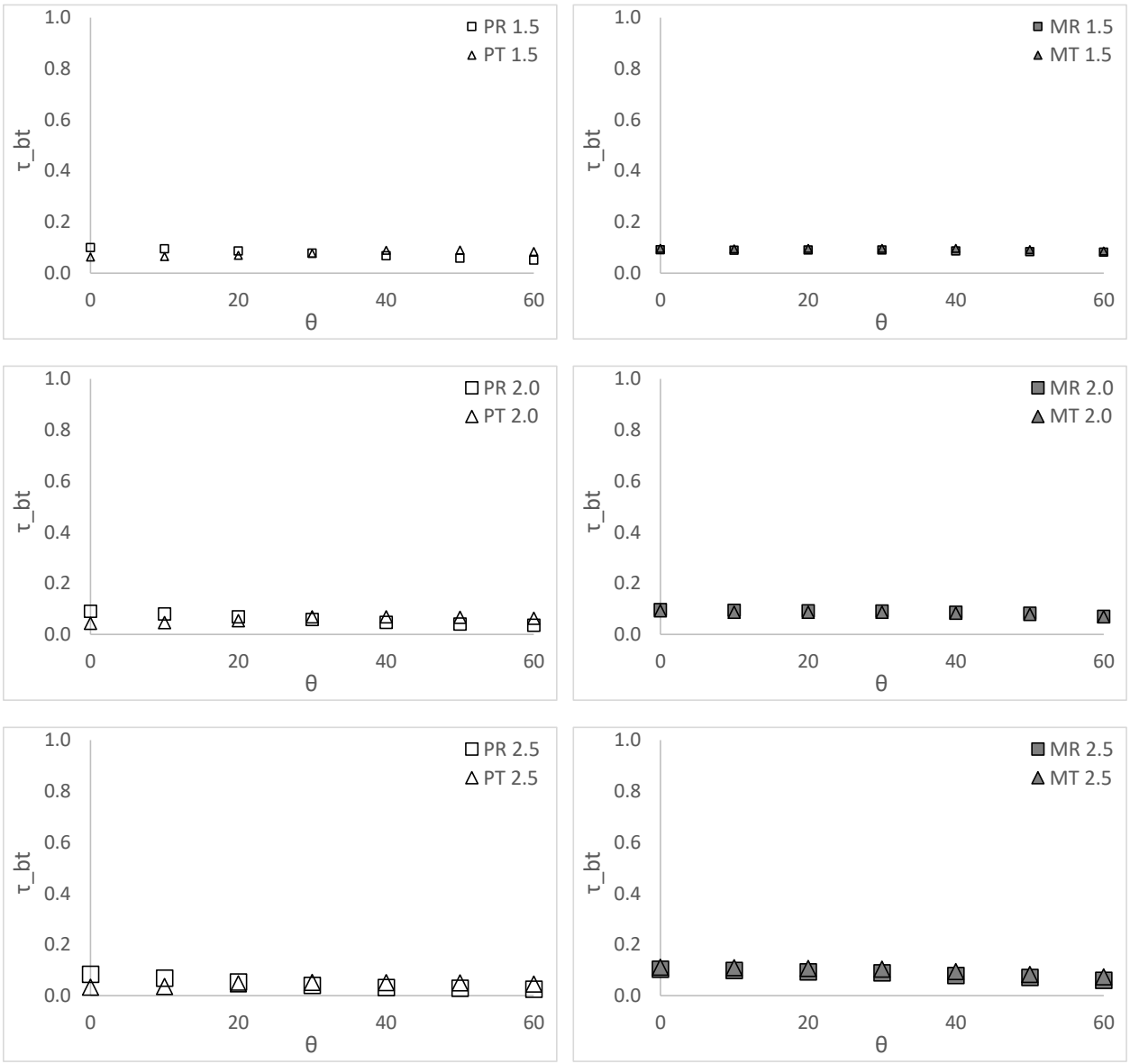

Figure 6.6: #08 DarkBrown01 – rectangular vs triangular profile

Table 6.4: #10 DecolineLining – calculated and measured τ_{bt} for various θ and Fr

#10 DecolineLining (τ_{bb} = 0.0520, τ_{bt} = 0.3329, ρ_{bt} = 0.6229)														
	Pleated Drape Models (P)							BAI-IS Measurements (M)						
		Rectangular (R)			Triangular (T)				Rectangular (R)			Triangular (T)		
θ	Flat	1.5	2.0	2.5	1.5	2.0	2.5	Flat	1.5	2.0	2.5	1.5	2.0	2.5
0	0.333	0.347	0.352	0.352	0.300	0.287	0.280	0.258	0.274	0.299	0.322	0.195	0.279	0.298
10	0.330	0.335	0.331	0.320	0.302	0.293	0.289	0.250	0.267	0.290	0.306	0.189	0.277	0.297
20	0.322	0.323	0.312	0.292	0.308	0.310	0.317	0.242	0.262	0.283	0.295	0.191	0.283	0.291
30	0.308	0.309	0.294	0.266	0.321	0.347	0.329	0.228	0.257	0.274	0.276	0.197	0.293	0.286
40	0.288	0.294	0.277	0.246	0.348	0.339	0.317	0.204	0.247	0.259	0.253	0.193	0.284	0.256
50	0.262	0.282	0.259	0.226	0.345	0.324	0.301	0.170	0.237	0.243	0.224	0.199	0.264	0.229
60	0.229	0.273	0.238	0.209	0.326	0.302	0.269	0.145	0.219	0.211	0.196	0.183	0.226	0.195

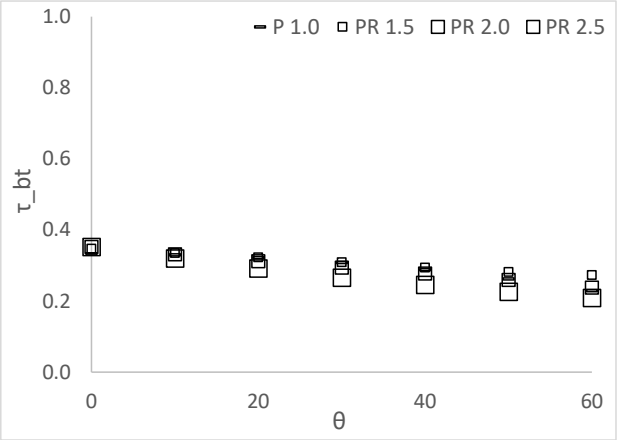

(a) Pleated Drape Model – Rectangular

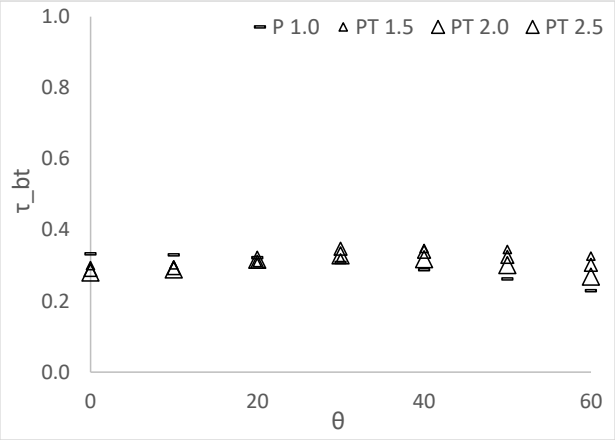

(b) Pleated Drape Model – Triangular

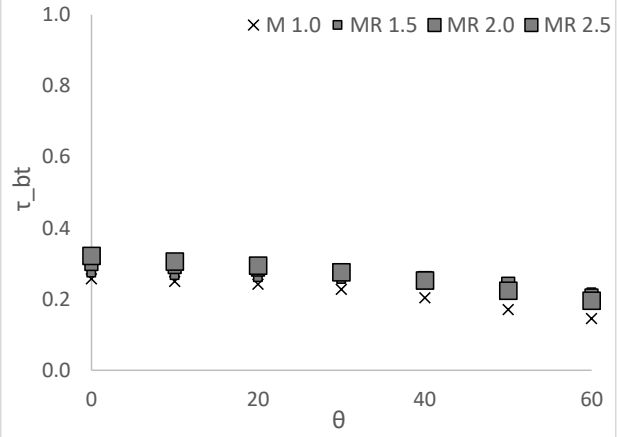

(c) BAI-IS Measurements – Rectangular

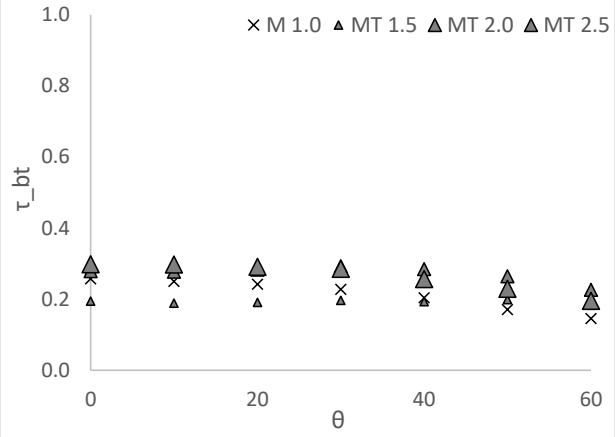

(d) BAI-IS Measurements – Triangular

Figure 6.7: #10 DecolineLining – calculated and measured τ_{bt} for various θ and Fr

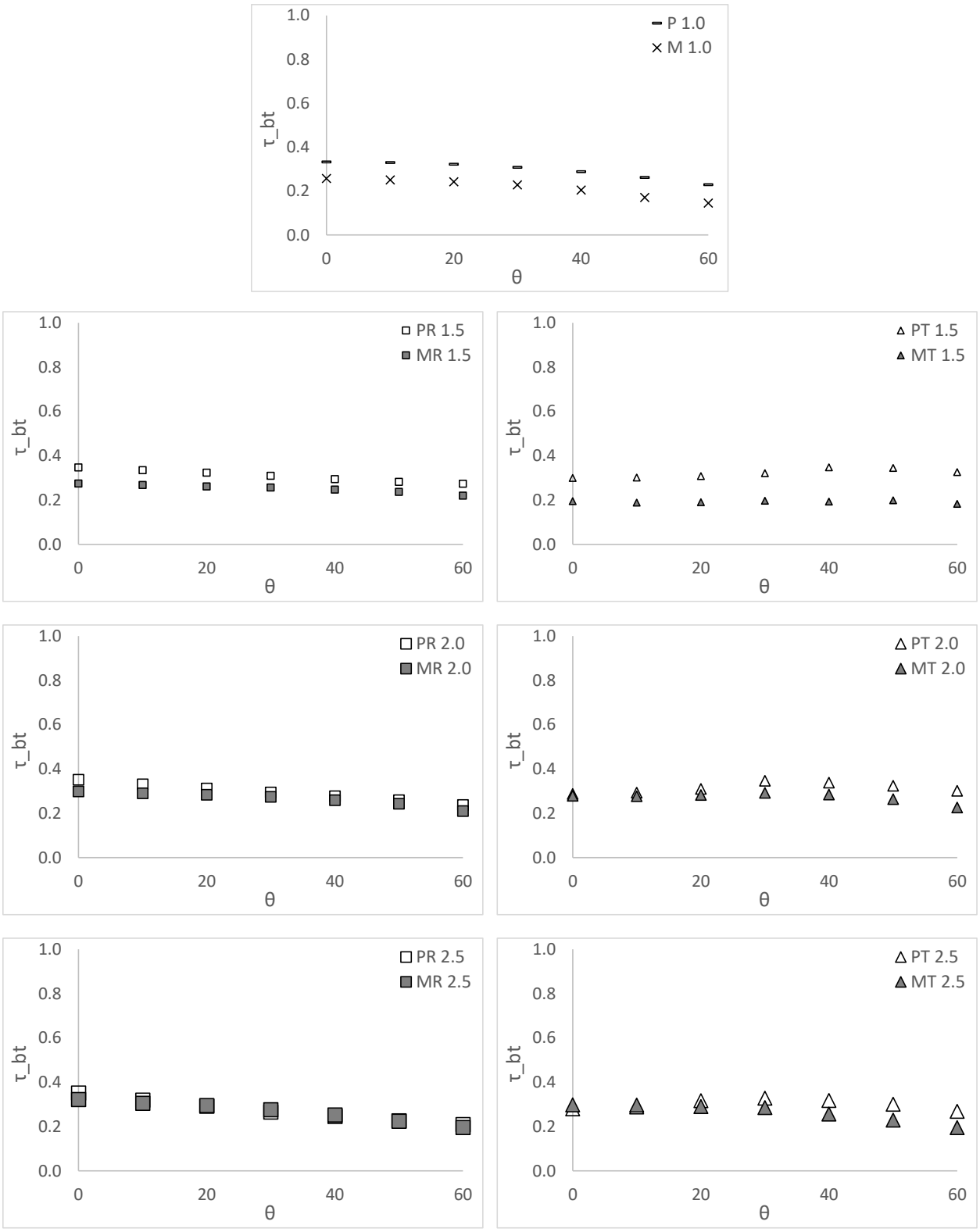

Figure 6.8: #10 DecolineLining – prediction vs measurement

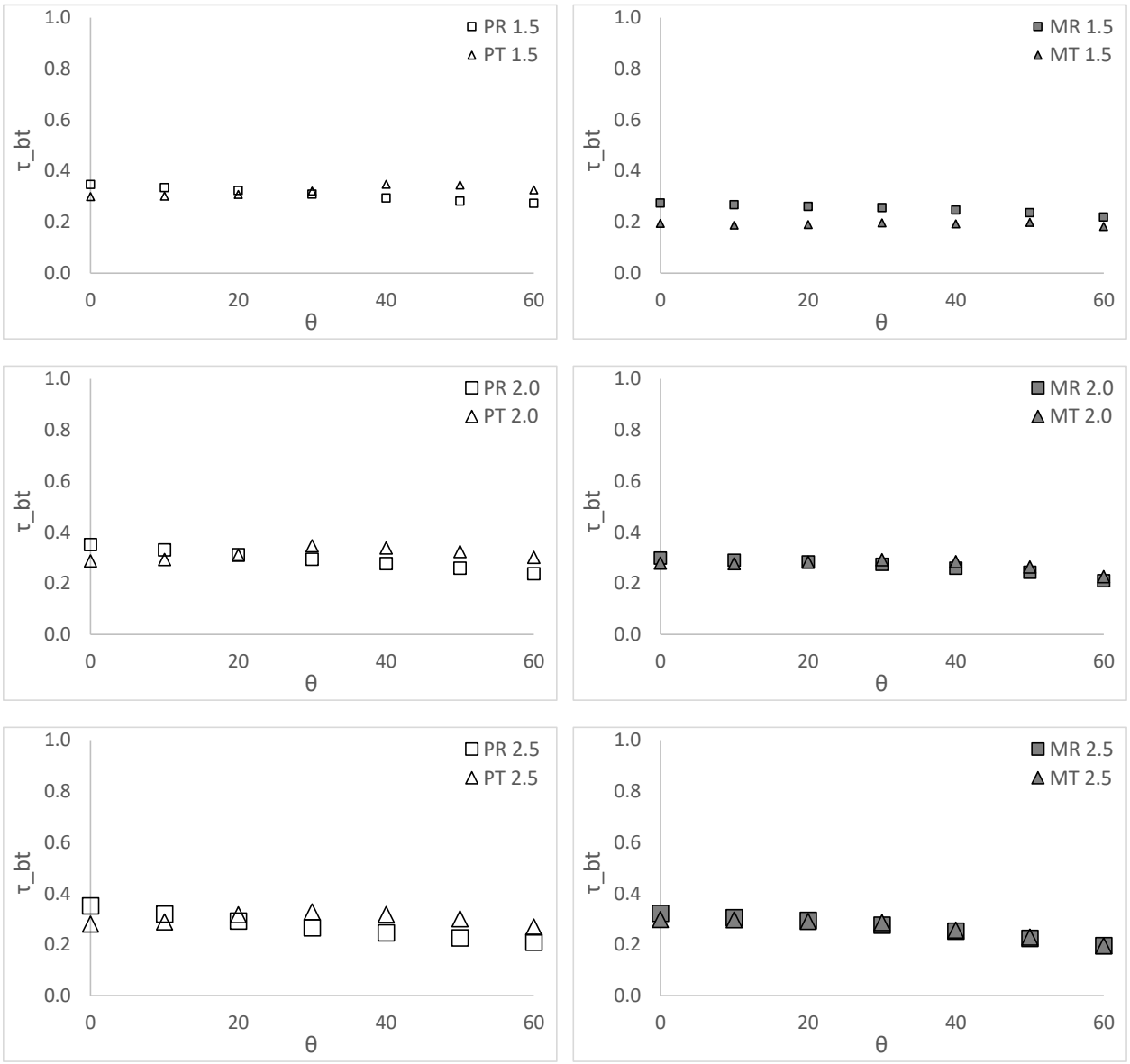

Figure 6.9: #10 DecolineLining – rectangular vs triangular profile

Table 6.5: #13 GreyOpen01 – calculated and measured τ_{bt} for various θ and Fr

#13 GreyOpen01 (τ_{bb} = 0.1919, τ_{bt} = 0.3170, ρ_{bt} = 0.1316)														
	Pleated Drape Models (P)							BAI-IS Measurements (M)						
		Rectangular (R)			Triangular (T)				Rectangular (R)			Triangular (T)		
θ	Flat	1.5	2.0	2.5	1.5	2.0	2.5	Flat	1.5	2.0	2.5	1.5	2.0	2.5
0	0.317	0.299	0.288	0.281	0.229	0.181	0.150	0.367	0.319	0.289	0.299	0.276	0.233	0.230
10	0.313	0.280	0.250	0.225	0.231	0.187	0.160	0.361	0.303	0.279	0.279	0.276	0.239	0.228
20	0.305	0.259	0.215	0.174	0.238	0.208	0.194	0.350	0.285	0.260	0.228	0.283	0.269	0.222
30	0.291	0.236	0.181	0.128	0.252	0.249	0.199	0.333	0.275	0.234	0.178	0.305	0.292	0.196
40	0.271	0.212	0.150	0.099	0.280	0.220	0.158	0.301	0.254	0.197	0.130	0.311	0.266	0.162
50	0.245	0.188	0.123	0.064	0.260	0.169	0.090	0.252	0.228	0.167	0.092	0.297	0.217	0.100
60	0.212	0.167	0.082	0.043	0.203	0.084	0.056	0.190	0.203	0.092	0.056	0.246	0.132	0.063

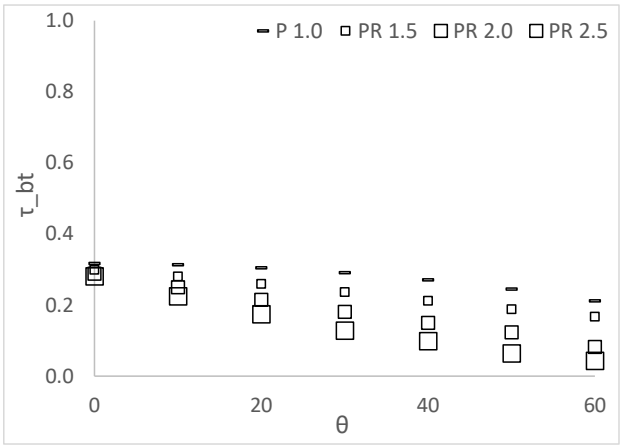

(a) Pleated Drape Model – Rectangular

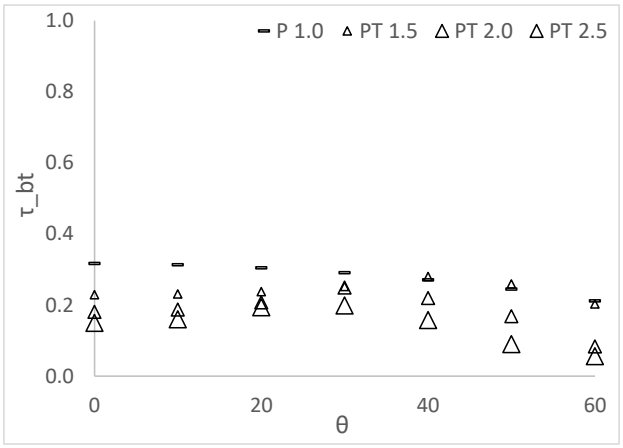

(b) Pleated Drape Model – Triangular

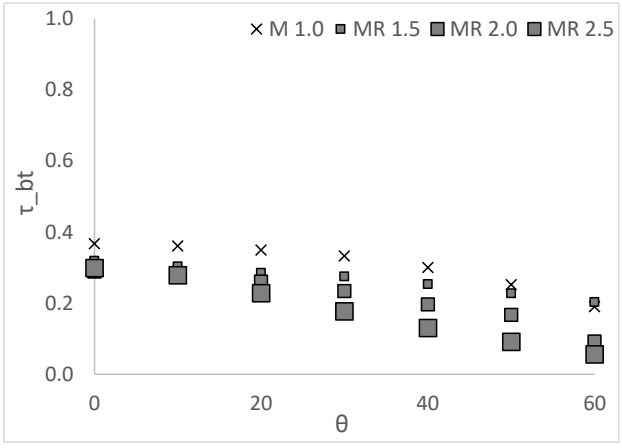

(c) BAI-IS Measurements – Rectangular

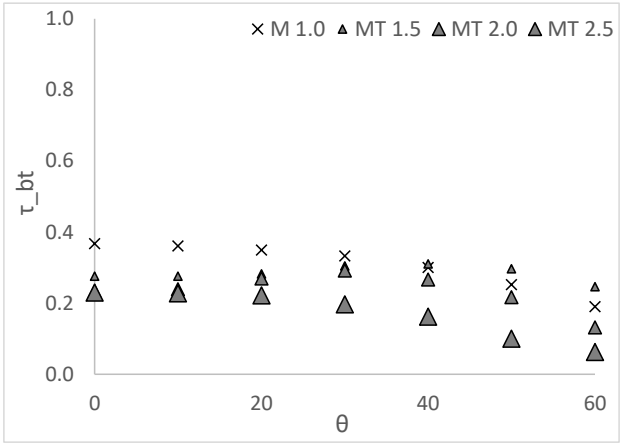

(d) BAI-IS Measurements – Triangular

Figure 6.10: #13 GreyOpen01 – calculated and measured τ_{bt} for various θ and Fr

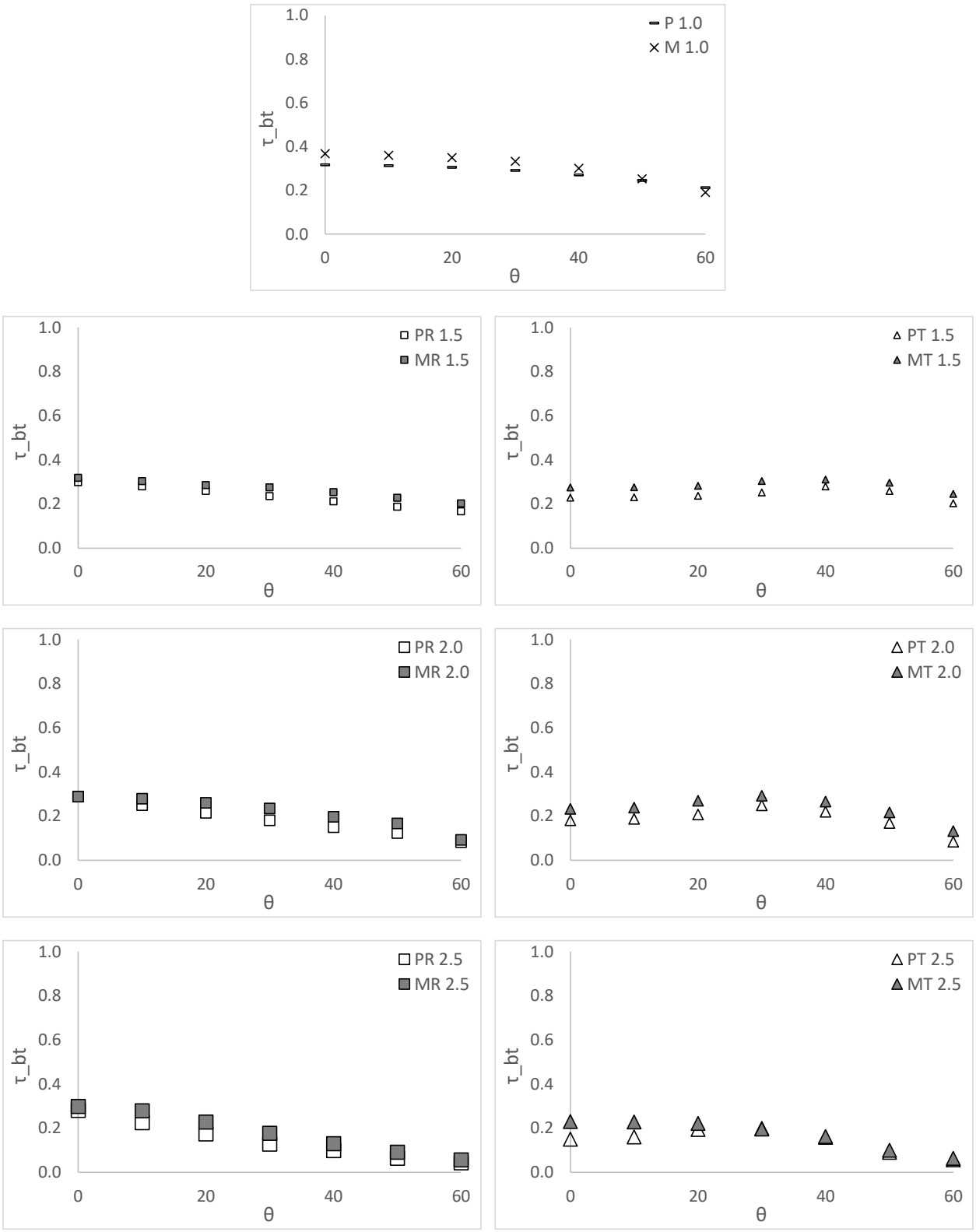

Figure 6.11: #13 GreyOpen01 – prediction vs measurement

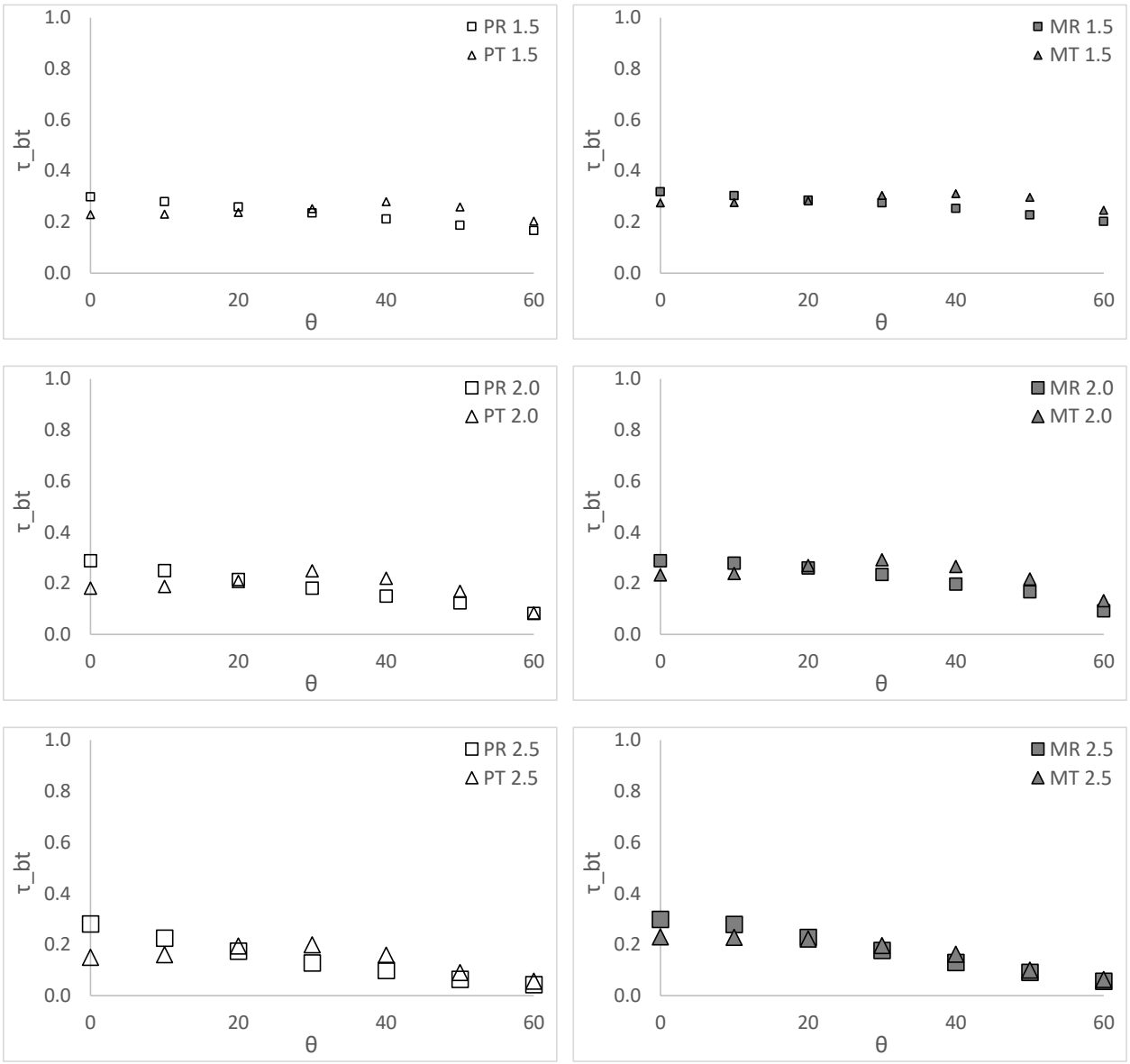

Figure 6.12: #13 GreyOpen01 – rectangular vs triangular profile

Table 6.6: #20 SheerBlack01 – calculated and measured τ_{bt} for various θ and Fr

#20 SheerBlack01 (τ_{bb} = 0.3451, τ_{bt} = 0.4993, ρ_{bt} = 0.1178)														
	Pleated Drape Models (P)							BAI-IS Measurements (M)						
		Rectangular (R)			Triangular (T)				Rectangular (R)			Triangular (T)		
θ	Flat	1.5	2.0	2.5	1.5	2.0	2.5	Flat	1.5	2.0	2.5	1.5	2.0	2.5
0	0.499	0.480	0.468	0.460	0.407	0.351	0.311	0.548	0.478	0.477	0.495	0.485	0.413	0.406
10	0.496	0.454	0.415	0.380	0.409	0.357	0.322	0.542	0.477	0.458	0.474	0.477	0.423	0.431
20	0.487	0.427	0.368	0.309	0.414	0.378	0.361	0.534	0.467	0.427	0.419	0.476	0.458	0.421
30	0.473	0.398	0.321	0.243	0.427	0.426	0.352	0.524	0.451	0.391	0.371	0.492	0.459	0.386
40	0.453	0.366	0.273	0.190	0.458	0.368	0.271	0.498	0.423	0.366	0.314	0.492	0.411	0.322
50	0.426	0.332	0.226	0.124	0.418	0.275	0.148	0.462	0.400	0.315	0.252	0.461	0.342	0.228
60	0.390	0.296	0.153	0.087	0.322	0.126	0.087	0.424	0.341	0.223	0.192	0.394	0.222	0.168

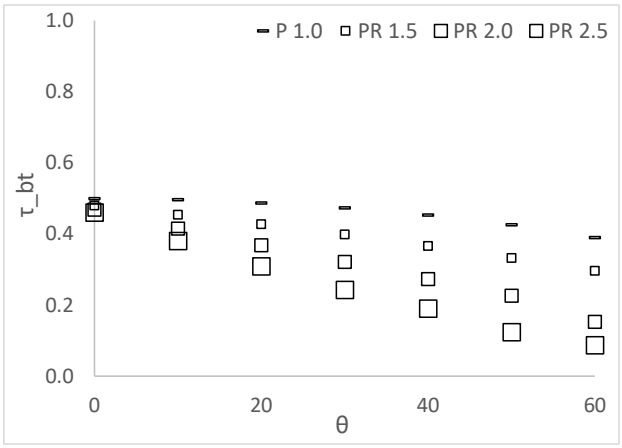

(a) Pleated Drape Model – Rectangular

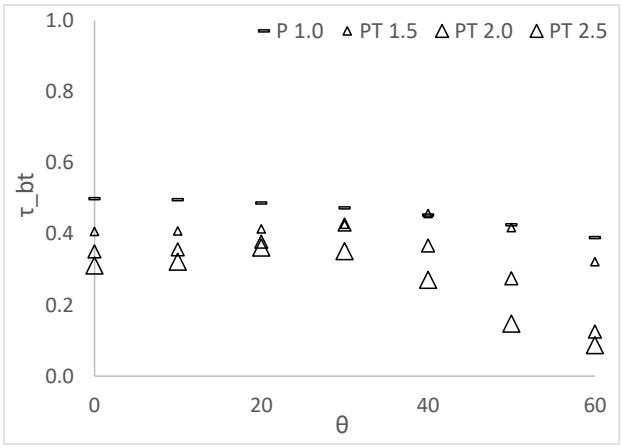

(b) Pleated Drape Model – Triangular

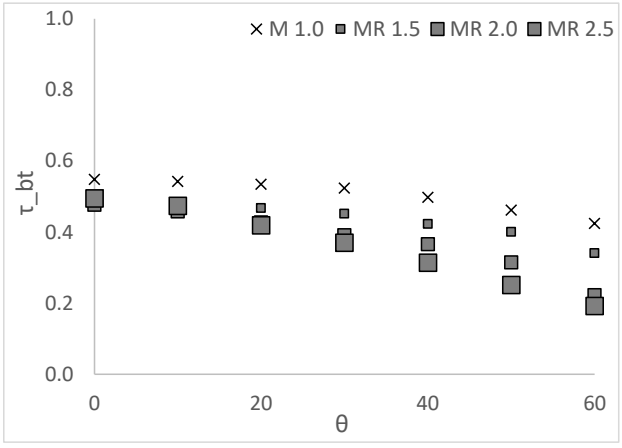

(c) BAI-IS Measurements – Rectangular

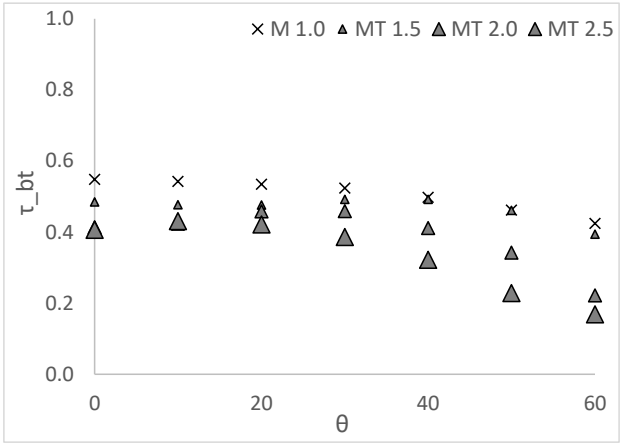

(d) BAI-IS Measurements – Triangular

Figure 6.13: #20 SheerBlack01 – calculated and measured τ_{bt} for various θ and Fr

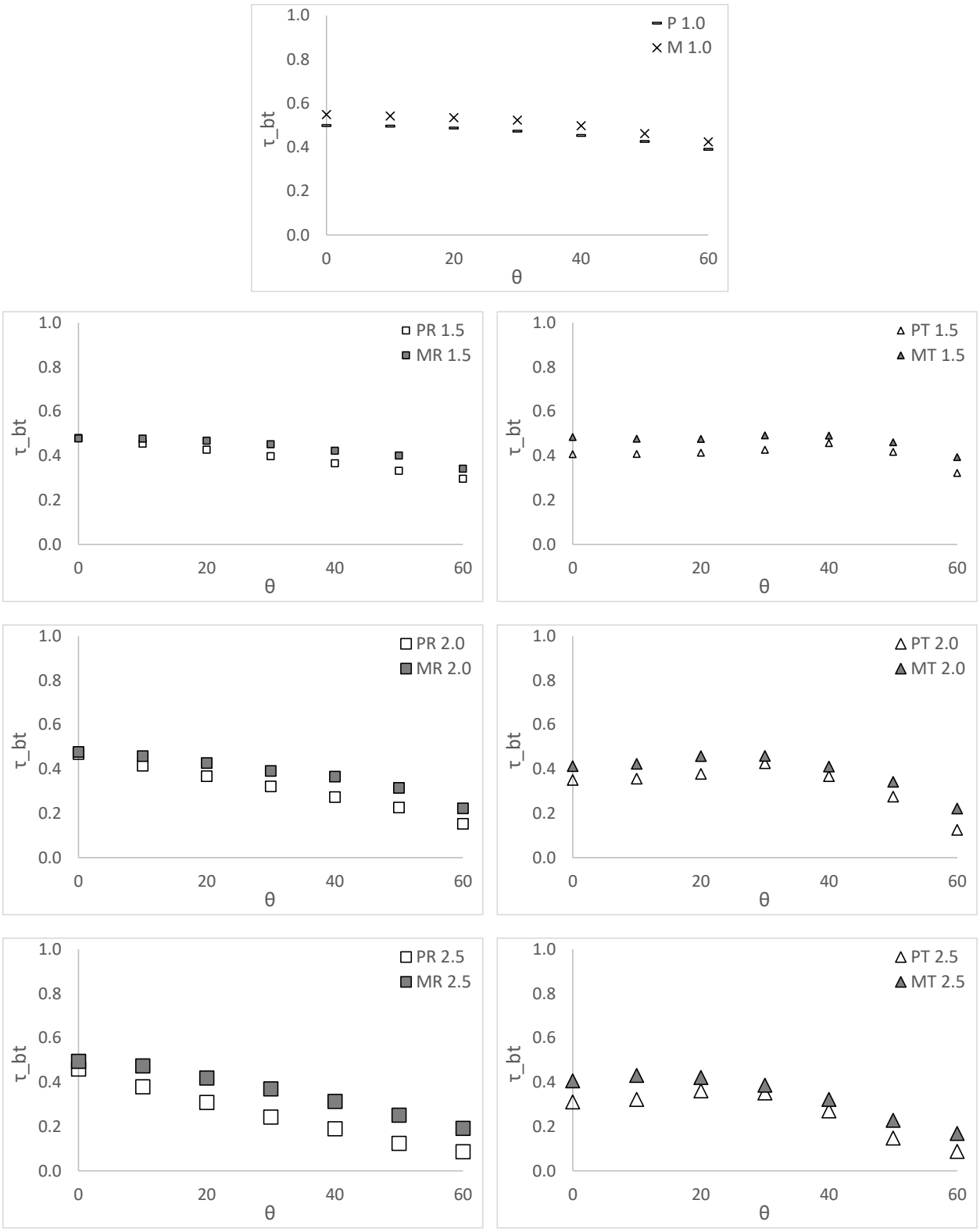

Figure 6.14: #20 SheerBlack01 – prediction vs measurement

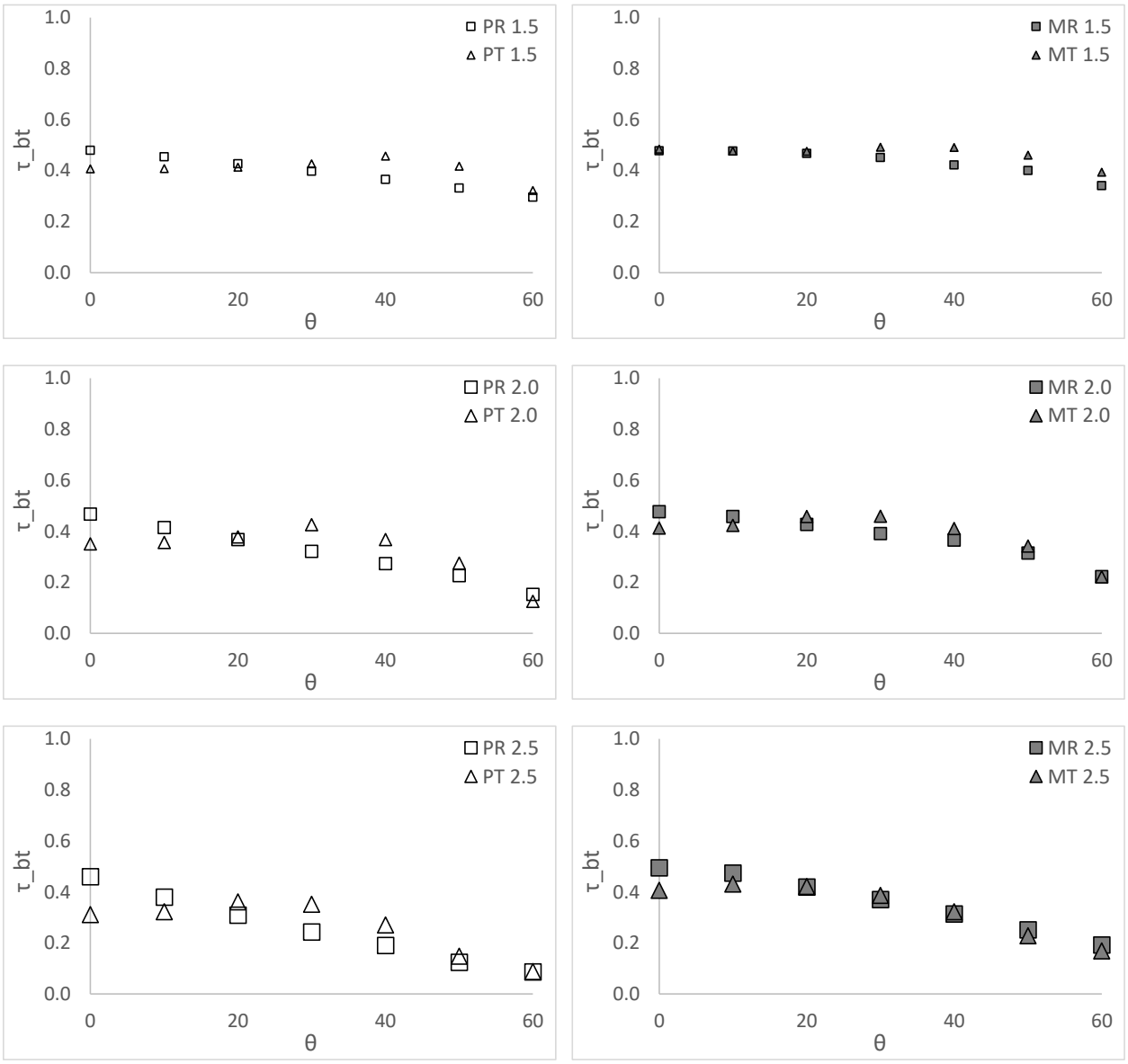

Figure 6.15: #20 SheerBlack01 – rectangular vs triangular profile

Table 6.7: #22 SheerWhite01 – calculated and measured τ_{bt} for various θ and Fr

#22 SheerWhite01 (τ_{bb} = 0.3169, τ_{bt} = 0.6496, ρ_{bt} = 0.2578)														
	Pleated Drape Models (P)							BAI-IS Measurements (M)						
		Rectangular (R)			Triangular (T)				Rectangular (R)			Triangular (T)		
θ	Flat	1.5	2.0	2.5	1.5	2.0	2.5	Flat	1.5	2.0	2.5	1.5	2.0	2.5
0	0.649	0.629	0.615	0.604	0.545	0.487	0.446	0.657	0.616	0.608	0.593	0.578	0.544	0.555
10	0.645	0.603	0.564	0.526	0.547	0.494	0.458	0.648	0.600	0.587	0.564	0.568	0.548	0.554
20	0.634	0.577	0.518	0.459	0.553	0.516	0.499	0.638	0.604	0.560	0.513	0.569	0.569	0.543
30	0.616	0.548	0.473	0.394	0.568	0.570	0.498	0.627	0.591	0.543	0.463	0.573	0.569	0.525
40	0.590	0.515	0.426	0.340	0.604	0.522	0.433	0.604	0.572	0.508	0.417	0.577	0.535	0.486
50	0.555	0.480	0.379	0.283	0.575	0.447	0.335	0.567	0.551	0.471	0.349	0.551	0.462	0.417
60	0.509	0.443	0.315	0.243	0.496	0.328	0.261	0.503	0.523	0.363	0.298	0.494	0.354	0.338

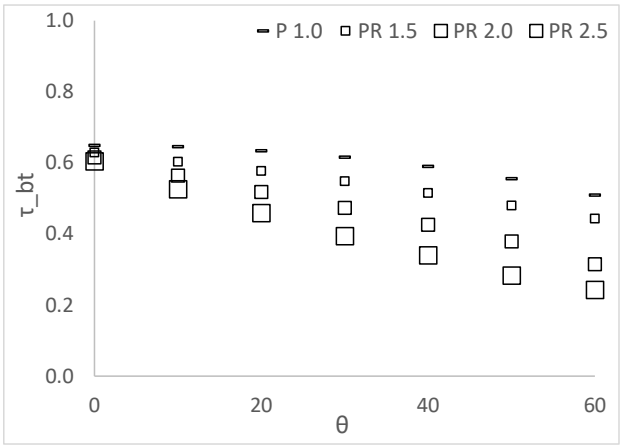

(a) Pleated Drape Model – Rectangular

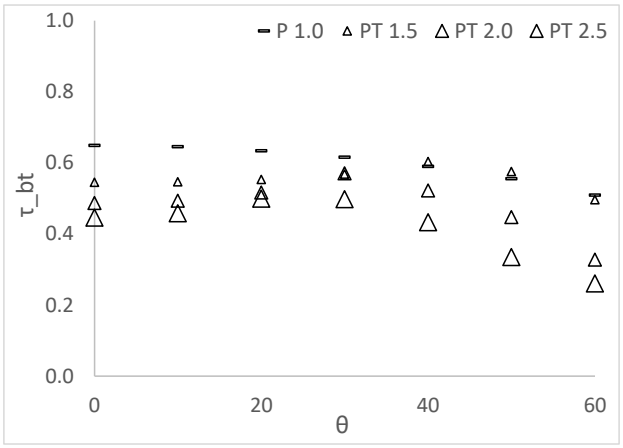

(b) Pleated Drape Model – Triangular

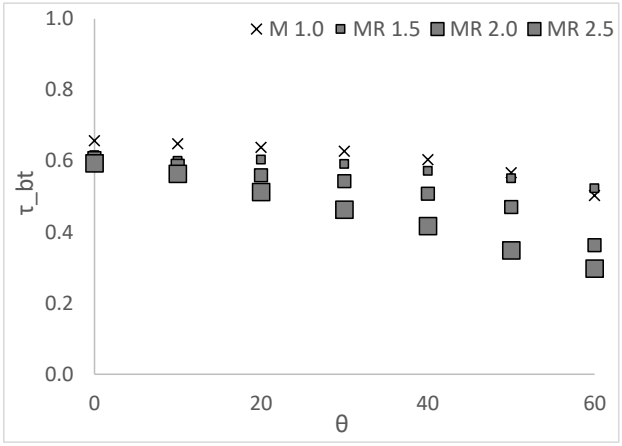

(c) BAI-IS Measurements – Rectangular

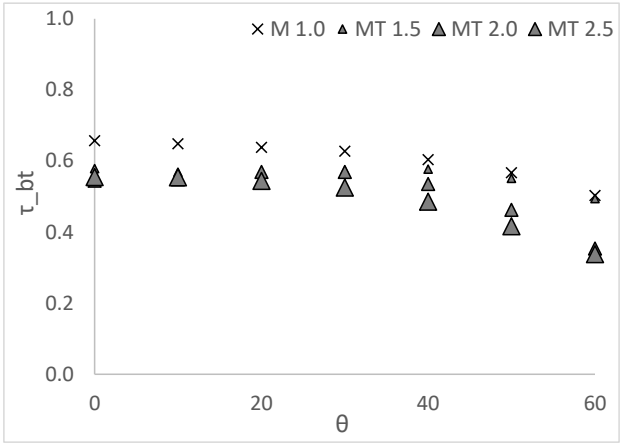

(d) BAI-IS Measurements – Triangular

Figure 6.16: #22 SheerWhite01 – calculated and measured τ_{bt} for various θ and Fr

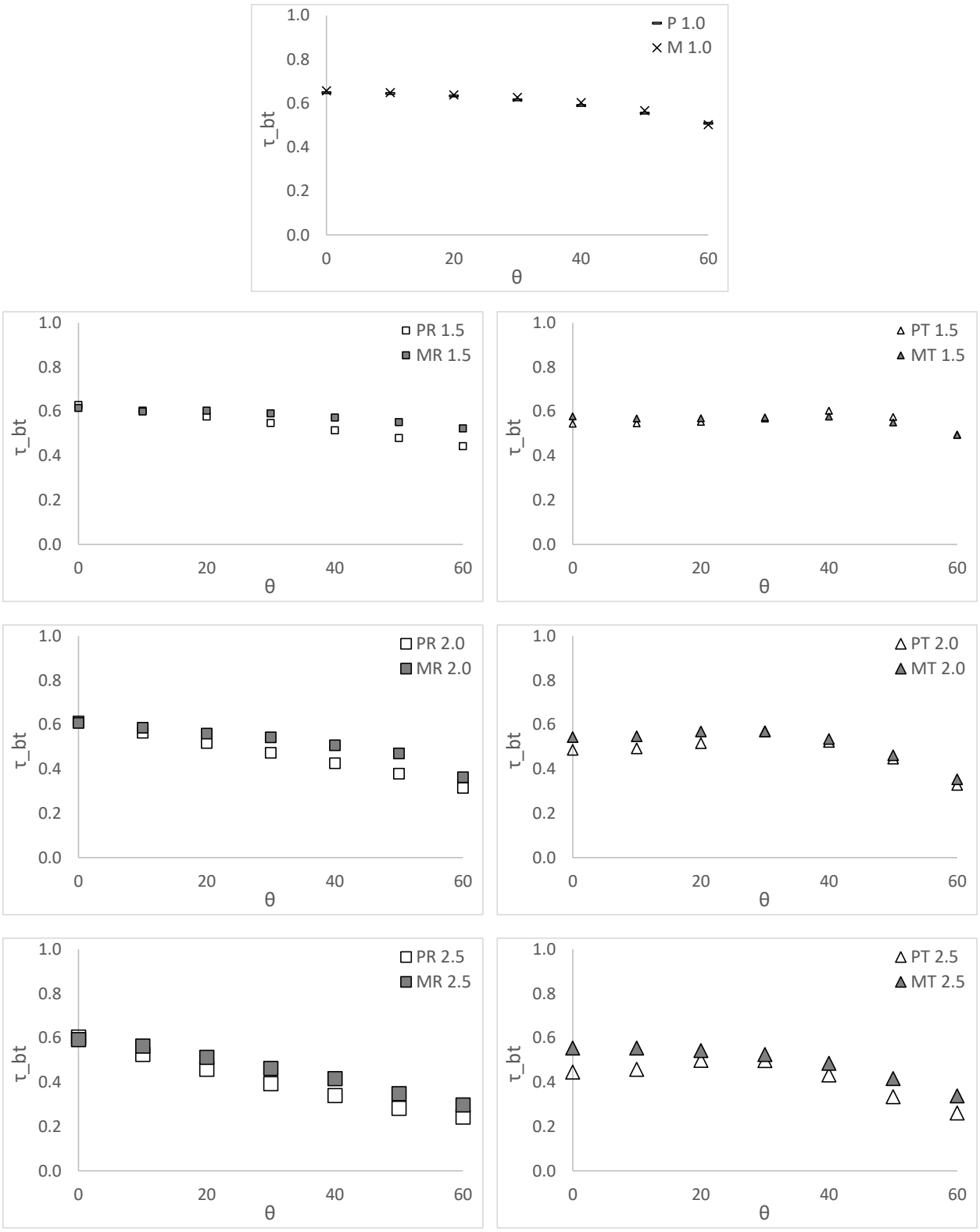

Figure 6.17: #22 SheerWhite01 – prediction vs measurement

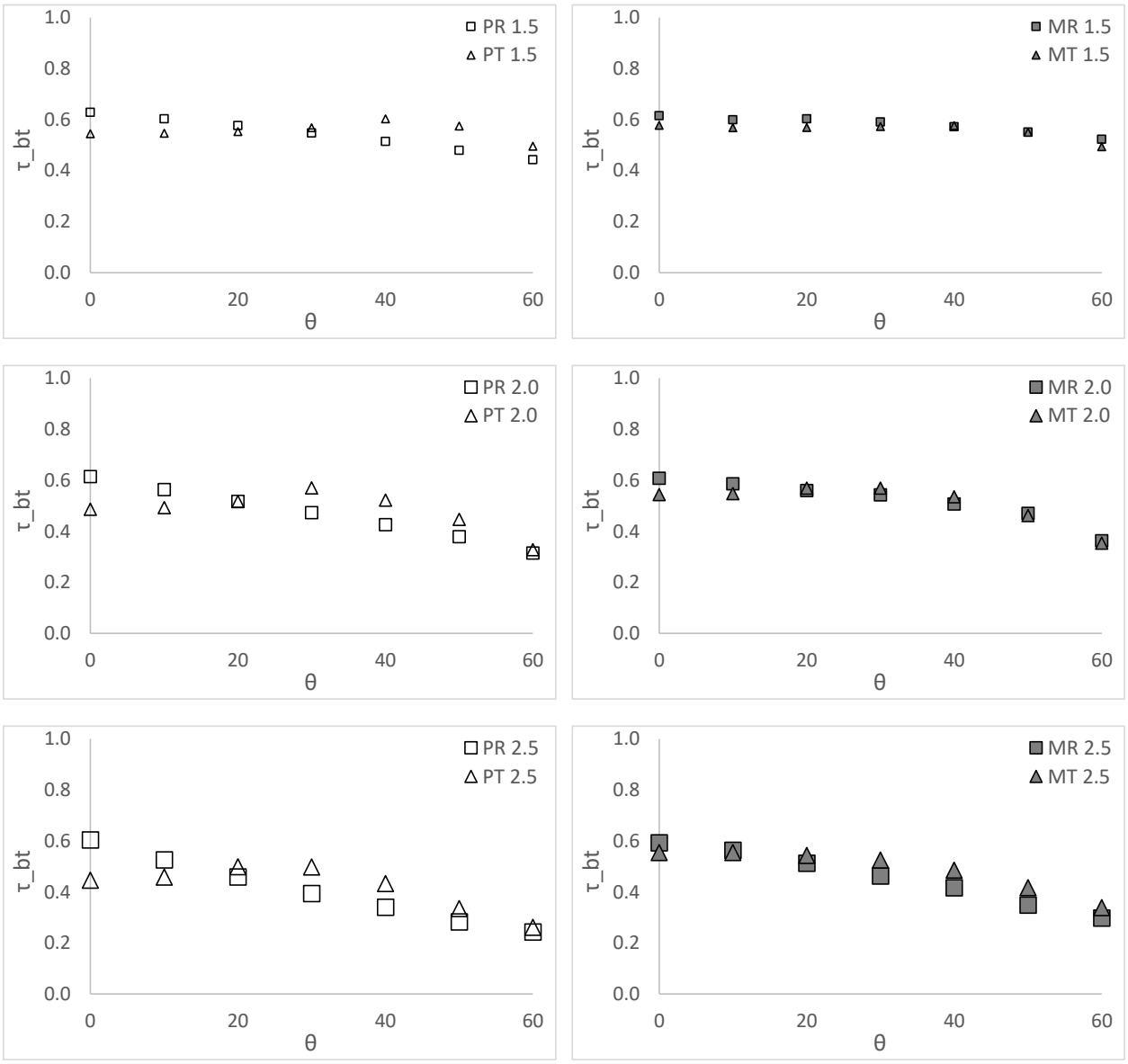

Figure 6.18: #22 SheerWhite01 – rectangular vs triangular profile

Table 6.8: #24 White05 – calculated and measured τ_{bt} for various θ and Fr

#24 White05 (τ_{bb} = 0.0006, τ_{bt} = 0.2196, ρ_{bt} = 0.6110)														
	Pleated Drape Models (P)							BAI-IS Measurements (M)						
		Rectangular (R)			Triangular (T)				Rectangular (R)			Triangular (T)		
θ	Flat	1.5	2.0	2.5	1.5	2.0	2.5	Flat	1.5	2.0	2.5	1.5	2.0	2.5
0	0.220	0.220	0.216	0.209	0.176	0.158	0.148	0.203	0.177	0.191	0.206	0.182	0.199	0.207
10	0.217	0.211	0.201	0.187	0.178	0.163	0.154	0.197	0.174	0.185	0.198	0.177	0.208	0.202
20	0.209	0.201	0.186	0.166	0.184	0.177	0.175	0.189	0.173	0.180	0.185	0.176	0.199	0.195
30	0.197	0.189	0.171	0.146	0.196	0.205	0.185	0.186	0.172	0.174	0.177	0.181	0.197	0.188
40	0.179	0.177	0.158	0.133	0.217	0.203	0.183	0.168	0.165	0.165	0.158	0.178	0.188	0.172
50	0.157	0.166	0.146	0.122	0.218	0.198	0.179	0.149	0.169	0.150	0.141	0.170	0.175	0.152
60	0.131	0.158	0.135	0.113	0.208	0.191	0.162	0.133	0.157	0.133	0.127	0.163	0.153	0.130

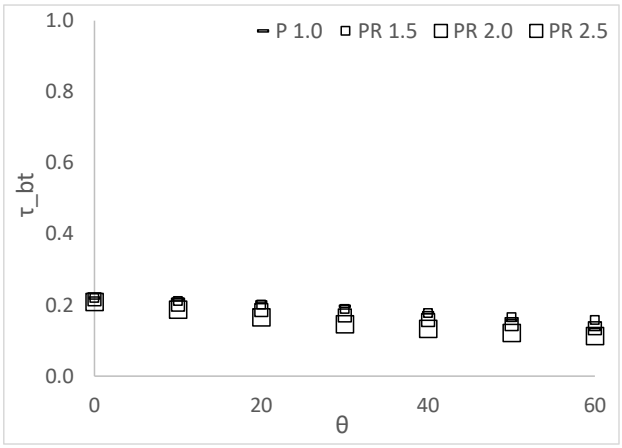

(a) Pleated Drape Model – Rectangular

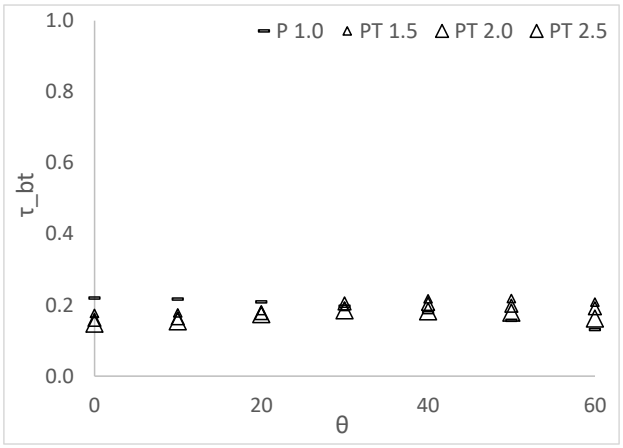

(b) Pleated Drape Model – Triangular

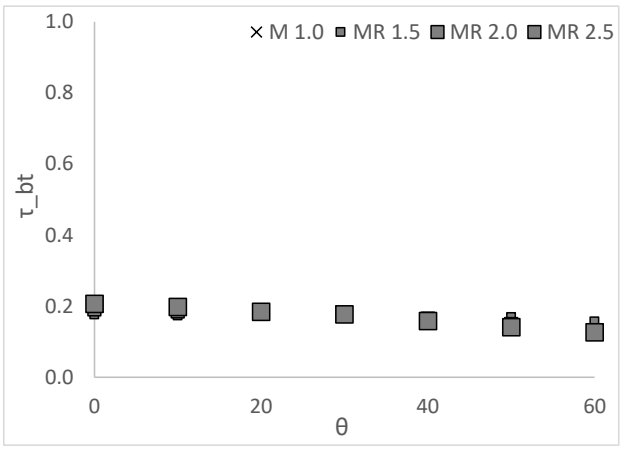

(c) BAI-IS Measurements – Rectangular

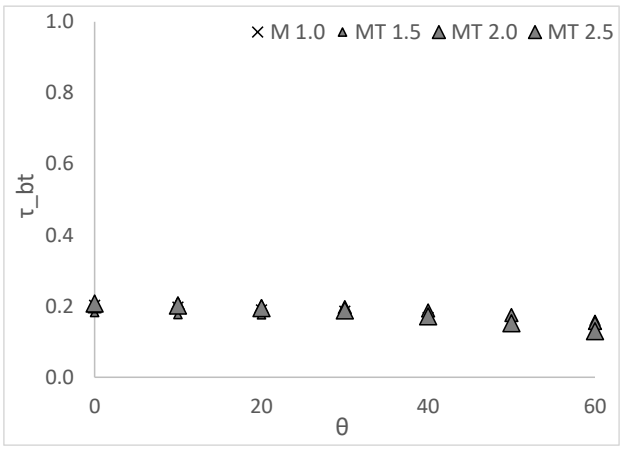

(d) BAI-IS Measurements – Triangular

Figure 6.19: #24 White05 – calculated and measured τ_{bt} for various θ and Fr

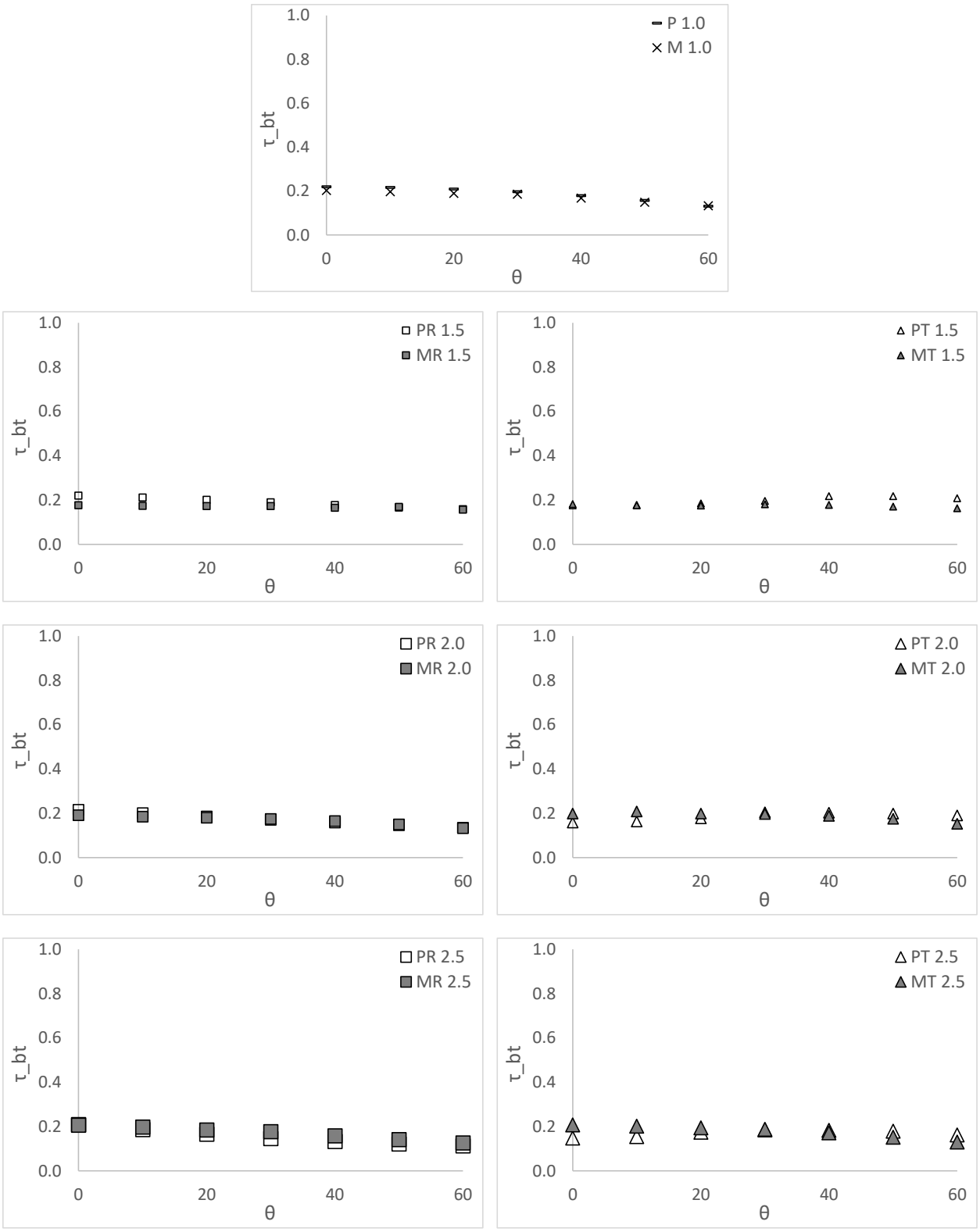

Figure 6.20: #24 White05 – prediction vs measurement

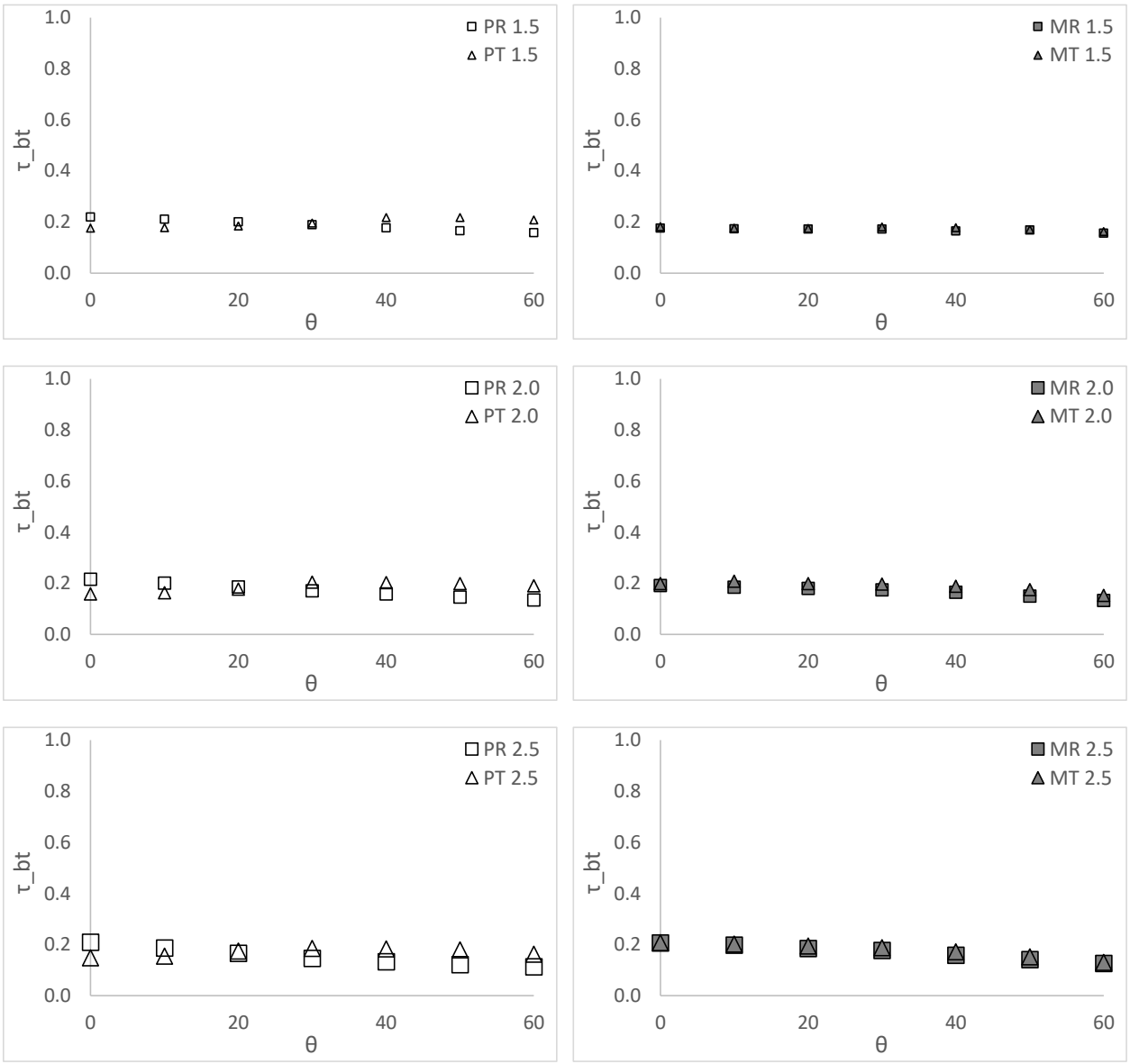

Figure 6.21: #24 White05 – rectangular vs triangular profile

Table 6.9: #26 BlueSoft01 – calculated and measured τ_{bt} for various θ and Fr

#26 BlueSoft01 (τ_{bb} = 0.0106, τ_{bt} = 0.1758, ρ_{bt} = 0.2622)														
	Pleated Drape Models (P)							BAI-IS Measurements (M)						
		Rectangular (R)			Triangular (T)				Rectangular (R)			Triangular (T)		
θ	Flat	1.5	2.0	2.5	1.5	2.0	2.5	Flat	1.5	2.0	2.5	1.5	2.0	2.5
0	0.175	0.154	0.139	0.130	0.104	0.072	0.056	0.179	0.150	0.131	0.140	0.137	0.109	0.138
10	0.173	0.145	0.124	0.107	0.105	0.076	0.060	0.174	0.144	0.127	0.132	0.134	0.107	0.135
20	0.166	0.134	0.108	0.085	0.111	0.087	0.075	0.171	0.141	0.121	0.117	0.137	0.114	0.142
30	0.154	0.122	0.091	0.063	0.121	0.107	0.082	0.161	0.133	0.114	0.104	0.144	0.125	0.137
40	0.139	0.108	0.075	0.051	0.138	0.106	0.078	0.144	0.126	0.107	0.091	0.148	0.118	0.124
50	0.119	0.094	0.064	0.045	0.137	0.100	0.073	0.128	0.115	0.096	0.078	0.143	0.098	0.097
60	0.096	0.083	0.056	0.039	0.127	0.091	0.064	0.105	0.106	0.083	0.069	0.134	0.085	0.088

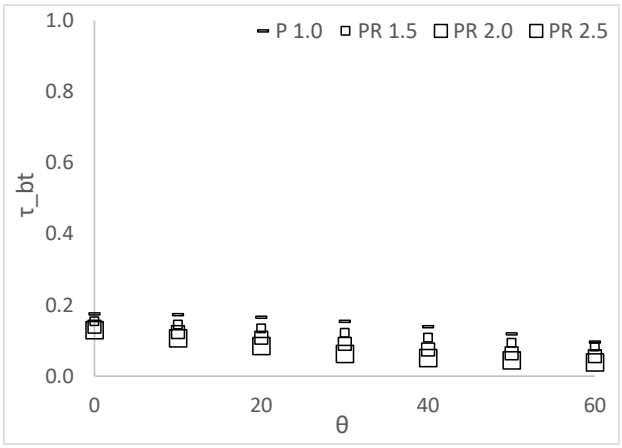

(a) Pleated Drape Model – Rectangular

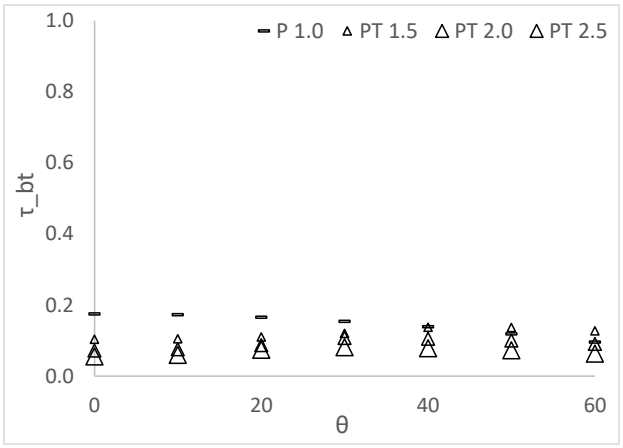

(b) Pleated Drape Model – Triangular

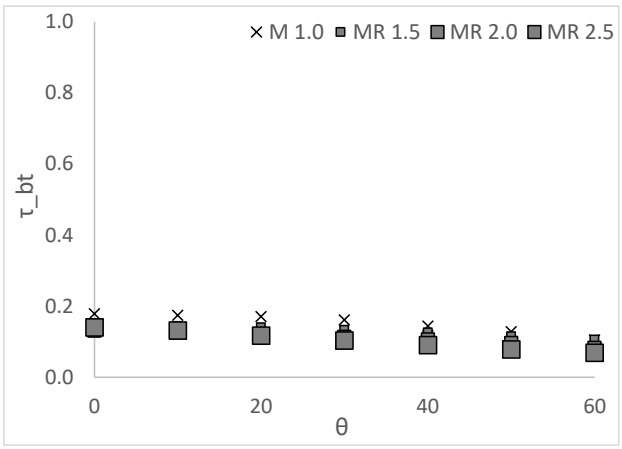

(c) BAI-IS Measurements – Rectangular

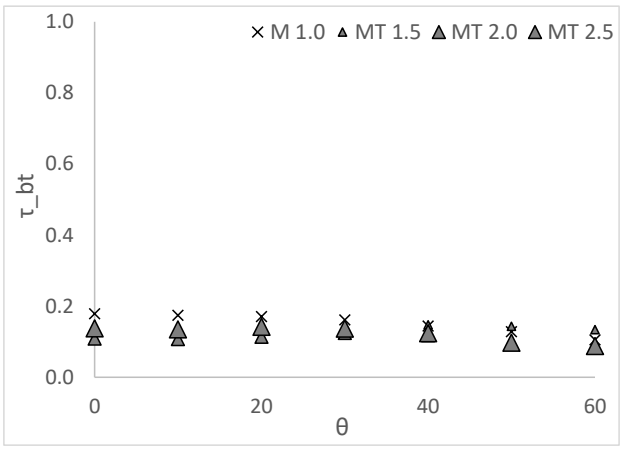

(d) BAI-IS Measurements – Triangular

Figure 6.22: #26 BlueSoft01 – calculated and measured τ_{bt} for various θ and Fr

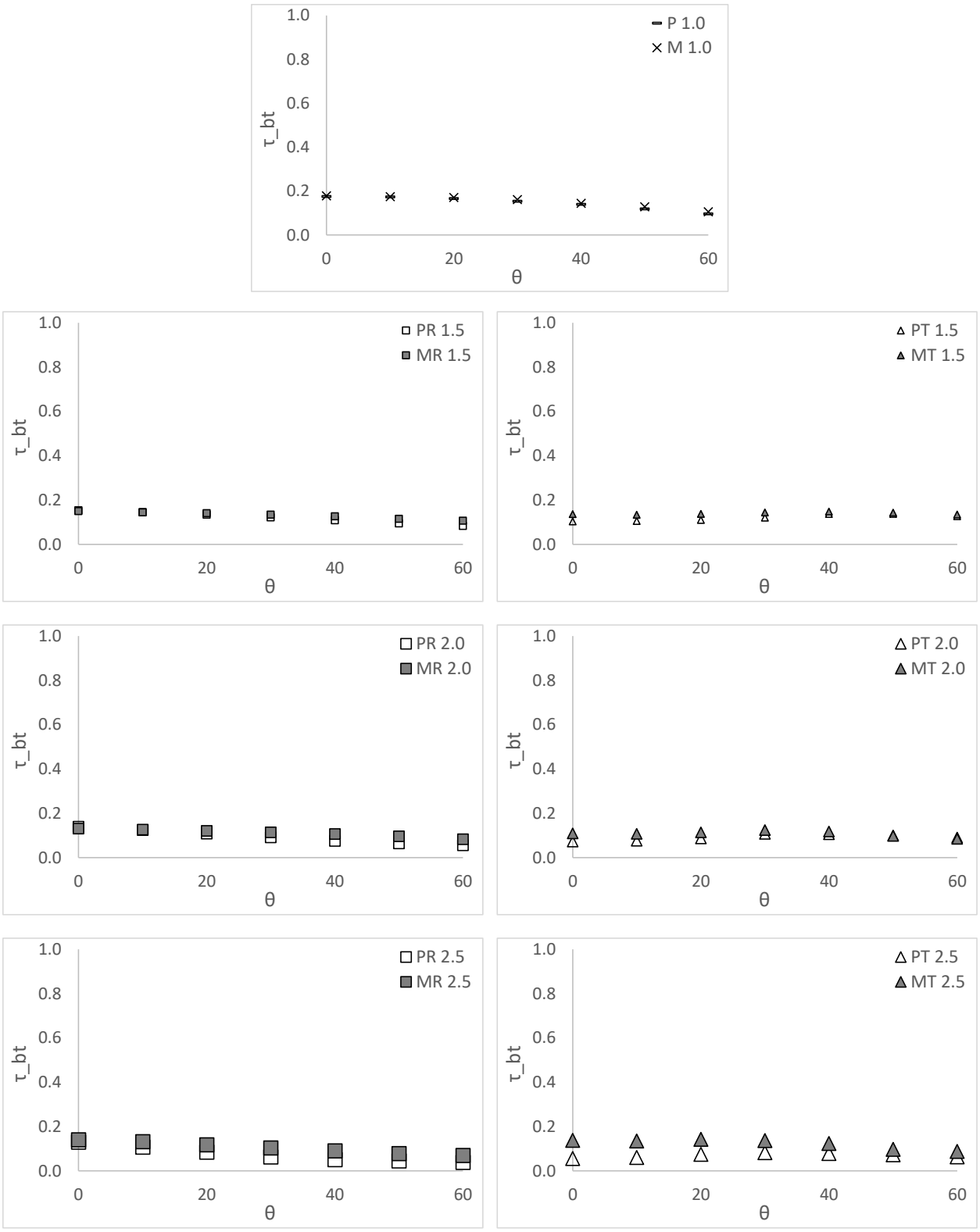

Figure 6.23: #26 BlueSoft01 – prediction vs measurement

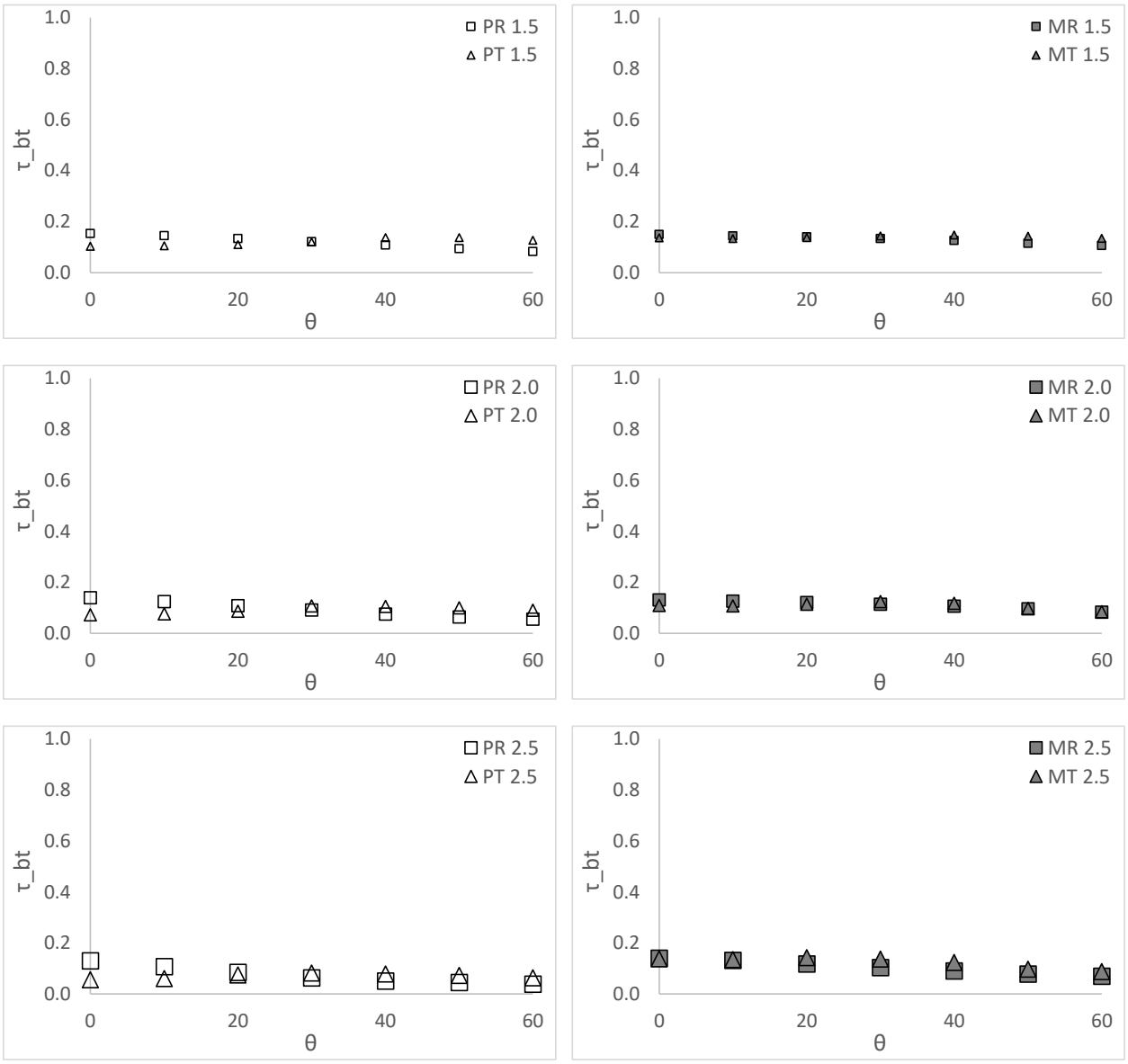

Figure 6.24: #26 BlueSoft01 – rectangular vs triangular profile

Table 6.10: #27 Yellow05 – calculated and measured τ_{bt} for various θ and Fr

#27 Yellow05 (τ_{bb} = 0.0012, τ_{bt} = 0.1506, ρ_{bt} = 0.5560)														
	Pleated Drape Models (P)							BAI-IS Measurements (M)						
		Rectangular (R)			Triangular (T)				Rectangular (R)			Triangular (T)		
θ	Flat	1.5	2.0	2.5	1.5	2.0	2.5	Flat	1.5	2.0	2.5	1.5	2.0	2.5
0	0.151	0.146	0.139	0.132	0.107	0.089	0.079	0.169	0.132	0.158	0.144	0.143	0.147	0.149
10	0.148	0.139	0.127	0.115	0.109	0.093	0.084	0.165	0.128	0.155	0.140	0.137	0.144	0.147
20	0.142	0.130	0.115	0.099	0.115	0.105	0.099	0.161	0.127	0.155	0.133	0.132	0.145	0.142
30	0.131	0.120	0.103	0.083	0.125	0.125	0.108	0.154	0.128	0.150	0.125	0.140	0.148	0.142
40	0.117	0.109	0.092	0.073	0.141	0.125	0.107	0.137	0.124	0.143	0.110	0.139	0.144	0.127
50	0.099	0.100	0.084	0.067	0.142	0.123	0.106	0.120	0.121	0.134	0.098	0.136	0.136	0.112
60	0.079	0.094	0.076	0.061	0.135	0.118	0.096	0.100	0.113	0.114	0.090	0.128	0.114	0.096

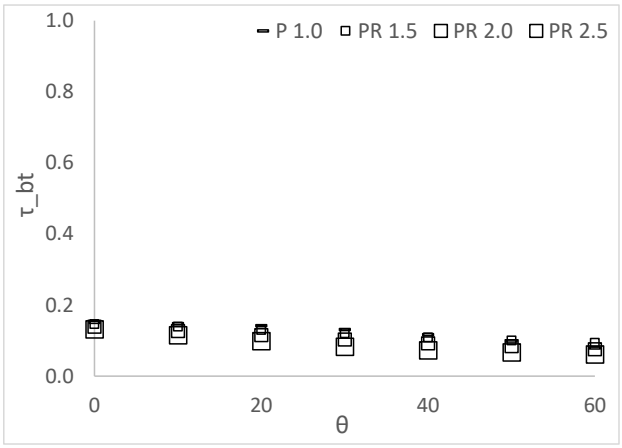

(a) Pleated Drape Model – Rectangular

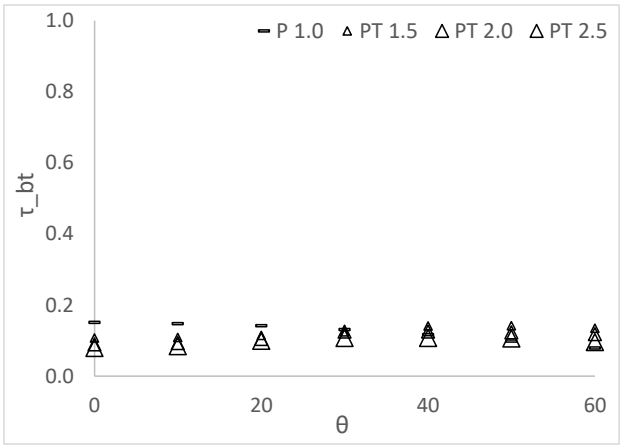

(b) Pleated Drape Model – Triangular

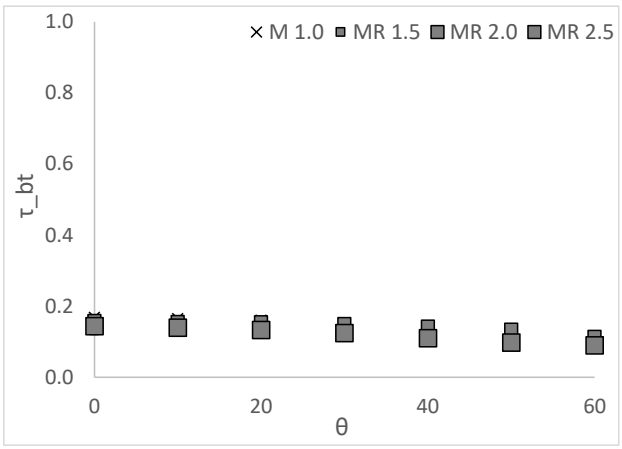

(c) BAI-IS Measurements – Rectangular

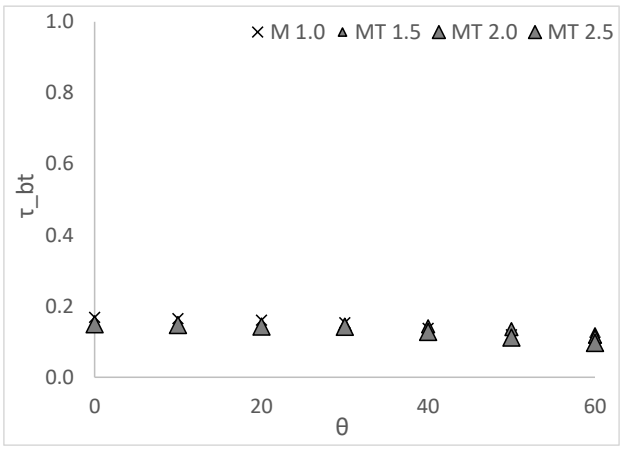

(d) BAI-IS Measurements – Triangular

Figure 6.25: #27 Yellow05 – calculated and measured τ_{bt} for various θ and Fr

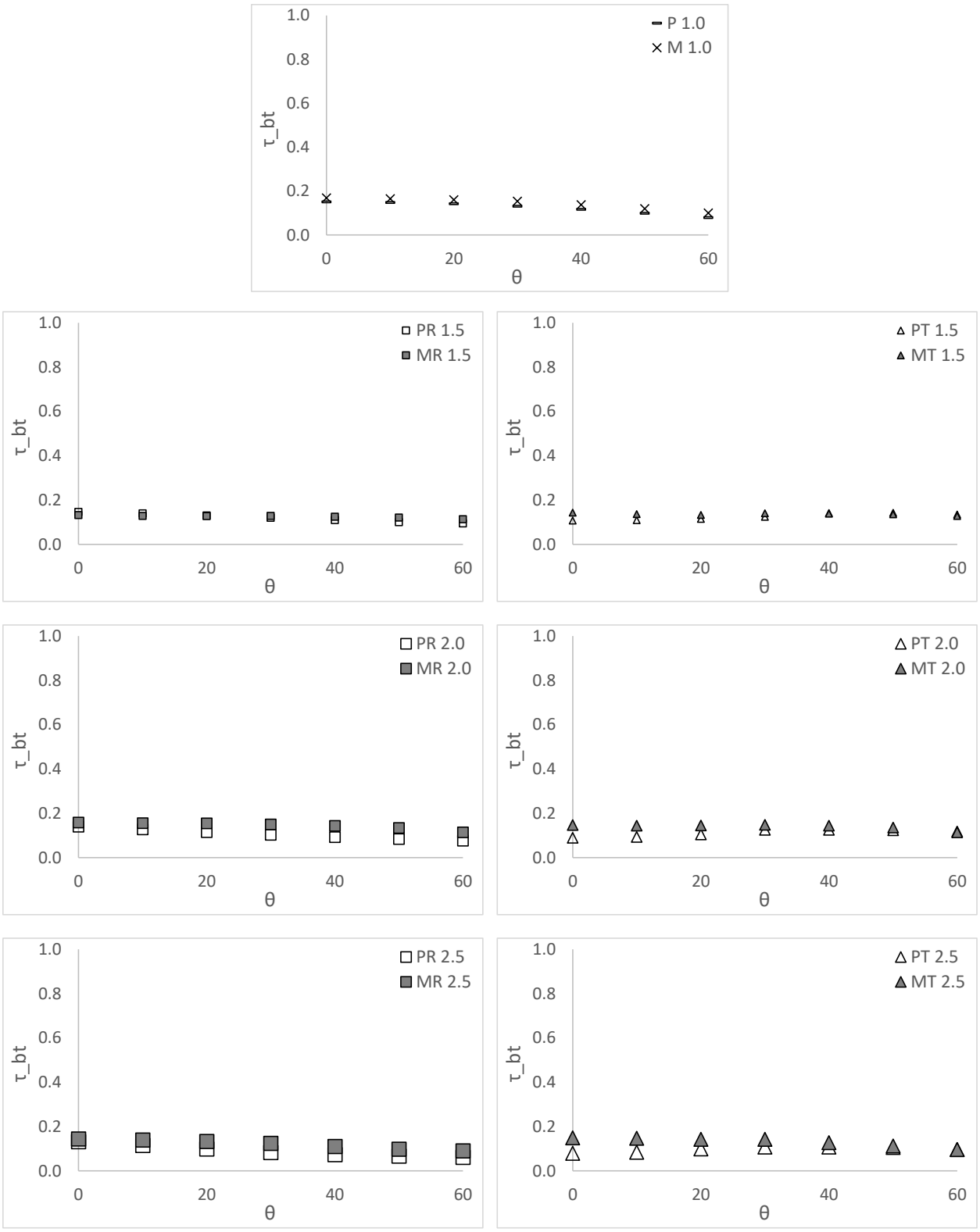

Figure 6.26: #27 Yellow05 – prediction vs measurement

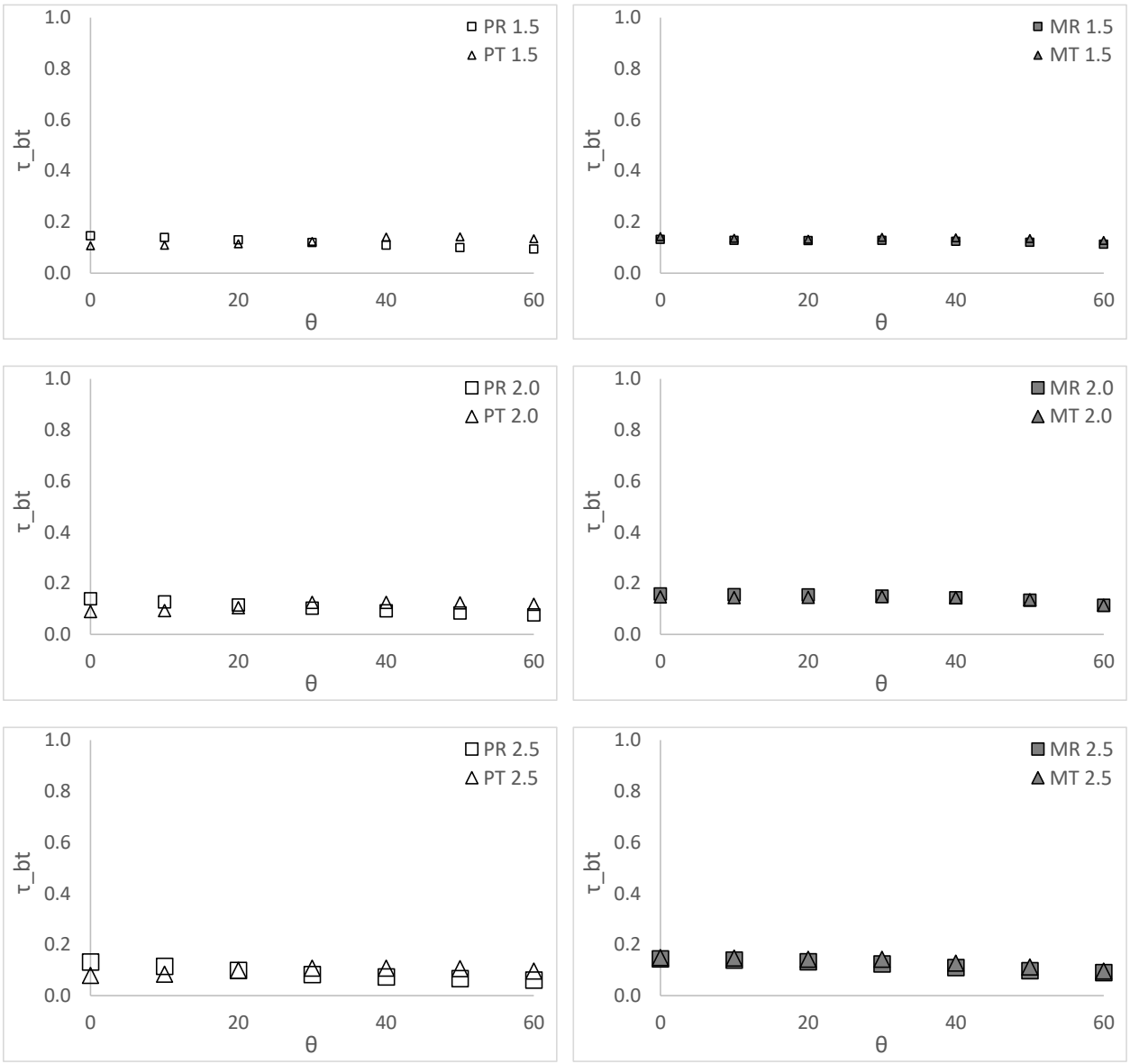

Figure 6.27: #27 Yellow05 – rectangular vs triangular profile

Table 6.11: #64 FashionBlack01 – calculated and measured τ_{bt} for various θ and Fr

#64 FashionBlack01 (τ_{bb} = 0.2412, τ_{bt} = 0.3780, ρ_{bt} = 0.1596)														
	Pleated Drape Models (P)							BAI-IS Measurements (M)						
		Rectangular (R)			Triangular (T)				Rectangular (R)			Triangular (T)		
θ	Flat	1.5	2.0	2.5	1.5	2.0	2.5	Flat	1.5	2.0	2.5	1.5	2.0	2.5
0	0.378	0.361	0.350	0.342	0.291	0.240	0.205	0.409	0.380	0.357	0.344	0.291	0.239	0.233
10	0.374	0.339	0.307	0.278	0.293	0.246	0.216	0.402	0.371	0.342	0.312	0.286	0.244	0.243
20	0.366	0.317	0.268	0.221	0.299	0.267	0.253	0.387	0.348	0.308	0.253	0.301	0.279	0.270
30	0.351	0.292	0.230	0.169	0.313	0.312	0.254	0.356	0.320	0.283	0.196	0.338	0.312	0.252
40	0.331	0.265	0.194	0.132	0.343	0.275	0.202	0.311	0.286	0.240	0.147	0.370	0.291	0.226
50	0.304	0.238	0.161	0.087	0.318	0.212	0.118	0.259	0.255	0.196	0.120	0.354	0.230	0.157
60	0.269	0.214	0.109	0.061	0.251	0.108	0.075	0.208	0.231	0.151	0.102	0.297	0.151	0.116

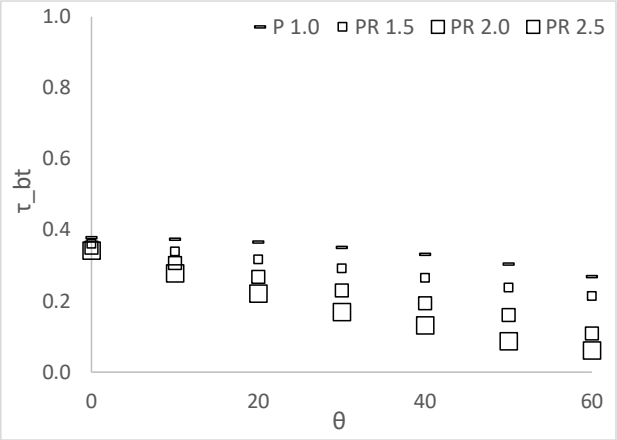

(a) Pleated Drape Model – Rectangular

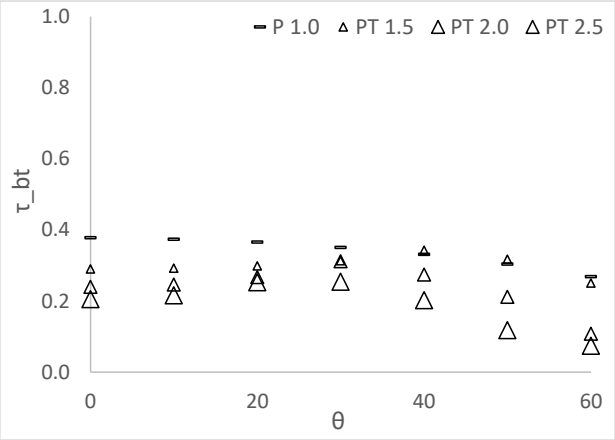

(b) Pleated Drape Model – Triangular

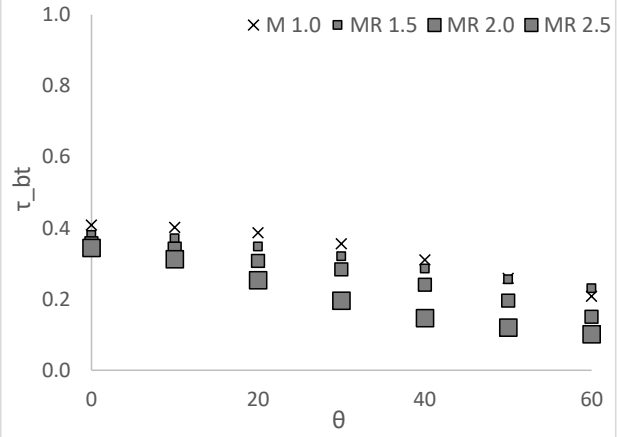

(c) BAI-IS Measurements – Rectangular

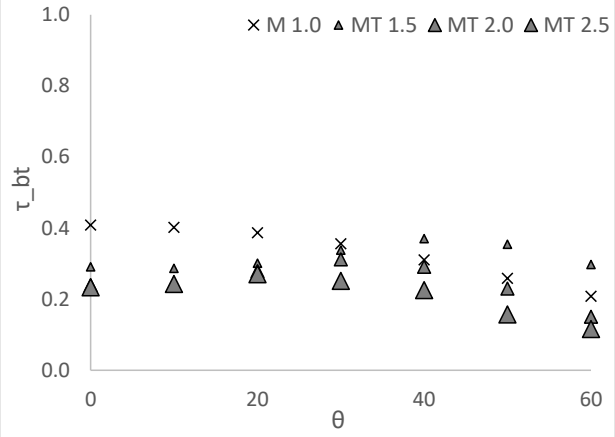

(d) BAI-IS Measurements – Triangular

Figure 6.28: #64 FashionBlack01 – calculated and measured τ_{bt} for various θ and Fr

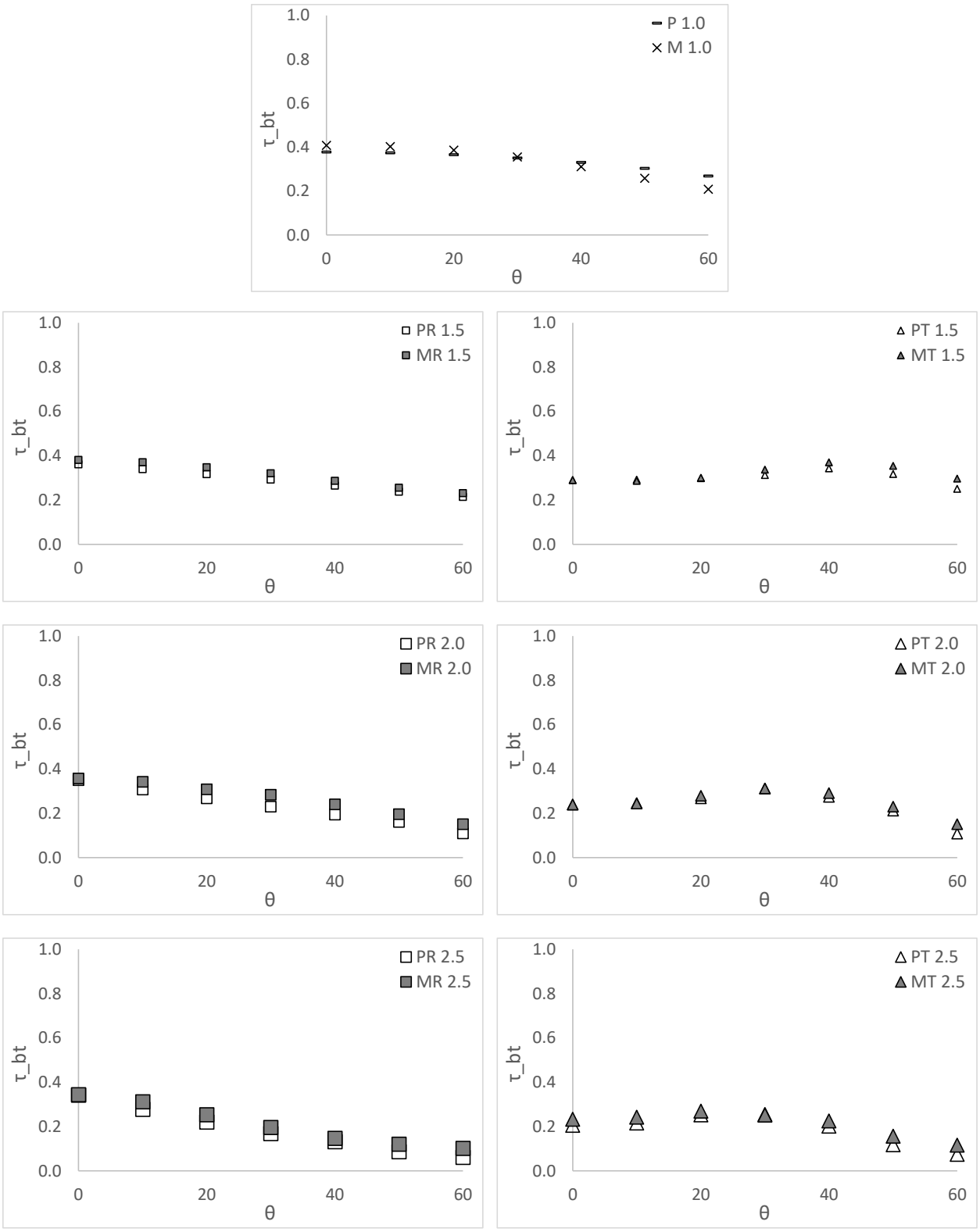

Figure 6.29: #64 FashionBlack01 – prediction vs measurement

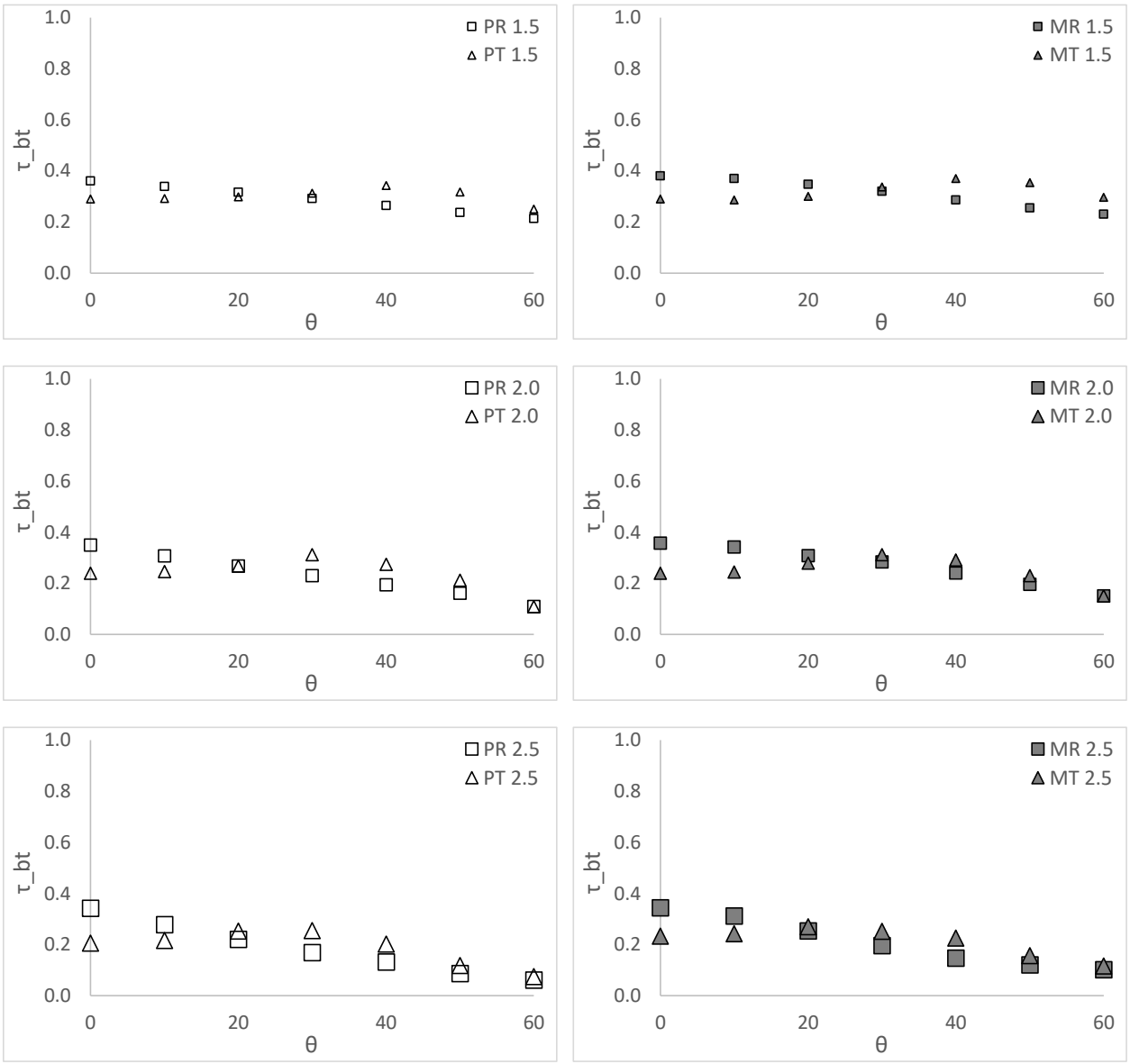

Figure 6.30: #64 FashionBlack01 – rectangular vs triangular profile

Table 6.12: #66 FashionLight01 – calculated and measured τ_{bt} for various θ and Fr

#66 FashionLight01 (τ_{bb} = 0.2537, τ_{bt} = 0.5332, ρ_{bt} = 0.3242)														
	Pleated Drape Models (P)							BAI-IS Measurements (M)						
		Rectangular (R)			Triangular (T)				Rectangular (R)			Triangular (T)		
θ	Flat	1.5	2.0	2.5	1.5	2.0	2.5	Flat	1.5	2.0	2.5	1.5	2.0	2.5
0	0.533	0.521	0.510	0.500	0.458	0.411	0.377	0.532	0.495	0.476	0.500	0.423	0.382	0.383
10	0.530	0.500	0.469	0.437	0.459	0.417	0.387	0.521	0.481	0.457	0.461	0.419	0.383	0.396
20	0.521	0.479	0.431	0.380	0.465	0.436	0.422	0.507	0.456	0.426	0.392	0.425	0.426	0.413
30	0.506	0.456	0.394	0.326	0.478	0.482	0.422	0.486	0.428	0.389	0.335	0.446	0.459	0.400
40	0.485	0.430	0.357	0.282	0.507	0.444	0.371	0.448	0.390	0.346	0.278	0.470	0.411	0.372
50	0.456	0.403	0.318	0.235	0.486	0.385	0.293	0.395	0.355	0.310	0.248	0.454	0.342	0.294
60	0.418	0.376	0.266	0.201	0.424	0.291	0.231	0.323	0.335	0.248	0.208	0.392	0.222	0.246

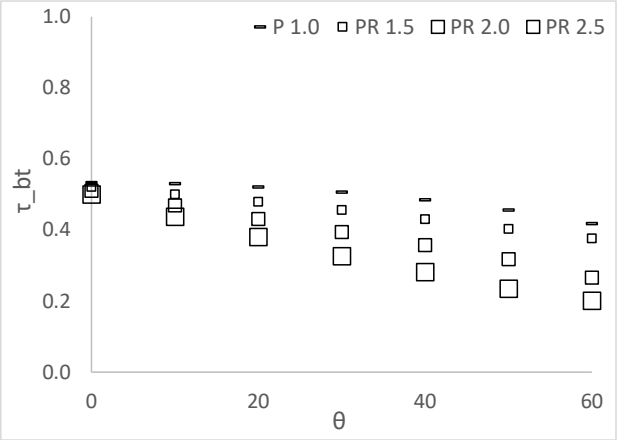

(a) Pleated Drape Model – Rectangular

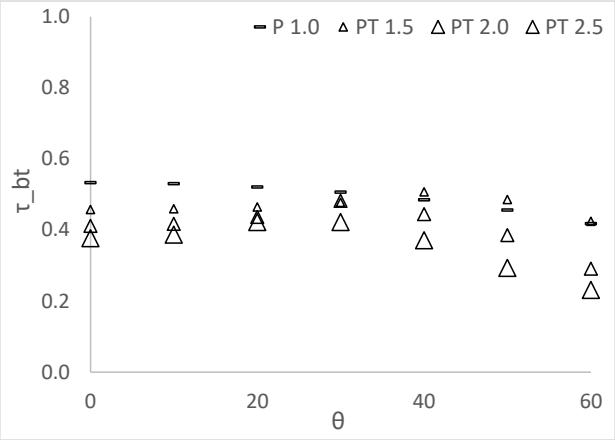

(b) Pleated Drape Model – Triangular

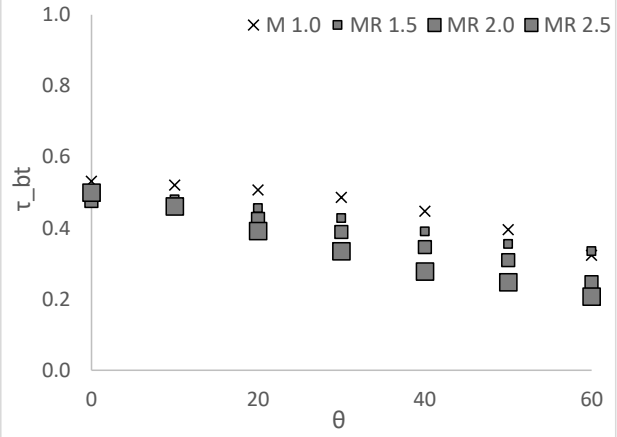

(c) BAI-IS Measurements – Rectangular

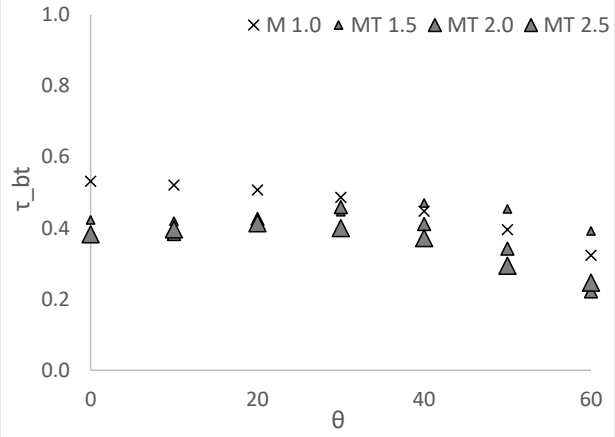

(d) BAI-IS Measurements – Triangular

Figure 6.31: #66 FashionLight01 – calculated and measured τ_{bt} for various θ and Fr

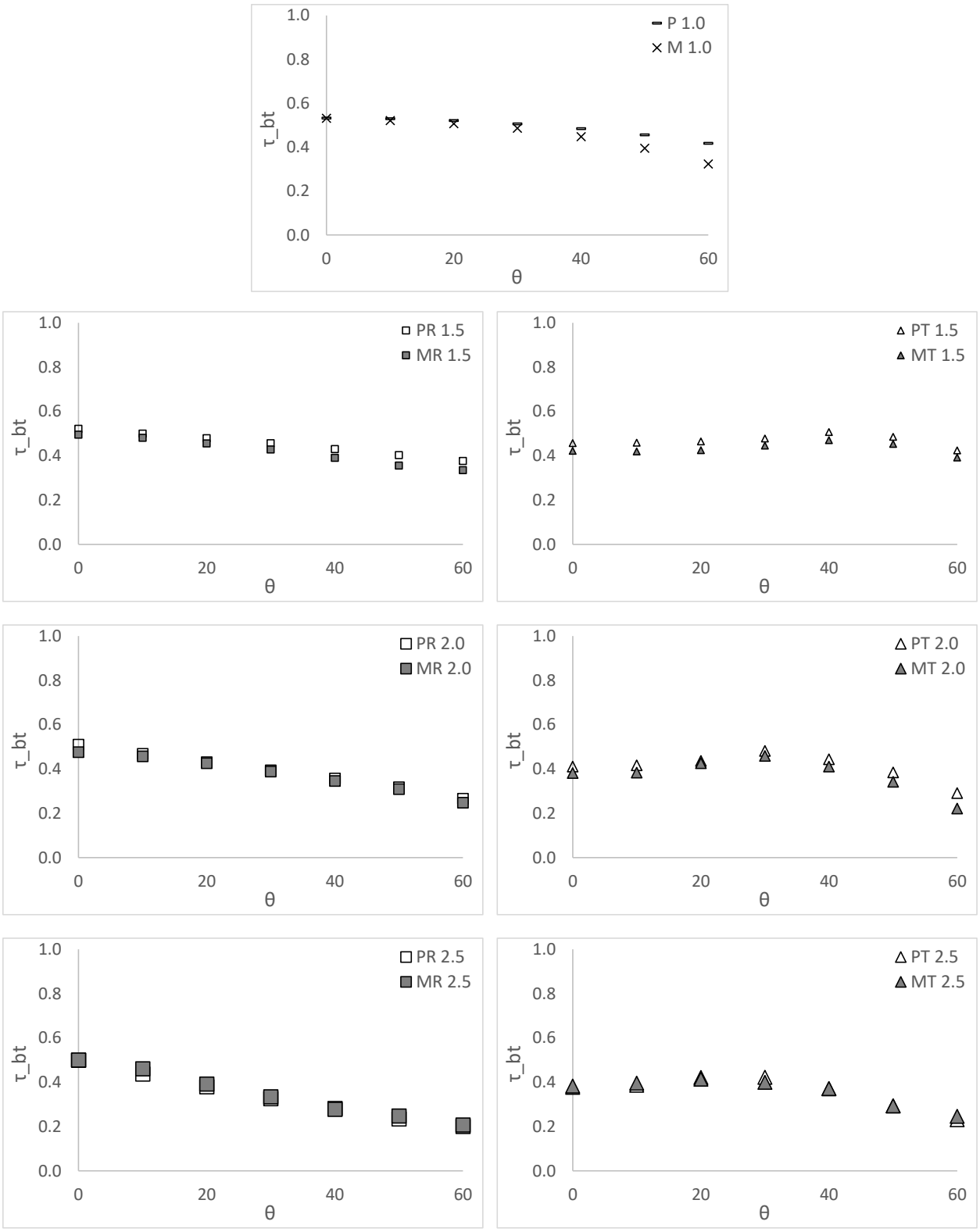

Figure 6.32: #66 FashionLight01 – prediction vs measurement

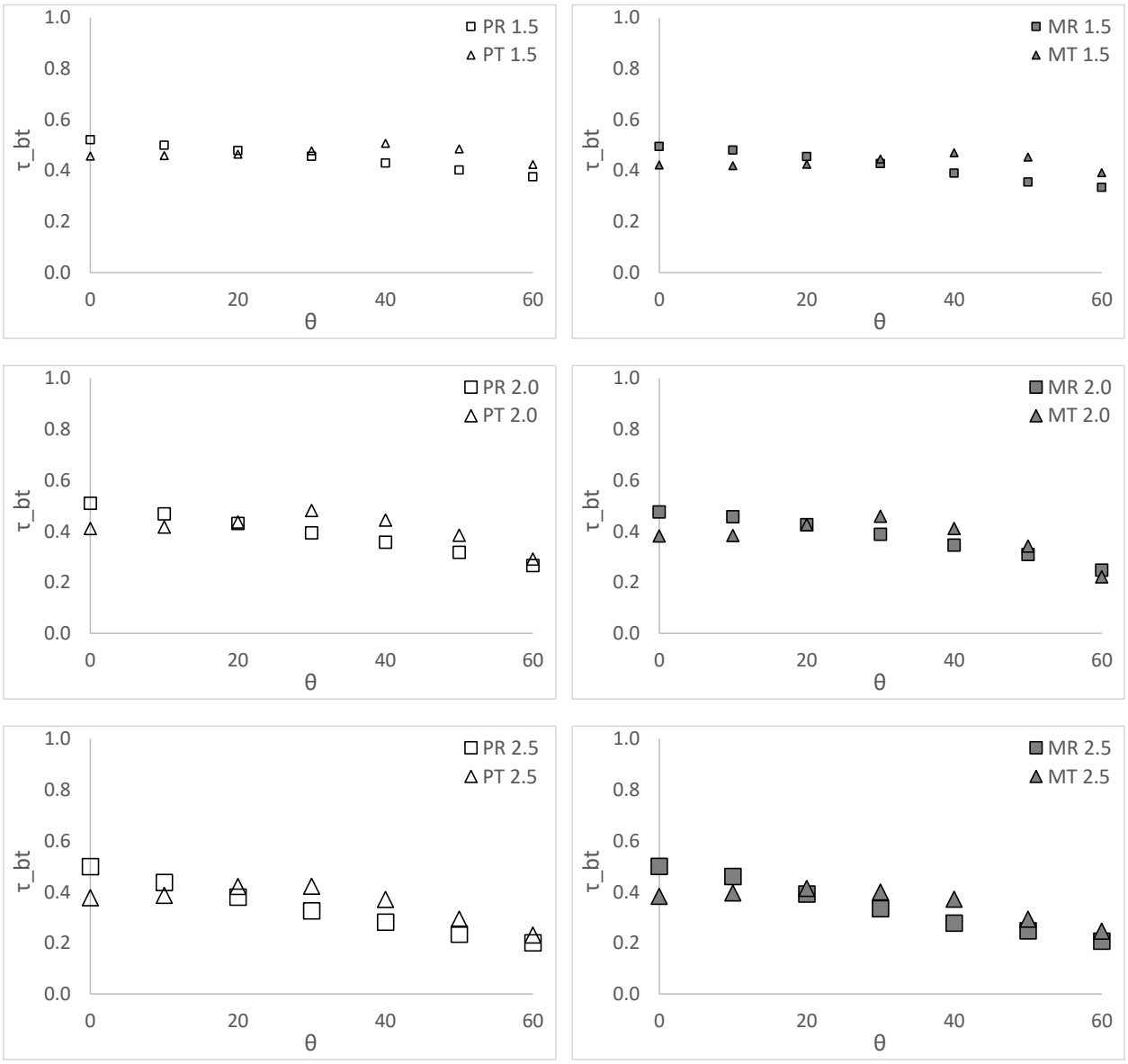

Figure 6.33: #66 FashionLight01 – rectangular vs triangular profile

Table 6.13: #68 GreenOpen01 – calculated and measured τ_{bt} for various θ and Fr

#68 GreenOpen01 (τ_{bb} = 0.1552, τ_{bt} = 0.4195, ρ_{bt} = 0.2863)														
	Pleated Drape Models (P)							BAI-IS Measurements (M)						
		Rectangular (R)			Triangular (T)				Rectangular (R)			Triangular (T)		
θ	Flat	1.5	2.0	2.5	1.5	2.0	2.5	Flat	1.5	2.0	2.5	1.5	2.0	2.5
0	0.419	0.396	0.378	0.365	0.328	0.274	0.236	0.429	0.375	0.345	0.351	0.364	0.324	0.334
10	0.416	0.377	0.342	0.309	0.329	0.279	0.246	0.419	0.370	0.334	0.325	0.359	0.326	0.331
20	0.407	0.358	0.307	0.258	0.335	0.298	0.277	0.406	0.367	0.317	0.294	0.366	0.335	0.321
30	0.393	0.336	0.274	0.209	0.348	0.338	0.282	0.392	0.356	0.299	0.254	0.373	0.331	0.303
40	0.373	0.312	0.240	0.176	0.376	0.314	0.249	0.365	0.330	0.272	0.212	0.363	0.305	0.270
50	0.345	0.288	0.211	0.144	0.362	0.273	0.196	0.330	0.306	0.236	0.169	0.344	0.264	0.215
60	0.310	0.265	0.174	0.122	0.318	0.208	0.155	0.284	0.290	0.176	0.144	0.292	0.183	0.172

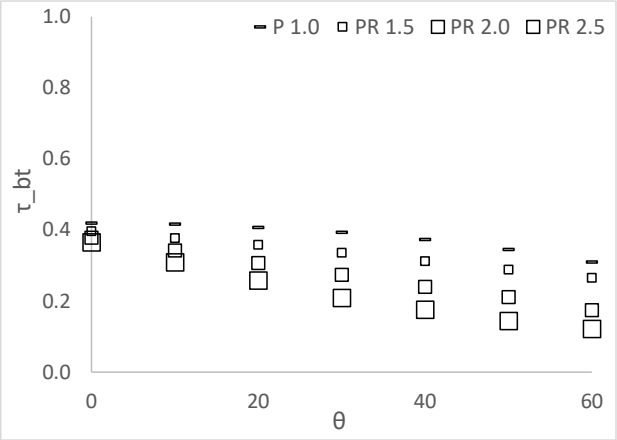

(a) Pleated Drape Model – Rectangular

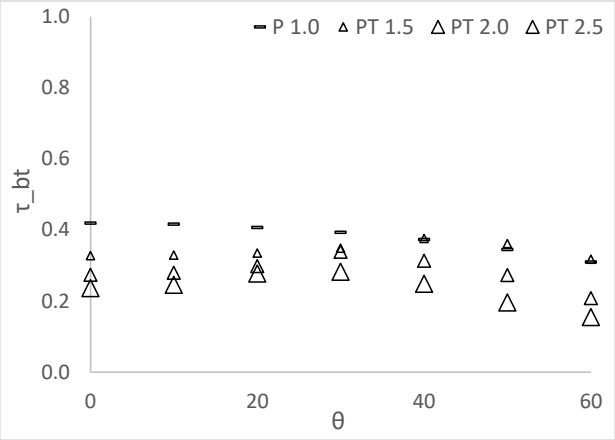

(b) Pleated Drape Model – Triangular

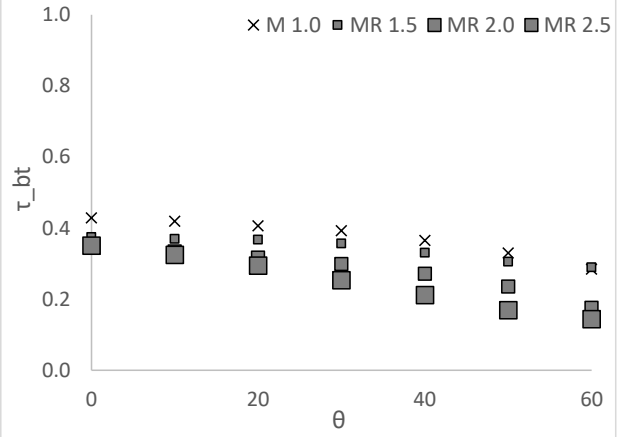

(c) BAI-IS Measurements – Rectangular

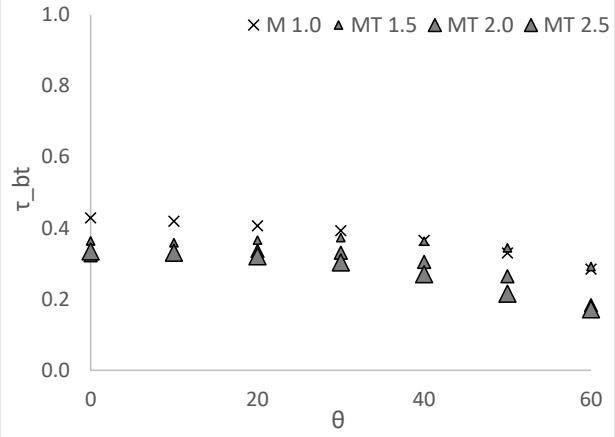

(d) BAI-IS Measurements – Triangular

Figure 6.34: #68 GreenOpen01 – calculated and measured τ_{bt} for various θ and Fr

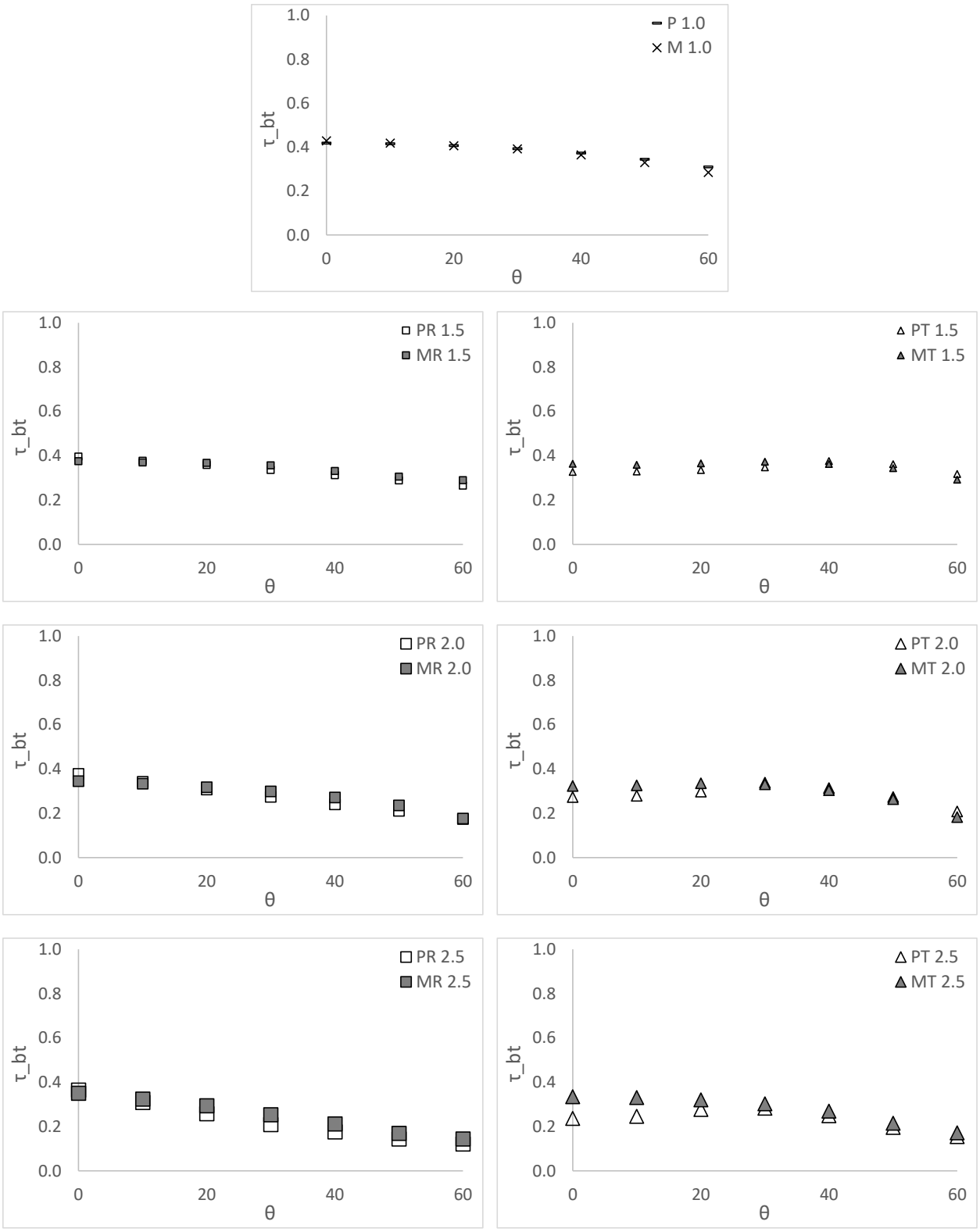

Figure 6.35: #68 GreenOpen01 – prediction vs measurement

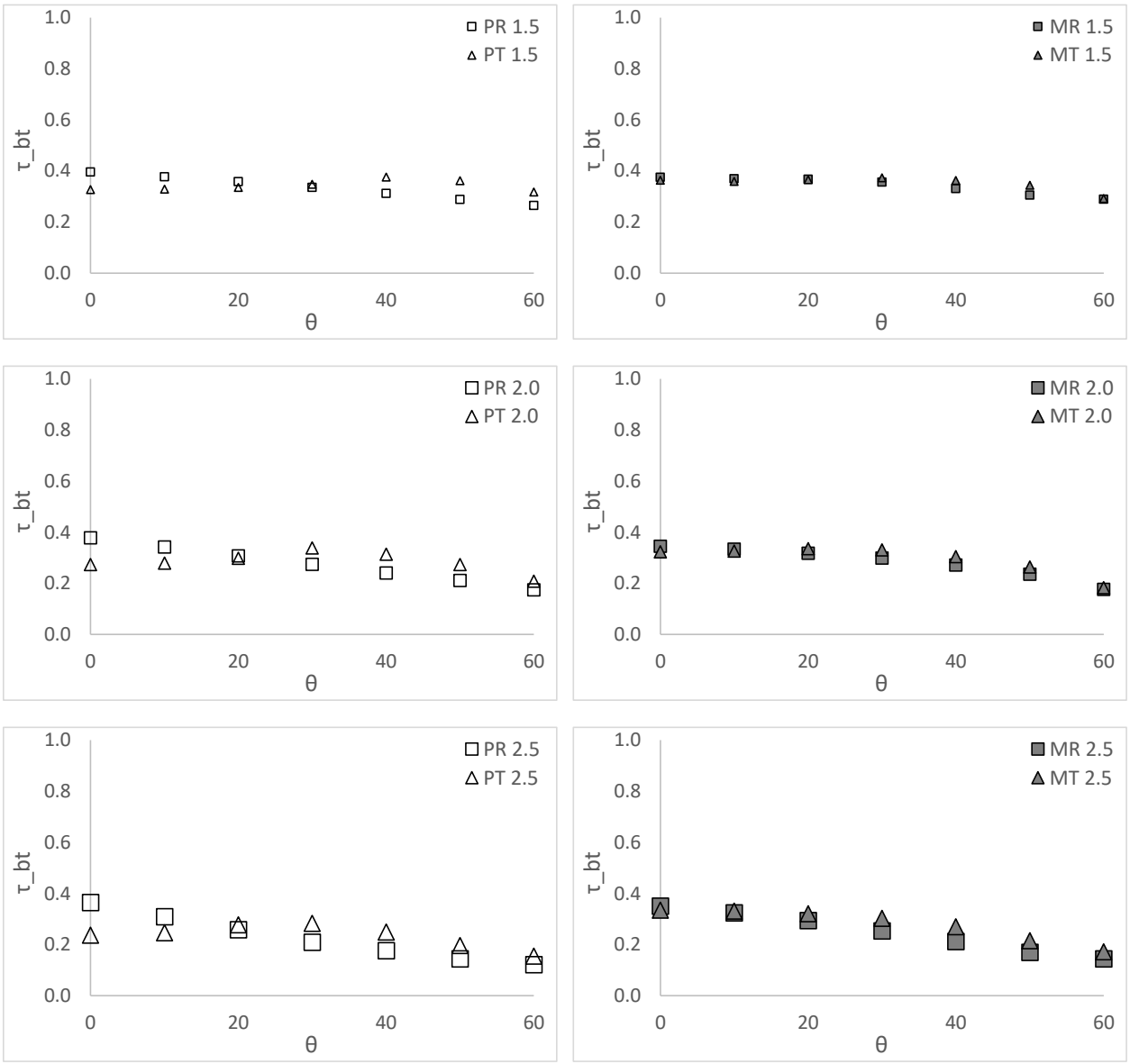

Figure 6.36: #68 GreenOpen01 – rectangular vs triangular profile

Table 6.14: #71 RoughRed – calculated and measured τ_{bt} for various θ and Fr

#71 RoughRed (τ_{bb} = 0.0404, τ_{bt} = 0.1873, ρ_{bt} = 0.3394)														
	Pleated Drape Models (P)							BAI-IS Measurements (M)						
		Rectangular (R)			Triangular (T)				Rectangular (R)			Triangular (T)		
θ	Flat	1.5	2.0	2.5	1.5	2.0	2.5	Flat	1.5	2.0	2.5	1.5	2.0	2.5
0	0.187	0.172	0.161	0.152	0.123	0.092	0.074	0.230	0.182	0.188	0.189	0.187	0.181	0.173
10	0.184	0.163	0.143	0.126	0.124	0.096	0.080	0.219	0.179	0.184	0.187	0.180	0.173	0.175
20	0.177	0.151	0.125	0.101	0.131	0.110	0.099	0.213	0.180	0.181	0.173	0.177	0.166	0.174
30	0.165	0.137	0.107	0.077	0.142	0.134	0.107	0.206	0.185	0.176	0.150	0.183	0.161	0.159
40	0.149	0.123	0.091	0.064	0.161	0.130	0.101	0.188	0.167	0.168	0.128	0.184	0.149	0.135
50	0.129	0.110	0.080	0.055	0.159	0.120	0.087	0.160	0.163	0.146	0.102	0.172	0.126	0.114
60	0.105	0.100	0.067	0.047	0.143	0.100	0.073	0.122	0.150	0.107	0.082	0.152	0.101	0.094

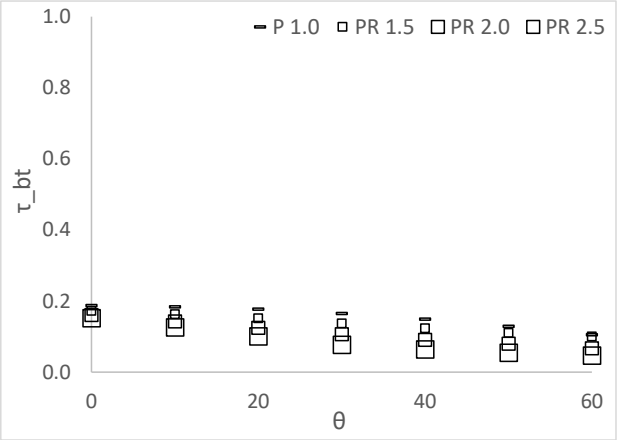

(a) Pleated Drape Model – Rectangular

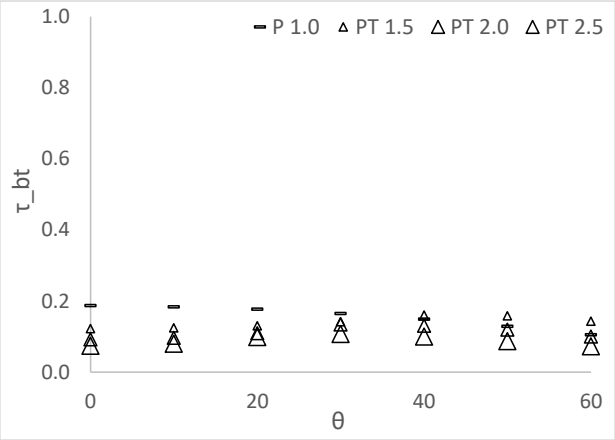

(b) Pleated Drape Model – Triangular

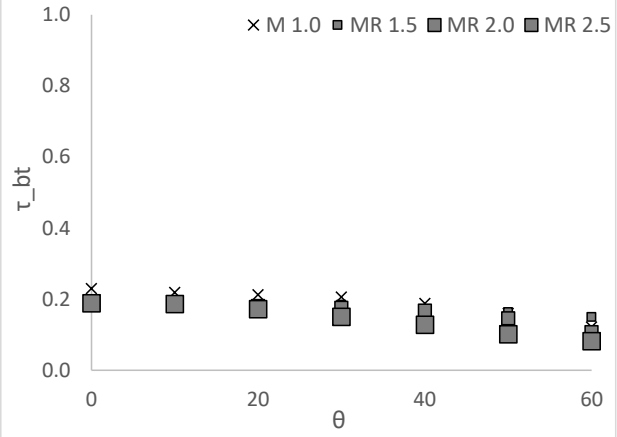

(c) BAI-IS Measurements – Rectangular

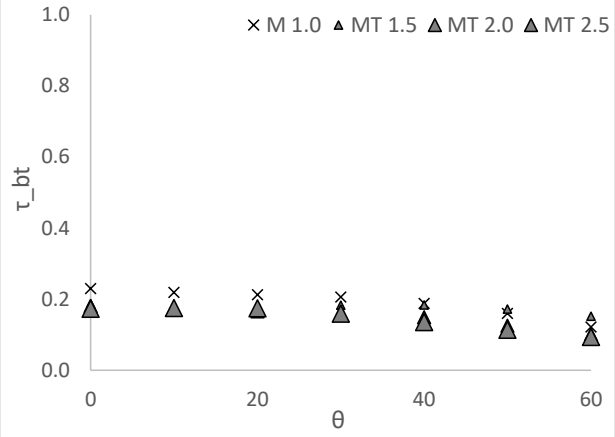

(d) BAI-IS Measurements – Triangular

Figure 6.37: #71 RoughRed – calculated and measured τ_{bt} for various θ and Fr

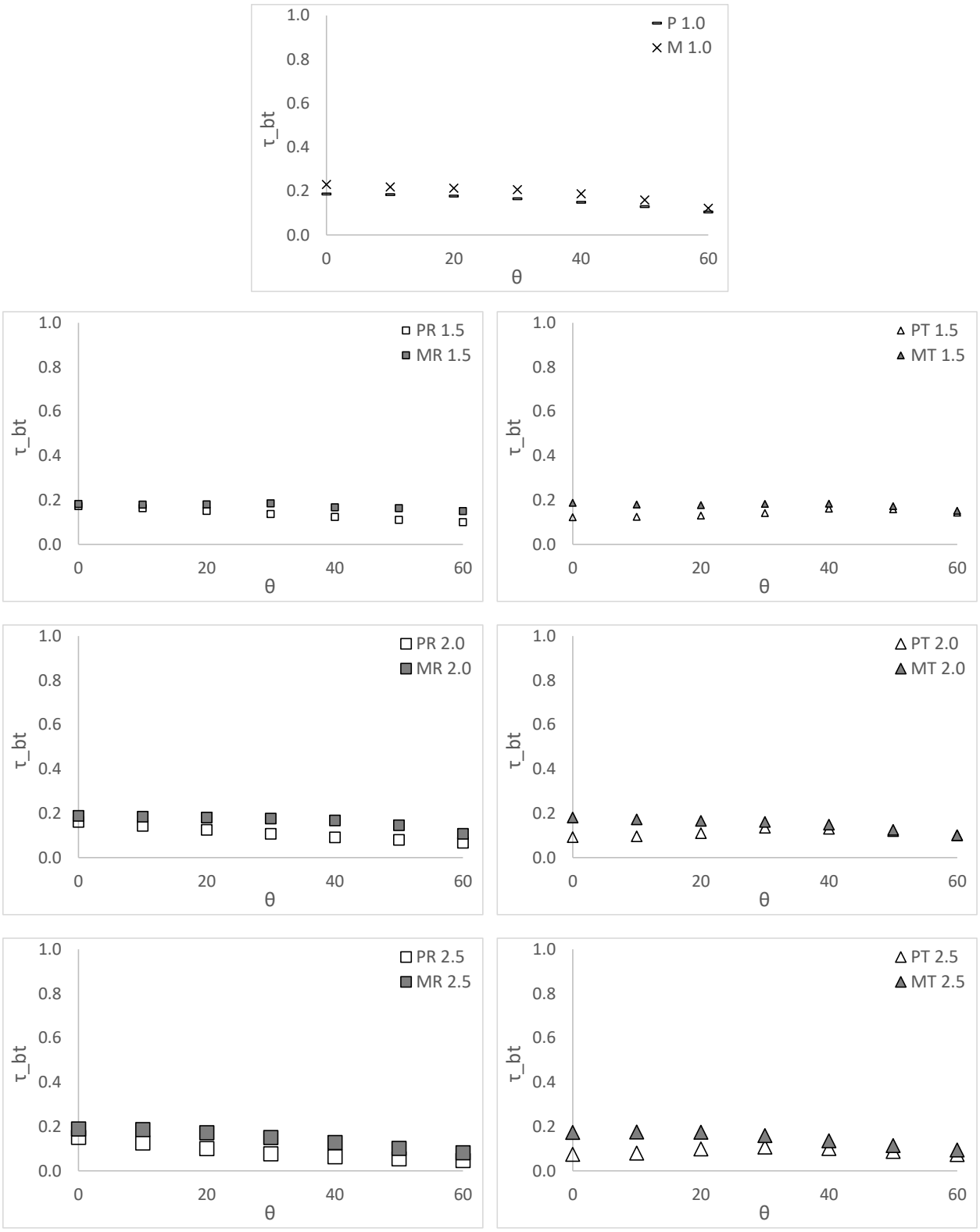

Figure 6.38: #71 RoughRed – prediction vs measurement

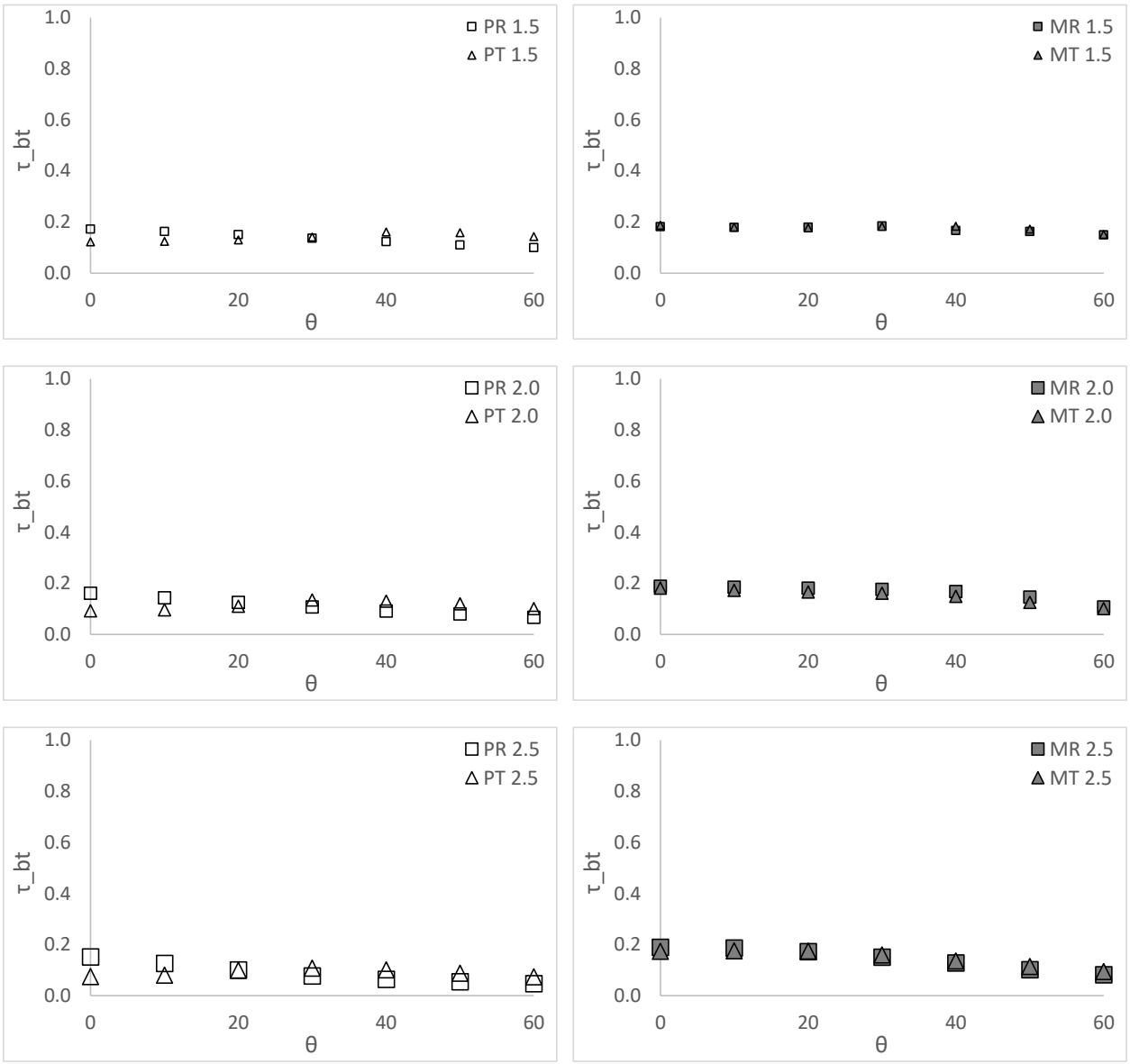

Figure 6.39: #71 RoughRed – rectangular vs triangular profile

Table 6.15: #72 Thin01 – calculated and measured τ_{bt} for various θ and Fr

#72 Thin01 (τ_{bb} = 0.4445, τ_{bt} = 0.7284, ρ_{bt} = 0.0918)														
	Pleated Drape Models (P)							BAI-IS Measurements (M)						
		Rectangular (R)			Triangular (T)				Rectangular (R)			Triangular (T)		
θ	Flat	1.5	2.0	2.5	1.5	2.0	2.5	Flat	1.5	2.0	2.5	1.5	2.0	2.5
0	0.728	0.695	0.674	0.661	0.584	0.508	0.457	0.762	0.699	0.680	0.682	0.703	0.681	0.670
10	0.723	0.660	0.606	0.558	0.586	0.516	0.471	0.753	0.687	0.671	0.660	0.693	0.680	0.640
20	0.711	0.625	0.545	0.469	0.594	0.542	0.520	0.741	0.685	0.650	0.610	0.683	0.683	0.619
30	0.690	0.586	0.484	0.383	0.611	0.605	0.504	0.724	0.673	0.631	0.573	0.682	0.665	0.576
40	0.661	0.543	0.421	0.313	0.651	0.527	0.399	0.696	0.646	0.567	0.505	0.653	0.624	0.503
50	0.621	0.494	0.358	0.231	0.600	0.408	0.242	0.664	0.614	0.515	0.426	0.604	0.559	0.413
60	0.569	0.441	0.268	0.180	0.474	0.218	0.161	0.622	0.547	0.387	0.357	0.514	0.420	0.354

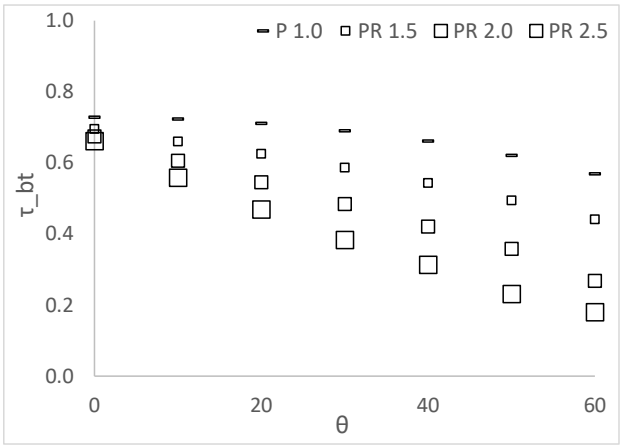

(a) Pleated Drape Model – Rectangular

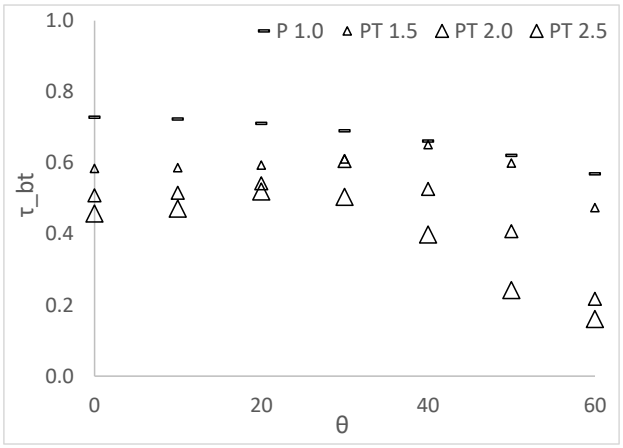

(b) Pleated Drape Model – Triangular

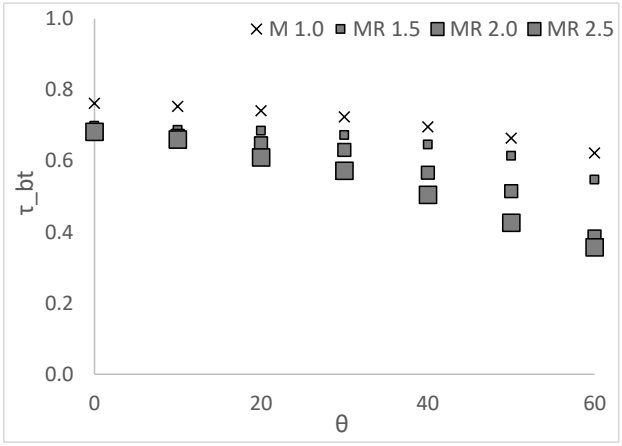

(c) BAI-IS Measurements – Rectangular

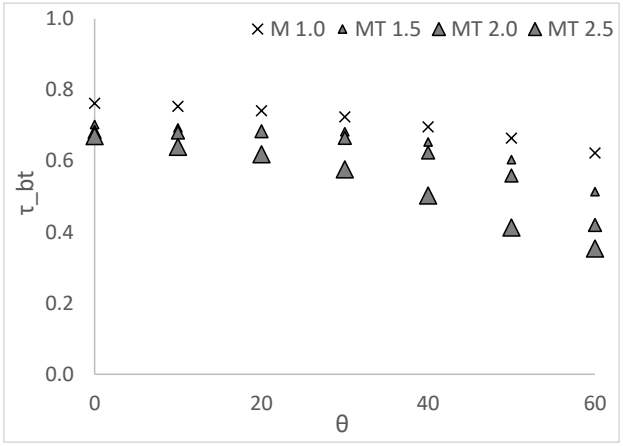

(d) BAI-IS Measurements – Triangular

Figure 6.40: #72 Thin01 – calculated and measured τ_{bt} for various θ and Fr

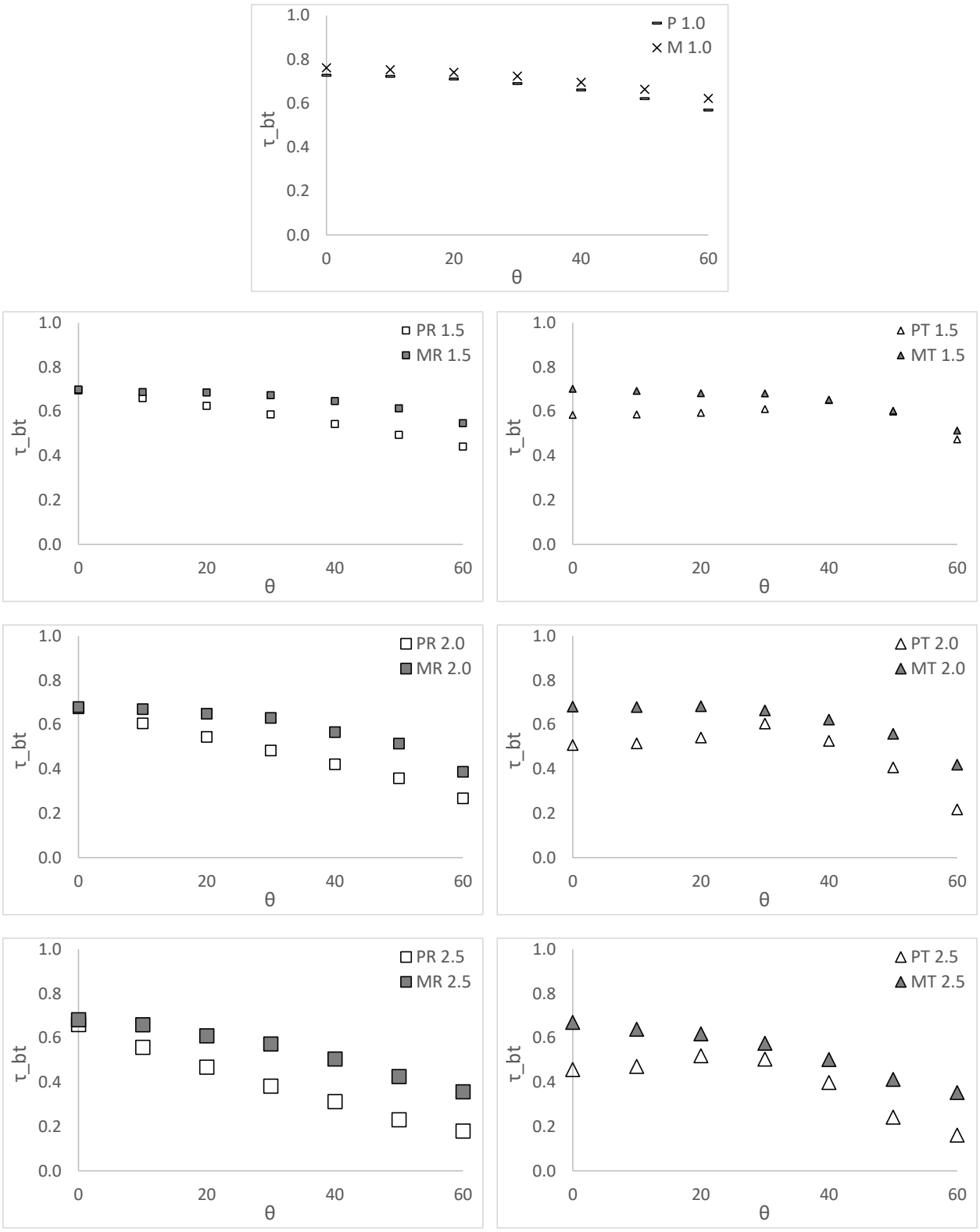

Figure 6.41: #72 Thin01 – prediction vs measurement

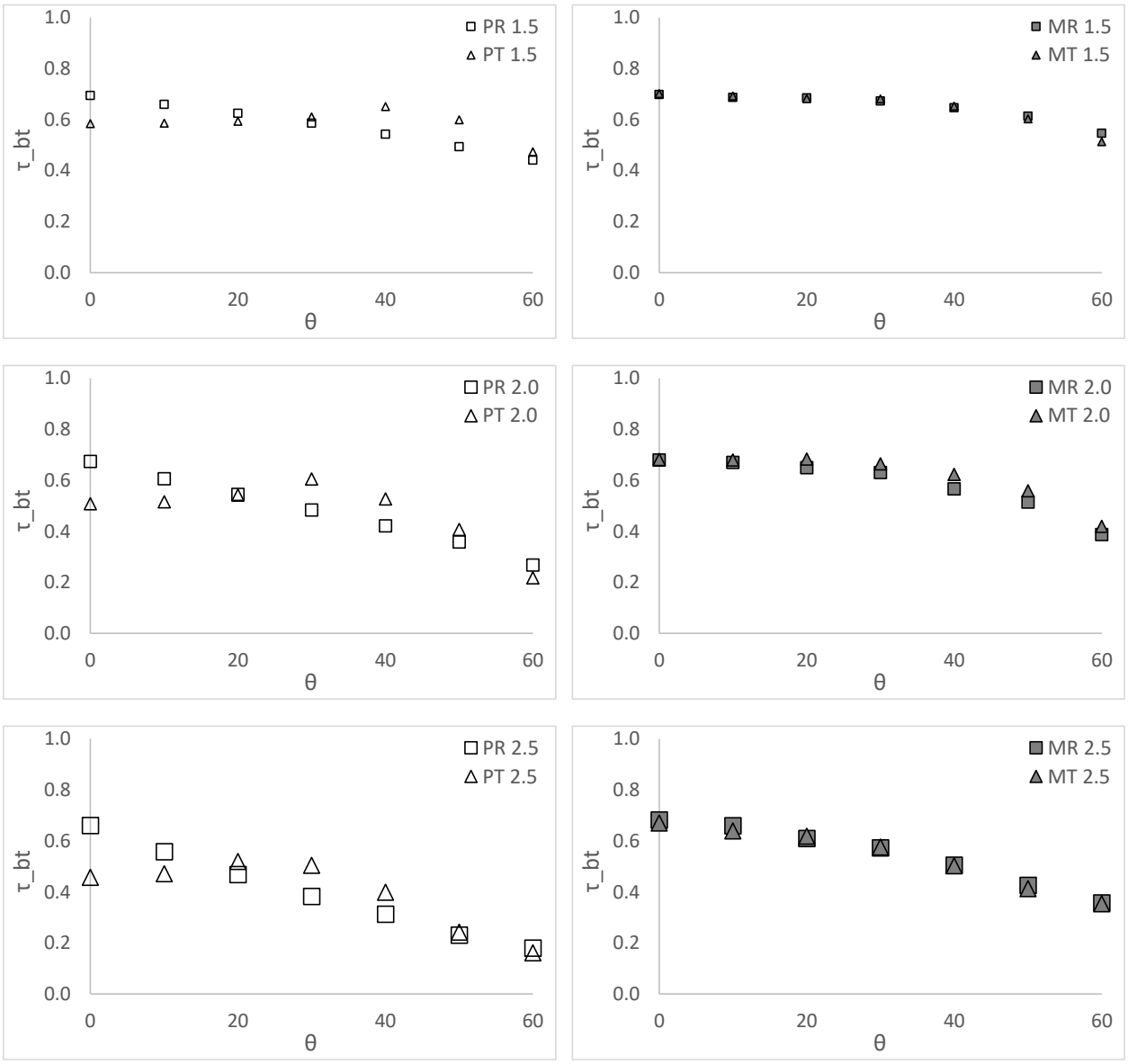

Figure 6.42: #72 Thin01 – rectangular vs triangular profile

Table 6.16: #73 Thin02 – calculated and measured τ_{bt} for various θ and Fr

#73 Thin02 (τ_{bb} = 0.3521, τ_{bt} = 0.5355, ρ_{bt} = 0.0922)														
	Pleated Drape Models (P)							BAI-IS Measurements (M)						
		Rectangular (R)			Triangular (T)				Rectangular (R)			Triangular (T)		
θ	Flat	1.5	2.0	2.5	1.5	2.0	2.5	Flat	1.5	2.0	2.5	1.5	2.0	2.5
0	0.535	0.510	0.496	0.485	0.428	0.365	0.322	0.566	0.527	0.514	0.518	0.523	0.482	0.506
10	0.532	0.482	0.439	0.400	0.430	0.372	0.334	0.554	0.525	0.497	0.491	0.519	0.478	0.495
20	0.522	0.453	0.388	0.325	0.436	0.394	0.375	0.540	0.519	0.471	0.449	0.512	0.487	0.471
30	0.507	0.422	0.338	0.254	0.449	0.445	0.365	0.523	0.502	0.445	0.409	0.522	0.480	0.433
40	0.486	0.388	0.287	0.199	0.482	0.383	0.280	0.493	0.471	0.397	0.360	0.506	0.442	0.371
50	0.457	0.351	0.237	0.131	0.440	0.286	0.152	0.455	0.453	0.334	0.298	0.479	0.381	0.285
60	0.418	0.311	0.162	0.093	0.339	0.131	0.091	0.408	0.383	0.228	0.202	0.415	0.283	0.210

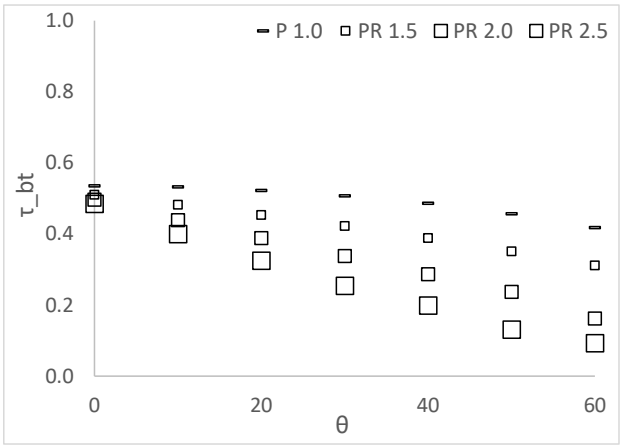

(a) Pleated Drape Model – Rectangular

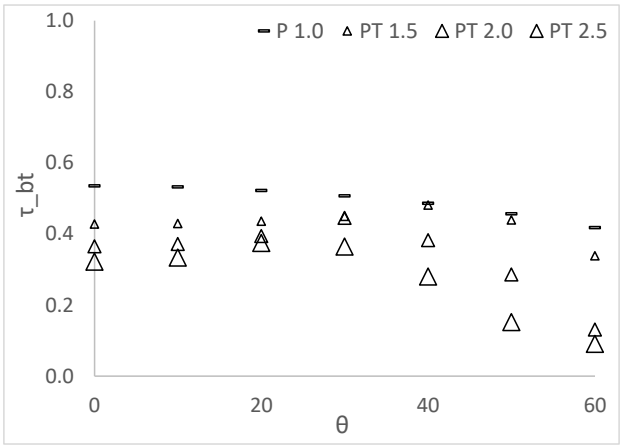

(b) Pleated Drape Model – Triangular

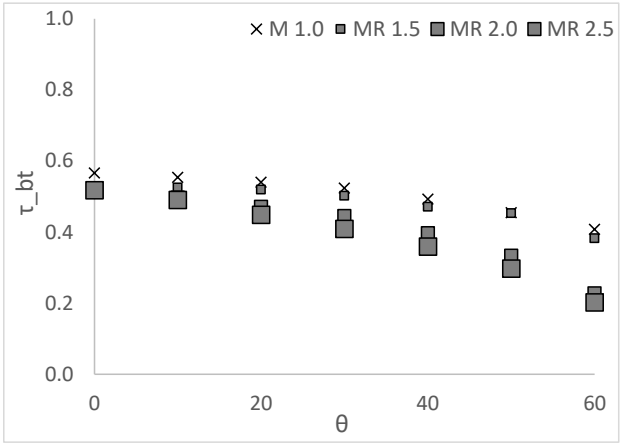

(c) BAI-IS Measurements – Rectangular

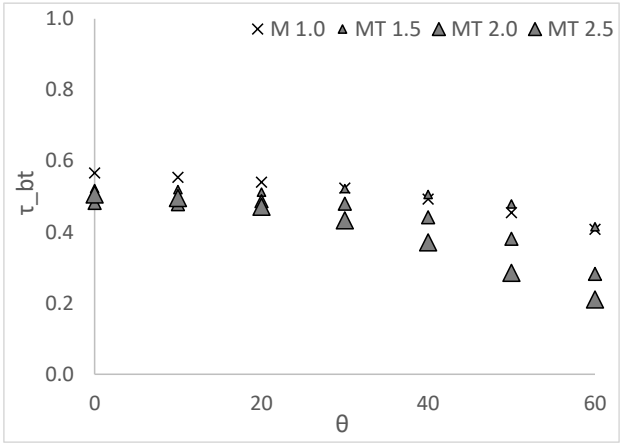

(d) BAI-IS Measurements – Triangular

Figure 6.43: #73 Thin02 – calculated and measured τ_{bt} for various θ and Fr

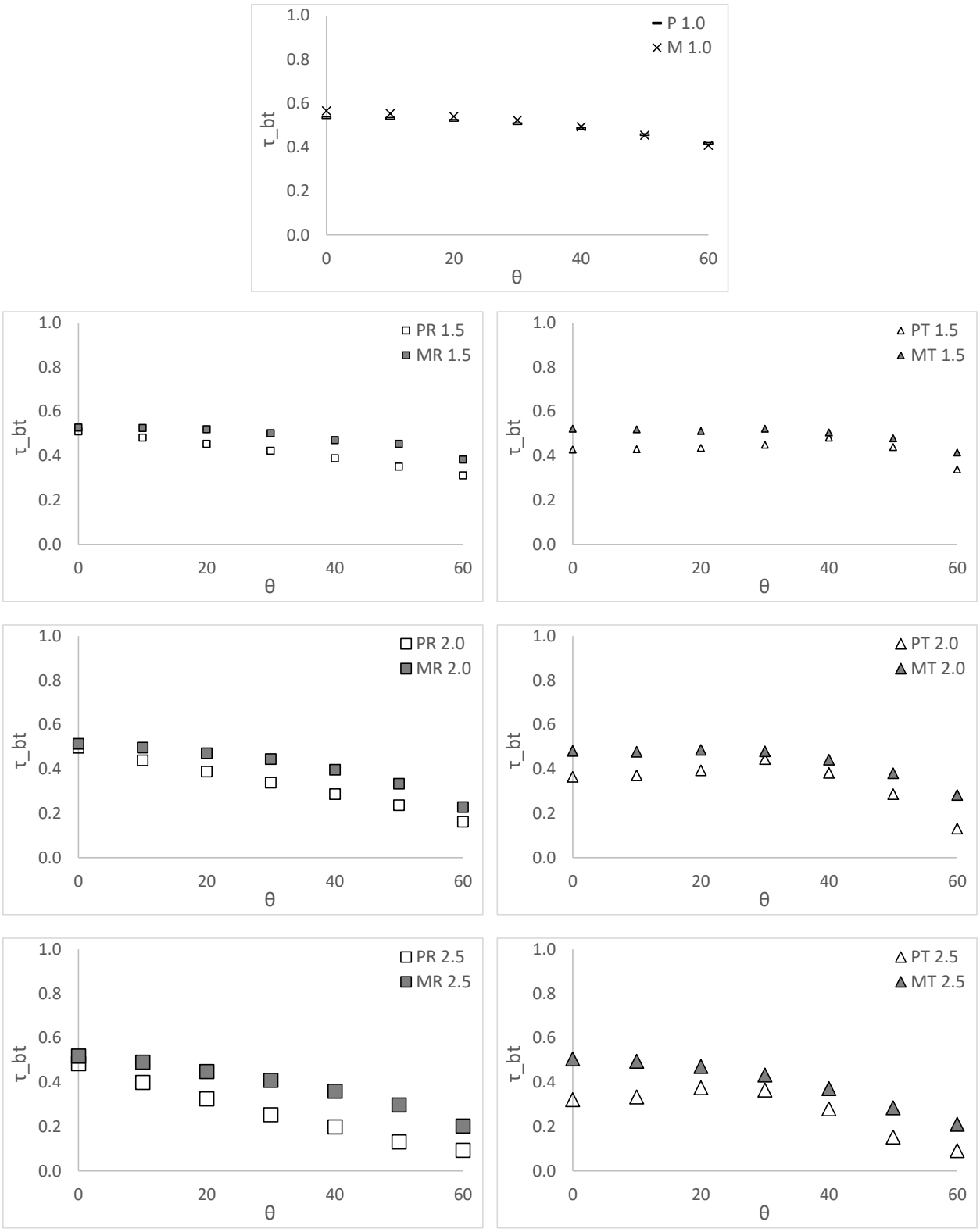

Figure 6.44: #73 Thin02 – prediction vs measurement

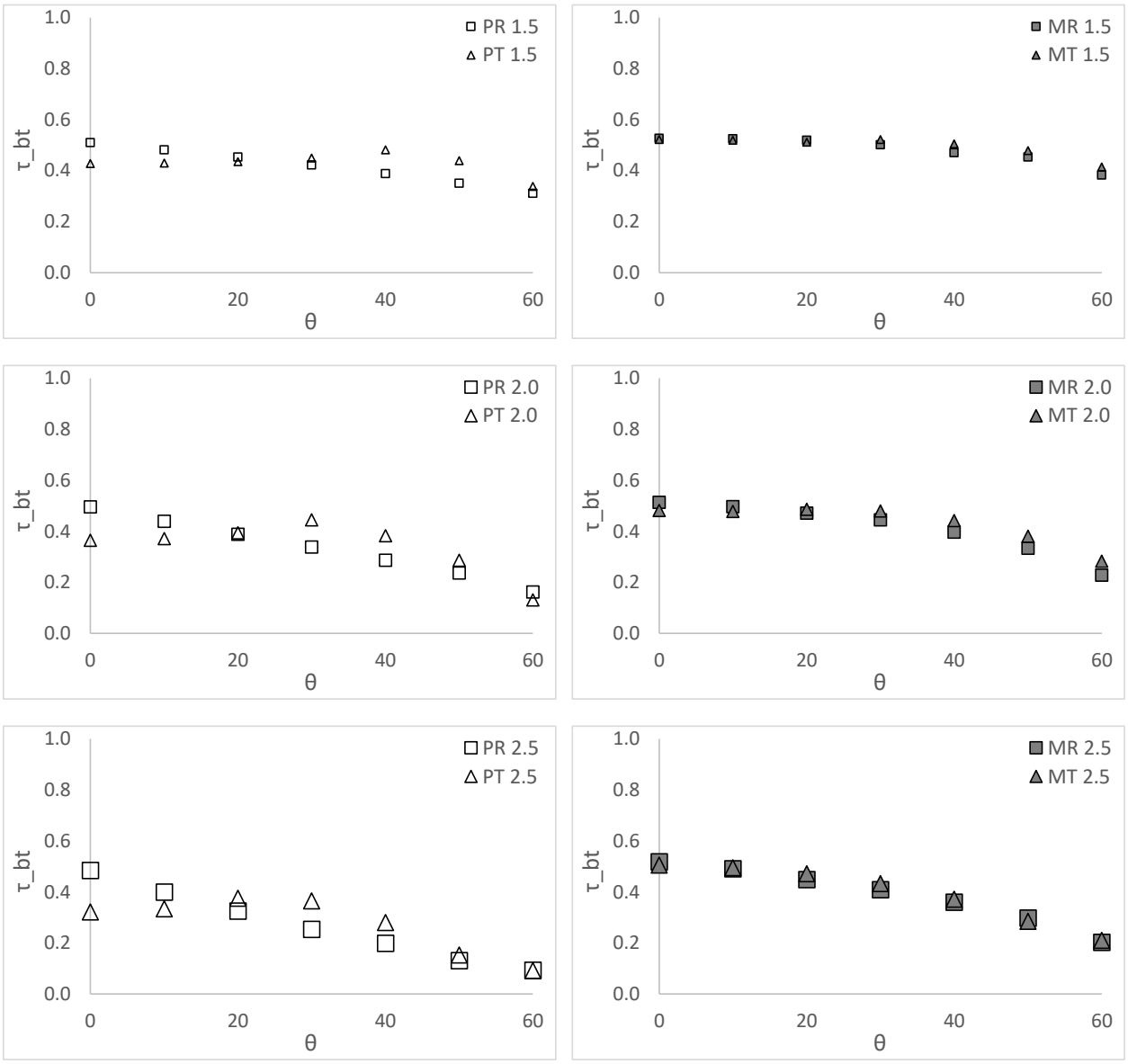

Figure 6.45: #73 Thin02 – rectangular vs triangular profile

Table 6.17: #75 Thin04 – calculated and measured τ_{bt} for various θ and Fr

#75 Thin04 (τ_{bb} = 0.4140, τ_{bt} = 0.6887, ρ_{bt} = 0.0962)														
	Pleated Drape Models (P)							BAI-IS Measurements (M)						
		Rectangular (R)			Triangular (T)				Rectangular (R)			Triangular (T)		
θ	Flat	1.5	2.0	2.5	1.5	2.0	2.5	Flat	1.5	2.0	2.5	1.5	2.0	2.5
0	0.688	0.655	0.635	0.621	0.550	0.475	0.424	0.738	0.692	0.664	0.658	0.664	0.663	0.659
10	0.684	0.622	0.569	0.522	0.552	0.482	0.438	0.727	0.687	0.654	0.636	0.656	0.654	0.651
20	0.672	0.588	0.510	0.436	0.559	0.508	0.485	0.713	0.679	0.627	0.605	0.653	0.635	0.614
30	0.653	0.551	0.452	0.353	0.575	0.568	0.472	0.697	0.672	0.594	0.560	0.648	0.613	0.572
40	0.625	0.510	0.391	0.286	0.614	0.495	0.373	0.669	0.627	0.523	0.508	0.614	0.557	0.514
50	0.588	0.464	0.331	0.209	0.566	0.383	0.226	0.630	0.606	0.481	0.426	0.576	0.472	0.418
60	0.538	0.414	0.246	0.162	0.448	0.206	0.150	0.587	0.533	0.354	0.334	0.495	0.366	0.339

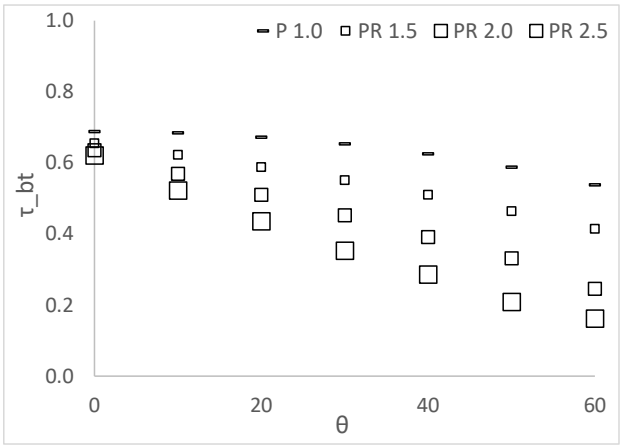

(a) Pleated Drape Model – Rectangular

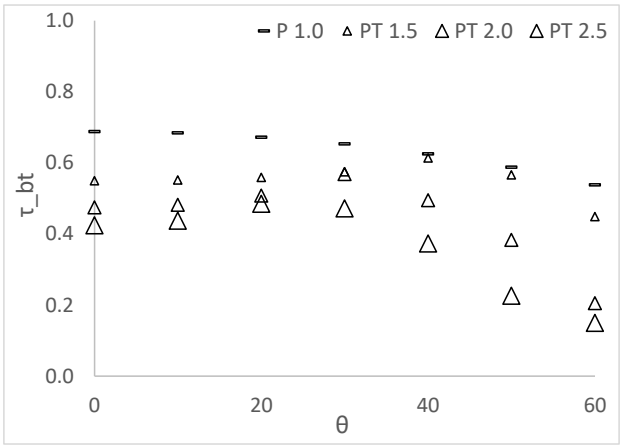

(b) Pleated Drape Model – Triangular

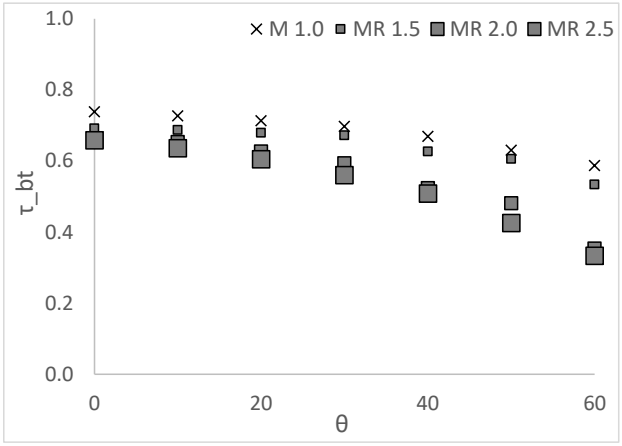

(c) BAI-IS Measurements – Rectangular

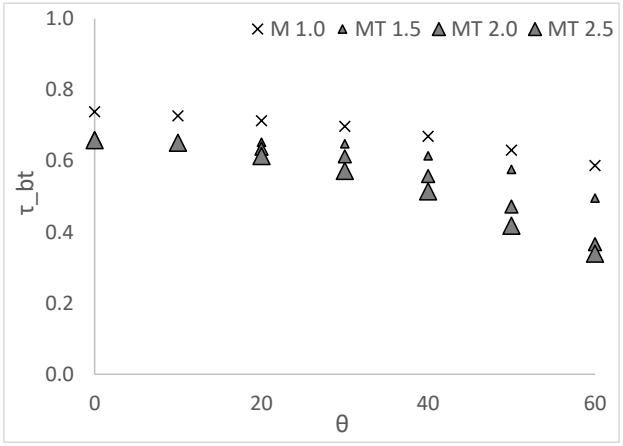

(d) BAI-IS Measurements – Triangular

Figure 6.46: #75 Thin04 – calculated and measured τ_{bt} for various θ and Fr

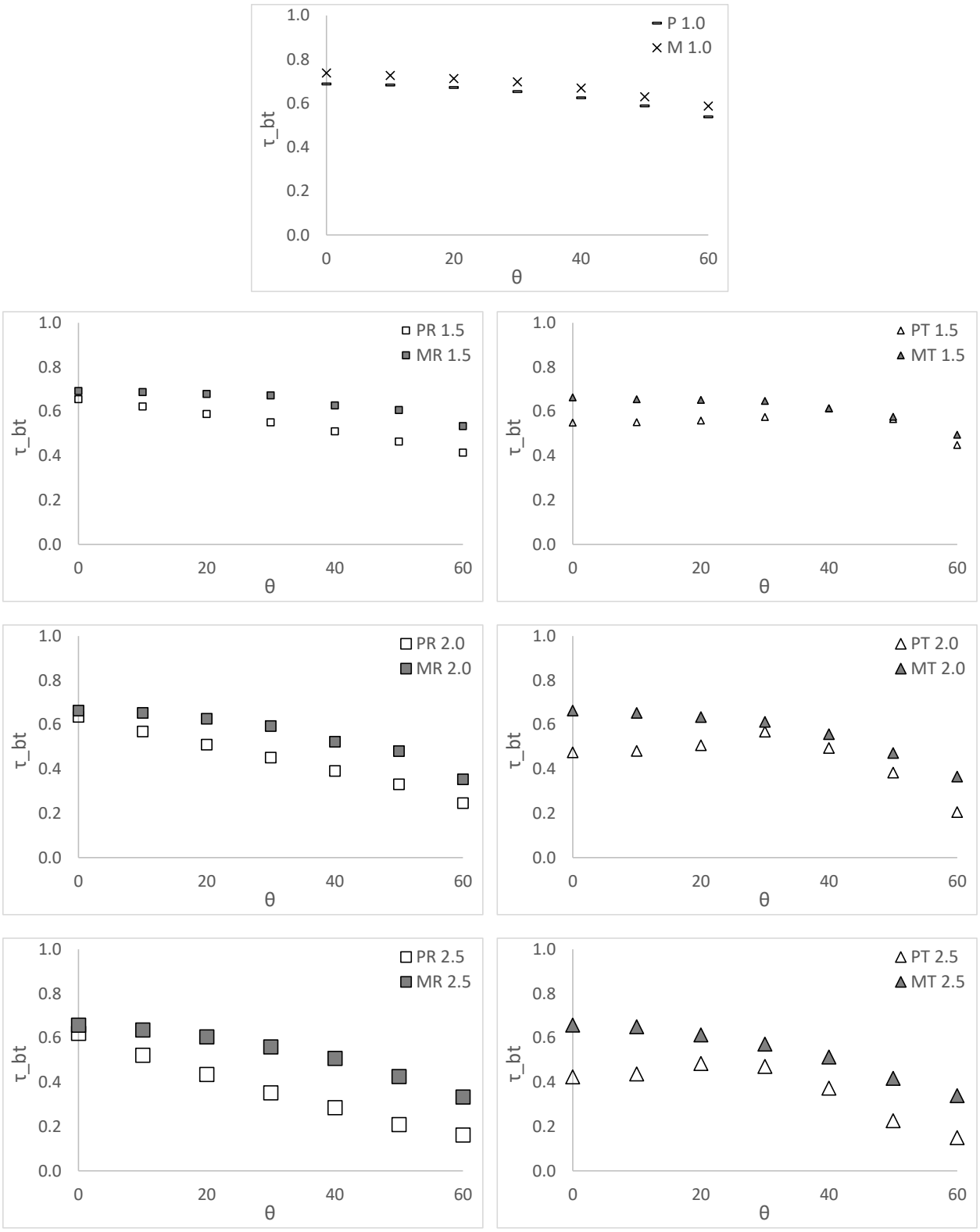

Figure 6.47: #75 Thin04 – prediction vs measurement

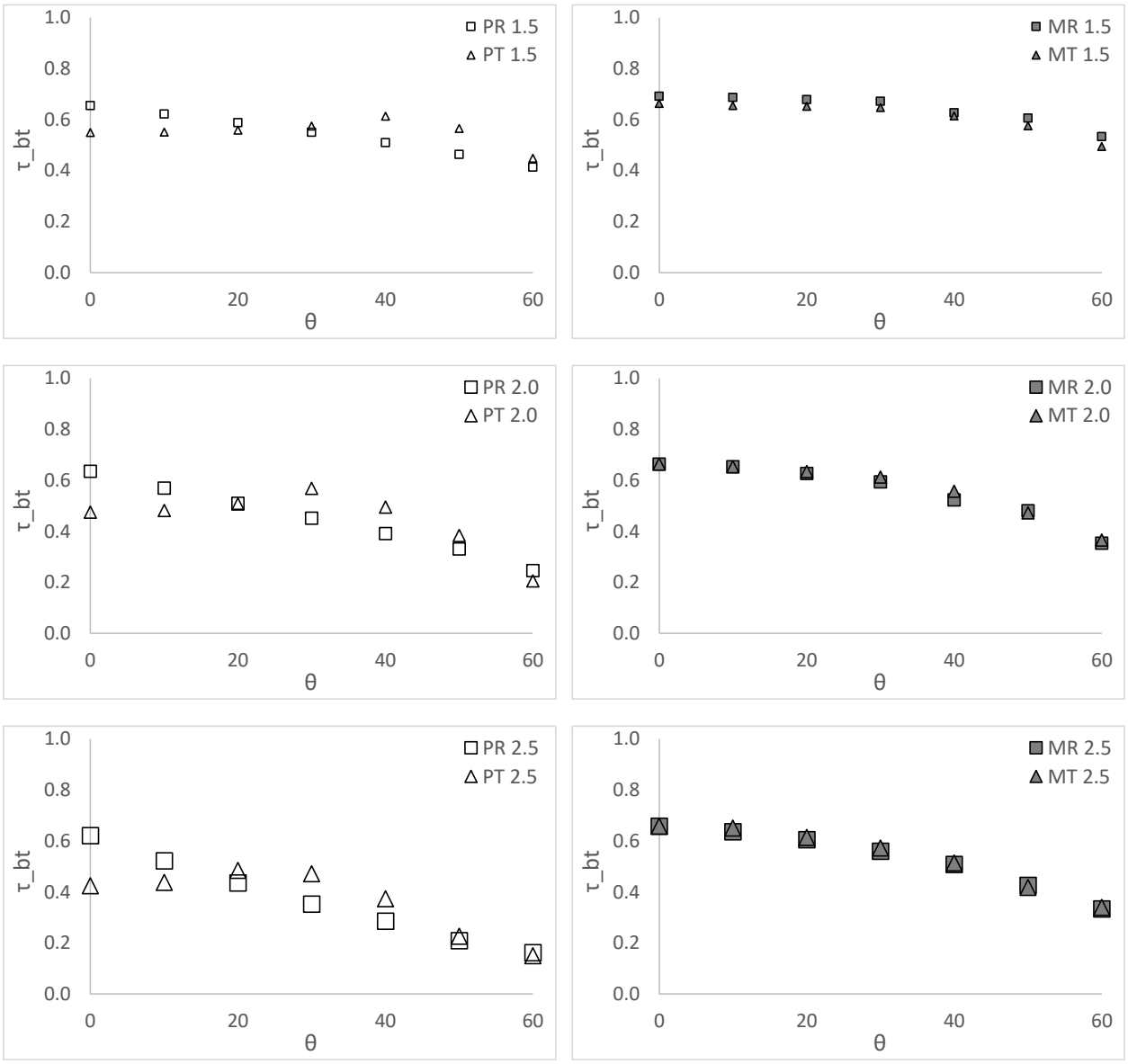

Figure 6.48: #75 Thin04 – rectangular vs triangular profile

Table 6.18: #77 WhiteOpen01 – calculated and measured τ_{bt} for various θ and Fr

#77 WhiteOpen01 (τ_{bb} = 0.1909, τ_{bt} = 0.5031, ρ_{bt} = 0.3525)														
	Pleated Drape Models (P)							BAI-IS Measurements (M)						
		Rectangular (R)			Triangular (T)				Rectangular (R)			Triangular (T)		
θ	Flat	1.5	2.0	2.5	1.5	2.0	2.5	Flat	1.5	2.0	2.5	1.5	2.0	2.5
0	0.503	0.489	0.476	0.465	0.428	0.383	0.349	0.512	0.461	0.447	0.462	0.459	0.449	0.438
10	0.500	0.470	0.439	0.408	0.430	0.388	0.358	0.502	0.447	0.445	0.440	0.454	0.446	0.437
20	0.491	0.451	0.405	0.365	0.435	0.406	0.390	0.492	0.440	0.425	0.398	0.457	0.452	0.415
30	0.478	0.430	0.372	0.307	0.447	0.447	0.393	0.478	0.438	0.406	0.359	0.471	0.449	0.391
40	0.457	0.407	0.338	0.268	0.475	0.418	0.353	0.451	0.414	0.374	0.312	0.463	0.421	0.340
50	0.430	0.383	0.304	0.230	0.458	0.371	0.293	0.421	0.389	0.330	0.265	0.439	0.379	0.274
60	0.394	0.359	0.261	0.202	0.410	0.299	0.239	0.376	0.335	0.242	0.205	0.393	0.285	0.228

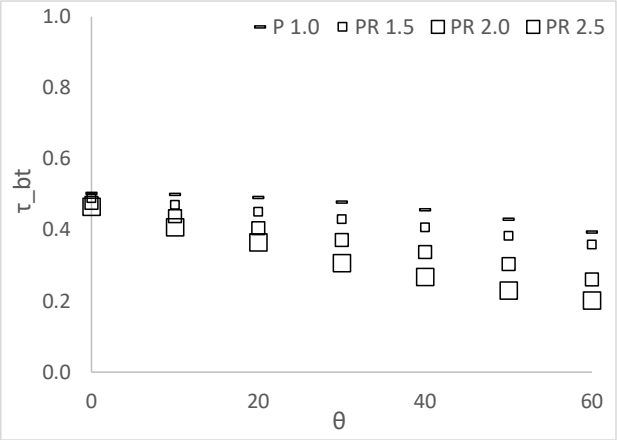

(a) Pleated Drape Model – Rectangular

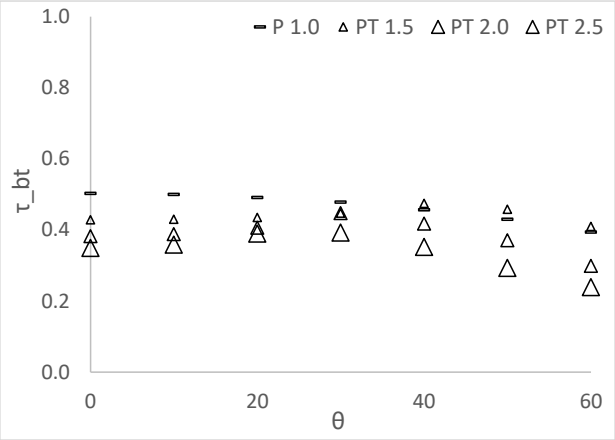

(b) Pleated Drape Model – Triangular

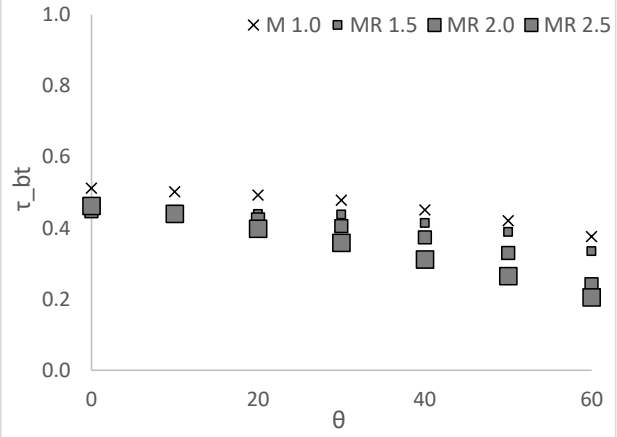

(c) BAI-IS Measurements – Rectangular

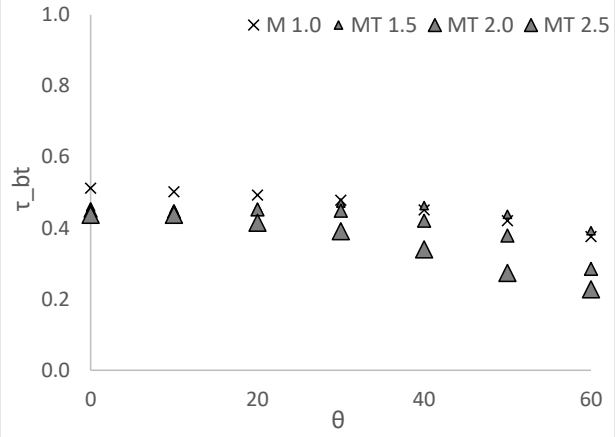

(d) BAI-IS Measurements – Triangular

Figure 6.49: #77 WhiteOpen01 – calculated and measured τ_{bt} for various θ and Fr

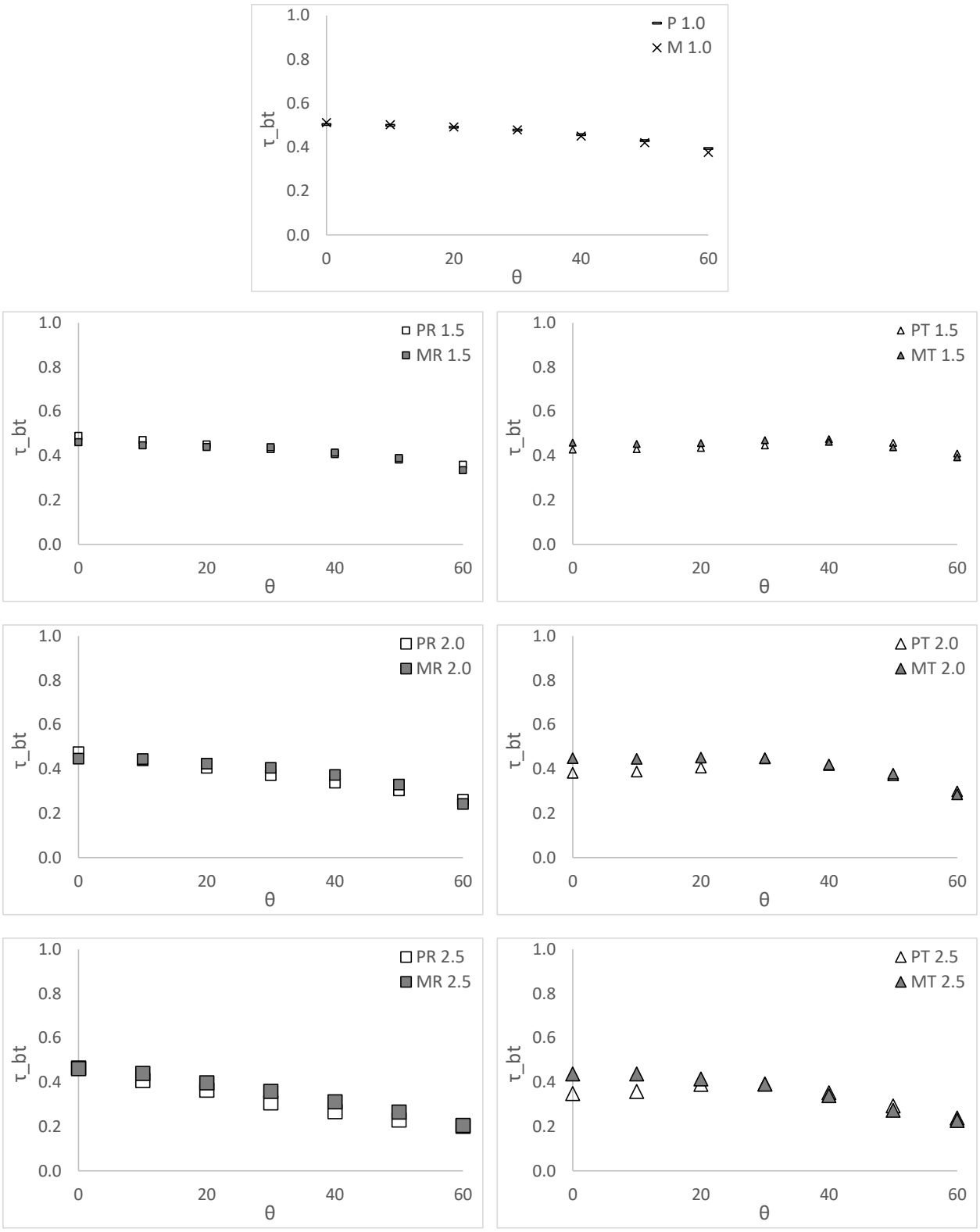

Figure 6.50: #77 WhiteOpen01 – prediction vs measurement

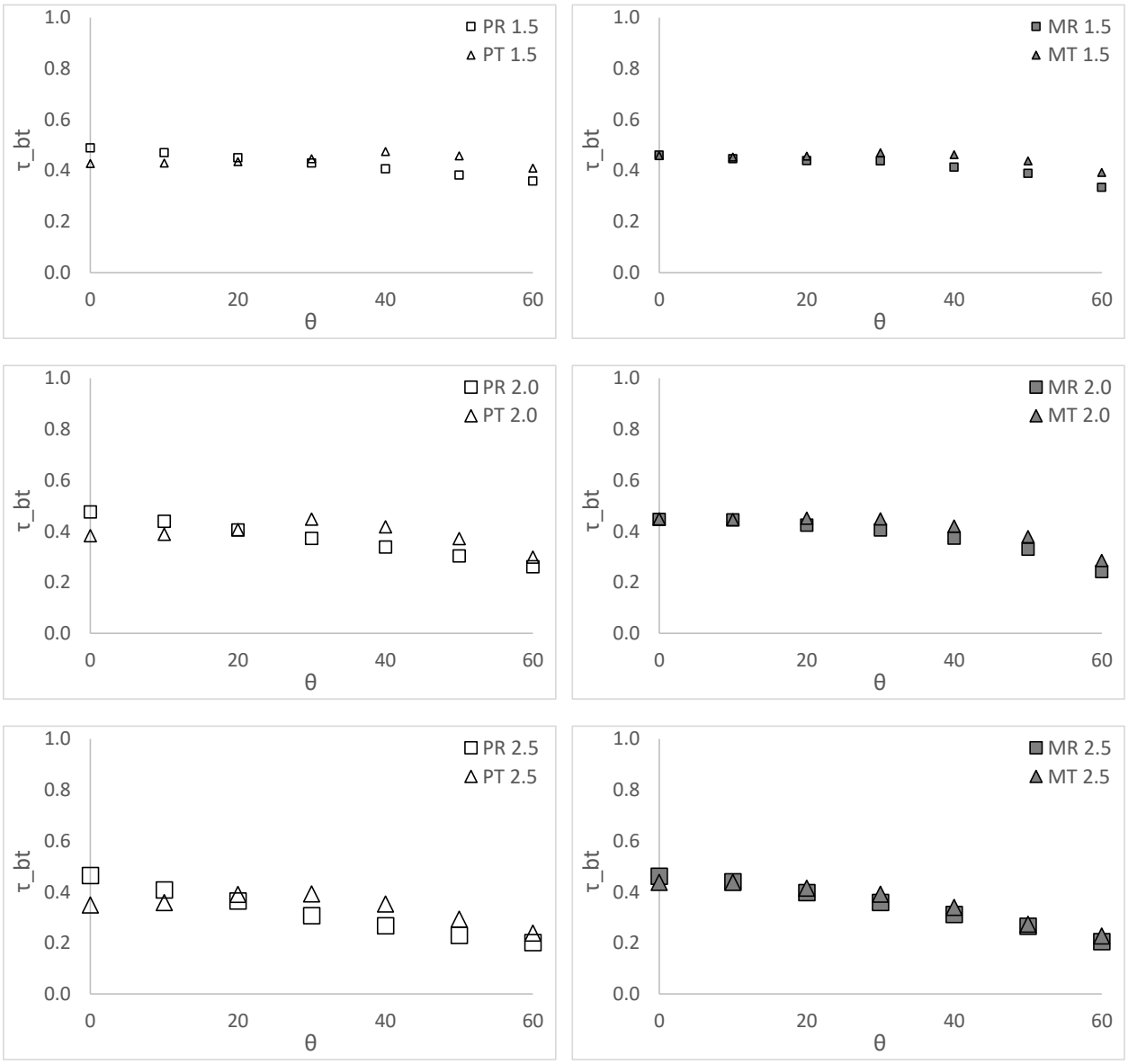

Figure 6.51: #77 WhiteOpen01 – rectangular vs triangular profile

Table 6.19: #92 PMB01 – calculated and measured τ_{bt} for various θ and Fr

#92 PowerMeshBlack01 (τ_{bb} = 0.0316, τ_{bt} = 0.1325, ρ_{bt} = 0.1431)														
	Pleated Drape Models (P)							BAI-IS Measurements (M)						
		Rectangular (R)			Triangular (T)				Rectangular (R)			Triangular (T)		
θ	Flat	1.5	2.0	2.5	1.5	2.0	2.5	Flat	1.5	2.0	2.5	1.5	2.0	2.5
0	0.132	0.116	0.106	0.101	0.071	0.046	0.033	0.170	0.139	0.125	0.108	0.091	0.071	0.079
10	0.130	0.108	0.092	0.080	0.073	0.049	0.037	0.161	0.133	0.118	0.091	0.096	0.077	0.079
20	0.124	0.098	0.077	0.059	0.078	0.060	0.051	0.151	0.118	0.107	0.074	0.109	0.094	0.080
30	0.114	0.086	0.062	0.039	0.088	0.078	0.058	0.133	0.101	0.095	0.064	0.121	0.118	0.073
40	0.101	0.074	0.048	0.031	0.102	0.075	0.052	0.100	0.087	0.083	0.043	0.126	0.114	0.077
50	0.084	0.063	0.040	0.024	0.100	0.066	0.041	0.070	0.082	0.071	0.036	0.118	0.094	0.062
60	0.066	0.055	0.032	0.019	0.086	0.050	0.033	0.052	0.083	0.058	0.033	0.100	0.059	0.040

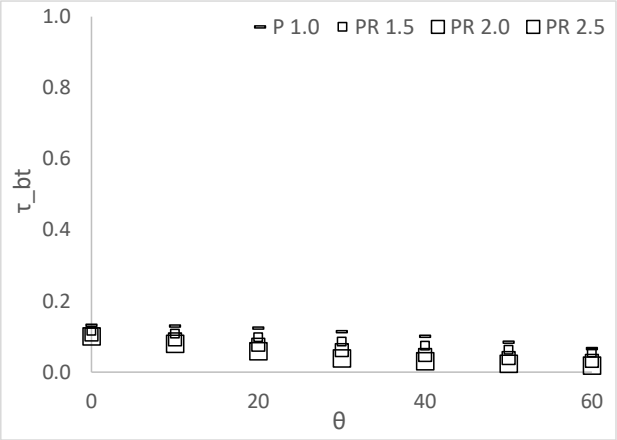

(a) Pleated Drape Model – Rectangular

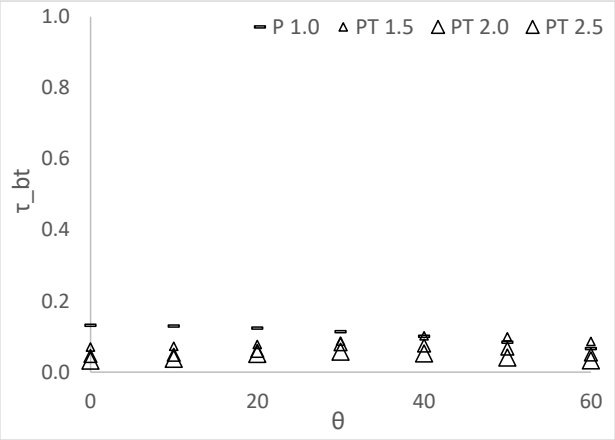

(b) Pleated Drape Model – Triangular

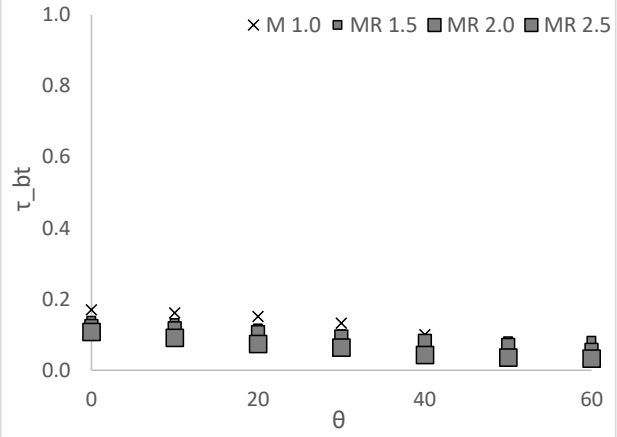

(c) BAI-IS Measurements – Rectangular

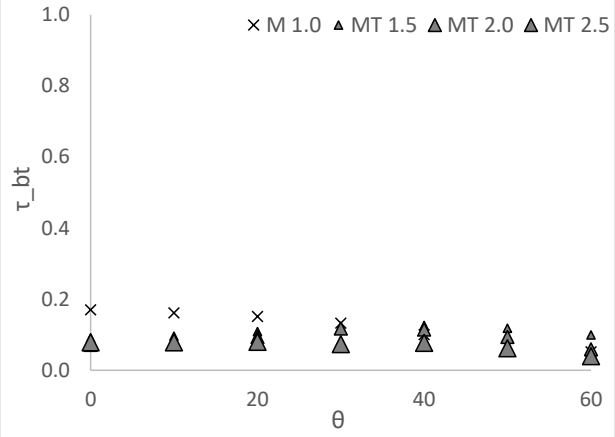

(d) BAI-IS Measurements – Triangular

Figure 6.52: #92 PMB01 – calculated and measured τ_{bt} for various θ and Fr

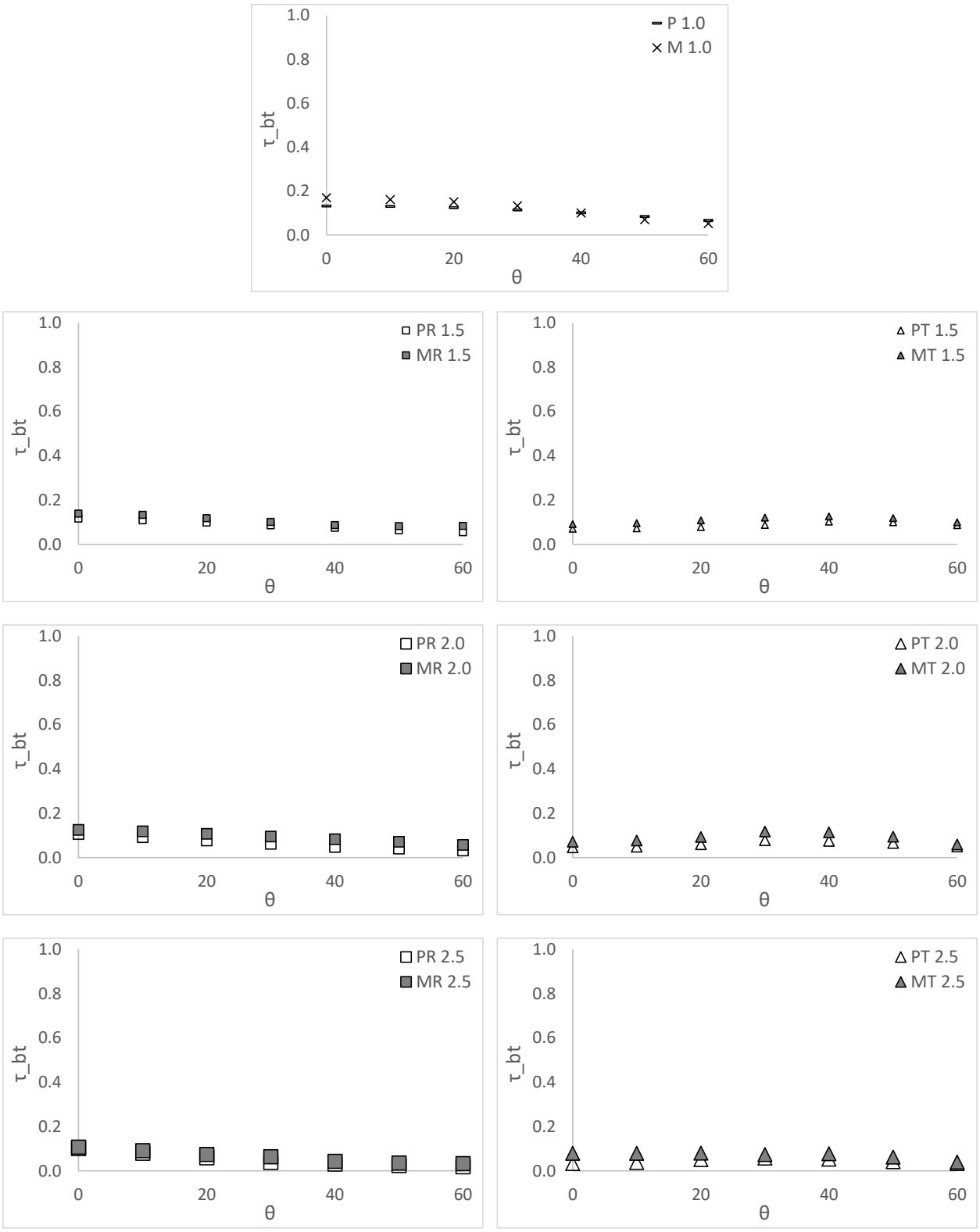

Figure 6.53: #92 PMB01 – prediction vs measurement

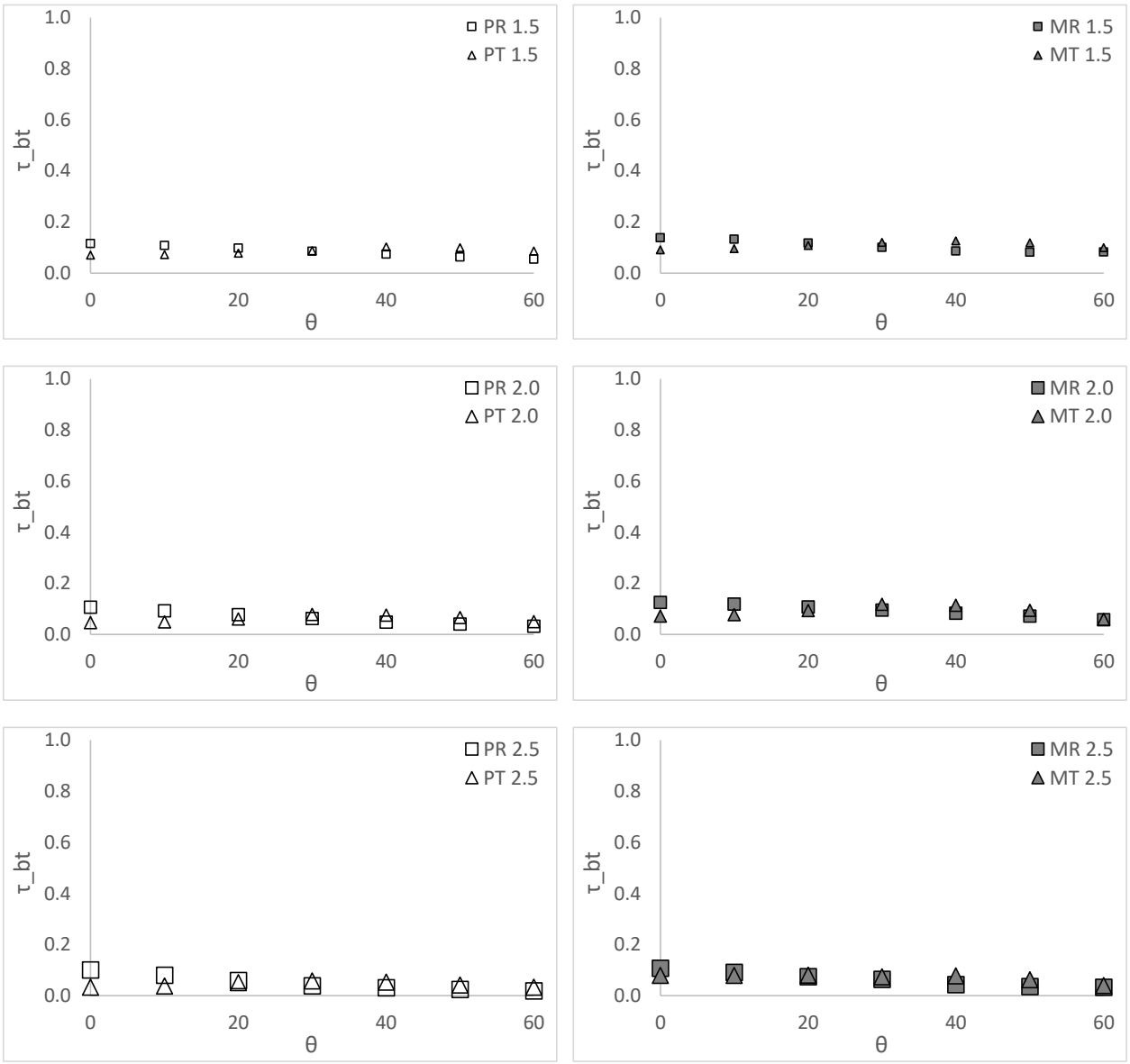

Figure 6.54: #92 PMB01 – rectangular vs triangular profile

Table 6.20: #94 PMBOpen – calculated and measured τ_{bt} for various θ and Fr

#94 PowerMeshBlackOpen (τ_{bb} = 0.2392, τ_{bt} = 0.3138, ρ_{bt} = 0.0854)														
	Pleated Drape Models (P)							BAI-IS Measurements (M)						
		Rectangular (R)			Triangular (T)				Rectangular (R)			Triangular (T)		
θ	Flat	1.5	2.0	2.5	1.5	2.0	2.5	Flat	1.5	2.0	2.5	1.5	2.0	2.5
0	0.314	0.303	0.296	0.292	0.234	0.190	0.161	0.381	0.348	0.330	0.326	0.234	0.169	0.149
10	0.310	0.281	0.255	0.231	0.236	0.196	0.172	0.373	0.345	0.310	0.273	0.236	0.177	0.150
20	0.302	0.259	0.217	0.177	0.243	0.218	0.208	0.355	0.317	0.271	0.199	0.257	0.219	0.197
30	0.288	0.235	0.181	0.128	0.258	0.262	0.210	0.326	0.289	0.229	0.122	0.290	0.251	0.205
40	0.268	0.209	0.148	0.096	0.287	0.224	0.158	0.275	0.259	0.185	0.074	0.325	0.228	0.184
50	0.242	0.184	0.119	0.052	0.260	0.160	0.073	0.198	0.227	0.151	0.058	0.325	0.164	0.100
60	0.209	0.162	0.068	0.028	0.190	0.054	0.035	0.070	0.199	0.113	0.048	0.258	0.074	0.054

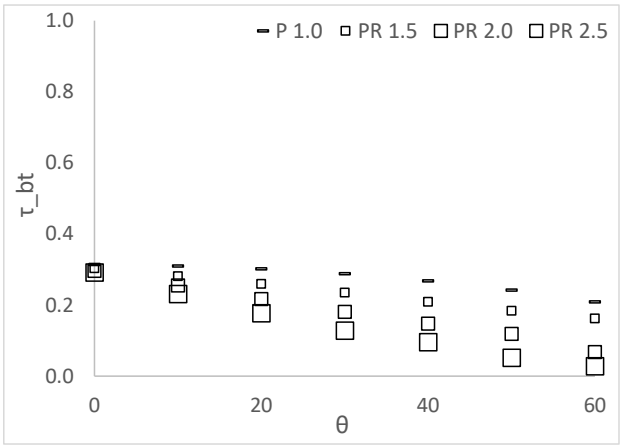

(a) Pleated Drape Model – Rectangular

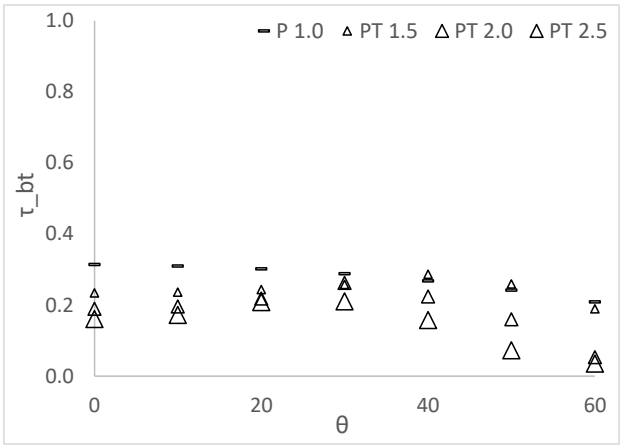

(b) Pleated Drape Model – Triangular

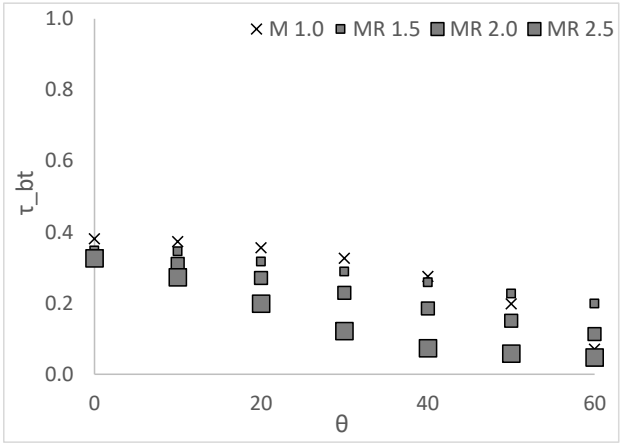

(c) BAI-IS Measurements – Rectangular

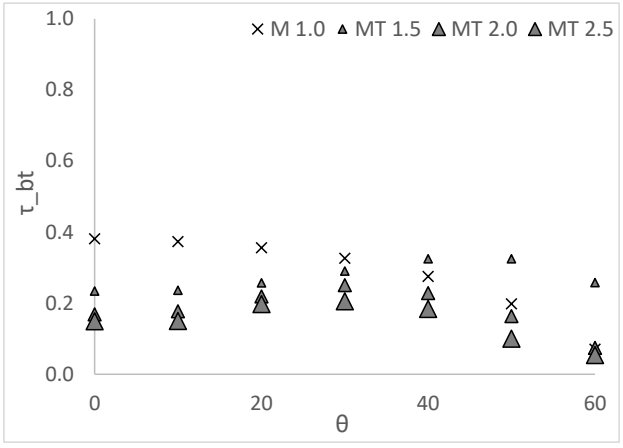

(d) BAI-IS Measurements – Triangular

Figure 6.55: #94 PMBOpen – calculated and measured τ_{bt} for various θ and Fr

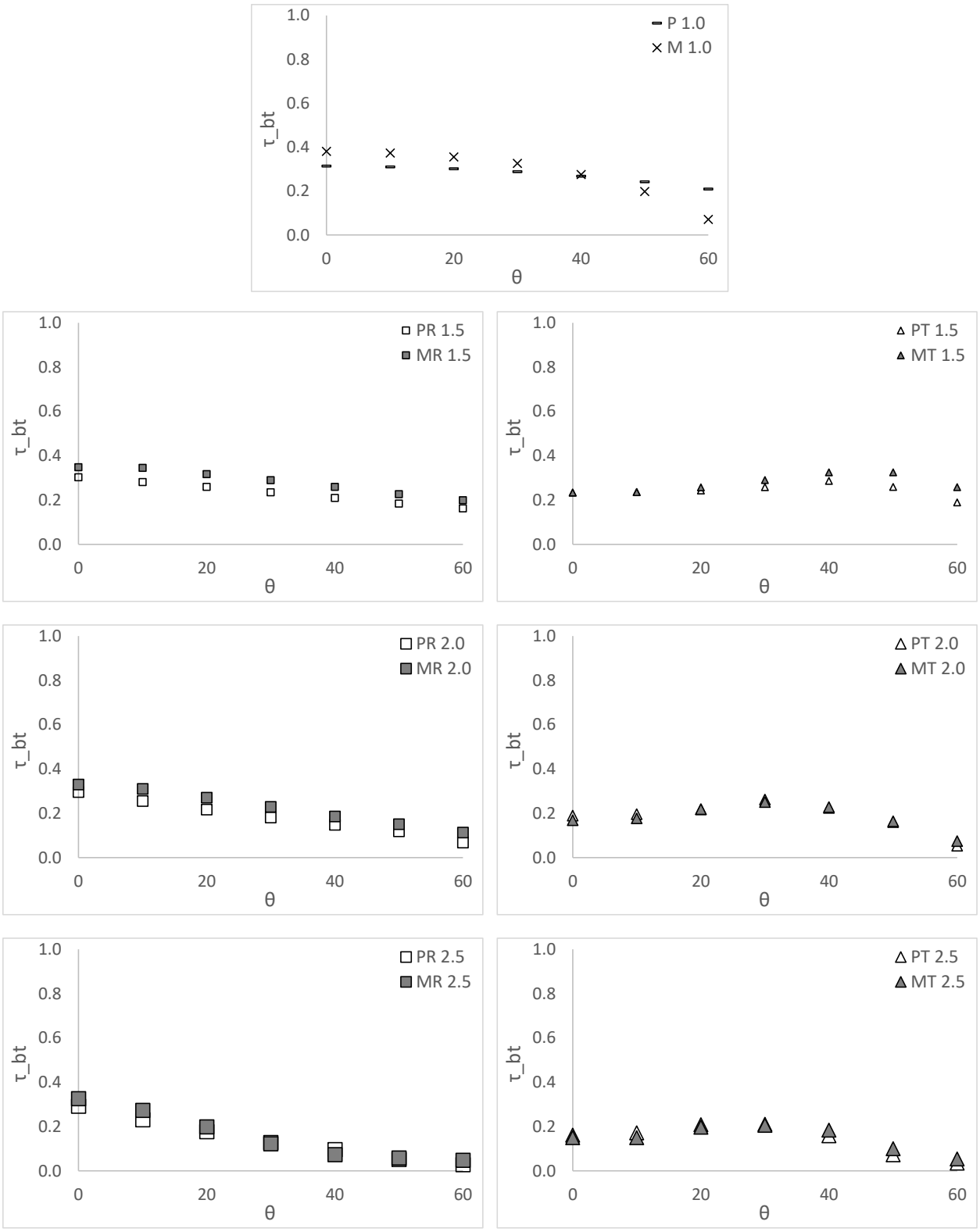

Figure 6.56: #94 PMBOpen – prediction vs measurement

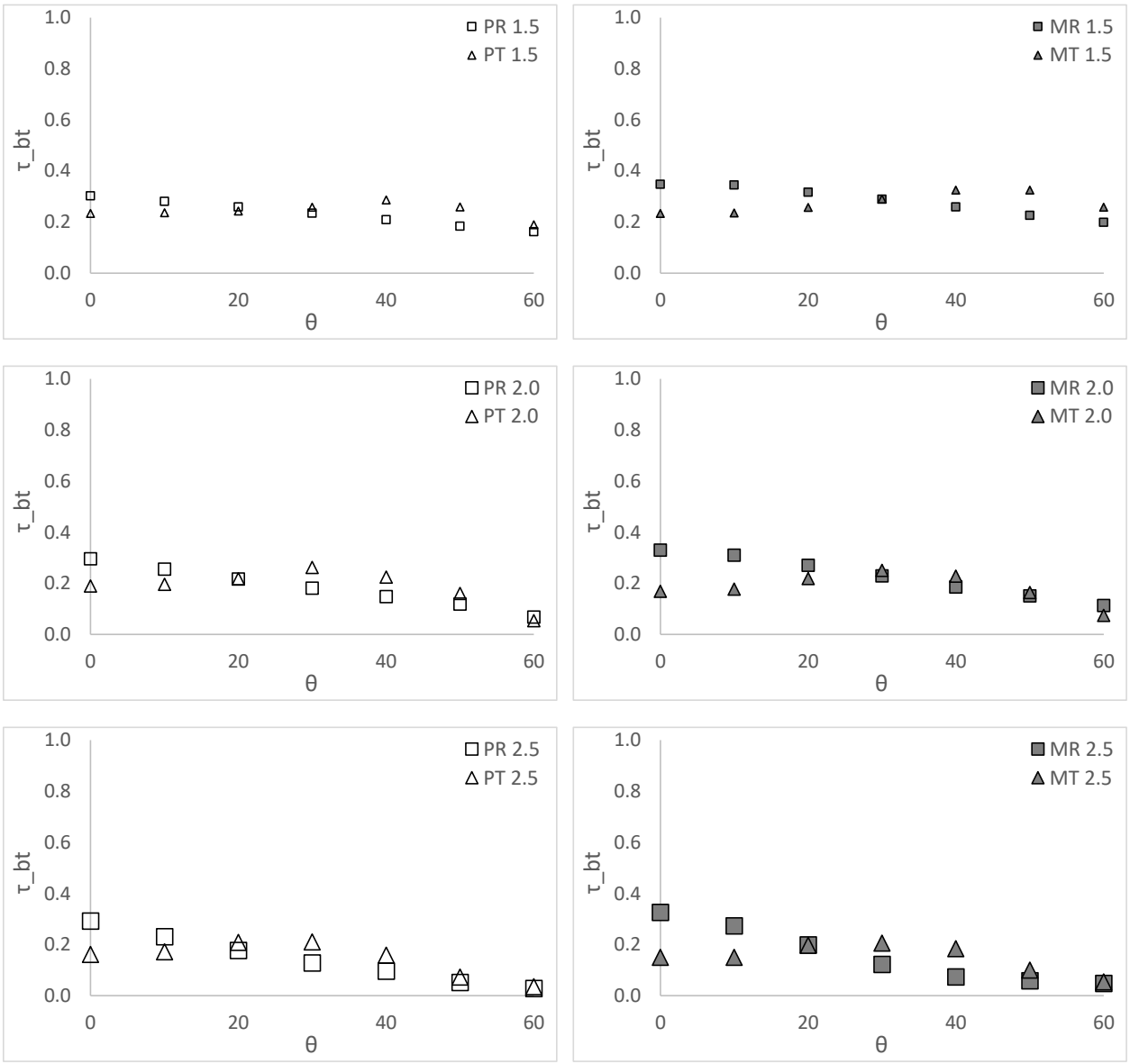

Figure 6.57: #94 PMBOpen – rectangular vs triangular profile

Table 6.21: #95 PMY – calculated and measured τ_{bt} for various θ and Fr

#95 PowerMeshYellow (τ_{bb} = 0.0838, τ_{bt} = 0.4717, ρ_{bt} = 0.4173)														
	Pleated Drape Models (P)							BAI-IS Measurements (M)						
		Rectangular (R)			Triangular (T)				Rectangular (R)			Triangular (T)		
θ	Flat	1.5	2.0	2.5	1.5	2.0	2.5	Flat	1.5	2.0	2.5	1.5	2.0	2.5
0	0.471	0.456	0.442	0.430	0.398	0.356	0.327	0.449	0.404	0.413	0.405	0.357	0.359	0.371
10	0.468	0.441	0.412	0.383	0.399	0.361	0.335	0.441	0.396	0.394	0.383	0.353	0.357	0.367
20	0.460	0.425	0.384	0.341	0.404	0.377	0.362	0.426	0.378	0.371	0.344	0.357	0.362	0.364
30	0.446	0.406	0.356	0.298	0.416	0.414	0.368	0.410	0.363	0.346	0.299	0.377	0.370	0.352
40	0.426	0.387	0.327	0.266	0.442	0.396	0.345	0.376	0.336	0.312	0.254	0.379	0.355	0.307
50	0.399	0.366	0.299	0.240	0.434	0.369	0.314	0.329	0.311	0.273	0.227	0.371	0.326	0.270
60	0.364	0.345	0.270	0.219	0.404	0.331	0.271	0.263	0.286	0.236	0.203	0.338	0.261	0.231

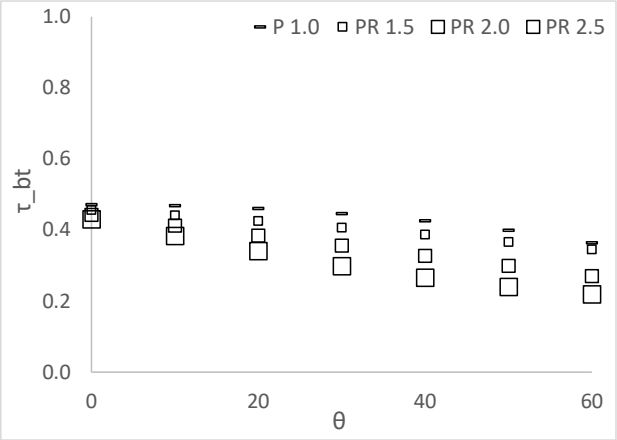

(a) Pleated Drape Model – Rectangular

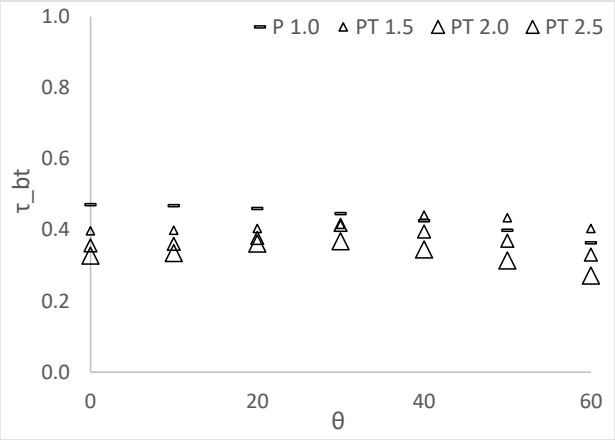

(b) Pleated Drape Model – Triangular

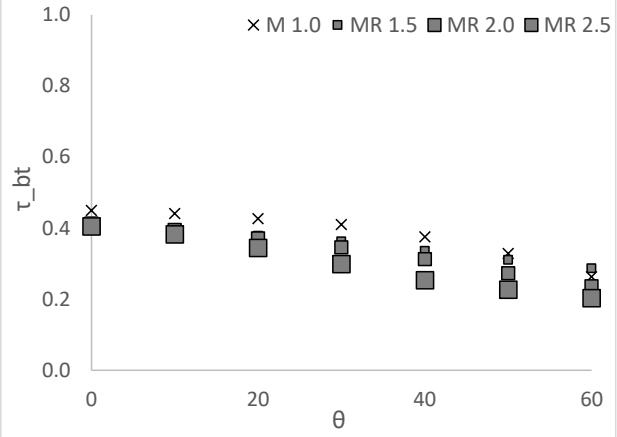

(c) BAI-IS Measurements – Rectangular

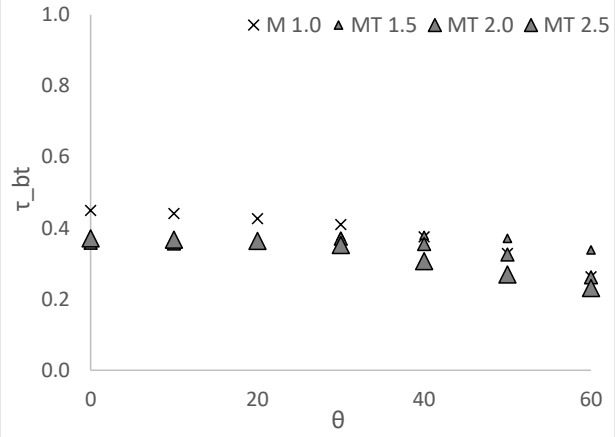

(d) BAI-IS Measurements – Triangular

Figure 6.58: #95 PMY – calculated and measured τ_{bt} for various θ and Fr

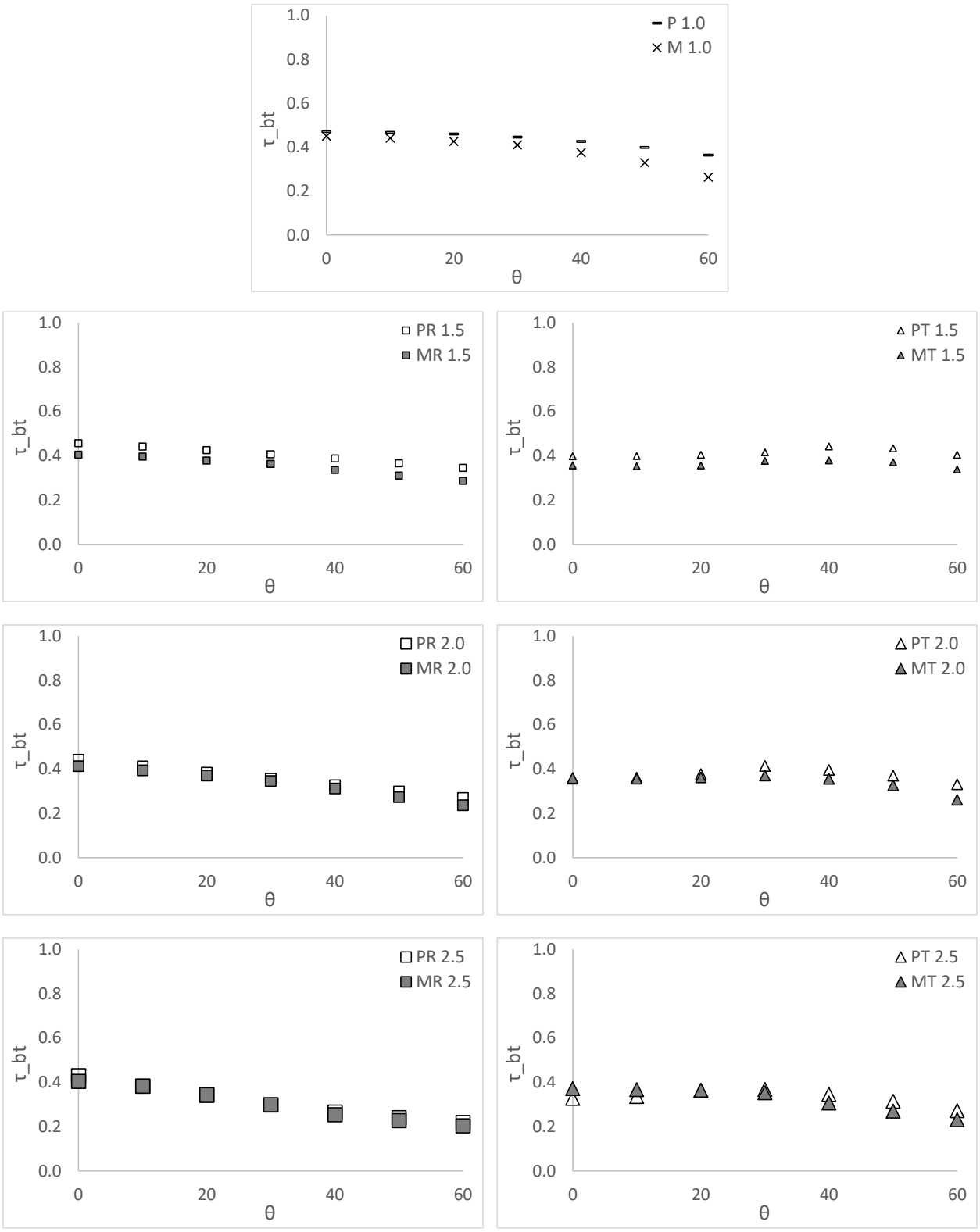

Figure 6.59: #95 PMY – prediction vs measurement

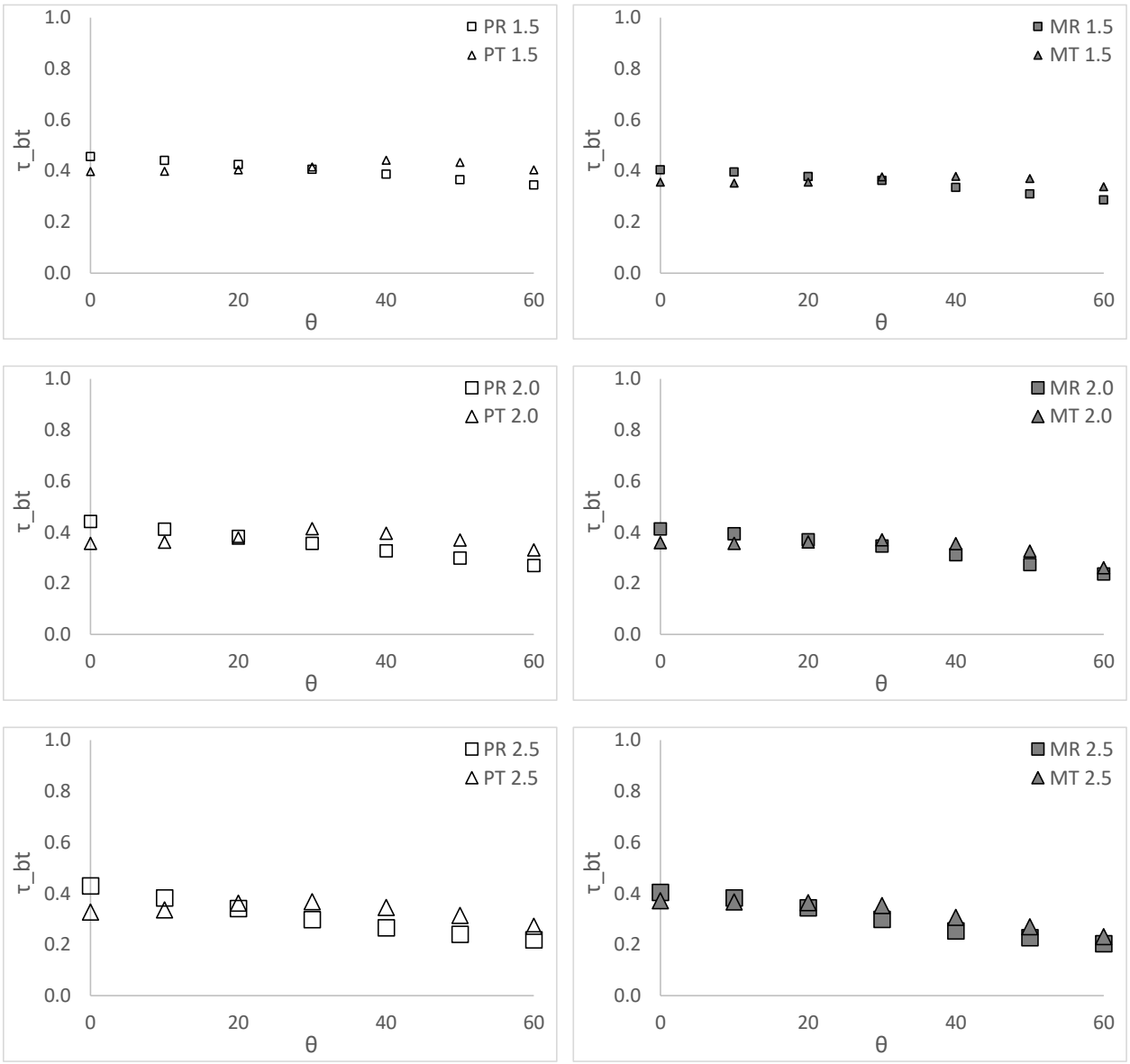

Figure 6.60: #95 PMY – rectangular vs triangular profile

6.3 Summary of Results

6.3.1 Predictions vs Measurements (P vs M)

Based on the results presented in the column (2) tables (i.e., Table 6.2 to Table 6.21), the differences between predicted τ_{bt} and measured τ_{bt} were averaged for the 49 cases in the test matrix for each fabric and listed as AVG in Table 6.22. The standard deviation of the differences (STD) is also given. In addition, the most underpredicted case (listed as Minimum Diff) and the most overpredicted case (listed as Maximum Diff) are also shown for each fabric in Table 6.22. In the cases where minimum and maximum differences are both negative (i.e., Fabrics #72 and #75), the pleated drape models always underpredict τ_{bt}.

- The P vs M comparisons are shown in the column (4) figures of Table 6.1. In general, the pleated drape models capture the effects of test variables discussed in Section 6.2 and provide trends that are comparable to those of BAI-IS measurements.

- Overall, the models tend to under-predict (AVG = -0.026 and STD = 0.051 for all cases of all 20 fabrics). On average, the models under-predict dark/medium color fabrics and slightly over-predict for light color fabrics. Note that fabrics with AVG near zero or above are all of light colors. And AVG is negative for all dark/medium color fabrics.

- AVG and STD are generally within ± 0.05 and 0.03, respectively, except for thin fabrics (i.e., #20, #22, #72, #73, and #75) where AVG can be as low as -0.110 and STD as high as 0.062. All of these fabrics are in the sheer category that has a high A_o and high τ_{bt}. This is likely due to the model simplification that τ_{bb} (which is very high for the fabrics considered here) is considered only for the first transmission. Any subsequent contact with fabric yields only diffuse radiation.

Table 6.22: Differences between pleated drape model predictions and BAI-IS measurements (-ve indicates under-prediction)

Fabrics	AVG	STD	Minimum		Maximum	
			Diff	Case	Diff	Case
#01 2600BX_Sheeting	-0.004	0.004	-0.013	Flat @ θ = 10°	0.004	R 2.0 @ θ = 0°
#08 DarkBrown01	-0.026	0.020	-0.078	T 2.5 @ θ = 0°	0.009	R 1.5 @ θ = 0°
#10 DecolineLining	0.054	0.042	-0.018	T 2.5 @ θ = 0°	0.154	T 1.5 @ θ = 40°
#13 GreyOpen01	-0.036	0.020	-0.080	T 2.5 @ θ = 0°	0.022	Flat @ θ = 60°
#20 SheerBlack01	-0.064	0.029	-0.128	R 2.5 @ θ = 30°	0.002	R 1.5 @ θ = 0°
#22 SheerWhite01	-0.035	0.034	-0.109	T 2.5 @ θ = 0°	0.027	T 1.5 @ θ = 40°
#24 White05	0.004	0.025	-0.060	T 2.5 @ θ = 0°	0.048	T 1.5 @ θ = 50°
#26 BlueSoft01	-0.022	0.020	-0.082	T 2.5 @ θ = 0°	0.008	R 2.0 @ θ = 0°
#27 Yellow05	-0.024	0.019	-0.070	T 2.5 @ θ = 0°	0.014	R 1.5 @ θ = 0°
#64 FashionBlack01	-0.020	0.022	-0.053	R 2.0 @ θ = 30°	0.061	Flat @ θ = 60°
#66 FashionLight01	0.020	0.023	-0.024	R 2.5 @ θ = 10°	0.095	Flat @ θ = 60°
#68 GreenOpen01	-0.014	0.027	-0.098	T 2.5 @ θ = 0°	0.033	R 2.0 @ θ = 0°
#71 RoughRed (Burlap)	-0.045	0.024	-0.099	T 2.5 @ θ = 0°	0.000	T 2.0 @ θ = 60°
#72 Thin01	-0.101	0.062	-0.213	T 2.5 @ θ = 0°	-0.002	T 1.5 @ θ = 40°
#73 Thin02	-0.080	0.048	-0.184	T 2.5 @ θ = 0°	0.010	Flat @ θ = 60°
#75 Thin04	-0.110	0.062	-0.234	T 2.5 @ θ = 0°	-0.001	T 1.5 @ θ = 40°
#77 WhiteOpen01	-0.011	0.028	-0.088	T 2.5 @ θ = 0°	0.029	R 2.0 @ θ = 0°
#92 PowerMeshBlack01	-0.022	0.012	-0.046	T 2.5 @ θ = 0°	0.014	Flat @ θ = 50°
#94 PowerMeshBlackOpen	-0.021	0.037	-0.068	T 1.5 @ θ = 60°	0.139	T 1.5 @ θ = 40°
#95 PowerMeshYellow	0.031	0.027	-0.044	T 2.5 @ θ = 0°	0.101	Flat @ θ = 60°

- For #01 2600BX_Sheeting, model predictions and BAI-IS measurements compare very well (AVG = -0.004 and STD = 0.004) with the worst case only being under-predicted with Minimum Diff = -0.013, a nearly perfect result. Though, as discussed in Section 6.2.6.1, the reason for this very good agreement is the insensitivity to any change in variables (i.e., due to very low solar-optical properties). So, for fabrics with extremely low solar-optical properties, either model can be used to predict τ_{bt}. Or even a constant τ_{bt} can be assigned in this case, and the result would still be excellent.

- In addition, AVG and STD are also calculated based on combinations of pleating profile and Fr (Table 6.23) and on θ (Table 6.24). Both models tend to under-predict the high Fr cases. STD is the lowest for flat profile and increases with Fr for both pleating profiles. For θ, no convincing trend is observed in the results.

Table 6.23: AVG and STD for combinations of pleating profiles and Fr

Profile/Fr	Flat	R 1.5	R 2.0	R 2.5	T 1.5	T 2.0	T 2.5
AVG	-0.004	-0.018	-0.032	-0.044	-0.012	-0.029	-0.045
STD	0.037	0.043	0.043	0.055	0.050	0.053	0.059

Table 6.24: AVG and STD for various θ

θ	0	10	20	30	40	50	60
AVG	-0.026	-0.031	-0.030	-0.027	-0.024	-0.025	-0.020
STD	0.052	0.048	0.043	0.046	0.050	0.057	0.059

6.3.2 Pleating Profiles – Rectangular vs Triangular (P vs T)

To see the effects of pleating profiles, column (5) figures of Table 6.1 compare τ_{bt} for the two profiles. The effect of pleating profiles in model prediction is more evident than that in measurements. In several cases, pleating profile did not affect the measured τ_{bt}. One reason is the physical limitation (i.e., the profile cannot be perfectly rectangular or triangular) in the pleated drape sample discussed in Section 5.3.2. As a result, the local θ effect discussed in Section 6.2.4 is also more evident in the model predictions than in the measurements.

CHAPTER 7
CONTRIBUTIONS, CONCLUSIONS AND RECOMMENDATIONS

7.1 Contributions to CFS Modelling

- An improved KUC that largely eliminated the bias and reduced the uncertainty present in the original KUC.

- The b&C model approach is a new methodology that enables efficient analysis in further KUC research.

- Customized KUC, an innovative way to express KUC through the b&C model approach and to increase the prediction accuracy, is the result of linking the convectional three-property KUC to a fourth fabric property, fabric thickness.

- As only rectangular models were previously available, a triangular pleated drape model was developed for comparison with the rectangular model and to aid the understanding of pleating.

- A comprehensive set of transmittance test results was attained based on a test matrix that covers four folding ratios (up to 2.5), two pleating profiles (rectangular and triangular), 20 fabrics (covering all original KUC categories plus sheer), seven angles of incidence (up to 60°). No previous measurement was done on the pleated drape layer alone. So this set of results is crucial for model development and validation.

7.2 Conclusions

CFS plays a key role in various aspects of building design. For controlling solar heat gain, CFS is practical and the most common. Early CFS research dates back to the 1930s, but development of computer-based CFS models is still at an early stage. Only within the last decade does the center-glass glazing analysis start to include CFS models for various window attachments. The ability to accurately and efficiently predict CFS energy performance is highly anticipated due to increasingly rigid energy efficiency regulations and indispensable indoor environmental quality requirements.

Drapes, the focus of this research and the most artistic among all window shadings, come with endless options in terms of textile, design, style, color, function, and etc. Conventionally, energy performance of drapes is rated with the three solar-optical properties of drape fabrics: reflectance, transmittance, and openness. This is the reason that the KUC is a useful tool in estimating the shading effect of drapes by providing a predetermined energy performance index based on the conventional rectangular pleated drape model with typical glazing units.

This study utilized a highly accurate spectrophotometer to generate the solar-optical properties for a set of fabrics and develop the improved KUC. The b&C model produces not only better results but also a methodology based on functional relationships that can be integrated into computer-based models. The functional relationship method leads to the finding of a fourth fabric property, fabric thickness, that has been confirmed to have an influence on how a KUC should be defined, giving a customized KUC based on the fourth property.

Parallel to the convectional rectangular pleated drape model, this study also built a triangular pleated drape model for comparison to better understand and quantify the effect of pleating. Similarly, the experiment performed with the BAI-IS dealt with both rectangular and triangular

pleated drape samples. A major limitation in the experiment was that pleated drape samples may not be comprised of the expected pleating profiles due to the physical properties of fabrics. Nevertheless, cross-examination of models versus measurements and rectangular profile versus triangular profile has aided to the understanding of pleating effect.

Overall, the models tend to under-predict (AVG = -0.026 and STD = 0.051 for all cases of all 20 fabrics). On average, the models under-predict dark/medium color fabrics and slightly over-predict for light color fabrics. Note that fabrics with AVG near zero or above are all of light colors. And AVG is negative for all dark/medium color fabrics. AVG and STD are generally within ± 0.05 and 0.03, respectively, except for thin fabrics where AVG can be as low as -0.110 and STD as high as 0.062. All of these fabrics are in the sheer category that has high A_o and high τ_{bt}. The model simplification that τ_{bb} is considered only for the first transmission could be the main cause for the under prediction.

7.3 Recommendations

7.3.1 Works to be done

- Replace the original KUC with the improved KUC and update the IAC table in the ASHRAE handbook accordingly.

- While all custom usage of the original KUC are retained with the improved KUC, the proposed customized KUC should be used for increased accuracy. In this case, each customized KUC needs a separate IAC table. The customized KUC can be incorporated into the pleated drape models to generate IAC tables.

- The above two tasks should be repeated with the triangular pleated drape model.

7.3.2 Future Research

- Fabric samples used in this work are more concentrated in the lower right region of the KUC. It is recommended to expand the current research to include a more balanced set of fabric samples.

- The customized KUC approach demonstrated that fabric thickness is linked to KUC. It is recommended to examine other fabric properties following the customized KUC method. Some possible controlling variables include fabric material, weave, thickness, and drape coefficient.

- Explore the applicability of the customized KUC approach for other window attachments such as insect screen and roller blind.

- The simplification assumed in the triangular pleated drape model should be re-examined for the high A_o fabrics. Considering beam-beam transmission only when beam radiation is incident on the fabric for the first time may lead to significant errors. For high A_o fabrics, subsequent transmission of incident beam radiation should be considered.

- While it is impractical to survey all pleating profiles, it is recommended to extend the BAI-IS measurements to include pleated drape samples that are comprised of sinusoidal pleats. Since sinusoidal pleats do not have sharp edges as in the cases of rectangular and triangular pleats, the uncertainty due to varying physical properties (e.g., drape coefficients) would be much reduced.

- The non-uniformity correction factor of fabrics should be considered in all future research.

REFERENCES

Apte J.S. and Arasteh D.K. (2006) Window-Related Energy Consumption in the US Residential and Commercial Building Stock. LBNL-60146, 38 pages. LBNL, Berkeley, CA.

ASHRAE (1965) ASHRAE Guide and Data Book. 1965 Edition. Chapter 26.

ASTM E 903 (1996) Standard Test Method for Solar Absorptance, Reflectance, and Transmittance of Materials Using Integrating Spheres. Annual Book of ASTM Standards.

Azeem A. et. al. (2015) Modeling and Optimization of Performance Properties of Drapery Fabrics Made by Cotton. International Journal of Textile Science 4(3): 60-65.

Barnaby C.S., Wright J.L., and Collins M.R. (2009) Improving load calculations for fenestration with shading devices. ASHRAE Transactions 115, Pt. 2.

Berardi U. (2015) Building Energy Consumption in US, EU, and BRIC Countries. Procedia Engineering 118: 128-136.

Blackshaw J.L. and Houghten F.C. (1934) Radiation of Energy through Glass. ASHVE Transactions 40: p93.

Carr M.L., Miller R.A., Orr L., and Shore D. (1939) A Study of the Heat Requirements of a Single-Glazed Test House and a Double-Glazed Test House. ASHVE Transactions 45: 195-212.

Chakroun W., Taylor R.P., Steele W.G., and Coleman H.W. (1993) Bias error reduction using ratios to baseline experiments – Heat transfer case study. Journal of Thermophysics and Heat Transfer 7(4): 754-757.

Chan Y.C., Tzempelikos A., and Protzman B. (2014) Solar Optical Properties of Roller Shades: Modeling Approaches, Measured Results and Impact on Energy Use and Visual Comfort. 3rd International High Performance Building Conference at Purdue, Paper 124, 14 pages.

Collins M.R., Huang N.Y.T., Wright J.L. (2016) An Examination of Keyes Universal Chart: 50 Years Later. ASHRAE Winter Conference, Orlando, Florida (OR-16-C056).

Energetics Incorporated. (2014) Windows and Building Envelope Research and Development: Roadmap for Emerging Technologies. Prepared for Building Technologies Office, Office of Energy Efficiency and Renewable Energy, US DOE.

Farber E.A., Smith W.A., Pennington C.W., Reed J.C. (1963) Theoretical Analysis of Solar Heat Gain Through Insulating Glass with Inside Shading. ASHRAE Transactions 69: 392-403.

Furler, R.A. (1991) Angular dependence of optical properties of homogeneous glasses. ASHRAE Transactions 97(2): 1129-1133.

Goebel D.G. (1967) Generalized Integrating-Sphere Theory. Applied Optics 6(1): 125-128.

Halder V. (2007) Upgrading a Broad Area Illuminating Integrating Sphere and Solar Transmittance Measurement of a Sheer Blind. MASc. Thesis. University of Waterloo, Waterloo, Ontario.

Hisdal B.J. (1965a) Reflectance of Perfect Diffuse and Specular Samples in Integrating Sphere. Journal of the Optical Society of America 55(9): 1122-1128.

Hisdal B.J. (1965b) Reflectance of Non-Perfect Surfaces in the Integrating Sphere. Journal of the Optical Society of America 55(10): 1255-1260.

Houghten F.C., Gutberlet C., and Blackshaw J.L. (1934) Studies of Solar Radiation through Bare and Shaded Windows. ASHVE Transactions 40: p101.

Houghten F.C. and Shore D. (1941) Heat Gain through Western Windows With and Without Shading. ASHVE Transactions 47: p251

IPCC. (2014) Climate Change 2014: Mitigation of Climate Change. Section 9.2.1: Energy and GHG Emissions from Buildings, 678-681.

Jacquez J.A., Kuppenheim H.F. (1955) Theory of Integrating Sphere. Journal of the Optical Society of America 45(6).

Jiang T. (2005) Transmittance Measurements of Louvered Blinds Using a Broad Area Illumination Integrating Sphere. MASc. Thesis. University of Waterloo, Waterloo, Ontario.

Kenkare N. and May-Plumlee T. (2005) Evaluation of drape characteristics in fabrics. International Journal of Clothing Science and Technology 17(2): 109 – 123.

Klems, J.H. (1994a) A New Method for Predicting the Solar Heat Gain of Complex Fenestration System – 1. Overview and Derivation of the Matrix Layer Calculation. ASHRAE Transactions 100(1): 1065-1072.

Klems, J.H. (1994b) A New Method for Predicting the Solar Heat Gain of Complex Fenestration System – 2. Detailed Description of the Matrix Layer Calculation. ASHRAE Transactions 100(1): 1073-1086.

Klems J.H. and Warner J.L. (1995) Measurement of bi-directional optical properties of complex shading devices. ASHRAE Transactions 101(1): 791-801.

Klems J.H. (2001) Solar Heat Gain through Fenestration Systems Containing Shading: Summary of Procedures for Estimating Performance from Minimal Data. ASHRAE Transactions 108(1): 512-524.

Keyes M.W. (1967) Analysis and Rating of Drapery Materials Used for Indoor Shading. ASHRAE Transactions 73(1): VIII.4.1-VIII.4.15.

Kotey N.A. (2009) Measurements and Models Related to Solar Optics in Windows with Shading Devices. PhD Thesis. University of Waterloo, Waterloo, Ontario.

Kotey N.A., Wright J.L., Collins M.R. (2008) Determining long wave radiative properties of flat shading materials. Proceedings of the 3rd SBRN and 33rd SESCI Joint Conference, Fredericton, 8 pages.

Kotey N.A., Wright J.L., Collins M.R. (2009a) Determining Off-Normal Solar Optical Properties of Drapery Fabrics. ASHRAE Transactions 115, Pt. 2.

Kotey N.A., Collins M.R., Wright J.L., Jiang T. (2009b) A Simplified Method For Calculating The Effective Solar Optical Properties Of A Venetian Blind Layer For Building Energy Simulation. ASME Journal of Solar Energy Engineering 131(2), 9 pages.

Kotey N.A., Wright J.L., Collins M.R. (2009c) A Detailed Model to Determine the Effective Solar Optical Properties of Draperies. ASHRAE Transactions 115, Pt. 1.

Kotey N.A., Wright J.L., Collins M.R. (2009d) Determining Off-Normal Solar Optical Properties of Roller Blind Materials. ASHRAE Transactions 115, Pt. 1.

Kotey N.A., Wright J.L., Collins M.R. (2009e) Determining Off-Normal Solar Optical Properties of Insect Screens. ASHRAE Transactions 115, Pt. 1.

Labsphere (2013) Technical Guide: Integrating Sphere Theory and Applications

LBNL, 2008. International Glazing Database (IGDB). http://windows.lbl.gov/materials/igdb/

Lomanowski B.A. and Wright J.L. (2009) Modelling Fenestration with Shading Devices in Building Energy Simulation: A Practical Approach. 11th International IBPSA Conference, Glasgow, Scotland.

Lomanowski B.A. and Wright J.L. (2012) The Complex Fenestration Construction: A Practical Approach for Modelling Windows with Shading Devices in ESP-r. Journal of Building Performance Simulation 5(3): 185-198.

McCluney R. and Mills L. (1993) Effect of Interior Shade on Window Solar Gain. ASHRAE Transactions 99(2): 565-570.

Milburn D. I. (1994) Measurement of Solar Transmittance of Advanced Glazing Materials. PhD Dissertation, University of Waterloo, Waterloo, Canada.

Miller R.A. and Black L.V. (1932) Transmission of Radiant Energy through Glass. ASHVE Transactions 38: p 63.

Moore G.L., and Pennington C.W. (1967) Measurement and Application of Solar Properties of Drapery Shading Materials. ASHRAE Transactions 73(1):VIII.3.1-VIII.3.15.

Ozisik N., and Schutrum L.F. (1959) Heat Flow through Glass with Roller Shades. ASHRAE Transactions 65: 697-716.

Ozisik N., and Schutrum L.F. (1960) Solar Heat Gain Factors for Windows with Drapes. ASHRAE Transactions 66: 228-239.

Parmelee G.V., Aubele W.W. and Huebscher G. (1948) Measurements of Solar Heat Transmission through Flat Glass. ASHVE Transactions 54: p158.

Parmelee G.V. and Aubele W.W. (1950) Heat Flow through Unshaded Flat Glass. ASHVE Transactions 56: p374.

Parmelee G.V. and Aubele W.W. (1952) The Shading of Sunlit Glass: An Analysis of the Effect of Uniformly Spaced Flat Opaque Slats. ASHVE Transactions 58: p377.

Parmelee G.V., Aubele W.W., and Vild D.J. (1953) The Shading of Sunlit Glass: An Experimental Study of Slat Type Sun Shades. ASHVE Transactions 59: p221.

Pennington C.W., Smith W.A., Farber E.A., and Reed J.C. (1964) Experimental Analysis of Solar Heat Gain Through Insulating Glass with Inside Shading. ASHRAE Transactions 70: 27-39.

Pettit, R.B. (1979) Hemispherical Transmittance Properties of Solar Glazings as a Function of Averaging Procedure and Incident Angle. Solar Energy Materials, Vol. 1: 125-140.

Pfrommer, P., Lomas, K.J., Seale, C., and Kupke, Chr. (1995) The Radiation Transfer through Coated and Tinted Glazing. Solar Energy 54(5): 287-299.

Roos, A. (1997) Optical Characterization of Coated Glazings at Oblique Angles of Incidence: Measurements versus Model Calculations. Journal of Non-Crystalline Solids 218: 247-255.

Rosa E.B., and Taylor A.H. (1922) Theory, Construction and Use of the Photometric Integrating Sphere. Scientific Papers of the Bureau of Standards. No. 447. Part of Volume 18. Department of Commerce. USA.

Sumpner W.E. (1892) Proceedings of the Physical Society of London. 12.

Tardy H.L. (1991) Matrix Method for Integrating-Sphere Calculations. Journal of the Optical Society of America 8(9): 1411-1418.

Van Dyck R.L. and Konen T.P. (1982) Energy Conservation through Interior Shading of Windows: An Analysis, Test and Evaluation of Reflective Venetian Blinds. LBL-14369 Report, LBNL, Berkeley, CA.

Wright J.L., Kotey N.A. (2006) Solar Absorption by Each Element in a Glazing/Shading Layer Array. ASHRAE Transactions 112(2): 3-12.

Wright J.L. (2008) Calculating Centre-Glass Performance Indices of Glazing Systems with Shading Devices. ASHRAE Transactions 114(2): 199-209.

Wright J.L., Huang N.Y.T., and Collins M.R. (2008) Thermal Resistance of a Window with an Enclosed Venetian Blind: A Simplified Model. ASHRAE Transactions 114(1): 471-482.

Wright J.L., Collins M.R., Barnaby C.S., and Kotey N.A. (2009) Improving Cooling Load Calculations for Fenestration with Shading Devices. ASHRAE 1311-RP. Final Report.

Wright J.L., Barnaby C.S., Niles P. and Rogalsky C.J. (2011) Efficient Simulation of Complex Fenestration Systems in heat Balance Room Models. Proc. of Building Simulation: 12th Conf. of Int. Building Performance Simulation Association (IBPSA): 2851-2858. Sydney, Australia.

Yahoda D.S., and Wright J.L. (2004) Methods for Calculating the Effective Longwave Radiative Properties of a Venetian Blind Layer. ASHRAE Transactions 110(1): 463-473.

Yellott J.L. (1965) Drapery Fabrics and their Effectiveness in Solar Heat Control. ASHRAE Transactions 71(1): 260-272.

Beckman DU Spectrophotometer Documents

Beckman Instruments. Beckman Instruction Manual – Model DU Spectrophotometer and Accessories. Document 305-A. 65 pages.

Beckman Instruments. Beckman Instruction Manual – Power Supply for DU Spectrophotometers. Document 546-H. 73 pages.

Beckman Instruments. Revision Sheet – Model DU Spectrophotometer. 305-A. 5 pages.

Beckman Instruments. Instructions for Servicing Beckman Model D and DU Photoelectric Quartz Spectrophotometers. Bulletin 150-C. 12 pages.

Beckman Instruments. Instructions for Servicing Beckman Model D and DU Spectrophotometers. Bulletin 150-D. 14 pages.

Beckman Instruments. Operating Instructions – Beckman Quartz Spectrophotometer. Bulletin 91-G. 14 pages.

Beckman Instruments. Operating Instructions. Bulletin 91-G. 10 pages.

Appendix A: List of Fabric Samples and Their Properties

		KUC		Weighted (400 – 1045 nm)			Weighted (250 – 2500 nm)		
ID	**Name**	**I,II,III**	**D,M,L**	τ_{bt}	ρ_{bt}	τ_{bd}	τ_{bt}	ρ_{bt}	τ_{bd}
1	2600BX_Sheeting	III	D	0.043	0.045	0.017	0.062	0.081	0.038
2	22111FV_Wide_LightYellow	II	L	0.388	0.572	0.376	0.371	0.553	0.360
3	22111FV_Wide_White	III	L	0.354	0.634	0.363	0.341	0.615	0.351
4	BlueRough01	III	M	0.142	0.446	0.139	0.116	0.406	0.114
5	SoftBlue31	II	M	0.327	0.323	0.316	0.317	0.309	0.307
6	Brown01	III	M	0.143	0.459	0.140	0.121	0.432	0.120
7	DadSolidFM	III	M	0.173	0.485	0.171	0.146	0.444	0.145
8	DarkBrown01	III	M	0.175	0.400	0.178	0.158	0.380	0.161
9	DarkGrey01	III	M	0.186	0.431	0.184	0.170	0.409	0.168
10	DecolineLining	II	L	0.435	0.589	0.390	0.420	0.561	0.374
11	GoldCut01	III	L	0.220	0.675	0.231	0.207	0.645	0.219
12	Grey01	III	L	0.213	0.516	0.205	0.196	0.494	0.190
13	GreyOpen01	I	D	0.407	0.155	0.158	0.409	0.157	0.163
14	Pink01	III	L	0.185	0.633	0.183	0.163	0.601	0.162
15	Pink02	III	L	0.181	0.519	0.175	0.164	0.496	0.158
16	Pink03	III	L	0.250	0.475	0.254	0.242	0.461	0.248
17	PurpleDark01	II	M	0.285	0.311	0.292	0.277	0.303	0.286
18	PurpleLight01	III	L	0.204	0.489	0.190	0.185	0.455	0.170
19	Rockton5865000FM	II	L	0.443	0.563	0.404	0.431	0.547	0.393
20	SheerBlack01	S	M	0.632	0.151	0.230	0.630	0.145	0.231
21	SheerRed01	S	M	0.650	0.171	0.273	0.647	0.169	0.273
22	SheerWhite01	S	L	0.732	0.261	0.399	0.727	0.250	0.396
23	SoilMusick01	II	L	0.298	0.470	0.297	0.282	0.449	0.281
24	White05	III	L	0.255	0.635	0.259	0.237	0.609	0.242
25	White07	III	L	0.247	0.713	0.249	0.225	0.684	0.227
26	BlueSoft01/SoftBlue30	II	M	0.248	0.335	0.237	0.235	0.323	0.224
27	Yellow05	III	L	0.195	0.595	0.182	0.171	0.555	0.158
28	YorklineLining	III	L	0.333	0.675	0.337	0.317	0.648	0.320
29	Black10	III	D	0.115	0.194	0.088	0.114	0.185	0.087

ID	Name	KUC		Weighted (400 – 1045 nm)			Weighted (250 – 2500 nm)		
		I,II,III	D,M,L	τ_{bt}	ρ_{bt}	τ_{bd}	τ_{bt}	ρ_{bt}	τ_{bd}
30	Brown10	III	M	0.191	0.427	0.190	0.180	0.409	0.179
31	Brown Open01	II	M	0.326	0.324	0.178	0.317	0.304	0.169
32	Green01	III	L	0.275	0.501	0.236	0.252	0.468	0.215
33	Grey10	III	M	0.220	0.381	0.184	0.203	0.360	0.168
34	S_Blue01	III	M	0.174	0.444	0.166	0.157	0.421	0.149
35	S_Brown01	III	L	0.175	0.502	0.170	0.157	0.477	0.153
36	S_Gold02	III	L	0.226	0.617	0.218	0.209	0.591	0.200
37	S_Grey01	III	M	0.158	0.424	0.151	0.143	0.402	0.136
38	S_Red01	III	M	0.157	0.462	0.157	0.141	0.437	0.140
39	S_Silver01	III	L	0.252	0.621	0.233	0.234	0.592	0.216
40	Silk01	III	L	0.223	0.579	0.222	0.203	0.555	0.202
41	SilkBlack01	III	M	0.178	0.412	0.161	0.157	0.380	0.142
42	White10	III	L	0.292	0.675	0.297	0.264	0.636	0.269
43	SingaporeChintzWhite01	III	L	0.377	0.625	0.381	0.362	0.610	0.366
44	SingaporeChintzOrange01	II	L	0.329	0.490	0.331	0.312	0.474	0.315
45	SingaporeChintzBlack01	II	M	0.250	0.359	0.243	0.233	0.340	0.227
46	SheerLight01	I	M	0.618	0.274	0.472	0.612	0.270	0.469
47	ReflexGabWhite01	III	L	0.312	0.697	0.310	0.296	0.674	0.294
48	ReflexGabOrange01	III	L	0.211	0.510	0.211	0.193	0.488	0.192
49	ReflexGabBrown01	III	M	0.190	0.424	0.189	0.172	0.401	0.171
50	HorizonSuitingDarkGreen	III	M	0.185	0.405	0.183	0.168	0.386	0.165
51	HorizonSuitingBlack	II	M	0.226	0.363	0.215	0.211	0.344	0.201
52	BlackSoft02	II	M	0.318	0.318	0.261	0.314	0.311	0.257
53	BlackSoft01	II	M	0.264	0.331	0.231	0.249	0.309	0.215
54	100PWoolMens Medium01	II	M	0.249	0.339	0.239	0.223	0.310	0.214
55	100PWoolMens Light01	II	M	0.316	0.417	0.293	0.284	0.381	0.262
56	100PWoolMens Dark01	III	D	0.132	0.234	0.129	0.131	0.227	0.129
57	BlueSoft20	II	M	0.236	0.362	0.227	0.232	0.353	0.223
58	RedSoft20	II	M	0.269	0.346	0.256	0.263	0.339	0.250
59	WhiteSheer20	S	L	0.720	0.257	0.390	0.715	0.251	0.386
60	YellowSoft20	II	L	0.395	0.485	0.381	0.388	0.479	0.374
61	Dark30	II	M	0.284	0.310	0.211	0.269	0.293	0.194
62	Dark31	II	M	0.286	0.322	0.189	0.269	0.302	0.172

ID	Name	KUC		Weighted (400 – 1045 nm)			Weighted (250 – 2500 nm)		
		I,II,III	D,M,L	τ_{bt}	ρ_{bt}	τ_{bd}	τ_{bt}	ρ_{bt}	τ_{bd}
63	Dark32	III	M	0.219	0.366	0.197	0.209	0.358	0.189
64	FashionBlack01	I	M	0.450	0.217	0.202	0.443	0.208	0.197
65	FashionGreen01	I	M	0.471	0.242	0.214	0.463	0.231	0.209
66	FashionLight01	I	L	0.560	0.339	0.304	0.553	0.330	0.298
67	FashionLight02	I	L	0.584	0.362	0.340	0.575	0.352	0.333
68	GreenOpen01	I	M	0.457	0.311	0.313	0.450	0.301	0.308
69	LightGreen30	II	L	0.434	0.469	0.324	0.418	0.456	0.310
70	RoughBlack	II	M	0.226	0.306	0.130	0.211	0.287	0.117
71	RoughRed	III	M	0.225	0.444	0.181	0.204	0.410	0.161
72	Thin01	S	D	0.805	0.064	0.227	0.804	0.063	0.229
73	Thin02	S	D	0.605	0.115	0.240	0.603	0.114	0.240
74	Thin03	I	M	0.465	0.235	0.333	0.463	0.225	0.331
75	Thin04	S	M	0.747	0.094	0.310	0.747	0.092	0.313
76	White30	II	L	0.429	0.522	0.350	0.413	0.512	0.334
77	WhiteOpen01	I	L	0.523	0.366	0.337	0.516	0.358	0.331
78	NigataSolids	III	M	0.138	0.310	0.138	0.115	0.370	0.114
79	NouvelleSkirts	III	M	0.203	0.412	0.192	0.188	0.336	0.178
80	S_GreyLight	III	M	0.156	0.466	0.150	0.142	0.445	0.135
81	IsakGrey	II	M	0.302	0.282	0.241	0.285	0.266	0.226
82	NathanGreen	II	M	0.268	0.321	0.248	0.258	0.310	0.239
83	Nathan ThickBlack	III	D	0.051	0.139	0.049	0.050	0.142	0.048
84	Nathan ThickDarkBlue	III	M	0.101	0.335	0.100	0.094	0.321	0.093
85	UnknownReflexGabBlack	III	M	0.168	0.396	0.166	0.152	0.364	0.149
86	NathanSheerBlack	II	D	0.274	0.123	0.091	0.299	0.147	0.114
87	NathanBlue	III	M	0.198	0.399	0.195	0.181	0.373	0.178
88	FashionSkin	I	L	0.569	0.317	0.294	0.563	0.310	0.289
89	UnknownGrey	III	M	0.238	0.412	0.227	0.224	0.404	0.213
90	IsakBlack2Pieces	II	M	0.305	0.296	0.270	0.300	0.289	0.266
91	IsakBlack1Piece	III	M	0.204	0.348	0.194	0.190	0.328	0.179
92	PowerMeshBlack01	II	D	0.188	0.200	0.155	0.199	0.205	0.166
93	PowerMeshBlack02	II	D	0.216	0.197	0.173	0.224	0.200	0.182
94	PowerMeshBlackOpen	I	D	0.409	0.112	0.126	0.426	0.124	0.143
95	PowerMeshYellow	II	L	0.501	0.501	0.413	0.482	0.392	0.394

ID	Name	KUC		Weighted (400 – 1045 nm)			Weighted (250 – 2500 nm)		
		I,II,III	D,M,L	τ_{bt}	ρ_{bt}	τ_{bd}	τ_{bt}	ρ_{bt}	τ_{bd}
00-1	Red01	III	M	0.227	0.439	0.198	0.222	0.424	0.193
00-10	Silver01	III	M	0.202	0.490	0.182	0.188	0.479	0.169
00-12	White02	II	L	0.382	0.583	0.287	0.364	0.558	0.270
00-13	White03	III	L	0.366	0.629	0.308	0.366	0.610	0.308
0-1	Black0001	I	M	0.584	0.163	0.248	0.581	0.156	0.248
0-2	Black0002	III	M	0.179	0.389	0.178	0.161	0.367	0.162
0-3	Orange0001	III	L	0.276	0.498	0.242	0.259	0.478	0.226
0-4	Red0002	S	M	0.670	0.170	0.289	0.669	0.164	0.290
0-5	Rough_Dark0001	II	M	0.339	0.272	0.165	0.328	0.248	0.155
0-6	Rough_Light0001	II	L	0.479	0.433	0.264	0.464	0.397	0.251
0-7	Rough_Medium0001	II	M	0.393	0.368	0.219	0.376	0.339	0.206
0-8	Sandy0001	III	L	0.209	0.533	0.201	0.193	0.510	0.186
0-9	White0001	S	L	0.773	0.245	0.395	0.769	0.237	0.392
N1	Cream_Sheer	S					0.800	0.190	0.350
N2	White1_IL	I	L				0.560	0.420	0.300
N3	White2_IIL	II	L				0.430	0.560	0.420
N4	White3_IIIL	III	L				0.300	0.680	0.290
N5	Brown_IM	I	M				0.640	0.230	0.310
N6	Green_IIM	II	M				0.280	0.320	0.260
N7	Blue_IIIM	III	M				0.200	0.380	0.190
N8	Black1_ID	I	D				0.320	0.150	0.090
N9	Black2_IID	II	D				0.230	0.210	0.180

Appendix B: Mathematical Formulation of KUC

Openness Lines Represented by Quadratic Functions

First, from the constant openness lines shown on the KUC, fabric transmittance, τ_{bt}, was read by eye from zero reflectance ($\rho_{bt} = 0$) to ρ_{bt} at the diagonal limit line, $\rho_{bt} = \rho_{bt,limit} = 1 - \tau_{bt,limit}$, at an increment of $\rho_{bt} = 0.05$. These (ρ_{bt}, τ_{bt}) points have been recorded along all constant A_o curves shown on the chart including A_o = 0.50, 0.40, 0.30, 0.25, 0.20, 0.10, 0.07, 0.05, 0.04, 0.03, 0.02, 0.01, and 0.01Limit. Table A.1 includes the data collected.

Second, the data points can be fitted using 2nd order polynomial of the form

$$\tau_{bt}(\rho_{bt}) = C_1 \rho_{bt}^2 + C_2 \rho_{bt} + C_3 \qquad \textbf{(A.1)}$$

That is to say that the constant A_o lines take the form of τ_{bt} as a function of ρ_{bt}. The fitting has been done in an Excel worksheet. The quadratic equations generated are shown in Figure A.1, each corresponding to a constant A_o line. The fitting is excellent with any difference between the original (solid) lines and the corresponding fitted (dashed) lines either not visible or insignificant. Figure A.1 shows the reproduced KUC, and Table A.2 summarizes the constant coefficients (C_1, C_2, and C_3) of the quadratic equations shown in Figure A.1. The nine categories plus the sheer are shown on the reproduced KUC for clarity (Figure A.2).

Table A.1: Points on Keyes' constant openness lines

$A_o = 0.50$		$A_o = 0.40$		$A_o = 0.30$		$A_o = 0.25$		$A_o = 0.20$		$A_o = 0.10$	
ρ_{bt}	τ_{bt}	ρ_{bt}	τ_{bt}	ρ_{bt}	τ_{bt}	ρ_{bt}	τ_{bt}	ρ_{bt}	τ_{bt}	ρ_{bt}	τ_{bt}
0.000	0.500	0.000	0.400	0.000	0.300	0.000	0.250	0.000	0.200	0.000	0.100
0.050	0.530	0.050	0.421	0.050	0.315	0.050	0.262	0.050	0.210	0.050	0.110
0.100	0.565	0.100	0.442	0.100	0.333	0.100	0.280	0.100	0.225	0.100	0.125
0.150	0.600	0.150	0.472	0.150	0.360	0.150	0.302	0.150	0.245	0.150	0.142
0.200	0.637	0.200	0.505	0.200	0.385	0.200	0.328	0.200	0.270	0.200	0.162
0.250	0.680	0.250	0.540	0.250	0.420	0.250	0.357	0.250	0.296	0.250	0.190
0.287	0.713	0.300	0.585	0.300	0.456	0.300	0.390	0.300	0.329	0.300	0.220
		0.350	0.633	0.350	0.498	0.350	0.428	0.350	0.365	0.350	0.250
		0.358	0.642	0.400	0.540	0.400	0.470	0.400	0.410	0.400	0.285
				0.430	0.570	0.450	0.513	0.450	0.453	0.450	0.322
						0.468	0.532	0.500	0.500	0.500	0.365
										0.550	0.410
										0.570	0.430

$A_o = 0.07$		$A_o = 0.05$		$A_o = 0.04$		$A_o = 0.03$		$A_o = 0.02$		$A_o = 0.01$	
ρ_{bt}	τ_{bt}	ρ_{bt}	τ_{bt}	ρ_{bt}	τ_{bt}	ρ_{bt}	τ_{bt}	ρ_{bt}	τ_{bt}	ρ_{bt}	τ_{bt}
0.000	0.070	0.000	0.050	0.000	0.04	0.000	0.030	0.000	0.02	0.000	0.010
0.050	0.081	0.100	0.071	0.100	0.06	0.100	0.046	0.100	0.034	0.100	0.020
0.100	0.098	0.200	0.108	0.200	0.093	0.200	0.075	0.200	0.059	0.200	0.036
0.150	0.117	0.300	0.157	0.300	0.139	0.300	0.115	0.300	0.092	0.300	0.060
0.200	0.139	0.400	0.218	0.400	0.195	0.400	0.167	0.400	0.135	0.400	0.094
0.250	0.161	0.500	0.287	0.500	0.259	0.500	0.228	0.500	0.189	0.500	0.134
0.300	0.188	0.600	0.364	0.600	0.335	0.600	0.298	0.600	0.255	0.600	0.183
0.350	0.215	0.620	0.380	0.637	0.363	0.657	0.343	0.681	0.319	0.700	0.248
0.400	0.248									0.732	0.268
0.450	0.280										
0.500	0.317										
0.550	0.355										
0.600	0.400										

0.01 Limit		$\rho_y = 0.25$		$\rho_y = 0.50$	
ρ_{bt}	τ_{bt}	ρ_{bt}	τ_{bt}	ρ_{bt}	τ_{bt}
0.000	0.000	0.250	0.000	0.500	0.000
0.100	0.001	0.247	0.050	0.499	0.050
0.200	0.003	0.241	0.100	0.497	0.100
0.300	0.013	0.230	0.150	0.493	0.150
0.350	0.022	0.219	0.200	0.488	0.200
0.400	0.033	0.207	0.250	0.479	0.250
0.450	0.047	0.196	0.300	0.461	0.300
0.500	0.060	0.183	0.350	0.435	0.350
0.550	0.076	0.172	0.400	0.410	0.400
0.600	0.094	0.146	0.500	0.382	0.450
0.650	0.115	0.124	0.585	0.355	0.500
0.700	0.137			0.299	0.600
0.750	0.164			0.270	0.650
0.800	0.190			0.251	0.682
0.805	0.195				

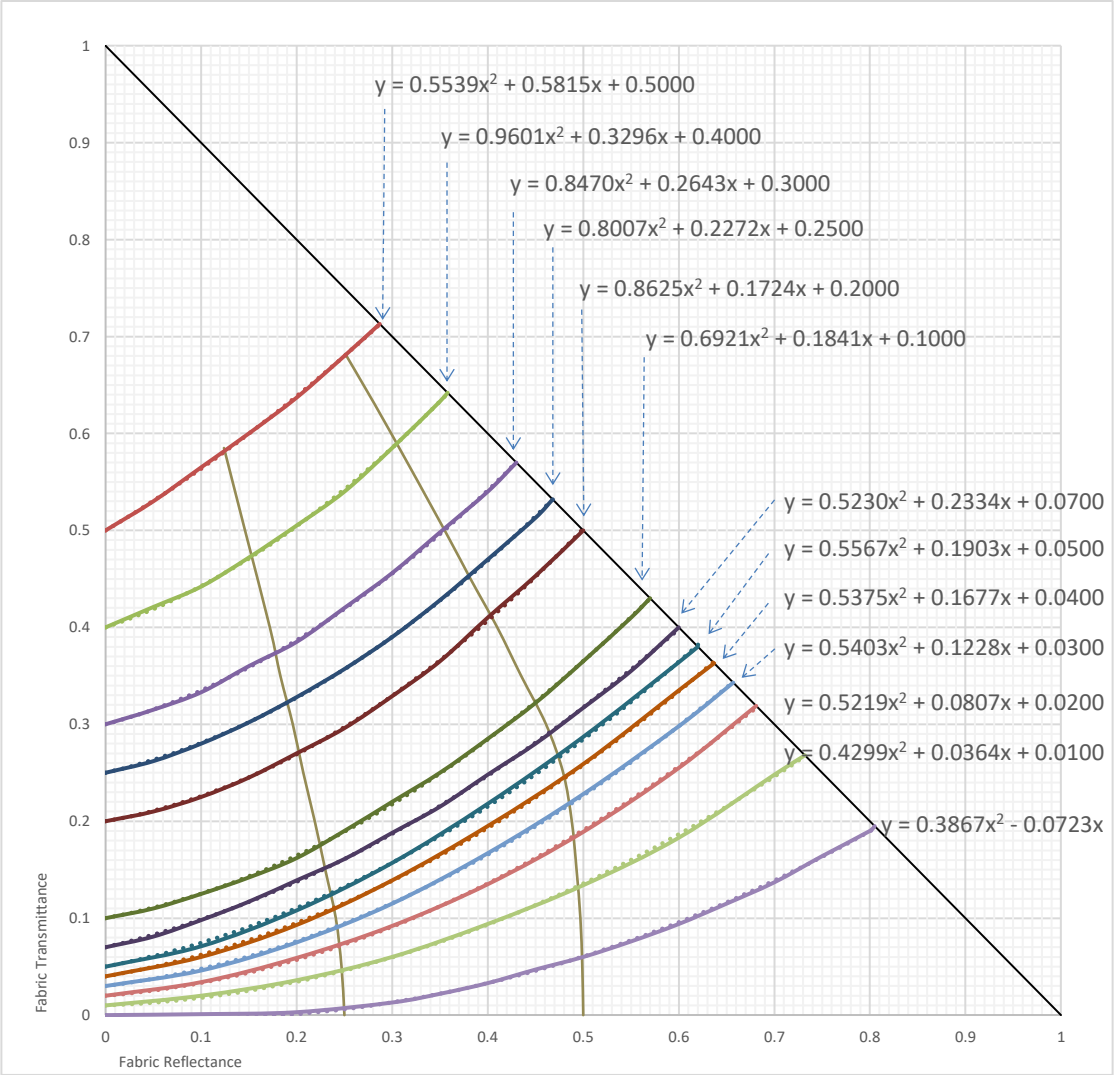

Figure A.1: Quadratic equations that represent the fitted openness lines

Table A.2: Coefficients C_1, C_2, and C_3 for quadratic equations representing A_o = constant lines

$$\tau_{bt}(\rho_{bt}) = C_1 \rho_{bt}^2 + C_2 \rho_{bt} + C_3$$

A_o	C_1	C_2	C_3
0.50	.5539	.5815	0.50
0.40	.9601	.3296	0.40
0.30	.8470	.2643	0.30
0.25	.8007	.2272	0.25
0.20	.8625	.1724	0.20
0.10	.6921	.1841	0.10
0.07	.5230	.2334	0.07
0.05	.5591	.1895	0.05
0.04	.5375	.1677	0.04
0.03	.5403	.1228	0.03
0.02	.5219	.0807	0.02
0.01	.4299	.0364	0.01
0.01 Limit	.3867	.0723	0

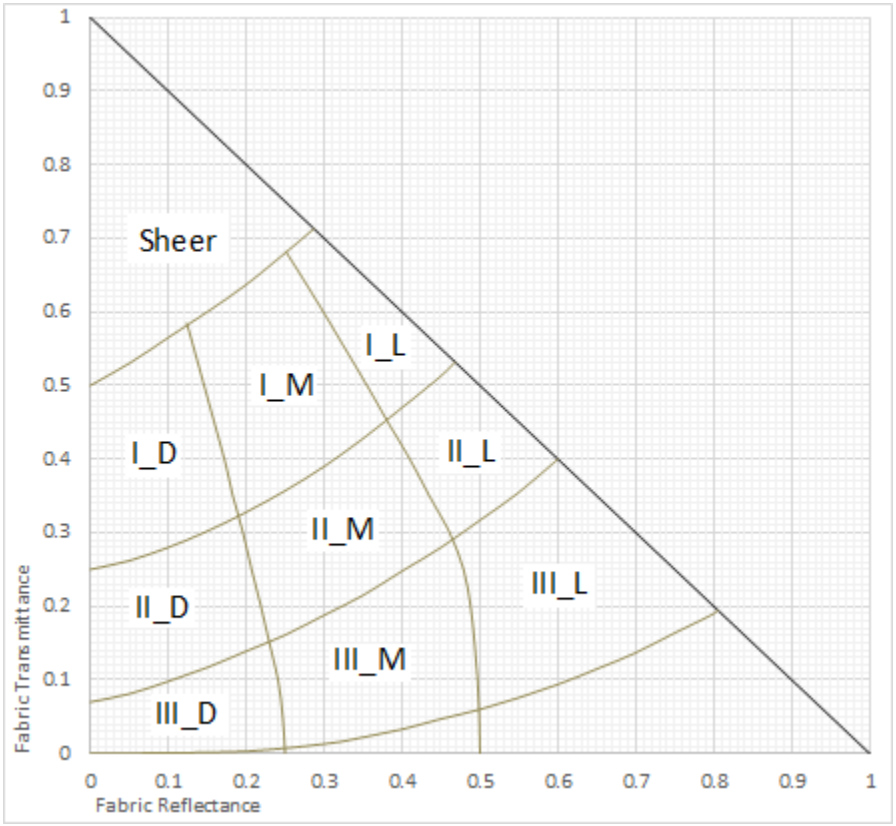

Figure A.2: Reproduced KUC showing the nine original fabric categories and a sheer fabric category

Arithmetic Relationship of ρ_{bt}, τ_{bt}, A_o Based on the Original KUC

Given any two properties of ρ_{bt}, τ_{bt}, and A_o, a point can be located and plotted on the KUC to determine the third property. This section offers a method to determine the third property arithmetically (without reading from the KUC).

On the KUC, a data point located by two of the three properties would lie in between two neighboring constant A_o lines, one above the point and one below it. Now, these two adjacent constant A_o lines, $\tau_{bt,Lower}(\rho_{bt})$ and $\tau_{bt,Upper}(\rho_{bt})$, have been represented by the quadratic equations discussed in Section 0. Note that at zero reflectance, $\rho_{bt} = 0$, $\tau_{bt,Lower}(\rho_{bt} =0) = A_{oLower}$ and $\tau_{bt,Upper}(\rho_{bt} =0) = A_{oUpper}$. In other words, equations of the two adjacent constant A_o lines bounding the data point are used to correlate the fabric properties.

The equation below relates the three optical properties, τ_{bt}, τ_{bb}, and ρ_{bt}, of a fabric:

$$\frac{\tau_{bb} - A_{oLower}}{A_{oUpper} - A_{oLower}} = \frac{\tau_{bt} - \tau_{bt,Lower}(\rho_{bt})}{\tau_{bt,Upper}(\rho_{bt}) - \tau_{bt,Lower}(\rho_{bt})} \qquad \textbf{(A.2)}$$

where

τ_{bb}, τ_{bt}, and ρ_{bt} are the solar optical properties of a fabric

A_{oUpper} is the openness of the nearest openness line above the point

A_{oLower} is the openness of the nearest openness line below the point

$\tau_{bt,Upper}$ (ρ_{bt}) is τ_{bt} calculated using the nearest openness line above the point

$\tau_{bt,Lower}$ (ρ_{bt}) is τ_{bt} calculated using the nearest openness line below the point

Equation (A.2) reflects the idea that the relative location of fabric openness between the two adjacent (Upper and Lower) A_o lines is the same at $\rho_{bt} = 0$ and at $\rho_{bt} = \rho_{bt}$. On the other hand, A_o is taken to be linear, with respect to τ_{bt}, between the values of A_o represented by Equation (A.1)

and Table A.2. Therefore, Equation (A.2) along with the C_1, C_2 and C_3 constants can be used to calculate the third unknown property given that the other two properties are known.

Note that either τ_{bb} alone or both of ρ_{bt} and τ_{bt} as a pair is required to choose the upper and lower constant A_o lines to be used in Equation (A.2). Therefore, any pair of the three properties satisfies the requirement. Additionally, if ρ_{bt} is the unknown in Equation (A.2), an iterative procedure (or root-finding calculation) can be used to find the solution. Otherwise, when τ_{bt} or τ_{bb} is the unknown, a more direct solution can be used.

Bounds of the KUC

Keyes (1967) neither considered fabrics with $A_o > 0.5$ nor discussed the region below $A_o = 0$. This sub-section deals with fabrics above the $A_o = 0.5$ line and below the $A_o = 0.01$ Limit line.

Below $A_o = 0.01$ Limit

Instead of using an $A_o = 0$ line, Keyes used a "0.01 Limit" line as his lower limit. As will be presented in the next section, note that none of the 117 fabrics (Section 2.3.2.2) examined in this study fall below the 0.01 Limit line of the Keyes Chart. Most likely, the fabric sample data used by Keyes were also all above the 0.01 Limit line although he did not explicitly deal with this topic. The 0.01 Limit line is assumed to be the zero openness ($A_o = 0$) line since this line starts at zero transmittance, $\tau_{bt} = 0$, at $\rho_{bt} = 0$. A fabric below the 0.01 Limit line, if any, is considered to have zero openness. For (ρ_{bt},τ_{bb}) or (τ_{bt}, τ_{bb}) with $\tau_{bb} = 0$, the 0.01 Limit line or $A_o = 0$ line is used to calculate the unknown property.

Above $A_o = 0.50$

For (ρ_{bt}, τ_{bb}) or (τ_{bt}, τ_{bb}) with $\tau_{bb} \geq 0.50$, a constant A_o line is assumed to have the same curvature as the $A_o = 0.50$ line. Similarly, the same curvature is also applied for any pair of (ρ_{bt}, τ_{bt}) that is

above the $A_o = 0.50$ line. Therefore, for $A_o > 0.50$, all constant A_o lines share the same C_1 and C_2 coefficients as the $A_o = 0.50$ line listed in Table A.2 while retaining the requirement that $C_3 = A_o$.

Beyond the Diagonal Limit Line

As explained in Section 2.2.4 and as shown in Figure 2.3, it is possible that a data point is located beyond the theoretical diagonal limit line. In this case, the constant A_o lines are simply assumed to follow Equation (A.1) while allowing the reflectance to go beyond the limit (i.e., $\rho_{bt} > \rho_{limit}$).

In summary, the method described here in has two functions:

1. Estimate the third, unknown, property of a fabric: With any two known solar optical properties, instead of reading by eye from the KUC, the third property can be estimated using Equation (A.2).

2. Plotting the triangles (Figure 2.3): With the three measured solar optical properties of a fabric, instead of a manual plot (e.g., Figure 2.3), Equation (A.2) can be used to generate the three points on the chart. The right angle point comes directly from the measured ρ_{bt} and τ_{bt}. For the other two points, either ρ_{bt} or τ_{bt} is assumed the unknown property. Then that "assumed" unknown property can be calculated using Equation (A.2). Combining the assumed unknown property and the measured known property gives a data point to be plotted on the KUC. Therefore, ($\rho_{bt,assumed\_unknown}$ and $\tau_{bt,measured}$) and ($\rho_{bt,measured}$ and $\tau_{bt,assumed\_unknown}$) are the other two points for the triangle.

This formulation will be useful for comparison between the original KUC and any improved KUC.

Appendix C: Measured Fabric Thickness

No.	Name	Thickness (mm)	
		Unpressed	Pressed
1	2600BX_Sheeting	0.25	0.21
2	22111FV_Wide_LightYellow	0.18	0.16
3	22111FV_Wide_White	0.16	0.13
4	BlueRough01	0.50	0.36
5	SoftBlue31	0.18	0.14
6	Brown01	0.89	0.71
7	DadSolidFM	0.42	0.32
8	DarkBrown01	0.47	0.31
9	DarkGrey01	0.50	0.34
10	DecolineLining	0.27	0.22
11	GoldCut01	0.31	0.25
12	Grey01	0.47	0.32
13	GreyOpen01	0.38	0.29
14	Pink01	0.81	0.67
15	Pink02	0.49	0.38
16	Pink03	0.23	0.18
17	PurpleDark01	0.23	0.17
18	PurpleLight01	0.79	0.49
19	Rockton5865000FM	0.17	0.14
20	SheerBlack01	0.12	0.11
21	SheerRed01	0.12	0.11
22	SheerWhite01	0.12	0.12
23	SoilMusick01	0.21	0.17
24	White05	0.48	0.28
25	White07	0.76	0.49
26	BlueSoft01/SoftBlue30	0.32	0.24
27	Yellow05	0.57	0.49
28	YorklineLining	0.28	0.21
29	Black10	0.18	0.15
30	Brown10	0.43	0.32
31	Brown Open01	0.43	0.33
32	Green01	0.44	0.36
33	Grey10	0.66	0.54
34	S_Blue01	0.47	0.39
35	S_Brown01	0.53	0.43
36	S_Gold02	0.51	0.40
37	S_Grey01	0.53	0.42
38	S_Red01	0.50	0.43
39	S_Silver01	0.48	0.37
40	Silk01	0.42	0.30
41	SilkBlack01	0.42	0.34
42	White10	0.50	0.38
43	SingaporeChintzWhite01	0.18	0.16
44	SingaporeChintzOrange01	0.18	0.16
45	SingaporeChintzBlack01	0.18	0.17
46	SheerLight01	0.13	0.12
47	ReflexGabWhite01	0.55	0.38
48	ReflexGabOrange01	0.57	0.38
49	ReflexGabBrown01	0.60	0.41
50	HorizonSuitingDarkGreen	0.47	0.32
51	HorizonSuitingBlack	0.45	0.36
52	BlackSoft02	0.14	0.10
53	BlackSoft01	0.44	0.35
54	100PWool Medium01	0.32	0.27
55	100PWool Light01	0.37	0.30
56	100PWool Dark01	0.40	0.32
57	BlueSoft20	0.16	0.12
58	RedSoft20	0.19	0.13
59	WhiteSheer20	0.12	0.11
60	YellowSoft20	0.22	0.17
61	Dark30	0.24	0.18
62	Dark31	0.23	0.18
63	Dark32	0.19	0.16
64	FashionBlack01	0.20	0.18
65	FashionGreen01	0.19	0.18
66	FashionLight01	0.21	0.17
67	FashionLight02	0.18	0.16
68	GreenOpen01	0.32	0.23
69	LightGreen30	0.21	0.15
70	RoughBlack	0.85	0.74
71	RoughRed	0.72	0.52
72	Thin01	0.40	0.11
73	Thin02	0.13	0.11
74	Thin03	0.20	0.18
75	Thin04	0.15	0.09
76	White30	0.21	0.17
77	WhiteOpen01	0.30	0.21
78	NigataSolids	0.86	0.46
79	NouvelleSkirts	0.53	0.35
80	S_GreyLight	0.50	0.36
81	IsakGrey	0.50	0.35
82	NathanGreen	0.21	0.17
83	Nathan ThickBlack	0.96	0.65
84	Nathan ThickDarkBlue	0.99	0.60
85	UnknownReflexGabBlack	0.57	0.40
86	NathanSheerBlack	0.63	0.51
87	NathanBlue	0.44	0.35
88	FashionSkin	0.18	0.15
89	UnknownGrey	0.37	0.29
90	IsakBlack2Pieces	0.13	0.10
91	IsakBlack1Piece	0.51	0.36
92	PowerMeshBlack01	0.63	0.44
93	PowerMeshBlack02	0.62	0.44
94	PowerMeshBlackOpen	0.37	0.31
95	PowerMeshYellow	0.50	0.33
00-1	Red01	0.17	0.14
00-10	Silver01	0.26	0.22
00-12	White02	0.59	0.48
00-13	White03	0.21	0.19
0-1	Black0001	0.13	0.12
0-2	Black0002	0.55	0.50
0-3	Orange0001	0.64	0.53
0-4	Red0002	0.15	0.13
0-5	Rough_Dark0001	0.86	0.67
0-6	Rough_Light0001	0.75	0.63
0-7	Rough_Medium0001	0.96	0.80
0-8	Sandy0001	0.56	0.40
0-9	White0001	0.12	0.11

Appendix D: Triangular Pleated Drape ILM

```
PROGRAM TRIANGULAR_MODEL

  IMPLICIT NONE

  REAL :: W                          ! INPUT -- PLEAT WIDTH (UNITS MUST BE CONSISTENT AND MUST BE GREATER
                                             THAN ZERO)
  REAL :: S                          ! INPUT -- PLEAT SPACING (MUST BE GREATER THAN ZERO AND S CANNOT BE
                                             GREATER THAN 2W)

  REAL :: OMEGA_H_DEG                ! INPUT -- HORIZONTAL INCIDENT ANGLE (IN DEGREE)
  REAL :: OMEGA_H_RAD                !      -- HORIZONTAL INCIDENT ANGLE (IN RADIAN)

  REAL :: M_TAU_F_BT0                ! INPUT -- MATERIAL (FABRIC) FRONT NORMAL BEAM-TOTAL   TRANSMITTANCE
  REAL :: M_TAU_F_BD0                ! INPUT -- MATERIAL (FABRIC) FRONT NORMAL BEAM-DIFFUSE TRANSMITTANCE
  REAL :: M_TAU_F_BB0                !      -- MATERIAL (FABRIC) FRONT NORMAL BEAM-BEAM
                                             TRANSMITTANCE = M_TAU_F_BT0 - M_TAU_F_BD0

  REAL :: M_RHO_F_BT0                !      -- MATERIAL (FABRIC) FRONT NORMAL BEAM-TOTAL   REFLECTANCE   =
                                             M_RHO_F_BD0
  REAL :: M_RHO_F_BD0                ! INPUT -- MATERIAL (FABRIC) FRONT NORMAL BEAM-DIFFUSE REFLECTANCE
  REAL :: M_RHO_F_BB0                !      -- MATERIAL (FABRIC) FRONT NORMAL BEAM-BEAM    REFLECTANCE

  REAL :: RHO_Y                      !      -- YARN REFLECTANCE

  REAL :: M_TAU_B_BT0                !      -- MATERIAL (FABRIC) BACK  NORMAL BEAM-TOTAL   TRANSMITTANCE
  REAL :: M_TAU_B_BD0                !      -- MATERIAL (FABRIC) BACK  NORMAL BEAM-DIFFUSE TRANSMITTANCE
  REAL :: M_TAU_B_BB0                !      -- MATERIAL (FABRIC) BACK  NORMAL BEAM-BEAM
                                             TRANSMITTANCE = M_TAU_B_BT0 – M_TAU_B_BD0

  REAL :: M_RHO_B_BT0                !      -- MATERIAL (FABRIC) BACK  NORMAL BEAM-TOTAL   REFLECTANCE   =
                                             M_RHO_B_BD0
  REAL :: M_RHO_B_BD0                !      -- MATERIAL (FABRIC) BACK  NORMAL BEAM-DIFFUSE REFLECTANCE
  REAL :: M_RHO_B_BB0                !      -- MATERIAL (FABRIC) BACK  NORMAL BEAM-BEAM    REFLECTANCE

  REAL, PARAMETER :: PI = 3.14159265358979
  REAL :: D_TO_R                     !      -- WORKING TEMP (CONVERT DEGREE TO RADIAN)

  REAL :: ALPHA                      !      -- PLEAT ANGLE IN RADIAN (PLEAT ANGLE = PI - FOLDING ANGLE)
                                     !      -- e.g., FOR RIGHT TRIANGULAR PLEATS, FLODING ANGLE = 2PI/3 SO PLEAT
                                             ANGLE = PI/3
  REAL :: W_LAYER                    !      -- PLEATED DRAPE LAYER WIDTH

  REAL :: ALPHA_1                    !      -- 90 DEGREES (PI/2) FROM NORMAL INCIDENCE
  REAL :: ALPHA_2                    !      -- MINIMUM INCIDENCE ANGLE AT WHICH THE BEAM RADIATION WILL PASS
                                             TWO FABRIC LAYERS OF THE TRIANGULARLY PLEATED DRAPE
  REAL :: ALPHA_3                    !      -- ANGLE FROM THE NORMAL INCIDENCE TO THE FABRIC (= ALPHA / 2)

  REAL :: THETA_DW_BK                !      -- INCIDENT ANGLE ON THE BACK  SIDE OF DOWN-SLOPE \ FABRIC PLEAT (IN
                                             RADIAN)
  REAL :: THETA_UP_FR                !      -- INCIDENT ANGLE ON THE FRONT SIDE OF   UP-SLOPE / FABRIC PLEAT (IN
                                             RADIAN)
  REAL :: THETA_DW_FR                !      -- INCIDENT ANGLE ON THE FRONT SIDE OF DOWN SLOPE \ FABRIC PLEAT (IN
                                             RADIAN)

  REAL :: S_P       ! -- S_P(S_PROJECTED) IS PLEAT SPACING (S) PROJECTED ONTO THE PLANE NORMAL TO INCIDENCE
  REAL :: S1P       ! -- SEE DRAWING FOR S1 AND S1P, S1P IS S1 PROJECTED ONTO THE PLANE NORMAL TO INCIDENCE
  REAL :: S3P       ! -- SEE DRAWING FOR S3 AND S3P, S3P IS S3 PROJECTED ONTO THE PLANE NORMAL TO INCIDENCE
  REAL :: S4P       ! -- SEE DRAWING FOR S4 AND S4P, S4P IS S4 PROJECTED ONTO THE PLANE NORMAL TO INCIDENCE

  INTEGER :: GROUP          ! -- CASE 1, 2, AND 3 -- DEPENDS ON OMEGA_H_RAD, W, AND S
                            ! -- DETERMINE THE CASE (1, 2, OR 3)
                            ! -- BASED ON THE PLEAT GEOMETRY AND THE INCIDENT ANGLE
```

```
REAL :: M_RHO_F_DD     !    -- MATERIAL (FABRIC) FRONT DIFFUSE-DIFFUSE   REFLECTANCE = M_RHO_F_BD
REAL :: M_TAU_F_DD     !    -- MATERIAL (FABRIC) FRONT DIFFUSE-DIFFUSE TRANSMITTANCE = M_TAU_F_BD
REAL :: M_RHO_B_DD     !    -- MATERIAL (FABRIC)  BACK DIFFUSE-DIFFUSE   REFLECTANCE = M_RHO_B_BD
REAL :: M_TAU_B_DD     !    -- MATERIAL (FABRIC)  BACK DIFFUSE-DIFFUSE TRANSMITTANCE = M_TAU_B_BD

REAL :: M_RHO_F_BD_UP_FR
REAL :: M_TAU_F_BB_UP_FR
REAL :: M_TAU_F_BD_UP_FR
REAL :: M_TAU_F_BT_UP_FR
REAL :: M_RHO_F_BD_DW_FR
REAL :: M_TAU_F_BB_DW_FR
REAL :: M_TAU_F_BD_DW_FR
REAL :: M_TAU_F_BT_DW_FR
REAL :: M_RHO_F_BD_DW_BK
REAL :: M_TAU_F_BB_DW_BK
REAL :: M_TAU_F_BD_DW_BK
REAL :: M_TAU_F_BT_DW_BK

REAL :: M_RHO_B_BD_UP_FR
REAL :: M_TAU_B_BB_UP_FR
REAL :: M_TAU_B_BD_UP_FR
REAL :: M_TAU_B_BT_UP_FR
REAL :: M_RHO_B_BD_DW_FR
REAL :: M_TAU_B_BB_DW_FR
REAL :: M_TAU_B_BD_DW_FR
REAL :: M_TAU_B_BT_DW_FR
REAL :: M_RHO_B_BD_DW_BK
REAL :: M_TAU_B_BB_DW_BK
REAL :: M_TAU_B_BD_DW_BK
REAL :: M_TAU_B_BT_DW_BK

REAL :: TAU_F_BB
REAL :: TAU_F_BD
REAL :: RHO_F_BD
REAL :: TAU_F_BT

! DISTANCES BETWEEN TWO POINTS (SEE DRAWINGS)
REAL :: AC, BD, AB, BC, CD, CF, BF, CG, AE, BE, DG, AF, FG, BG, CE, EF, DF, AH

! VIEW FACTORS
REAL :: F1B3B, F1B4B, F2B3B, F2B4B, &
        F3B1B, F4B1B, F3B2B, F4B2B, &
        F1B7B, F2B7B, F3B7B, F4B7B, F7B4B
REAL :: F1F3F, F1F4F, F2F3F, F2F4F, &
        F3F1F, F4F1F, F3F2F, F4F2F, &
        F1F7F, F2F7F, F3F7F, F4F7F, F7F4F

! VIEW FACTORS
REAL :: F5F1F, F5F2F, F5F3F, F5F4F, F5F7F
REAL :: F6B1B, F6B2B, F6B3B, F6B4B, F6B7B

REAL :: Z1B_BD, Z4B_BD, Z7B_BD, Z1F_BD, Z4F_BD, Z7F_BD

! SEE DRAWINGS FOR SURFACE NUMBERS
REAL :: J1B , J2B , J3B , J4B , J6B , J7B          ! J = RADIOSITY, #B = BACK SURFACES
REAL :: J1F , J2F , J3F , J4F , J5F , J7F          ! J = RADIOSITY, #F = FRONT SURFACES
REAL :: G5F , G6B                                                         ! G = IRRADIANCE

INTEGER, PARAMETER :: N = 12
! ********************THIS NUMBER IS DETERMINED BY THE MODEL**********************************
REAL :: A ( N , N + 2 )
REAL :: XSOL ( N )

INTEGER I

!!!!!!!!!!!!!!!!!!!!!!!!!!!!!!!!!!!!!!!!!!!!!!!!!!!!!!!!!!!!!!!!!!!!!!!!!!!!!!!!!!!!!!!!!!!!!!!!!!!!!!!!!!!!!!!!!!!!!!!!!!!!
!
!
!!!!!!!!!!!!!!!!!!!!!!!!!!!!!!!!!!!!!!!!!!!!!!!!!!!!!!!!!!!!!!!!!!!!!!!!!!!!!!!!!!!!!!!!!!!!!!!!!!!!!!!!!!!!!!!!!!!!!!!!!!!!
```

```
! INPUTS: PLEAT GEOMETRY AND INCIDENT ANGLE
        W = 3.75                                        ! INPUT -- INPUT A VALUE
        S = 3.00                                        ! INPUT -- INPUT A VALUE -- NOTE THAT S CAN'T BE > 2*W
        OMEGA_H_DEG = 0.00      ! INPUT -- INPUT A VALUE -- LIMIT OMEGA_H_DEG FROM -89.99 TO +89.99 BY
                                ! SYMMETRY, OPTICAL PROPERTIES ARE THE SAME AT +/- ANGLE


! INPUTS: FABRIC PROPERTIES (M_TAU_F_BT0, M_TAU_F_BD0, M_RHO_F_BD0 ARE RESULTS OF CARY 5000
! MEASUREMENTS)
M_TAU_F_BT0 = 0.4717                    ! INPUT -- INPUT A VALUE
M_TAU_F_BD0 = 0.3879                    ! INPUT -- INPUT A VALUE
M_RHO_F_BD0 = 0.4173                    ! INPUT -- INPUT A VALUE

! TAU_BT = TAU_BB + TAU_BD
M_TAU_F_BB0 = M_TAU_F_BT0 - M_TAU_F_BD0

! EQUATION 4.1/4.2 AND 4.3/4.4
M_RHO_F_BB0 = 0.00              ! ASSUMED TO BE 0 - SEE CHAPTER OF NATHAN'S THESIS (EQUATION 4.1 AND 4.2)
M_RHO_F_BT0 = M_RHO_F_BD0 + M_RHO_F_BB0
                                ! M_RHO_F_BT0 = M_RHO_F_BD0 SINCE M_RHO_F_BB0 = 0
RHO_Y = MAX ( 0.00001, M_RHO_F_BT0 / MAX ( 0.00001, 1.0 - M_TAU_F_BB0 ) )
                                ! EQUATION 4.3/4.4 WITH MINIMUM YAR REFLECTANCE = 0.00001

! ASSUME FRONT AND BACK FABRIC PROPERTIES ARE THE SAME UNLESS FRONT AND BACK SURFACES OF A FABRIC
! ARE DIFFERENT
M_TAU_B_BB0 = M_TAU_F_BB0
M_TAU_B_BT0 = M_TAU_F_BT0
M_TAU_B_BD0 = M_TAU_F_BD0
M_RHO_B_BB0 = M_RHO_F_BB0
M_RHO_B_BT0 = M_RHO_F_BT0
M_RHO_B_BD0 = M_RHO_F_BD0

! CHECK FOR CORRECT INPUT RANGE: S MUST BE < 2W
IF      ( W < S / 2.0 ) THEN
        WRITE (*,*) 'INPUT ERROR: S SHOULD BE > 2W'
        STOP
ELSE IF ( W < 0.0)  THEN
        WRITE (*,*) 'INPUT ERROR: W SHOULD BE POSITIVE'
        STOP
ELSE IF ( S < 0.0)  THEN
        WRITE (*,*) 'INPUT ERROR: S SHOULD BE POSITIVE'
        STOP
END IF

! CHECK FOR CORRECT INPUT RANGE: OMEGA_H_DEG SHOULD BE WITHIN +90 TO -90 DEGREES
IF ( OMEGA_H_DEG < -90.0 .OR. OMEGA_H_DEG > 90.0 ) THEN
        WRITE (*,*) 'INPUT ERROR: INCIDENT ANGLE MUST BE WITHIN +- 90 DEGREES'
        STOP
END IF

IF ( M_TAU_F_BT0 < M_TAU_F_BD0 ) THEN
        WRITE (*,*) 'WARNING: INPUT FABRIC PROPERTIES TAU_F_BT0 < TAU_F_BD0'
        WRITE (*,*) 'CHECK FABRIC PROPERTIES MEASUREMENTS AND THEIR DIFFERENCE'
END IF

! FACTOR CONVERTING DEGREE TO RADIAN
D_TO_R = PI / 180.0


DO I = 1, 7

! CONSIDER POSITITVE INCIDENT ANGLE ONLY, LIMIT ANGLE FROM -89.999999 TO 89.999999
! THEN CONVERT TO RADIAN
OMEGA_H_DEG = ABS ( MAX ( -89.99999 , MIN ( 89.99999 , OMEGA_H_DEG ) ) )
OMEGA_H_RAD = OMEGA_H_DEG * D_TO_R

! CALCULATE WORKING TEMPS BASED ON S, W, AND INCIDENT ANGLE. SEE DRAWINGS FOR MORE DETAILS
ALPHA = 2.0 * ASIN ( ( S / 2.0 ) / W )
W_LAYER = W * COS ( ALPHA / 2.0 )
```

```
! NORMAL INCIDENCE (OMEGA_H = 0) AND THE THREE ALPHA_# DETERMINE THE RANGES OF THE THREE CASES
ALPHA_1 = PI / 2.0
ALPHA_2 = ATAN( 1.5 * S / W_LAYER )
ALPHA_3 = ALPHA / 2.0



! PROJECTED SURFACES ON THE PLANE PERPENDICULAR TO INCIDENT RADIATION
S_P = S * COS ( OMEGA_H_RAD )
S1P = ( 1.5 * S - W_LAYER * TAN ( OMEGA_H_RAD ) ) * COS ( OMEGA_H_RAD )
S3P = W * SIN ( ALPHA / 2.0 - OMEGA_H_RAD )
S4P = W * SIN ( ALPHA / 2.0 + OMEGA_H_RAD )

! DETERMINE THE CASE I, II, OR III
IF                    ( OMEGA_H_RAD > ALPHA_2 .AND. OMEGA_H_RAD <= ALPHA_1 ) THEN
        GROUP = 1
        THETA_DW_BK = ABS( PI / 2.0 - OMEGA_H_RAD + ALPHA / 2.0 )
        THETA_UP_FR = ABS( PI / 2.0 - OMEGA_H_RAD - ALPHA / 2.0 )
        !THETA_DW_FR = 0.0
ELSE IF ( OMEGA_H_RAD > ALPHA_3 .AND. OMEGA_H_RAD <= ALPHA_2 ) THEN
        GROUP = 2
        THETA_DW_BK = ABS( PI / 2.0 - OMEGA_H_RAD + ALPHA / 2.0 )
        THETA_UP_FR = ABS( PI / 2.0 - OMEGA_H_RAD - ALPHA / 2.0 )
        !THETA_DW_FR = 0.0
ELSE IF ( OMEGA_H_RAD >= 0.0    .AND. OMEGA_H_RAD <= ALPHA_3 ) THEN
        GROUP = 3
        !THETA_DW_BK = 0.0
        THETA_UP_FR = ABS( PI / 2.0 - OMEGA_H_RAD - ALPHA / 2.0 )
        THETA_DW_FR = ABS( PI / 2.0 + OMEGA_H_RAD - ALPHA / 2.0 )
ELSE
        WRITE (*,*) 'IF YOU SEE THIS MESSAGE, THERE IS SOMETHING WRONG WITH THE CODE'
        STOP
END IF

! (CASE I)   FRONT SIDE OF UP SLOPE SURFACE AND  BACK SIDE OF DOWN SLOPE SURFACE
! (CASE II)  FRONT SIDE OF UP SLOPE SURFACE AND  BACK SIDE OF DOWN SLOPE SURFACE
! (CASE III) FRONT SIDE OF UP SLOPE SURFACE AND FRONT SIDE OF DOWN SLOPE SURFACE
!THETA_DW_BK = ABS( PI / 2.0 - OMEGA_H_RAD + ALPHA / 2.0 )
!THETA_UP_FR = ABS( PI / 2.0 - OMEGA_H_RAD - ALPHA / 2.0 )
!THETA_DW_FR = ABS( PI / 2.0 + OMEGA_H_RAD - ALPHA / 2.0 )


CALL FM_SOL_DIFFUSE             &
            (                   &
            M_RHO_F_BT0 ,       &
            M_TAU_F_BT0 ,       &
            M_TAU_F_BB0 ,       &
            M_RHO_F_DD ,        &
            M_TAU_F_DD          &
            )
CALL FM_SOL_DIFFUSE             &
            (                   &
            M_RHO_B_BT0 ,       &
            M_TAU_B_BT0 ,       &
            M_TAU_B_BB0 ,       &
            M_RHO_B_DD ,        &
            M_TAU_B_DD          &
            )
! SOLVING FOR UP SLOPE FRONT SURFACE FABRIC PROPERTIES
CALL FM_SOL_BEAM                &
          (                     &
          THETA_UP_FR ,         &
          M_RHO_F_BT0 ,         &
          M_TAU_F_BB0 ,         &
          M_TAU_F_BT0 ,         &
          M_RHO_F_BD_UP_FR ,    &
          M_TAU_F_BB_UP_FR ,    &
          M_TAU_F_BD_UP_FR      &
          )
          M_TAU_F_BT_UP_FR = M_TAU_F_BB_UP_FR + M_TAU_F_BD_UP_FR
```

```
! SOLVING FOR DOWN SLOPE FRONT SURFACE FABRIC PROPERTIES
CALL FM_SOL_BEAM                &
          (                     &
          THETA_DW_FR ,         &
          M_RHO_F_BT0 ,         &
          M_TAU_F_BB0 ,         &
          M_TAU_F_BT0 ,         &
          M_RHO_F_BD_DW_FR ,    &
          M_TAU_F_BB_DW_FR ,    &
          M_TAU_F_BD_DW_FR      &
          )
M_TAU_F_BT_DW_FR = M_TAU_F_BB_DW_FR + M_TAU_F_BD_DW_FR
! SOLVING FOR DOWN SLOPE BACK SURFACE FABRIC PROPERTIES
          CALL FM_SOL_BEAM      &
          (                     &
          THETA_DW_BK ,         &
          M_RHO_B_BT0 ,         &
          M_TAU_B_BB0 ,         &
          M_TAU_B_BT0 ,         &
          M_RHO_B_BD_DW_BK ,    &
          M_TAU_B_BB_DW_BK ,    &
          M_TAU_B_BD_DW_BK      &
          )
M_TAU_B_BT_DW_BK = M_TAU_B_BB_DW_BK + M_TAU_B_BD_DW_BK



! THE FOLLOWING SET OF DISTANCES (EACH BETWEEN TWO POINTS) CAN BE USED FOR ALL 3 CASES
! BUT THE VIEW FACTORS HAVE TO BE DEFINED SEPARATELY FOR EACH CASE
AC = S
BD = S
AB = W
BC = W
CD = W
CF = S * SIN ( PI / 2 - OMEGA_H_RAD ) / SIN ( OMEGA_H_RAD + ALPHA / 2 )
BF = W - CF
CG = CF * SIN ( PI - OMEGA_H_RAD - ALPHA / 2 ) / SIN ( OMEGA_H_RAD - ALPHA / 2 )
AE = CG
BE = W - AE
DG = BE
AF = S * SIN ( PI / 2 - ALPHA / 2 ) / SIN ( OMEGA_H_RAD + ALPHA / 2 )
FG = CF * AF / BF
BG = SQRT ( BF**2 + FG**2 - 2 * BF * FG * COS ( OMEGA_H_RAD + ALPHA / 2 ) )
CE = SQRT (  S**2 + AE**2 - 2 *  S * AE * COS (  PI / 2 - ALPHA / 2 ) )
EF = SQRT ( AF**2 + AE**2 - 2 * AF * AE * COS ( OMEGA_H_RAD - ALPHA / 2 ) )
DF = SQRT (  S**2 + BF**2 - 2 *  S * BF * COS (  PI / 2 - ALPHA / 2 ) )
! AH ONLY APPLIES TO CASE 3
AH = W * SIN ( ALPHA / 2 - OMEGA_H_RAD ) / SIN ( PI / 2 + OMEGA_H_RAD )

SELECT CASE (GROUP)
CASE (1)
                    ! DETERMINE TAU_F_BB FOR CASE 1
                    TAU_F_BB = 0.0
                    ! CASE 1 VIEW FACTORS
                    F1B3B = ( ( BC + FG ) - ( CF + BG ) ) / ( 2 * CG )
                    F1B4B = ( ( CF + CG ) - ( FG     ) ) / ( 2 * CG )
                    F2B3B = ( ( BG + DF ) - ( FG + BD ) ) / ( 2 * DG )
                    F2B4B = ( ( FG + CD ) - ( CG + DF ) ) / ( 2 * DG )
                    F3B1B = F1B3B * CG / BF
                    F4B1B = F1B4B * CG / CF
                    F3B2B = F2B3B * DG / BF
                    F4B2B = F2B4B * DG / CF
                    !
                    !F1B7B = 0.0
                    !F2B7B = 0.0
                    !F3B7B = 0.0
                    F4B7B = 0.0
                    F7B4B = 0.0
                    !F1F7F = 0.0
                    !F2F7F = 0.0
```

```
!F3F7F = 0.0
F4F7F = 0.0
F7F4F = 0.0
!
F1F3F = ( ( AB + EF ) - ( AF + BE ) ) / ( 2 * AE )
F1F4F = ( ( AF + CE ) - ( AC + EF ) ) / ( 2 * AE )
F2F3F = ( ( BE + BF ) - ( EF     ) ) / ( 2 * BE )
F2F4F = ( ( BC + EF ) - ( CE + BF ) ) / ( 2 * BE )
F3F1F = F1F3F * AE / BF
F4F1F = F1F4F * AE / CF
F3F2F = F2F3F * BE / BF
F4F2F = F2F4F * BE / CF
!
F5F1F = ( ( AC + AE ) - ( CE     ) ) / ( 2 * AC )
F5F2F = ( ( AB + CE ) - ( AE + BC ) ) / ( 2 * AC )
F5F3F = ( ( BC + AF ) - ( AB + CF ) ) / ( 2 * AC )
F5F4F = ( ( AC + CF ) - ( AF     ) ) / ( 2 * AC )
F5F7F = 0.0
!
F6B1B = ( ( BG + CD ) - ( BC + DG ) ) / ( 2 * BD )
F6B2B = ( ( DG + BD ) - ( BG     ) ) / ( 2 * BD )
F6B3B = ( ( BF + BD ) - ( DF     ) ) / ( 2 * BD )
F6B4B = ( ( BC + DF ) - ( BF + CD ) ) / ( 2 * BD )
F6B7B = 0.0

Z1B_BD = M_TAU_F_BB_UP_FR * M_RHO_B_BD_DW_BK * S / AE
Z4B_BD = M_TAU_F_BD_UP_FR * S / CF
Z7B_BD = 0.0

Z1F_BD = M_TAU_F_BB_UP_FR * M_TAU_B_BD_DW_BK * S / AE
Z4F_BD = M_RHO_F_BD_UP_FR * S / CF
Z7F_BD = 0.0
```

CASE (2)

```
! DETERMINE TAU_F_BB FOR CASE 2
TAU_F_BB = S1P / S_P * M_TAU_F_BB_UP_FR
! CASE 2 VIEW FACTORS
F1B3B = ( ( BC + DF ) - ( CF + BD ) ) / ( 2 * CD )
F1B4B = ( ( CD + CF ) - ( DF     ) ) / ( 2 * CD )
F2B3B = 0.0
F2B4B = 0.0
F3B1B = F1B3B * CD / BF
F4B1B = F1B4B * CD / CF
F3B2B = 0.0
F4B2B = 0.0
!F1B7B = 0.0
!F2B7B = 0.0
!F3B7B = 0.0
F4B7B = 0.0
F7B4B = 0.0
F1F3F = ( ( AB + BF ) - ( AF     ) ) / ( 2 * AB )
F1F4F = ( ( AF + BC ) - ( AC + BF ) ) / ( 2 * AB )
F2F3F = 0.0
F2F4F = 0.0
F3F1F = F1F3F * AB / BF
F4F1F = F1F4F * AB / CF
F3F2F = 0.0
F4F2F = 0.0
!F1F7F = 0.0
!F2F7F = 0.0
!F3F7F = 0.0
F4F7F = 0.0
F7F4F = 0.0

F5F1F = ( ( AB + AC ) - ( BC     ) ) / ( 2 * AC )
F5F2F = 0.0
F5F3F = ( ( BC + AF ) - ( AB + CF ) ) / ( 2 * AC )
F5F4F = ( ( AC + CF ) - ( AF     ) ) / ( 2 * AC )
F5F7F = 0.0
```

```
                F6B1B = ( ( BD + CD ) - ( BC     ) ) / ( 2 * BD )
                F6B2B = 0.0
                F6B3B = ( ( BF + BD ) - ( DF     ) ) / ( 2 * BD )
                F6B4B = ( ( BC + DF ) - ( BF + CD ) ) / ( 2 * BD )
                F6B7B = 0.0

                Z1B_BD = M_TAU_F_BB_UP_FR * M_RHO_B_BD_DW_BK * S / AE
                Z4B_BD = M_TAU_F_BD_UP_FR * S / CF
                Z7B_BD = 0.0

                Z1F_BD = M_TAU_F_BB_UP_FR * M_TAU_B_BD_DW_BK * S / AE
                Z4F_BD = M_RHO_F_BD_UP_FR * S / CF
                Z7F_BD = 0.0

CASE (3)
                ! DETERMINE TAU_F_BB FOR CASE 3
                TAU_F_BB = ( S3P * M_TAU_F_BB_DW_FR + S4P * M_TAU_F_BB_UP_FR ) / S_P
                ! CASE 3 VIEW FACTORS
                F1B3B = 0.0
                F1B4B = 0.0
                F2B3B = 0.0
                F2B4B = 0.0
                F3B1B = 0.0
                F4B1B = 0.0
                F3B2B = 0.0
                F4B2B = 0.0
                !F1B7B = 0.0
                !F2B7B = 0.0
                !F3B7B = 0.0
                F4B7B = ( BC + CD - BD ) / ( 2 * CD )
                F7B4B = F4B7B
                F1F3F = 0.0
                F1F4F = 0.0
                F2F3F = 0.0
                F2F4F = 0.0
                F3F1F = 0.0
                F4F1F = 0.0
                F3F2F = 0.0
                F4F2F = 0.0
                !F1F7F = 0.0
                !F2F7F = 0.0
                !F3F7F = 0.0
                F4F7F = F4B7B
                F7F4F = F4B7B

                F5F1F = 0.0
                F5F2F = 0.0
                F5F3F = 0.0
                F5F4F = ( ( AC + BC ) - ( AB     ) ) / ( 2 * AC )
                F5F7F = F5F4F

                F6B1B = 0.0
                F6B2B = 0.0
                F6B3B = 0.0
                F6B4B = F5F4F
                F6B7B = F5F4F

                Z1B_BD = 0.0
                Z4B_BD = M_TAU_F_BD_UP_FR * S / CF
                Z7B_BD = M_TAU_F_BD_DW_FR * AH / W

                Z1F_BD = 0.0
                Z4F_BD = M_RHO_F_BD_UP_FR * S / CF
                Z7F_BD = M_RHO_F_BD_DW_FR * AH / W

END SELECT

A      = 0.0                    ! INITIALIZE RADIOSITY MATRIX COEFFICIENTS
XSOL   = 0.0                    ! INITIALIZE SOLUTION VECTOR COEFFICIENTS
```

```
A(1,1)  = -1.0
A(1,2)  = 0.0
A(1,3)  = M_RHO_B_DD * F1B3B
A(1,4)  = M_RHO_B_DD * F1B4B
A(1,5)  = 0.0
A(1,6)  = 0.0
A(1,7)  = 0.0
A(1,8)  = 0.0
A(1,9)  = M_TAU_F_DD * F1F3F
A(1,10) = M_TAU_F_DD * F1F4F
A(1,11) = 0.0
A(1,12) = 0.0
A(1,13) = -Z1B_BD
A(2,1)  = 0.0
A(2,2)  = -1.0
A(2,3)  = M_RHO_B_DD * F2B3B
A(2,4)  = M_RHO_B_DD * F2B4B
A(2,5)  = 0.0
A(2,6)  = 0.0
A(2,7)  = 0.0
A(2,8)  = 0.0
A(2,9)  = M_TAU_F_DD * F2F3F
A(2,10) = M_TAU_F_DD * F2F4F
A(2,11) = 0.0
A(2,12) = 0.0
A(2,13) = 0.0
A(3,1)  = M_RHO_B_DD * F3B1B
A(3,2)  = M_RHO_B_DD * F3B2B
A(3,3)  = -1.0
A(3,4)  = 0.0
A(3,5)  = 0.0
A(3,6)  = 0.0
A(3,7)  = M_TAU_F_DD * F3F1F
A(3,8)  = M_TAU_F_DD * F3F2F
A(3,9)  = 0.0
A(3,10) = 0.0
A(3,11) = 0.0
A(3,12) = 0.0
A(3,13) = 0.0
A(4,1)  = M_RHO_B_DD * F4B1B
A(4,2)  = M_RHO_B_DD * F4B2B
A(4,3)  = 0.0
A(4,4)  = -1.0
A(4,5)  = 0.0
A(4,6)  = M_RHO_B_DD * F4B7B
A(4,7)  = M_TAU_F_DD * F4F1F
A(4,8)  = M_TAU_F_DD * F4F2F
A(4,9)  = 0.0
A(4,10) = 0.0
A(4,11) = 0.0
A(4,12) = M_TAU_F_DD * F4F7F
A(4,13) = -Z4B_BD
A(5,1)  = 0.0
A(5,2)  = 0.0
A(5,3)  = 0.0
A(5,4)  = 0.0
A(5,5)  = -1.0
A(5,6)  = 0.0
A(5,7)  = 0.0
A(5,8)  = 0.0
A(5,9)  = 0.0
A(5,10) = 0.0
A(5,11) = 0.0
A(5,12) = 0.0
A(5,13) = 0.0
A(6,1)  = 0.0
A(6,2)  = 0.0
A(6,3)  = 0.0
A(6,4)  = M_RHO_B_DD * F7B4B
A(6,5)  = 0.0
```

```
A(6,6)  = -1.0
A(6,7)  = 0.0
A(6,8)  = 0.0
A(6,9)  = 0.0
A(6,10) = M_TAU_F_DD * F7F4F
A(6,11) = 0.0
A(6,12) = 0.0
A(6,13) = -Z7B_BD
A(7,1)  = 0.0
A(7,2)  = 0.0
A(7,3)  = M_TAU_B_DD * F1B3B
A(7,4)  = M_TAU_B_DD * F1B4B
A(7,5)  = 0.0
A(7,6)  = 0.0
A(7,7)  = -1.0
A(7,8)  = 0.0
A(7,9)  = M_RHO_F_DD * F1F3F
A(7,10) = M_RHO_F_DD * F1F4F
A(7,11) = 0.0
A(7,12) = 0.0
A(7,13) = -Z1F_BD
A(8,1)  = 0.0
A(8,2)  = 0.0
A(8,3)  = M_TAU_B_DD * F2B3B
A(8,4)  = M_TAU_B_DD * F2B4B
A(8,5)  = 0.0
A(8,6)  = 0.0
A(8,7)  = 0.0
A(8,8)  = -1.0
A(8,9)  = M_RHO_F_DD * F2F3F
A(8,10) = M_RHO_F_DD * F2F4F
A(8,11) = 0.0
A(8,12) = 0.0
A(8,13) = 0.0
A(9,1)  = M_TAU_B_DD * F3B1B
A(9,2)  = M_TAU_B_DD * F3B2B
A(9,3)  = 0.0
A(9,4)  = 0.0
A(9,5)  = 0.0
A(9,6)  = 0.0
A(9,7)  = M_RHO_F_DD * F3F1F
A(9,8)  = M_RHO_F_DD * F3F2F
A(9,9)  = -1.0
A(9,10) = 0.0
A(9,11) = 0.0
A(9,12) = 0.0
A(9,13) = 0.0
A(10,1) = M_TAU_B_DD * F4B1B
A(10,2) = M_TAU_B_DD * F4B2B
A(10,3) = 0.0
A(10,4) = 0.0
A(10,5) = 0.0
A(10,6) = M_TAU_B_DD * F4B7B
A(10,7) = M_RHO_F_DD * F4F1F
A(10,8) = M_RHO_F_DD * F4F2F
A(10,9) = 0.0
A(10,10) = -1.0
A(10,11) = 0.0
A(10,12) = M_RHO_F_DD * F4F7F
A(10,13) = -Z4F_BD
A(11,1) = 0.0
A(11,2) = 0.0
A(11,3) = 0.0
A(11,4) = 0.0
A(11,5) = 0.0
A(11,6) = 0.0
A(11,7) = 0.0
A(11,8) = 0.0
A(11,9) = 0.0
A(11,10) = 0.0
```

```
            A(11,11) = -1.0
            A(11,12) = 0.0
            A(11,13) = 0.0
            A(12,1) = 0.0
            A(12,2) = 0.0
            A(12,3) = 0.0
            A(12,4) = M_TAU_B_DD * F7B4B
            A(12,5) = 0.0
            A(12,6) = 0.0
            A(12,7) = 0.0
            A(12,8) = 0.0
            A(12,9) = 0.0
            A(12,10) = M_RHO_F_DD * F7F4F
            A(12,11) = 0.0
            A(12,12) = -1.0
            A(12,13) = -Z7F_BD

   CALL SOLMATS ( N , A , XSOL )

            J1B = XSOL(1)
            J2B = XSOL(2)
            J3B = XSOL(3)
            J4B = XSOL(4)
            J6B = XSOL(5)
            J7B = XSOL(6)
            J1F = XSOL(7)
            J2F = XSOL(8)
            J3F = XSOL(9)
            J4F = XSOL(10)
            J5F = XSOL(11)
            J7F = XSOL(12)

            G5F = F5F1F * J1F + F5F2F * J2F + F5F3F * J3F + F5F4F * J4F + F5F7F * J7F
            G6B = F6B1B * J1B + F6B2B * J2B + F6B3B * J3B + F6B4B * J4B + F6B7B * J7B

            TAU_F_BD = G6B
            RHO_F_BD = G5F
            TAU_F_BT = TAU_F_BD + TAU_F_BB


   WRITE (*,*) 'INCIDENT ANGLE = ' , OMEGA_H_DEG
   WRITE (*,*) 'GROUP = '  , GROUP
   WRITE (*,*) 'TAU_BT = ' , TAU_F_BT
   WRITE (*,*) 'TAU_BD = ' , TAU_F_BD
   WRITE (*,*) 'RHO_BD = ' , RHO_F_BD

   OMEGA_H_DEG = OMEGA_H_DEG + 10.00

   END DO

   CONTAINS

!*****************************************************************************************************************************
!           SUBROUTINE: FM_SOL_DIFFUSE
!
!           PURPOSE: CALCULATES THE DIFFUSE-DIFFUSE SOLAR OPTICAL PROPERTIES OF A FABRIC BY INTEGRATING
!         THE CORRESPONDING PROPERTIES OVER THE HEMISPHERE USING ROMBERG'S INTEGRATION
!*****************************************************************************************************************************
!
!                       INPUT:
!           TAUFF_BB_NORM = FORWARD FACING FABRIC BEAM-BEAM  TRANSMITTANCE AT NORMAL INCIDENCE
!           TAUFF_BT_NORM = FORWARD FACING FABRIC BEAM-TOTAL TRANSMITTANCE AT NORMAL INCIDENCE
!                                   (TAUFF_BT_NORM = TAUFF_BB_NORM + TAUFF_BD_NORM)
!           RHOFF_BT_NORM = FORWARD-FACING FABRIC BEAM-TOTAL REFLECTANCE   AT NORMAL INCIDENCE
!
!                       INTERMEDIATE VARIABLES:
!           IMAX      = 2**N - 1
!           JMAX      = NUMBER OF COLUMNS IN TABLEAU
!           NXMJP2    = NMAX - J + 2
!           I                   = INDEX ON REPEATED SUM
```

```
!           J                       = COLUMN SUBSCRIPT FOR  TABLEAUS
!           N                       = ROW SUBSCRIPT FOR TABLEAUS
!           NMAX    = MAXIMUM VALUE OF N
!           MMAX    = MAXIMUM VALUE OF M
!           PROP    = A FLAG THAT SELECTS THE APPROPRIATE FABRIC SOLAR OPTICAL PROPERTY TO BE INTEGRATED
!           T                       = MATRIX CONTAINING ROMBERG'S TABLEAU
!           F                       = THE INTEGRAND FUNCTION
!           H                       = B - A
!           FR                      = ( B - A ) / 2**N
!           FORJM1  = 4**( J - 1 )
!           THETA_RAD                       = ANGLE OF INCIDENCE IN RADIANS (VARIES FROM 0 RADIANS TO PI/2 RADIANS)
!           TAUFF_BD_NORM  = FORWARD FACING FABRIC BEAM-DIFFUSE TRANSMITTANCE AT NORMAL INCIDENCE
!
!                   OUTPUT:
!           RHOFF_DD = FORWARD-FACING FABRIC SURFACE REFLECTANCE FOR INCIDENT DIFFUSE RADIATION
!           TAUFF_DD = FORWARD FACING FABRIC SURFACE TRANSMITTANCE FOR INCIDENT DIFFUSE RADIATION
!*****************************************************************************************************************
   SUBROUTINE FM_SOL_DIFFUSE ( RHOFF_BT_NORM , TAUFF_BT_NORM , TAUFF_BB_NORM , RHOFF_DD , TAUFF_DD )

           IMPLICIT NONE

           REAL :: TAUFF_BB_NORM
           REAL :: TAUFF_BT_NORM
           REAL :: RHOFF_BT_NORM

           REAL :: RHOFF_DD
           REAL :: TAUFF_DD

           INTEGER :: IMAX
           INTEGER :: JMAX
           INTEGER :: NXMJP2
           INTEGER :: I
           INTEGER :: J
           INTEGER :: N
           INTEGER :: NMAX
           INTEGER :: MMAX
           INTEGER :: PROP
           REAL, DIMENSION ( 10 , 10 , 2 ) :: T
           !REAL :: F
           REAL :: H
           REAL :: FR
           REAL :: FORJM1
           REAL :: THETA_RAD
           REAL :: TAUFF_BD_NORM

           REAL :: PI
           REAL :: THETA_RAD_A
           REAL :: THETA_RAD_B

           PI = 3.14159265358979
           THETA_RAD_A =  0.000001 * PI / 180.0
           THETA_RAD_B = 89.999999 * PI / 180.0

           TAUFF_BD_NORM = TAUFF_BT_NORM - TAUFF_BB_NORM

           MMAX = 4
           NMAX = 5
           JMAX = 6 ! Why did Nathan use JMAX = 4?

           DO PROP = 1 , 2 , 1             ! 1 FOR RHO AND 2 FOR TAU

                   ! COMPUTE H AND FIRST INTEGRAL APPROXIMATION
                   H = THETA_RAD_B - THETA_RAD_A
                   T ( 1 , 1 , PROP ) =                                                                    &
                     (                                                                                     &
                     F ( THETA_RAD_A , RHOFF_BT_NORM , TAUFF_BB_NORM , TAUFF_BT_NORM , PROP ) +            &
                     F ( THETA_RAD_B , RHOFF_BT_NORM , TAUFF_BB_NORM , TAUFF_BT_NORM , PROP )              &
                     ) * H / 2.0

                   ! HALVE INTERVAL REPEATEDLY, COMPUTE T(N+1,1)
```

```
                DO N = 1 , NMAX
                        T ( N + 1 , 1 , PROP ) = 0.0
                        FR = H / 2.0**N
                        IMAX = 2**N - 1
                        DO I = 1 , IMAX , 2
                                !WRITE (*,*) FLOAT (I) * FR + THETA_RAD_A
                                T ( N + 1 , 1 , PROP ) =                        &
                                        T ( N + 1 , 1 , PROP ) +                &
                                        F                                       &
                                        (                                       &
                                        FLOAT(I) * FR + THETA_RAD_A ,           &
                                        RHOFF_BT_NORM ,                         &
                                        TAUFF_BB_NORM ,                         &
                                        TAUFF_BT_NORM ,                         &
                                        PROP                                    &
                                        )
                                        ! NOTE: WHEN THE LINE IS TOO LONG, THE CODE WON'T WORK
                        END DO
                        T ( N + 1 , 1 , PROP ) = T ( N , 1 , PROP ) / 2.0 + H * T ( N + 1 , 1 , PROP ) / 2.0**N
                END DO

                ! COMPUTE ROMBERG TABLEAU
                DO J = 2 , JMAX
                        NXMJP2 = NMAX - J + 2
                        FORJM1 = 4.0**( J - 1 )
                        DO N = 1 , NXMJP2
                           T ( N , J , PROP ) = ( FORJM1 * T ( N + 1 , J - 1 , PROP ) - T ( N , J - 1 , PROP ) ) / ( FORJM1 - 1.0 )
                        END DO
                END DO

                IF ( PROP == 1 ) THEN
                        RHOFF_DD = T ( 1 , 6 , PROP )
                ELSE IF ( PROP == 2 ) THEN
                        TAUFF_DD = T ( 1 , 6 , PROP )
                ELSE
                        WRITE (*,*) 'ERROR: CHECK THE CODE'
                END IF

        END DO

  END SUBROUTINE FM_SOL_DIFFUSE

!*****************************************************************************************************************************
!       FUNCTION: F
!
!       PURPOSE: CALCULATES THE INTEGRAND FUNCTION TO BE USED IN THE ROMBERG INTEGRATION
!*****************************************************************************************************************************
!
!               INPUT:
!       THETA_RAD       = ANGLE OF INCIDENCE IN RADIANS (VARIES FROM 0 RADIANS TO PI/2 RADIANS)
!       TAUFF_BB_NORM   = FABRIC BEAM-BEAM TRANSMITTANCE AT NORMAL INCIDENCE
!       TAUFF_BT_NORM   = FORWARD-FACING FABRIC BEAM-TOTAL TRANSMITTANCE AT NORMAL INCIDENCE
!                               (TAUFF_BT_NORM = TAU_BB_NORM + TAUFF_BD_NORM)
!       RHOFF_BT_NORM   = FORWARD-FACING FABRIC BEAM-TOTAL REFLECTANCE   AT NORMAL INCIDENCE
!       PROP            = A FLAG THAT SELECTS THE APPROPRIATE FABRIC SOLAR OPTICAL PROPERTY TO BE
!                               INTEGRATED
!
!       INTERMEDIATE VARIABLES:
!       RHOFF_BD                = BEAM-TO-DIFFUSE REFLECTANCE   OF THE FABRIC (FRONT SURFACE)
!       TAUFF_BB                = BEAM-TO-BEAM    TRANSMITTANCE OF THE FABRIC (FRONT SURFACE)
!       TAUFF_BD                = BEAM-TO-DIFFUSE TRANSMITTANCE OF THE FABRIC (FRONT SURFACE)
!*****************************************************************************************************************************
  REAL FUNCTION F ( THETA_RAD , RHOFF_BT_NORM , TAUFF_BB_NORM , TAUFF_BT_NORM , PROP )

        IMPLICIT NONE

        REAL :: THETA_RAD
        REAL :: RHOFF_BT_NORM
        REAL :: TAUFF_BB_NORM
        REAL :: TAUFF_BT_NORM
```

```
        INTEGER :: PROP
        REAL :: RHOFF_BD
        REAL :: TAUFF_BB
        REAL :: TAUFF_BD
        !WRITE (*,*) THETA_RAD


        CALL FM_SOL_BEAM        &
            (                   &
            THETA_RAD ,         &
            RHOFF_BT_NORM ,     &
            TAUFF_BB_NORM ,     &
            TAUFF_BT_NORM ,     &
            RHOFF_BD ,          &
            TAUFF_BB ,          &
            TAUFF_BD            &
            )

        IF ( PROP == 1 ) THEN
                !F =                ( COS ( THETA_RAD ) ) * ( RHOFF_BD )
                F = 2.0 * ( SIN ( THETA_RAD ) ) * ( COS ( THETA_RAD ) ) * ( RHOFF_BD )
                !CHECK THE ORIGINAL CODE (CFSShadeMod.f90) DOES NOT HAVE THE SIN PART HERE
        ELSE IF ( PROP == 2 ) THEN
                !F =                ( COS ( THETA_RAD ) ) * ( TAUFF_BB + TAUFF_BD )
                F = 2.0 * ( SIN ( THETA_RAD ) ) * ( COS ( THETA_RAD ) ) * ( TAUFF_BB + TAUFF_BD )
        ELSE
                WRITE (*,*) 'ERROR'
        END IF

  END FUNCTION F

!*****************************************************************************************************************************
!       SUBROUTINE: FM_SOL_BEAM
!
!       PURPOSE: CALCULATES THE SOLAR OPTICAL PROPERTIES OF A FABRIC FOR BEAM RADIATION INCIDENT ON
!       THE FORWARD FACING SURFACE
!       USING OPTICAL PROPERTIES AT NORMAL INCIDENCE  USING SEMI-EMPIRICAL RELATIONS.
!       IF YOU WANT THE SOLAR OPTICAL PROPERTIES FOR THE BACKWARD FACING SURFACE, CALL THE SUBROUTINE
!       AGAIN AND SUPPY IT
!       WITH THE CORRESPONDING BACKWARD FACING SURFACE OPTICAL PROPERTIES      AT NORMAL INCIDENCE.
!*****************************************************************************************************************************
!
!               INPUT:
!       THETA_RAD = ANGLE OF INCIDENCE IN RADIANS (VARIES FROM 0 RADIANS TO PI/2 RADIANS)
!       TAUFF_BB_NORM = FORWARD-FACING FABRIC BEAM-BEAM  TRANSMITTANCE AT NORMAL INCIDENCE
!       TAUFF_BT_NORM = FORWARD FACING FABRIC BEAM-TOTAL TRANSMITTANCE AT NORMAL INCIDENCE
!       (TAUFF_BT_NORM = TAU_BB_NORM + TAUFF_BD_NORM)
!       RHOFF_BT_NORM = FORWARD-FACING FABRIC BEAM-TOTAL REFLECTANCE   AT NORMAL INCIDENCE
!
!               INTERMEDIATE VARIABLES:
!       THETA = DUMMY VARIABLE
!       RHOFF_BT_90DEG = FORWARD-FACING FABRIC BEAM-TOTAL REFLECTANCE   AT 90 DEGREES INCIDENCE
!       TAUFF_BT_90DEG = FORWARD-FACING FABRIC BEAM-TOTAL TRANSMITTANCE AT 90 DEGREES INCIDENCE
!       RHOFF_BT_EXPO = EXPONENT IN THE FABRIC OFF-NORMAL BEAM-TOTAL REFLECTANCE   MODEL (FRONT SIDE)
!       TAUFF_BB_EXPO = EXPONENT IN THE FABRIC OFF-NORMAL BEAM-BEAM  TRANSMITTANCE MODEL
!       TAUFF_BT_EXPO = EXPONENT IN THE FABRIC OFF-NORMAL BEAM-TOTAL TRANSMITTANCE MODEL (FRONT
!       SIDE)
!       TAUFF_BD_NORM = FORWARD FACING FABRIC BEAM-DIFFUSE TRANSMITTANCE AT NORMAL INCIDENCE
!       TAUFF_BT = BEAM-TO-TOTAL TRANSMITTANCE OF THE FABRIC (FRONT SURFACE)
!
!               OUTPUT:
!       RHOFF_BD = BEAM-TO-DIFFUSE REFLECTANCE   OF THE FABRIC (FRONT SURFACE)
!       TAUFF_BB = BEAM-TO-BEAM    TRANSMITTANCE OF THE FABRIC (FRONT SURFACE)
!       TAUFF_BD = BEAM-TO-DIFFUSE TRANSMITTANCE OF THE FABRIC (FRONT SURFACE)
!*****************************************************************************************************************************
  SUBROUTINE FM_SOL_BEAM ( THETA_RAD , RHOFF_BT_NORM , TAUFF_BB_NORM , TAUFF_BT_NORM , RHOFF_BD ,
TAUFF_BB , TAUFF_BD )

        IMPLICIT NONE
```

```
      REAL, INTENT (IN) :: THETA_RAD
      REAL, INTENT (IN) :: TAUFF_BB_NORM
      REAL, INTENT (IN) :: TAUFF_BT_NORM
      REAL, INTENT (IN) :: RHOFF_BT_NORM
      REAL, INTENT (OUT) :: RHOFF_BD
      REAL, INTENT (OUT) :: TAUFF_BB
      REAL, INTENT (OUT) :: TAUFF_BD
      REAL :: TAUFF_BT_90DEG
      REAL :: RHOFF_BT_90DEG
      REAL :: TAUFF_BD_NORM
      REAL :: RHOFF_BT_EXPO
      REAL :: TAUFF_BB_EXPO
      REAL :: TAUFF_BT_EXPO
      REAL :: TAUFF_BT
      REAL :: THETA
      REAL :: RHO_YARN
      REAL, PARAMETER :: PI = 3.14159265359

      TAUFF_BD_NORM = TAUFF_BT_NORM - TAUFF_BB_NORM

      RHO_YARN = ( RHOFF_BT_NORM ) / ( 1.0 - TAUFF_BB_NORM )

      RHOFF_BT_90DEG = RHOFF_BT_NORM + ( 1.0 - RHOFF_BT_NORM ) * ( 0.7 * RHO_YARN**0.7 )

      RHOFF_BT_EXPO = 0.6

      TAUFF_BB_EXPO = MAX ( -0.5 * ( LOG ( MAX ( TAUFF_BB_NORM , 0.01 ) ) ) , 0.35 )  ! why 0.001 was used instead of 0.01

      TAUFF_BT_EXPO = MAX ( -0.5 * ( LOG ( MAX ( TAUFF_BT_NORM , 0.01 ) ) ) , 0.35 )  ! why 0.001 was used instead of 0.01

      IF ( THETA_RAD > 90.01 * PI / 180.0 .OR. THETA_RAD < -90.01 * PI / 180.0 ) THEN
            !WRITE (*,*) THETA_RAD
            WRITE (*,*) 'ERROR: CHECK CODE AND INPUT INCIDENT ANGLEAAAAAAAAAA'
      ELSE IF ( THETA_RAD >  89.99 * PI / 180.0 ) THEN    ! FOR INCIDENT ANGLE =  90 DEGREE, MAKE IT =  89.99 DEGREE
            THETA =  89.99 * PI / 180.0
      ELSE IF ( THETA_RAD < -89.99 * PI / 180.0 ) THEN    ! FOR INCIDENT ANGLE = -90 DEGREE, MAKE IT = -89.99 DEGREE
            THETA = -89.99 * PI / 180.0
      ELSE
            THETA = THETA_RAD                           ! USUAL ACTION
      END IF
            THETA = ABS ( THETA )         ! BY SYMMETRY, OPTICAL PROPERTIES CALCULATES FOR POSITIVE
                                          !INCIDENCE ANGLES ARE THE SAME FOR CORRESPONDING
                                          ! PROPERTIES AT NEGATIVE INCIDENCE ANGLES

      !CALCULATE BEAM-DIFFUSE REFLECTANCE OF FABRIC
      RHOFF_BD = RHOFF_BT_NORM + ( RHOFF_BT_90DEG - RHOFF_BT_NORM ) * ( 1.0 - ( COS              &
      ( THETA ) )**RHOFF_BT_EXPO )
      IF( RHOFF_BD < 0.0 ) RHOFF_BD = 0.0

      !CALCULATE BEAM-BEAM TRANSMITTANCE OF FABRIC
      TAUFF_BB = TAUFF_BB_NORM * ( ( COS ( THETA ) )**TAUFF_BB_EXPO )
      IF ( TAUFF_BB < 0.0 ) TAUFF_BB = 0.0

      !CALCULATE BEAM-TOTAL TRANSMITTANCE OF FABRIC
      TAUFF_BT = TAUFF_BT_NORM * ( ( COS ( THETA ) )**TAUFF_BT_EXPO )
      IF ( TAUFF_BT < 0.0 ) TAUFF_BT = 0.0

      !CALCULATE BEAM-DIFFUSE TRANSMITTANCE
      TAUFF_BD = TAUFF_BT - TAUFF_BB
      IF ( TAUFF_BD < 0.0 ) TAUFF_BD = 0.0

   END SUBROUTINE FM_SOL_BEAM

!*****************************************************************************************************************
!  SUBROUTINE USED TO SOLVE MATRIX BY THE ELIMINATION METHOD SUPPLEMENTED BY A SEARCH FOR THE LARGEST
!  PIVOTAL ELEMENT AT EACH STAGE
!                                                                    SINGLE PRECISION VERSION
!*****************************************************************************************************************
   SUBROUTINE SOLMATS( N , A , XSOL )
```

```
        IMPLICIT NONE

        INTEGER N                                       ! NO. OF ACTIVE ROWS IN A
        REAL A(:,:) , XSOL(:)           ! MINIMUM REQUIRED DIMENSIONS: A ( N , N + 2 ), XSOL ( N )
        REAL CMAX , TEMP , C , Y , D
        INTEGER NM1 , NP1 , NP2 , I , J , L , LP , NOS , NI , NJ

        NM1 = N - 1
        NP1 = N + 1
        NP2 = N + 2

        DO I = 1 , N
                A ( I , NP2 ) = 0.0
                ! DO 1 J=1,NP1          ! TODO ?
        END DO

        DO I = 1 , N
                DO J = 1 , NP1
                        A ( I , NP2 ) = A ( I , NP2 ) + A ( I , J )
                END DO
        END DO

        DO L = 1 , N - 1
                CMAX = A ( L , L )
                LP = L + 1
                NOS = L

                DO I = LP , N
                        IF ( ABS ( CMAX ) .LT. ABS ( A ( I , L ) ) ) THEN
                                CMAX = A ( I , L )
                                NOS = I
                        END IF
                END DO

                !    Swap rows
                IF ( NOS .NE. L ) THEN
                        DO J = 1 , NP2
                                TEMP = A ( L , J )
                                A ( L , J ) = A ( NOS , J )
                                A ( NOS , J ) = TEMP
                        END DO
                END IF

                DO I = LP , N
                        C = 0.0
                        Y = -A ( I , L ) / A ( L , L )
                        DO J = L , NP2
                                A ( I , J ) = A ( I , J ) + Y * A ( L , J )
                        END DO
                        DO J = L , NP1
                                C = C + A ( I , J )
                        END DO
                END DO
        END DO

        !  NOW BACKSUBSTITUTE
        XSOL ( N ) = A ( N , NP1 ) / A ( N , N )
        DO I = 1 , NM1
                NI = N - I
                D = 0.0
                DO J = 1 , I
                        NJ = N + 1 - J
                        D = D + A ( NI , NJ ) * XSOL ( NJ )
                END DO
                XSOL ( NI ) = ( A ( NI , NP1 ) - D ) / A ( NI , NI )
        END DO
    END SUBROUTINE SOLMATS

END PROGRAM TRIANGULAR_MODEL
```

Appendix E: Uncertainty Analysis

0^{th} Order Uncertainty

The photodetector has an uncertainty of ±1% of Full Scale (FS) Reading (Halder 2007). The gain accuracy of the PLA is ±1% of actual reading (as specified in datasheet). For the DAQ, the absolute accuracy is provided in the Accuracy Table. Based on the datasheet, the uncertainty of DAQ ranges from ±0.02% for the highest voltage range to ±0.04% for the lowest voltage range. Any uncertainty in this range is extremely small compared to those of detector and PLA. As a result, it is safe to ignore the DAQ uncertainty.

Therefore, the uncertainty in the voltage reading can be estimated as:

$$\frac{\delta V_S}{V_S} = \frac{\delta V_R}{V_R} = \pm\sqrt{\left(\frac{\delta V_{PD}}{V_{FS}}\right)^2 + \left(\frac{\delta V_{PLA}}{V_{PLA}}\right)^2}$$

Note that V_{FS} = Full Scale Voltage. And if the detector signal is not at full scale, the uncertainty should then be estimated as:

$$\frac{\delta V_S}{V_S} = \frac{\delta V_R}{V_R} = \pm\sqrt{\left(\frac{\delta V_{PD}}{V_{FS}} \times \frac{V_{FS}}{V_{PD}}\right)^2 + \left(\frac{\delta V_{PLA}}{V_{PLA}}\right)^2}$$

Then,

$$\frac{\delta \tau}{\tau} = \pm\sqrt{\left(\frac{\delta V_S}{V_S}\right)^2 + \left(\frac{\delta V_R}{V_R}\right)^2}$$

For $\delta V_{PD}/V_{FS} = \pm 1\%$ and $\delta V_{PLA}/V_{PLA} = \pm 1\%$, Table A.3 below lists the calculated $\delta V/V$ vs V_{FS}/V_{PD} and the resulting $\delta\tau/\tau$.

Table A.3: Zeroth order uncertainty in spectral transmittance for various relative detector signal strength

V_{FS}/V_{PD}	$\delta V/V$	$\delta\tau/\tau$
1	±1.4%	±2.0%
2	±2.2%	±3.2%
5	±5.1%	±7.2%
10	±10%	±14.2%

In general, $\delta V_S/V_S$ is greater than $\delta V_R/V_R$ because V_S has to be smaller than V_R for a given transmittance measurement. For example, assume $\tau(\lambda) = 0.5$, then V_S is half of V_R. This implies that, assuming V_R is at full scale, $\delta\tau/\tau$ can be be calculated as $\delta\tau/\tau = (0.014^2+0.022^2)^{0.5} = \pm 2.6\%$. In other words, the lower the spectral transmittance of a sample, the higher the uncertainty in its transmittance measurements. Table A.4 shows the resulting uncertainty in measured spectral transmittance for various transmittance assuming the reference signal is at full scale.

Table A.4: Zeroth order uncertainty in spectral transmittance for various transmittance

$\tau(\lambda)$	$\delta V_R/V_R$	$\delta V_S/V_S$	$\delta\tau/\tau$
1.0	±1.4%	±1.4%	±2.0%
0.5	±1.4%	±2.2%	±2.6%
0.2	±1.4%	±5.1%	±5.3%
0.1	±1.4%	±10%	±10.1%

Table A.4 summarizes the zeroth order single-sample analysis that provides the lowest possible uncertainty in measured spectral transmittance of samples for several τ (λ).

1st Order Uncertainty

First order uncertainty is the temporal variation in measured quantities, V_S and V_R in this case. The sources of the temporal variation include stability of the light source and the data processing system of BAI-IS.

To estimate the 1st order uncertainty, two sets of tests were performed. For the first set of tests, data were taken continuously for several periods of time at various frequencies without a sample in place. As well, the PLA has adjustable time constant (100 μs to 30 s) and sensitivity (3 μV to 1 V). Time constant and sensitivity should be adjusted according to the detector's signal level. Therefore, the second set of tests were carried out to check the effect of time constant and sensitivity on signal stability over a time period. Several typical combinations of time constant and sensitivity were chosen for the experiment. Details and results of the two sets of tests are discussed as follows.

The first set includes a series of three tests, using the following settings.

- Monochromator: Slit Width = 0.1 mm and Nominal Wavelength = 1000 nm
- PLA: Time Constant = 100 ms and Sensitivity = 30 mV

Number of sample, frequency of data reading, and the duration of the test are listed in Table A.5. As well, average (AVG), standard deviation (STD), and % STD in terms of the average reading (STD/AVG) are given Table A.5.

Table A.5: Results of the first set tests showing AVG, STD, and STD/AVG %

Test	1	2	3
No. of Samples	10000	600	600
Frequency (Hz)	1000	10	100
Duration (s)	10	60	6
AVG	0.49736	0.49672	0.49716
STD	0.00082	0.00082	0.00082
STD/AVG (%)	0.165	0.165	0.165

As shown in Table A.5, STD is 0.165% of the average reading for all three cases. The results of these three test are essentially the same. All averages are within one standard deviation of each other. Therefore, taking more than 600 samples for longer than 6 seconds will not reduce uncertainty of the results.

The second set includes a series of five tests, using the following settings, and results are shown in Table A4.

- Monochromator: Slit Width = 0.1 mm and Nominal Wavelength = 1000 nm
- Number of Samples = 10000 and Frequency = 1000

Table A.6: Results of the second set tests showing AVG, STD, and STD/AVG %

Test	1	2	3	4	5
Time Constant (ms)	10	30	100	300	100
Sensitivity (mV)	100	100	100	100	30
AVG	0.1491	0.1524	0.1524	0.1521	0.4974
STD	0.0019	0.0008	0.0005	0.0005	0.0008
STD/AVG (%)	1.253	0.516	0.340	0.320	0.165

The results show that STD decreases as time constant increases up to about 300 ms in this case. As shown in Table A.6, STD/AVG reduces from 1.25% to 0.32% as time constant increases from 10 ms to 300 ms. To further reduce uncertainty, one can use a higher sensitivity setting (e.g., test case 5 uses 30 mV compared to 100 mV for all other cases). Note that case 5 of the second set is case 1 of the first set.

Both increasing time constant and increasing sensitivity will reduce the uncertainty. However, signal saturation occurs when sensitivity is too high. In addition, increasing time constant will also increase settling time (longer wait time before signal can be read).

Uncertainty associated with the stability of light source and data processing system can be estimated as two standard deviation of the sample readings. Therefore, based on the two sets of tests, the uncertainty ranges from ±0.33% to ±2.5%. Following the manufacturer's procedures for adjusting time constant and sensitivity (i.e., first set of tests), the uncertainty is ±0.33%. For the transmittance experiment, time constant less than 100 ms is not necessary. Time saved is definitely not worth the added uncertainty. So the maximum uncertainty is ±0.68% based on time constant ≥ 100 ms. This source of uncertainty can be safely neglected if proper procedures for adjusting time constant and sensitivity are followed. For example, ±0.33% is less than ¼ of the minimum uncertainty (±1.4%) shown in Table A.3. Even the maximum of ±0.68% is still not significant compared to the accuracy of data processing system (±1.4% to ±10%).